

Washington University in St. Louis  
**Washington University Open Scholarship**

---

All Theses and Dissertations (ETDs)

---

Summer 9-1-2014

# Fine Particle and Mercury Formation and Control during Coal Combustion

Xiaofei Wang

*Washington University in St. Louis*

Follow this and additional works at: <https://openscholarship.wustl.edu/etd>

---

## Recommended Citation

Wang, Xiaofei, "Fine Particle and Mercury Formation and Control during Coal Combustion" (2014). *All Theses and Dissertations (ETDs)*. 1360.

<https://openscholarship.wustl.edu/etd/1360>

This Dissertation is brought to you for free and open access by Washington University Open Scholarship. It has been accepted for inclusion in All Theses and Dissertations (ETDs) by an authorized administrator of Washington University Open Scholarship. For more information, please contact [digital@wumail.wustl.edu](mailto:digital@wumail.wustl.edu).

WASHINGTON UNIVERSITY

School of Engineering and Applied Science  
Department of Energy, Environmental and Chemical Engineering

Dissertation Examination Committee:

Pratim Biswas, Chair

Richard Axelbaum

Jeffrey Catalano

John Fortner

Constance Senior

Brent Williams

Fine Particle and Mercury Formation and Control during Coal Combustion

By

Xiaofei Wang

A dissertation presented to the  
Graduate School of Arts and Sciences  
of Washington University in  
partial fulfillment of the  
requirements for the degree  
of Doctor of Philosophy

August 2014  
Saint Louis, Missouri

## Contents

<b>List of Figures.....</b>	<b>vi</b>
<b>List of Tables .....</b>	<b>xii</b>
<b>Acknowledgments .....</b>	<b>xiii</b>
<b>Abstract of the Dissertation .....</b>	<b>xv</b>
<b>Chapter 1. Introduction .....</b>	<b>1</b>
1.1 Background and motivation.....	2
1.2 Dissertation outline .....	14
1.3 References.....	16
<b>Chapter 2. Characterization of Organic and Black Carbon Aerosols from Coal Combustion: An Experimental Study in a 1 Megawatt Pilot Scale Coal Combustor .....</b>	<b>26</b>
Abstract.....	27
2.1 Introduction.....	28
2.2 Experimental Section .....	29
2.3 Results and Discussion .....	32
2.4 Conclusions.....	40
2.5 References.....	42
<b>Chapter 3. Characterization of organic aerosol produced from pulverized coal combustion in a drop-tube furnace .....</b>	<b>47</b>
Abstract.....	48
3.1 Introduction.....	49
3.2 Experimental Section .....	52
3.3 Results and Discussion .....	56

3.4 Conclusions.....	71
3.5 References.....	72
<b>Chapter 4. Formation mechanism of organic aerosol during coal combustion: Roles of pyrolysis .....</b>	<b>80</b>
Abstract.....	81
4.1 Introduction.....	82
4.2 Experimental Section.....	83
4.3 Results and Discussion .....	88
4.4 Conclusions.....	99
4.5 Reference .....	101
<b>Chapter 5. Effect of sulfur content in coal on organic aerosol formation during coal combustion.....</b>	<b>106</b>
Abstract.....	107
5.1 Introduction.....	108
5.2 Experimental Section.....	109
5.3 Results and Discussion .....	112
5.4 References.....	128
<b>Chapter 6. Mercury Removal during Coal Combustion by Injection of Vanadium Pentoxide (V<sub>2</sub>O<sub>5</sub>) .....</b>	<b>134</b>
Abstract.....	135
6.1 Introduction.....	136
6.2 Experimental Section.....	139
6.3 Results and Discussion .....	142
6.4 Conclusions.....	154
6.5 References.....	156

<b>Chapter 7. Role of Exhaust Gas Recycle on Submicrometer Particle Formation during Oxy-Coal Combustion .....</b>	<b>163</b>
Abstract .....	164
7.1 Introduction.....	165
7.2 Experimental section.....	167
7.3 Results and discussion .....	170
7.4 Conclusions.....	181
7.5 References.....	183
<b>Chapter 8. Conclusions.....</b>	<b>188</b>
8.1 Organic aerosol formation during coal combustion (Chapter 2, 3, 4 and 5) .....	189
8.2 Mercury removal during coal combustion by injection of Vanadium Pentoxide ( $V_2O_5$ ) (Chapter 6) .....	190
8.3 Submicrometer particle formation during oxy-coal combustion (Chapter 7).....	191
8.4 Implications for “Real World” .....	191
<b>Chapter 9. Future Work.....</b>	<b>193</b>
9.1 Further elucidation of formation pathways of organic aerosols during coal combustion .....	194
9.2 Atmospheric aging of coal combustion aerosols .....	199
9.3 Mercury oxidation in electrostatic precipitator (ESP) .....	200
9.4 Formation of organic carbon and black carbon aerosols during oxy-coal combustion .....	200
<b>Appendix I. Supporting materials for Chapter 3.....</b>	<b>202</b>
<b>Appendix II. Supporting materials for Chapter 4.....</b>	<b>207</b>
<b>Appendix III. Supporting materials for Chapter 5.....</b>	<b>222</b>
<b>Appendix IV. Description of ACERF Test Facility .....</b>	<b>225</b>

<b>Appendix V: Description of the Drop-tube furnace .....</b>	<b>230</b>
A5.1. Introduction.....	230
A5.2. Detailed Description .....	232
A5.3. Residence time calculations .....	237
A5.4. Temperature history of a burning coal.....	239
A5.5. Reference .....	247
<b>Appendix VI. Advanced instrumentation for aerosol measurement: AMS and TAG .....</b>	<b>248</b>
A6.1. High-Resolution Time-of-Flight Aerosol Mass Spectrometer (HR-ToF-AMS) ...	248
A6.2 Thermal Desorption Aerosol Gas Chromatograph Mass Spectrometer (TAG).....	249
A6.3 References:.....	250
<b>Appendix VII. List of papers and presentations .....</b>	<b>251</b>
<b>Appendix VIII. list of Raw data included in the attached CD.....</b>	<b>255</b>
<b>Xiaofei Wang - Curriculum Vitae .....</b>	<b>256</b>

## LIST OF FIGURES

Figure 1.1 Schematic diagram of combustion process of a single coal particle .....	5
Figure 1.2 Submicrometer particle formation during coal combustion (Taken from Suriyawong et al. (Suriyawong et al. 2006a)) .....	7
Figure 1.3 Schematic drawing of oxy-fuel combustion process (Taken from <a href="http://www.vattenfall.com/en/ccs/oxyfuel-combustion.htm">http://www.vattenfall.com/en/ccs/oxyfuel-combustion.htm</a> ). .....	12
Figure 2.1 Schematic drawing of ACERF system (no recycled flue gas was used in this study) 31	
Figure 2.2 Size distributions of particles in coal combustion flue gas for Experiment Set #1. ....	33
Figure 2.3 Pictures of aerosol samples collected on filters during the combustion for Experiment Set #1 (Top: Telfon filter; Bottom: Quartz filter). .....	34
Figure 2.4 EC/OC emissions under different fuel-air equivalence ratios for Experiment Set #1	34
Figure 2.5 Size distribution (Nano DMA data) of ultrafine particles in coal combustion flue gas .....	36
Figure 2.6 Size distributions of particles in coal combustion flue gas for Experiment Set #2 ....	38
Figure 2.7 Elemental compositions of submicrometer particles in coal combustion flue gas for Experiment Set #2 .....	39
Figure 2.8 BC/OC aerosol concentrations under oxy-coal combustion (Experiment Set #2) .....	40
Figure 3.1 Schematic drawing of the laboratory-scale pulverized coal combustion system with measurement instruments identified. ....	53
Figure 3.2. (A) Average organic mass spectra for fine particulate matter from pulverized coal combustion under different oxygen/coal ratios. Each mass spectrum corresponds to one oxygen/coal ratio. The mass spectra were obtained by an Aerodyne Aerosol Mass Spectrometer (AMS); (B) High resolution AMS spectrum and (C) Some important high resolution peak	

patterns for fine particulate matter from pulverized coal combustion under the oxygen/coal ratio at 12.0. CHOgt1 represents a group of high resolution ions, including  $\text{CO}_2^{+2}$ ,  $\text{CO}_2^+$ ,  $^{13}\text{CO}_2^+$ ,  $\text{CH}_2\text{O}_2^+$ ,  $\text{C}_3\text{O}_2^+$ ,  $\text{C}_8\text{H}_5\text{O}_3^+$ ,  $\text{C}_8\text{H}_7\text{O}_4^+$ ,  $\text{C}_{16}\text{H}_{23}\text{O}_4^+$  ..... 59

Figure 3.3. **(A)** Emission factors of particulate matter, total carbon, elemental carbon and organic carbon from coal combustion. **(B)** GC-MS measurements of extracts from coal combustion particles. Different chemical compounds were separated depending on their retention time in GC column. Major compounds were identified according to their mass spectra: *A. Benzaldehyde, 3-methoxy-4-[(trimethylsilyl)oxy]-, O-methyloxime; B. 3-Hydroxybutyric acid, t-butyl ester; C. Benzaldehyde, 2-methyl-; D. 1,3-Benzenediol, o-(4-methylbenzoyl)-o-(2-methoxybenzoyl)-; E. Benzene, 1,3-bis(1,1-dimethylethyl)-; F. 2-Isopropyl-5-methyl-1-heptanol; G. Phenol, 2,4-bis(1,1-dimethylethyl)-; H. Benzoic acid, 3,5-bis(1,1-dimethylethyl)-4-hydroxy-, ethyl ester; I. 13-Docosen-1-ol, (Z)-; J. Hexadecanoic acid, methyl ester; K. n-Hexadecanoic acid; L. 14-Pentadecenoic acid; M. Oxtadecanoic acid, methyl ester; N. Oxtadecanoic acid.* The presence of some esters may be due to the derivatization of acids with BSTFA; **(C)** Positive and negative mass spectra for extract of fine particulate matter from pulverized coal combustion. The mass spectra were obtained by an Aerosol Time-of-flight Mass Spectrometer (ATOFMS) ..... 62

Figure 3.4. **(A)** Average organic mass spectra and **(B)** Size distributions for different additional- $\text{N}_2/\text{Air}$  ratios while coal feed rate was fixed at 3.0 g/hr. The mass spectra were obtained by AMS, while the size distributions were measured by SMPS. Each color of mass spectrum or size distribution corresponds to certain additional- $\text{N}_2/\text{Air}$  ratios: (Blank: Air; Red: 10%  $\text{N}_2$  + 90% Air; Green: 20%  $\text{N}_2$  + 80% Air; Blue: 40%  $\text{N}_2$  + 60% Air); **(C)** Oxygen/Carbon (O/C) elemental ratios with error bars of organic matter for different additional- $\text{N}_2/\text{Air}$  ratios. .... 68

Figure 3.5. Proposed formation mechanisms of OA from coal combustion. .... 69

Figure 4.1. Schematic drawing of the experimental setup: (a) Drop-tube furnace system; (b) Flat-flame system ..... 85

Figure 4.2. AMS spectrum of (a) organic products from pyrolysis of PRB coal and (b) organic aerosols from combustion of PRB coal ..... 89



Figure 4.3. TAG chromatography of (a) organic aerosol from combustion of PRB coal; and (b) organic products from pyrolysis of PRB coal .....	91
Figure 4.4. Summary of organic aerosol formation during coal combustion .....	93
Figure 4.5. AMS spectrum of (a) organic aerosols from combustion of ILL#6 coal; and (b) organic products from pyrolysis of ILL#6 coal .....	94
Figure 4.6. TAG chromatography of (a) organic aerosol from combustion of ILL#6; and (b) organic products from pyrolysis of ILL#6 coal .....	97
Figure 4.7. Activation energy distributions for PRB coal and ILL#6 coal obtained by DAEM model .....	98
Figure 5.1. Schematic diagram of the experimental set-up .....	111
Figure 5.2. Size distribution of submicrometer particles from the combustion of ILL#6 coal ..	114
Figure 5.3 (A) AMS mass spectrum; and (B) High resolution peak patterns for fine organic particulate matter from combustion of ILL#6 coal, a high sulfur content coal. CHOgt1 represents a group of high resolution ions, including CHOgt1, which represents a group of high resolution ions, including $\text{CO}_2^{+2}$ , $\text{CO}_2^+$ , $^{13}\text{CO}_2^+$ , $\text{CH}_2\text{O}_2^+$ , $\text{C}_3\text{O}_2^+$ , $\text{C}_8\text{H}_5\text{O}_3^+$ , $\text{C}_8\text{H}_7\text{O}_4^+$ , $\text{C}_{16}\text{H}_{23}\text{O}_4^+$ .....	116
Figure 5.4 Elemental ratios for fine organic particulate matter from the combustion of ILL#6 coal, a high sulfur content coal. ....	117
Figure 5.5 (A) AMS organic spectrum; (B) Size distributions; (C) Elemental compositions; and (D) Correlation of concentration between SO4 species and the organic matter of submicrometer particles from the combustion of PRB coals mixed with different contents of sulfur .....	121
Figure 5.6 High resolution organic AMS spectrum of submicrometer particles from the combustion of PRB coals mixed with 4% sulfur .....	122
Figure 5.7 Formation mechanism of particulate nitrogen-containing organic matter during combustion high sulfur content coal .....	125

Figure 6.1. Schematic diagram of the experimental set-up .....	140
Figure 6.2. Combustion of PRB coal mixed with V <sub>2</sub> O <sub>5</sub> at different ratios: (a) Mercury concentrations in the flue gas; (b) Fine particle size distribution; and (c) Elemental compositions of fine particulate matter .....	144
Figure 6.3. (a) Particle size distribution from pure V <sub>2</sub> O <sub>5</sub> experiment; (b) SEM image of V <sub>2</sub> O <sub>5</sub> particles collected from the outlet of the drop-tube furnace; (c) SEM image of original V <sub>2</sub> O <sub>5</sub> particles; and (d) X-ray Diffraction (XRD) spectrum of the collected particles from pure V <sub>2</sub> O <sub>5</sub> experiment .....	148
Figure 6.4. Illustration of ultrafine V <sub>2</sub> O <sub>5</sub> particles formation .....	149
Figure 6.5. Effect of chlorine content in coal on mercury concentrations in the flue gas: (a) Mercury concentrations in the flue gas; (b) Fine particle size distribution; and (c) Elemental compositions of fine particulate matter .....	151
Figure 6.6. Comparison of material cost among the V <sub>2</sub> O <sub>5</sub> injection, activated carbon injection and bromine-impregnated activated carbon injection for mercury capture .....	154
Figure 7.1. <b>a)</b> Schematic diagram of drop-tube furnace system for oxy-combustion studies with exhaust gas recycle; <b>b)</b> O <sub>2</sub> /CO <sub>2</sub> ratios at the furnace inlet under different recycle ratios .....	168
Figure 7.2. Ash particle formation pathways during oxy-coal combustion; adapted from Suriyawong et al. (2006a). Illustrated is the impact of recycle exhaust gas. ....	171
Figure 7.3. Combustion of PRB coal (Experiment Set #1): <b>a)</b> Particle size distributions under different recycle ratios with filtration of recycled exhaust gas; Comparisons of size distributions between with filtration and without filtration of recycled exhaust gas under recycle ratio: <b>b)</b> 20%; <b>b)</b> 40%; <b>d)</b> 60% .....	172
Figure 7.4. X-ray diffractograms of submicrometer ash particles, comparing conventional coal-air with oxy-coal combustion without recycle and oxy-coal combustion with recycle (S: SiO <sub>2</sub> , A: Al <sub>2</sub> O <sub>3</sub> , C: CaO, H: Fe <sub>2</sub> O <sub>3</sub> ) .....	175

Figure 7.5. Comparisons of size distributions between with and without moisture addition of recycled exhaust gas under recycle ratio: <b>a)</b> 20%; <b>b)</b> 40%; <b>c)</b> 60% .....	177
Figure 7.6. Combustion of PRB coal at the lower feed rate (Experiment Set #2): <b>A)</b> Particle size distributions under different recycle ratios with filtration of recycled exhaust gas; Comparisons of size distributions between with filtration and without filtration of recycled flue gas under recycle ratio: <b>B)</b> 20%; <b>C)</b> 40%; <b>D)</b> 60% .....	179
Figure 7.7. Combustion of PRB coal at higher O <sub>2</sub> /CO <sub>2</sub> ratio (Experiment Set #3): <b>a)</b> Particle size distributions under different recycle ratios with filtration of recycled exhaust gas; Comparisons of size distributions between with filtration and without filtration of recycled exhaust gas under recycle ratio: <b>b)</b> 20%; <b>c)</b> 40%; <b>d)</b> 60% .....	181
Figure A4.1; Process flow diagram of the test facility .....	227
Figure A4.2: Cross section of the vertically down-fired combustor .....	228
Figure A4.3: Burner of the test facility .....	229
Figure A5.1. Picture and schematic drawing of the drop-tube furnace .....	230
Figure A5.2 Schematic drawing of a 285 MW furnace (Provided by Ameren Energy) .....	231
Figure A5.3. Overall inlet system into combustor (source: Smallwood's thesis(Smallwood 2005)) .....	233
Figure A5.4. Outlet system at combustor exit (source: Smallwood's thesis(Smallwood 2005)) .....	234
Figure A5.5. Schematic drawing of the coal feeder (source: William Linak) .....	236
Figure A5.6. (A) Schematic drawing of the connection between the coal feeder and the drop-tube furnace; (B) Air velocity contour (unit: m/s) in the drop-tube furnace (calculated using <i>Fluent</i> ) .....	237

Figure A5.7. Temperature profile along the alumina tube when the furnace temperature is fixed at 1100°C ..... 239

Figure A6.1 Schematic drawing of TAG (picture courtesy: Brent Williams) ..... 249

## LIST OF TABLES

Table 1.1 Summary of MATS for the emission limits of mercury and other heavy metal from coal-fired power plants (adapted from <a href="http://www.epa.gov/mats/actions.html">http://www.epa.gov/mats/actions.html</a> ) .....	9
Table 2.1 Test plan of experimental conditions in ACERF system .....	31
Table 2.2 Flue gas composition for each experimental condition .....	35
Table 3.1 Summary of experimental conditions for drop-tube furnace study of pulverized coal combustion .....	54
Table 5.1. Proximate and ultimate analysis of coals .....	110
Table 5.2. Identified Organic Compounds of the Methanol Extract from Submicrometer Particles Collected from the Combustion of PRB Coal Mixing with 4% Sulfur (by UPLC/ESI(+)/UHR-TOFMS) .....	126
Table 6.1. Experimental test plan for this study .....	141
Table 7.1. Summary of oxy-coal combustion test conditions (Q1 and Q2 are indicated in Fig. 7.1a). .....	169

## ACKNOWLEDGMENTS

I would like to express my deepest and most sincere gratitude to Professor Pratim Biswas, my PhD advisor, for his great guidance and continuous support on my scientific research. I have learned so much from him. And I am sure that my entire life will benefit a lot from his guidance.

I thank Drs. Richard L. Axelbaum, Jeffrey G. Catalano (from the Department of Earth & Planetary Sciences), John D. Fortner, Constance Senior (from ADA-ES, Inc.) and Brent J. Williams for serving on my dissertation committee and providing important and valuable comments and suggestions to improve this dissertation.

I also thank the colleagues in the Aerosol & Air Quality Research Laboratory for providing their helps and assistances. Especially I want to thank Dr. Wei-Ning Wang for his valuable help and guidance on my research; Michael Daukoru for teaching me how to operate the drop-tube system; and Jing He for his collaboration and tremendous help on our projects. I also want to thank Sijia Li, Emma Cotter, Hugo Sabin and other master/undergraduate/visiting students who helped me a lot on conducting experiments. Many thanks also go to my friends in the EECE department and the McDonnell International Academy. And I also would like to express my thanks to the staffs in EECE department.

I want to thank the McDonnell Academy, Peabody Energy and Consortium for Clean Coal Utilization (CCCU) for supporting me to do the coal combustion research and pursue my Ph.D.

In particular, I want to offer my sincere thanks to Professor Brent Williams. He provided me guidance on using the aerosol mass spectrometry and lots of great suggestions for our papers. I

also want to thank Professor Xin Yang at Fudan University, who was my master's degree advisor. We collaborated with him on several projects. He provided me many ambient data and valuable suggestions. I also want to express my thanks to Dr. Axelbaum's group. Drs. Benjamin Kumfer and Bhupesh Dhungel helped us a lot on doing pilot-scale coal combustion studies. I also thank Dr. Michael Gross and his student Hanliu Wang, who provided me many help on analyze the coal fly ash samples using their powerful mass spectrometry.

Finally, I do want to express my special thanks to my family, my lovely wife Yaping Zhang and my daughter Hanna Wang. And many thanks should also go to my parents, Jiusheng Wang and Xiaoyun Wang, for their tremendous support for my PhD. studies. And I would like to thank my parents in law, for their support and help on taking care of our baby girl.

Xiaofei Wang

*Washington University in St. Louis*

*August 2014*

# ABSTRACT OF THE DISSERTATION

Fine Particle and Mercury Formation and Control during Coal Combustion

by

Xiaofei Wang

Doctor of Philosophy in Energy, Environmental & Chemical Engineering

Washington University in St. Louis, 2014

Professor Pratim Biswas, Chair

Pulverized coal combustion is widely used worldwide for the production of electricity. However, it is one of the primary emission sources of air pollutants, including particulate matter (fly ash) and mercury (Hg), into the atmosphere. This dissertation investigated three aspects of pollutant formation and control from the coal combustion process: (1) organic aerosol formation during coal combustion, (2) mercury removal during coal combustion by injection of Vanadium Pentoxide ( $V_2O_5$ ), and (3) submicrometer particle formation during oxy-coal combustion.

**Part. 1.** While the characterization and formation of the mineral matter component of aerosol during coal combustion has been well studied and understood, the characterization and fate of corresponding organic matter content was not examined in detail earlier. The first part of this dissertation studies the formation mechanism of organic aerosols during coal combustion. Pilot-scale experiments were conducted in a 1 MW coal combustor, and showed that black carbon aerosol formation was greatly enhanced by increasing the fuel-air equivalence ratio. However, organic carbon aerosol formation was lowered by increasing the fuel-air equivalence ratio, which was opposite to the trend of black carbon aerosol formation. This phenomenon indicates that the formation mechanism of organic carbon aerosol is different from black carbon (soot) aerosol.



Detailed organic aerosol formation mechanisms have been studied in a laboratory-scale system. Aerosol mass spectrometry techniques were applied to characterize both coal combustion aerosols from a drop-tube coal combustor and coal pyrolysis products from a flat-flame coal pyrolyzer. The chemical composition of major species for both combustion organic aerosols and pyrolysis products are hydrocarbons, carboxylic acids and aromatic compounds. The similarities of the chemical compositions demonstrate that the products from coal pyrolysis, (the initial step of coal combustion), are the precursors of organic aerosols. More carboxylic acids and oxygenated organic compounds were found in the combustion aerosols, indicating that many pyrolysis products are oxidized before they are converting to organic aerosols.

A strong correlation between inorganic and organic aerosol formation mechanisms has been found in this work, demonstrating that inorganic particles play a critical role as carriers of organic species. Sulfate species in inorganic aerosols play a particularly important role in organic aerosol formation. Enhanced organic aerosol formation during the combustion of high sulfur content coal has been observed for the first time. High resolution mass spectra analysis shows the presence of amine-like organics in the aerosols. The correlation between particulate sulfate and organics suggests that acidic sulfate particles may absorb basic amine-like organics, a major coal pyrolysis product, from the gas phase into the particle phase via acid-base neutralization reactions.

**Part. 2.** Coal combustion is a major source of atmospheric mercury. High-temperature sorbent injection is an efficient method to capture metallic species during combustion. This part of the study examines the performance on Hg capture from pulverized coal combustion in a drop-tube furnace.  $V_2O_5$  was tested as a sorbent and demonstrated good performance on elemental mercury capture, which results from the formation of ultrafine  $V_2O_5$  particles during the

combustion process. It is proposed that the ultrafine  $V_2O_5$  particles catalyzed  $Hg^0$  oxidation on their large surfaces.  $Hg^{2+}$ , the oxidation product, may condense on fly ash particle surfaces or on tubing surfaces, thereby being removed from the flue gas.

**Part. 3.** Coal combustion is the largest single contributor to global anthropogenic  $CO_2$  emissions. Oxy-coal combustion replaces the air with oxygen and uses recycled flue gas (RFG) as a diluent, resulting in a higher concentration (>98%) of  $CO_2$  in the exhaust, which promotes more effective control, capture, and possible conversion of  $CO_2$ . This part of the dissertation investigates the effects of recycling (up to recycle ratios of 60%) on submicrometer particle formation in a drop-tube furnace system. The recycled exhaust gas containing lower  $O_2$  concentration and higher  $CO_2$  concentration suppressed submicrometer particle formation. However, it was found that water vapor in recycled exhaust gas greatly enhanced the formation of submicrometer particles. The gas composition changes that result from exhaust-gas recycling significantly affected the size distribution of submicrometer particles at the exit of the combustor. Differences in the particle size distribution with and without the filtration of recycled exhaust gas were insignificant. The composition of the resultant particles in oxy-coal combustion and conventional coal-air combustion as determined by X-ray diffraction was similar.

## **CHAPTER 1. INTRODUCTION**

## 1.1 Background and motivation

Pulverized coal combustion is widely used for the production of electricity, ranging from 45% in the United States to greater than 70% in India and China (Biswas et al. 2011). However, it is a major primary emission source of many air pollutants (Quann et al. 1982, Senior and Flagan 1982, Linak and Wendt 1994, Seinfeld and Pandis 2006, Skeen et al. 2010), including particulate matter (fly ash), mercury, and other gaseous pollutants such as CO<sub>2</sub>, SO<sub>2</sub> and NO<sub>x</sub>. Control of these air pollutants from coal combustion is of vital importance to the environment and to human health.

Particulate matter draws much attention because it affects human health and radiative climate forcing (Poschl 2005). Particles emitted from coal combustion usually contain inorganic constituents; including major species, such as SiO<sub>2</sub>, MgO, Fe<sub>2</sub>O<sub>3</sub>, elemental carbon, and trace species, such as Pb, Hg and Se (Linak and Wendt 1994). Organic matter also constitutes a relatively low but important fraction of total particle mass (Zhang et al. 2008, Linak et al. 2007). Coal combustion produces particles with diameters varying from several nanometers up to hundreds of micrometers (Quann et al. 1982). Submicrometer particles are particularly important due to their ability to penetrate deep in the respiratory system (Poschl 2005). Additionally, it is found that many heavy metals and carbonaceous materials are enriched in submicrometer particles, which pose serious health risks to human beings (Haynes et al. 1982a, Linak and Wendt 1994, Linak et al. 2007). Therefore, it is very important to study submicrometer particle formation from coal combustion. The formation mechanism of inorganic particles during coal combustion had been well established (Linak and Wendt 1994, Biswas and Wu 1998, Zhuang and Biswas 2001, Damle et al. 1982a, Quann et al. 1982). However, the

detailed formation mechanisms of organic aerosols are still not clear. This work has studied organic aerosol formation during coal combustion in detail.

Coal combustion is also a dominant source of anthropogenic emission of mercury (Senior, Helble, et al. 2000, Senior, Sarofim, et al. 2000), which is very harmful to people's brains, hearts, kidneys, lungs, and immune systems (Clarkson 1997). In 2011, the US EPA issued national standards (Mercury and Air Toxics Standards) for emissions of mercury and other heavy metals from power plants. Consequently, to control mercury (Hg) and other heavy metals emissions is an urgent issue. In coal combustion flue gas, mercury can be present in both the gas and particle phases. And most of heavy metals are present in the particle phase. Thus, the main goal of emission control is to capture both gaseous Hg and particulate matter from coal combustion. Many technologies have been proposed for either Hg or particulate matter capture. However, a technology which can reduce emissions of both Hg and particulate matter efficiently and economically is strongly preferred. Sorbent injection is a potentially promising method to control emissions of Hg and particulate matter. In this work, a sorbent injection method has been developed to control Hg and particulate matter emissions.

Coal combustion is a main source of CO<sub>2</sub> emission, which is a main greenhouse gas associated with climate change. Oxy-coal combustion coupled with carbon capture and sequestration (CCS) is a promising technology to reduce CO<sub>2</sub> emission from coal combustion (Chen et al. 2012). Oxy-coal combustion conditions are very different from conventional coal combustion conditions. There is limited knowledge on how submicrometer particles are formed during the new oxy-coal combustion conditions. Although some studies did investigate submicrometer particle formation during oxy-coal combustion, most of these laboratory-scale studies do not include exhaust gas recycling, a key aspect of oxy-coal combustion systems. The roles of

exhaust gas recycle in submicrometer particle formation during oxy-coal combustion are largely unknown. Thus, this work has investigated submicrometer particle formation during oxy-coal combustion with exhaust gas recycling.

### *1.1.1 Submicrometer aerosol formation during coal combustion*

The process of a single coal particle burning is considered to occur in three basic steps (shown in Fig. 1.1) (Warnatz et al. 2006, Suriyawong et al., 2006a): *I) Devolatilization (or Pyrolysis) of coal*: the molecular structure of coal can be represented as clusters of many fused aromatic rings connected with other clusters via aliphatic bridges or loops. These aromatic rings are more stable than the aliphatic bridges and loops: when coal particles enter a furnace, they are rapidly heated up (at a heating rate  $\sim 10^5$  K/s). The bridges and loops in coal molecular structure break up before the aromatic rings, which are relatively more stable. Some small aromatic cluster fragments, referred to as “tar”, are released in the gas phase due to their higher volatility. Meanwhile, larger molecular-weight fragments remain in parent coal particles due to their lower volatility. The remaining particles are called “char”. Typically, the devolatilization process takes less than 100 ms; *II) Burning of tar*: after released in the gas phase, tars can undergo secondary pyrolysis to produce light gases, such as CO, H<sub>2</sub>. Some of tar may form soot particles after the secondary pyrolysis. However, under high temperature, these carbonaceous species are quickly oxidized and form a bright flame. The presence of soot particles makes the flame brighter; *III) Burning of char*: char particle is basically a mixture of elemental carbon and inorganic ash. The carbon in char particle first reacts with CO<sub>2</sub> to form CO, which is then oxidized by O<sub>2</sub> and form CO<sub>2</sub> in the gas phase. The burning of char particles may take about 2 seconds in a full scale coal combustor.

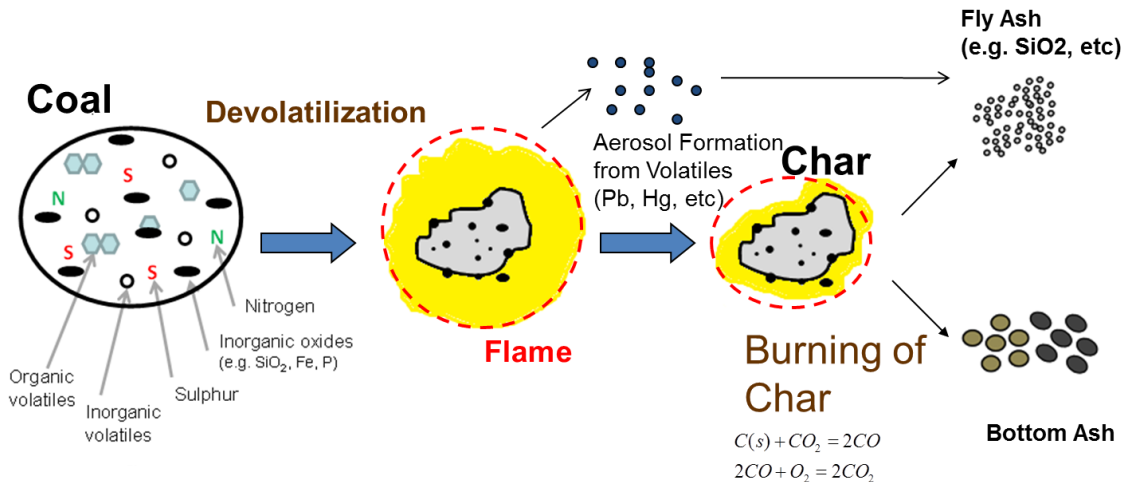


Figure 1.1 Schematic diagram of combustion process of a single coal particle (the diagram was made based on Warnatz et al. 2006)

Coal combustion produces high concentrations of submicrometer particles and supermicrometer particles in its exhaust gas. Inorganic mineral matter is a main component of these particles. The general formation pathway of submicrometer inorganic particles during coal combustion has been well established (Fig. 1.2) (Damle et al. 1982a, Haynes et al. 1982a, Biswas and Wu 1998, Linak and Wendt 1994). Coal contains a certain amount of mineral matter, such as CaO, Al<sub>2</sub>O<sub>3</sub>, and SiO<sub>2</sub>. After the devolatilization of coal particles in a combustor, volatile matter is released and char particles are formed. CO is formed in the vicinity of char, which creates a reducing environment. Some metal oxides are reduced by CO at the char surfaces and thus produce metal or metal sub-oxides, which are relatively more volatile. These metal or sub-oxides may be released into the gas phase and then experience rapid re-oxidation to form stable metal-oxide nuclei. Subsequently they grow into submicrometer aerosols by coagulation and condensation (Quann et al. 1982, Quann and Sarofim 1982, Linak and Wendt 1994, Biswas and Wu 1998).

Coal combustion also produces ultrafine soot particles (Bond et al. 2004, Olmez et al. 1988, Cho et al. 2009). Brown and Fletcher (1998) proposed a model to describe soot formation during coal combustion. They proposed that tar vapors are the precursors of soot. The formation of soot during coal burning is very different from that during light hydrocarbon gas combustion. In light hydrocarbon gas combustion, light gas may break up into acetylene and may undergo cyclization to form aromatic rings if there is no aromatic species in the light gas. Then those aromatic rings keep growing and finally form fine soot particles (Mansurov 2005). In contrast, tar vapors from coal pyrolysis are relative larger molecules. Thus they can directly lose H and O atoms to form soot.

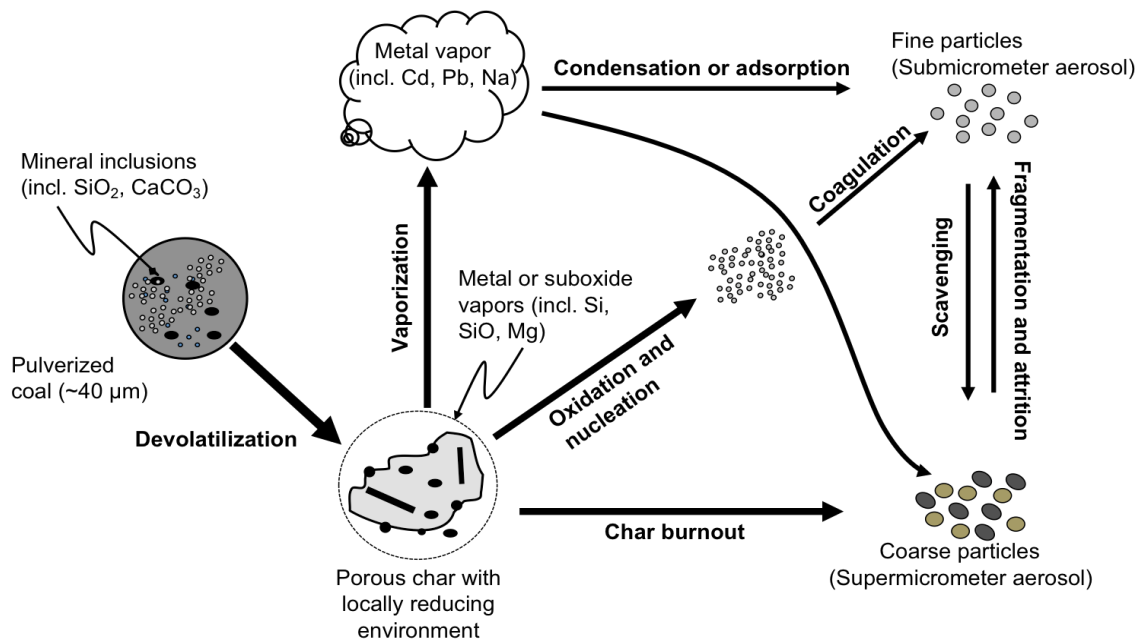




Figure 1.2 Submicrometer particle formation during coal combustion (Taken from Suriyawong et al. (Suriyawong et al. 2006a))

As mentioned above, the formation of inorganic particles, including minerals and soot, in submicrometer size range has been studied extensively. However, the organic content of particles has not been examined in detail. In recent years, there has been renewed interest in the organic matter content of coal fly ash, due to both climate change and health concerns (Zhang et al. 2008, Cho et al. 2009, Jacobson et al. 2000). Coal combustion has been identified as one of the major sources of atmospheric organic aerosol in some developing countries, such as China (Sun et al. 2013, Hu et al. 2013, Wang, Williams, et al. 2013b).

However, few studies have focused on organic aerosol formation during coal combustion. Zhang et al. (2008) measured the emission factors of particulate organic carbon, which range from 0.3 to 17.1 mg kg<sup>-1</sup> coal. The characterization of organic aerosol shows that the main components are alkanes, aliphatic acids, aromatic acids, and PAHs. And the emission factors of several types of particulate PAHs, which draw much attention due to their carcinogenicity, were also determined. Generally, there is very limited knowledge on either the chemical characteristics of organic aerosol or their formation pathways during coal combustion.

### *1.1.2. Removal of Hg and other heavy metals from coal combustion*

In 2011, the US EPA established the Mercury and Air Toxics Standard (MATS) which strictly regulates the emissions of Hg and other pollutants from power plants. Table 1.1 summarizes the standards for coal-fired power plants. According to the standard, if a new coal-fired power plant uses coal with the following characteristics — Hg content: 50 ppb, Heating value: 28 MJ/kg, assumed thermal efficiency for electrical generators is 30% — then at least 91.5% of Hg needs to

be captured. MATS also regulates the emissions of other toxic metals, which are mainly present in particulate form.

Mercury (Hg) content in coal varies from about 0.049 to 0.126 ppm (w/w) (Pavlish et al. 2003). During coal combustion, Hg is released in its elemental form  $\text{Hg}^0(\text{g})$ . In the post combustion environment with its lower temperature,  $\text{Hg}^0(\text{g})$  may be oxidized to  $\text{Hg}^{2+}$  by HCl and  $\text{Cl}_2$ .  $\text{Hg}^{2+}$  species can easily condense on particle surface and form particulate Hg, Hg(p) (Galbreath and Zygarlicke 2000, Senior, Helble, et al. 2000, Senior, Sarofim, et al. 2000). Thus, there are three forms of Hg in exhaust gas: 1)  $\text{Hg}^0(\text{g})$ ; 2)  $\text{Hg}^{2+}(\text{g})$ ; and 3) Hg(p).  $\text{Hg}^{2+}(\text{g})$  is water-soluble and can be readily removed by wet flue gas desulfurization (WFGD) systems (Zhuang et al. 2004). Hg(p) can also be easily removed by particulate matter control devices such as fabric filter (FF) baghouses or electrostatic precipitators (ESP). But it is much more difficult to capture  $\text{Hg}^0(\text{g})$  (Pavlish et al. 2003). In order to capture  $\text{Hg}^0(\text{g})$ , many control methods have been developed, such as: (1) Activated carbon injection; (2) Oxidation (or catalytic oxidation) of  $\text{Hg}^0(\text{g})$  in flue gas; and (3) Sorbent injection during combustion.

Activated carbon injection is a widely used and commercially available technology for mercury capture. Basically, powdered activated carbon particles are injected into flue gas ductwork to absorb  $\text{Hg}^0(\text{g})$ . Then a particulate control device removes them and fly ash. For activated carbon injection processes, the carbon/mercury (C/Hg) ratio (on a weight basis) may reach 5,000-100,000:1 to achieve >90% removal efficiency for mercury (Hsi et al. 1998, Pavlish et al. 2003). The large C/Hg ratio may result from mass-transfer limitations, from the limited mercury adsorption capacity of activated carbon, or from the limited surface reactivity of carbon. Fly ash can be used as a cement replacement in concrete. It requires that the carbon content in fly ash is less than 5 ~ 6 % (Pflughoeft-Hassett et al. 2009). However, carbon content above 1% can still

adversely affect the salability of fly ash. Thus, it limits the amount of activated carbon injection. A desirable C/Hg ratio should be less than 5,000 to 10,000:1.

Table 1.1 Summary of MATS for the emission limits of mercury and other heavy metal from coal-fired power plants (adapted from <http://www.epa.gov/mats/actions.html>)

<b>Emission limits for Pollutants</b>	<b>New or Reconstructed Coal-fired unit (lb/GWh)</b>	<b>Existing Coal-fired units (lb/GWh)</b>
Particulate matter	7.0	300
Antimony (Sb)	$8.0 \times 10^{-3}$	$8.0 \times 10^{-3}$
Arsenic (As)	$3.0 \times 10^{-3}$	$2.0 \times 10^{-2}$
Beryllium (Be)	$6.0 \times 10^{-4}$	$2.0 \times 10^{-3}$
Cadmium (Cd)	$4.0 \times 10^{-4}$	$3.0 \times 10^{-3}$
Chromium (Cr)	$7.0 \times 10^{-3}$	$3.0 \times 10^{-2}$
Cobalt (Co)	$2.0 \times 10^{-3}$	$8.0 \times 10^{-3}$
Lead (Pb)	$2.0 \times 10^{-3}$	$2.0 \times 10^{-2}$
Manganese (Mn)	$4.0 \times 10^{-3}$	$5.0 \times 10^{-2}$
Nickel (Ni)	$4.0 \times 10^{-2}$	$4.0 \times 10^{-2}$
Selenium (Se)	$6.0 \times 10^{-2}$	$6.0 \times 10^{-2}$
Mercury (Hg)	$2.0 \times 10^{-4}^* \sim 4.0 \times 10^{-2}^{**}$	$1.3 \times 10^{-2}^* \sim 4.0 \times 10^{-2}^{**}$

\*: for other kinds of coal (not lignite coal)

\*\* : for lignite coal

It is easier to capture  $\text{Hg}^{2+}(\text{g})$  than  $\text{Hg}^0(\text{g})$ . Therefore, a way to control Hg emission is to oxidize  $\text{Hg}^0(\text{g})$  to  $\text{Hg}^{2+}$  in flue gas and then to use scrubber to capture it. Many halogen species can oxidize  $\text{Hg}^0(\text{g})$ . For example, chlorine is a major halogen specie in flue gas and plays a critical role in Hg oxidation (Senior, Sarofim, et al. 2000). Bromine and iodine can be injected into coal combustor or flue gas ductwork to enhance  $\text{Hg}^0(\text{g})$  oxidation significantly (Liu et al. 2007, Li, Daukoru, et al. 2009). The catalytic oxidation of  $\text{Hg}^0(\text{g})$  has also been extensively studied. One approach is to utilize selective catalytic reduction (SCR) units, a  $\text{NO}_x$  control device. A SCR catalyst typically consists of  $\text{V}_2\text{O}_5$ ,  $\text{WO}_3$  or zeolite supported on various carriers such as  $\text{TiO}_2$ . It catalyzes the reduction of  $\text{NO}_x$  to  $\text{N}_2$ . Many studies report that SCR catalysts can also oxidize  $\text{Hg}^0(\text{g})$ , particularly in the presence of halogen species (Cao, Chen, et al. 2007). Aside from SCR catalysts, other metal or metal oxide catalysts, such as  $\text{Fe}_2\text{O}_3$ ,  $\text{CuO}$ , and some precious metals (gold, silver, and palladium), have also been studied (Galbreath et al. 2005, Ghorishi et al. 2005, Zhao et al. 2006). Recently, some studies reported that  $\text{TiO}_2$  based photocatalysts have a good performance in  $\text{Hg}^0(\text{g})$  oxidation (Li, Li, et al. 2011b, Li et al. 2012, Li, Wu, et al. 2011, Li et al. 2008, Pitoniak et al. 2005).

The sorbent injection into combustor (high temperature sorbent injection) is an efficient method to control heavy metal emissions from combustion (Biswas and Wu 1998, Gale and Wendt 2005, 2003, 2002, Wendt and Lee 2010, Yoo et al. 2005). As mentioned in Part 1.1.1, during coal combustion, metallic species may be released into the gas phase and form vapors. At the exit of the combustor, these vapors undergo homogeneous nucleation or heterogeneous condensation and form submicrometer aerosols when the temperature drops. If additional sorbent particles are injected into the combustor, some metallic vapors can condense on the preexisting sorbent particles. Therefore, these metallic species are associated with sorbent particles, which usually

have a larger particle size. They can be easily removed by particulate matter control devices. This methodology can also be applied for Hg removal. Wu et al. (1998) reported a method using TiO<sub>2</sub> as sorbent: the sorbent precursor was added into a high-temperature environment (like combustor). Then the precursor was oxidized to form high concentrations of TiO<sub>2</sub> agglomerate, which can efficiently oxidize and capture Hg<sup>0</sup>(g) under ultraviolet irradiation.

### *1.1.3 Submicrometer particle formation during oxy-fuel combustion*

Coal combustion is the single largest contributor to global anthropogenic CO<sub>2</sub> emissions, contributing 42% of total CO<sub>2</sub> emissions from anthropogenic sources and 73% of the CO<sub>2</sub> emissions associated with electricity and heat generation (Baumert et al. 2005). Oxy-coal combustion coupled with carbon capture and storage (CCS) is a promising technology to reduce CO<sub>2</sub> emission. Instead of air, pure oxygen is used to combust coal particles, resulting in a high concentration of CO<sub>2</sub> in exhaust that facilitates the control, capture, and possible conversion of CO<sub>2</sub> (Abraham et al. 1982, Buhre, Elliott, et al. 2005, Croiset and Thambimuthu 1999). Combustion in pure oxygen could have a very high flame temperature. To reduce it, oxy-coal combustion utilizes recycled flue gas (RFG) as a diluent. The concept of oxy-coal combustion is summarized in Fig. 1.3. Oxy-coal combustion has similar heat transfer characteristics to conventional pulverized coal combustion (Tan et al. 2006). And it also has many advantages, including lower NO<sub>x</sub> emissions (Okazaki and Ando 1997, Hu et al. 2001, 2003), reduced flue gas volume (Buhre, Elliott, et al. 2005), and relatively lower cost compared to post-combustion capture techniques (Singh et al. 2003, Beér 2007). However, the effects of oxy-coal combustion conditions on emissions (both gaseous and particulate) are still unclear and require detailed study, since these emissions may have negative impacts both on environment (Samet et al. 2000, Ramanathan et al. 2001) and downstream processes, such as CO<sub>2</sub> compression and sequestration.

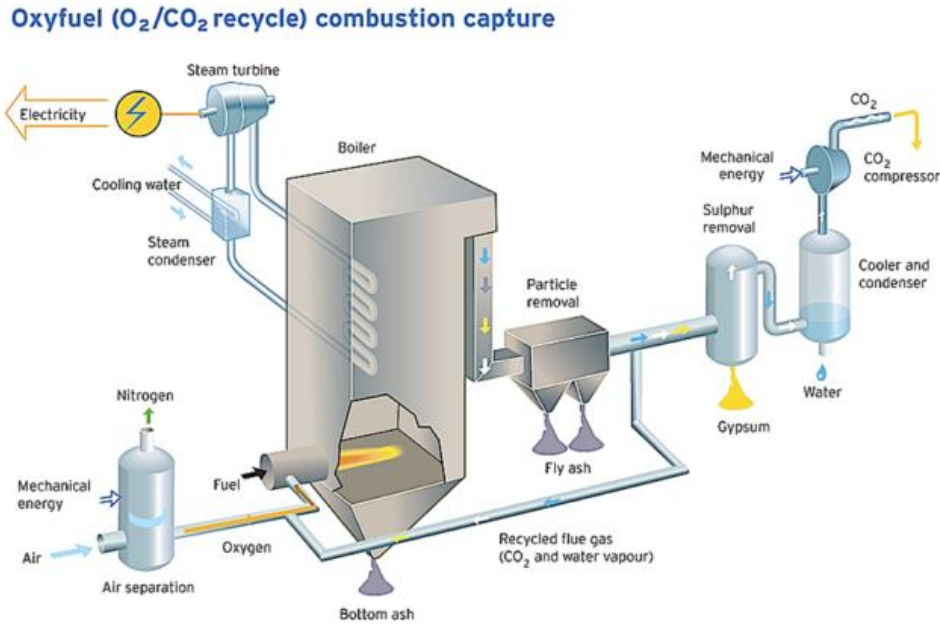


Figure 1.3 Schematic drawing of oxy-fuel combustion process (Taken from <http://www.vattenfall.com/en/ccs/oxyfuel-combustion.htm>).

Many studies have investigated the effects of oxy-coal combustion on combustion characteristics and gaseous pollutant emissions. However, not many studies focused on submicrometer particle formation (Suriyawong et al. 2006a, Sheng et al. 2007, Zhuang and Pavlish 2012). The formation of submicrometer particles bears continued relevance due to their penetration through conventional particle control devices (Li, Suriyawong, et al. 2009, Suriyawong et al. 2008) and concerns about their harmful effects on human health (Samet et al. 2000). Understanding the formation mechanisms of submicrometer particles under various oxy-coal combustion conditions that include exhaust gas recycle, is therefore an important step in increasing the efficiency of particle control devices and systems. Suriyawong et al. (2006a) studied submicrometer particle formation during oxy-coal combustion in a drop-tube furnace, and they found that the surface temperature of burning char is a key parameter affecting the formation of submicrometer metal-oxide particles via the effect of temperature on metal-oxide/metal vaporization rates. Sheng and

co-workers (Sheng et al. 2007, Sheng and Li 2008) studied submicrometer particle formation during the oxy-coal combustion of a low-rank Chinese coal using a drop-tube furnace and confirmed the CO<sub>2</sub> suppression of submicrometer particle formation via the vaporization-nucleation pathway. They also studied mineral transformations in the total ash formed during the oxy-coal combustion of four other Chinese coals and the result shows that, in comparison to conventional O<sub>2</sub>-N<sub>2</sub> systems, oxy-coal combustion in O<sub>2</sub>-CO<sub>2</sub> did not affect the mineral phases detected but did affect the relative amounts in which those phases were present in the total residual ash. Morris et al. (2013) characterized particle emission from air- and oxy-coal combustion with actual flue gas recycling in a pilot-scale coal combustor (37 KW). The authors reported that concentrations of soot particles were much lower in the oxy-coal combustion mode than in the air-firing mode, especially with an actual flue gas recycle, which may send the soot particles back to the furnace and diminish them. In addition, size distribution of sodium was reported and there is no significant difference of sodium partitioning between air-firing and oxy-coal combustion.

Most of these studies were performed using single pass flow-through drop-tube furnace studies that did not include exhaust gas recycling, an important aspect of oxy-coal combustion systems. This is a particularly important consideration as the exhaust gas usually contains high concentrations of aerosols and moisture. Recycling of the exhaust gas can introduce them back into the combustion chamber, and this may affect the resultant particle formation processes during coal combustion. In this work, the role of exhaust gas recycle in submicrometer particle formation during oxy-coal combustion is studied.

## 1.2 Dissertation outline

This dissertation has three main objectives:

- 1) To understand formation mechanisms of organic aerosols produced during pulverized coal combustion;
- 2) To evaluate the performance of mercury capture using high temperature sorbents technologies; and
- 3) To investigate formation of submicrometer particle during oxy-coal combustion with flue gas recycling

The three objectives are studied and described in six chapters of the dissertation. This dissertation is organized such that each chapter is self-contained with an introduction, experimental section, results, discussion, and conclusions. Chapters 2 and 3 provide a systematic study of the characteristics of organic aerosol emission from a 1-megawatt pilot-scale coal combustor and a laboratory-scale coal combustor (drop-tube furnace), respectively. They investigate organic aerosol emissions under various combustion conditions and propose a general pathway for organic aerosol formation during coal combustion. Then, to prove the proposed pathway, Chapter 4 compares the chemical compositions of organic aerosol from coal combustion and organic products from coal pyrolysis. Chapter 5 studies the effects of sulfur content in coal on sulfate/organic aerosol formation during coal combustion. Chapter 6 reports mercury removal from coal combustion by injecting vanadium pentoxide ( $V_2O_5$ ) as a high temperature sorbent. And Chapter 7 studies the role of exhaust gas recycle on submicrometer



particle formation during oxy-coal combustion. Finally, the conclusions of this dissertation are summarized in Chapter 8.

### 1.3 References

- Abraham, B. M., J. G. Asbury, E. P. Lynch, and A. P. S. Teotia. 1982. "Coal-oxygen process provides carbon dioxide for enhanced recovery." *Oil Gas J* no. 80 (11):68-70.
- Baumert, K. A., T. Herzog, and J. Pershing. 2005. *Navigating the Numbers: Greenhouse Gas Data and International Climate Policy*. World Resources Institute.
- Beér, J. M. 2007. "High efficiency electric power generation: The environmental role." *Progress in Energy and Combustion Science* no. 33 (2):107-134. doi: 10.1016/j.pecs.2006.08.002.
- Biswas, P., W. N. Wang, and W. J. An. 2011. "The energy-environment nexus: aerosol science and technology enabling solutions." *Frontiers of Environmental Science & Engineering in China* no. 5 (3):299-312. doi: 10.1007/s11783-011-0351-1.
- Biswas, P., and C. Y. Wu. 1998. "Control of toxic metal emissions from combustors using sorbents: A review." *Journal of the Air & Waste Management Association* no. 48 (2):113-127.
- Bond, T. C., D. G. Streets, K. F. Yarber, S. M. Nelson, J.-H. Woo, and Z. Klimont. 2004. "A technology-based global inventory of black and organic carbon emissions from combustion." *J. Geophys. Res.* no. 109 (D14):D14203. doi: 10.1029/2003jd003697.
- Brown, A. L., and T. H. Fletcher. 1998. "Modeling Soot Derived from Pulverized Coal." *Energy & Fuels* no. 12 (4):745-757. doi: 10.1021/ef9702207.
- Buhre, B., L. Elliott, C. Sheng, R. P. Gupta, and T. F. Wall. 2005. "Oxy-fuel combustion technology for coal-fired power generation." *Progress in Energy and Combustion Science* no. 31 (4):283-307. doi: 10.1016/j.pecs.2005.07.001.

Cao, Y., B. Chen, J. Wu, H. Cui, J. Smith, C. K. Chen, P. Chu, and W. P. Pan. 2007. "Study of mercury oxidation by a selective catalytic reduction catalyst in a pilot-scale slipstream reactor at a utility boiler burning bituminous coal." *Energy & Fuels* no. 21 (1):145-156. doi: 10.1021/ef0602426.

Chen, L., S. Z. Yong, and A. F. Ghoniem. 2012. "Oxy-fuel combustion of pulverized coal: Characterization, fundamentals, stabilization and CFD modeling." *Progress in Energy and Combustion Science* no. 38 (2):156-214. doi: 10.1016/j.pecs.2011.09.003.

Cho, S. H., J. I. Yoo, A. T. Turley, C. A. Miller, W. P. Linak, J. O. L. Wendt, F. E. Huggins, and M. I. Gilmour. 2009. "Relationships between composition and pulmonary toxicity of prototype particles from coal combustion and pyrolysis." *Proceedings of the Combustion Institute* no. 32:2717-2725. doi: 10.1016/j.proci.2008.05.016.

Clarkson, T. W. 1997. "The toxicology of mercury." *Critical Reviews in Clinical Laboratory Sciences* no. 34 (4):369-403. doi: 10.3109/10408369708998098.

Croiset, E., and K. Thambimuthu. 1999. "Coal combustion with flue gas recirculation for CO<sub>2</sub> recovery." In *Greenhouse gas technologies*, edited by P. Riemer, B. Eliasson and A. Wokaun, 581-6. Amsterdam: Elsevier Science.

Damle, A. S., D. S. Ensor, and M. B. Ranade. 1982. "Coal Combustion Aerosol Formation Mechanisms - A Review." *Aerosol Science and Technology* no. 1 (1):119-133.

Galbreath, K. C., and C. J. Zygarlicke. 2000. "Mercury transformations in coal combustion flue gas." *Fuel Processing Technology* no. 65:289-310. doi: 10.1016/s0378-3820(99)00102-2.

Galbreath, K. C., C. J. Zygarlicke, J. E. Tibbetts, R. L. Schulz, and G. E. Dunham. 2005. "Effects of NO<sub>x</sub>, alpha-Fe<sub>2</sub>O<sub>3</sub>, gamma-Fe<sub>2</sub>O<sub>3</sub>, and HCl on mercury transformations in a 7-kW coal combustion system." *Fuel Processing Technology* no. 86 (4):429-448. doi: 10.1016/j.fuproc.2004.03.003.

Gale, T. K., and J. O. L. Wendt. 2002. "High-temperature interactions between multiple-metals and kaolinite." *Combustion and Flame* no. 131 (3):299-307. doi: Pii s0010-2180(02)00404-2  
10.1016/s0010-2180(02)00404-2.

Gale, T. K., and J. O. L. Wendt. 2003. "Mechanisms and models describing sodium and lead scavenging by a kaolinite aerosol at high temperatures." *Aerosol Science and Technology* no. 37 (11):865-876. doi: 10.1080/02786820390225808.

Gale, T. K., and J. O. L. Wendt. 2005. "In-furnace capture of cadmium and other semi-volatile metals by sorbents." *Proceedings of the Combustion Institute* no. 30:2999-3007. doi: 10.1016/j.proci.2004.08.197.

Ghorishi, S. B., C. W. Lee, W. S. Jozewicz, and J. D. Kilgroe. 2005. "Effects of fly ash transition metal content and flue gas HCl/SO<sub>2</sub> ratio on mercury speciation in waste combustion." *Environmental Engineering Science* no. 22 (2):221-231. doi: 10.1089/ees.2005.22.221.

Haynes, B. S., M. Neville, R. J. Quann, and A. F. Sarofim. 1982. "Factors Governing the Surface Enrichment of Fly-ash in Volatile Trace Species." *Journal of Colloid and Interface Science* no. 87 (1):266-278.

Hsi, H. C., S. G. Chen, M. Rostam-Abadi, M. J. Rood, C. F. Richardson, T. R. Carey, and R. Chang. 1998. "Preparation and evaluation of coal-derived activated carbons for removal of

mercury vapor from simulated coal combustion flue gases." *Energy & Fuels* no. 12 (6):1061-1070. doi: 10.1021/ef9801064.

Hu, W. W., M. Hu, B. Yuan, J. L. Jimenez, Q. Tang, J. F. Peng, W. Hu, M. Shao, M. Wang, L. M. Zeng, Y. S. Wu, Z. H. Gong, X. F. Huang, and L. Y. He. 2013. "Insights on organic aerosol aging and the influence of coal combustion at a regional receptor site of central eastern China." *Atmos. Chem. Phys.* no. 13 (19):10095-10112. doi: 10.5194/acp-13-10095-2013.

Hu, Y. Q., N. Kobayashi, and M. Hasatani. 2001. "The reduction of recycled-NO<sub>x</sub> in coal combustion with O<sub>2</sub>/recycled flue gas under low recycling ratio." *Fuel* no. 80 (13):1851-1855.

Hu, Y. Q., N. Kobayashi, and M. Hasatani. 2003. "Effects of coal properties on recycled-NO<sub>x</sub> reduction in coal combustion with O<sub>2</sub>/recycled flue gas." *Energy Conversion and Management* no. 44 (14):2331-2340.

Jacobson, M. C., H. C. Hansson, K. J. Noone, and R. J. Charlson. 2000. "Organic atmospheric aerosols: Review and state of the science." *Reviews of Geophysics* no. 38 (2):267-294. doi: 10.1029/1998rg000045.

Li, H., Y. Li, C.-Y. Wu, and J. Zhang. 2011. "Oxidation and capture of elemental mercury over SiO<sub>2</sub>-TiO<sub>2</sub>-V<sub>2</sub>O<sub>5</sub> catalysts in simulated low-rank coal combustion flue gas." *Chemical Engineering Journal* no. 169 (1-3):186-193. doi: 10.1016/j.cej.2011.03.003.

Li, H., C.-Y. Wu, Y. Li, and J. Zhang. 2011. "CeO<sub>2</sub>-TiO<sub>2</sub> Catalysts for Catalytic Oxidation of Elemental Mercury in Low-Rank Coal Combustion Flue Gas." *Environmental Science & Technology* no. 45 (17):7394-7400. doi: 10.1021/es2007808.

Li, H., C.-Y. Wu, Y. Li, and J. Zhang. 2012. "Superior activity of MnO<sub>x</sub>-CeO<sub>2</sub>/TiO<sub>2</sub> catalyst for catalytic oxidation of elemental mercury at low flue gas temperatures." *Applied Catalysis B-Environmental* no. 111:381-388. doi: 10.1016/j.apcatb.2011.10.021.

Li, Y., M. Daukoru, A. Suriyawong, and P. Biswas. 2009. "Mercury Emissions Control in Coal Combustion Systems Using Potassium Iodide: Bench-Scale and Pilot-Scale Studies." *Energy & Fuels* no. 23 (1):236-243. doi: 10.1021/ef800656v.

Li, Y., P. D. Murphy, C.-Y. Wu, K. W. Powers, and J.-C. J. Bonzongo. 2008. "Development of silica/vanadia/titania catalysts for removal of elemental mercury from coal-combustion flue gas." *Environmental Science & Technology* no. 42 (14):5304-5309. doi: 10.1021/es8000272.

Li, Y., A. Suriyawong, M. Daukoru, Y. Zhuang, and P. Biswas. 2009. "Measurement and Capture of Fine and Ultrafine Particles from a Pilot-Scale Pulverized Coal Combustor with an Electrostatic Precipitator." *J. Air & Waste Manage. Assoc.* no. 59 (5):553-9. doi: [10.3155/1047-3289.59.3.1](https://doi.org/10.3155/1047-3289.59.3.1).

Linak, W. P., and J. O. L. Wendt. 1994. "Trace metal transformation mechanisms during coal combustion." *Fuel Processing Technology* no. 39 (1-3):173-198.

Linak, W. P., J.-I. K. Yoo, S. J. Wasson, W. Zhu, J. O. L. Wendt, F. E. Huggins, Y. Chen, N. Shah, G. P. Huffman, and M. I. Gilmour. 2007. "Ultrafine ash aerosols from coal combustion: Characterization and health effects." *Proceedings of the Combustion Institute* no. 31:1929-1937. doi: 10.1016/j.proci.2006.08.086.

Liu, S.-H., N.-Q. Yan, Z.-R. Liu, Z. Qu, P. Wang, S.-G. Chang, and C. Miller. 2007. "Using bromine gas to enhance mercury removal from flue gas of coal-fired power plants."

*Environmental Science & Technology* no. 41 (4):1405-1412. doi: 10.1021/es061705p.

Mansurov, Z. A. 2005. "Soot formation in combustion processes (review)." *Combustion Explosion and Shock Waves* no. 41 (6):727-744.

Morris, W. J., D. Yu, J. O. L. Wendt. 2013. "A comparison of soot, fine particle and sodium emissions for air- and oxy-coal flames, with recycled flue gases of various compositions."

*Proceedings of the Combustion Institute* no. 34: 3453-3461

Okazaki, K., and T. Ando. 1997. "NO<sub>x</sub> reduction mechanism in coal combustion with recycled CO<sub>2</sub>." *Energy* no. 22 (2/3).

Olmez, I., A. E. Sheffield, G. E. Gordon, J. E. Houck, L. C. Pritchett, J. A. Cooper, T. G. Dzubay, and R. L. Bennett. 1988. "Compositions of Particles from Selected Sources in Philadelphia for Receptor Modeling Applications." *Japca-the International Journal of Air Pollution Control and Hazardous Waste Management* no. 38 (11):1392-1402.

Pavlish, J. H., E. A. Sondreal, M. D. Mann, E. S. Olson, K. C. Galbreath, D. L. Laudal, and S. A. Benson. 2003. "State review of mercury control options for coal-fired power plants." *Fuel Processing Technology* no. 82 (2-3):89-165. doi: 10.1016/s0378-3820(03)00059-6.

Pflughoeft-Hassett, D. F., D. J. Hassett, T. D. Buckley, L. V. Heebink, and J. H. Pavlish. 2009. "Activated carbon for mercury control: Implications for fly ash management." *Fuel Processing Technology* no. 90 (11):1430-1434. doi: 10.1016/j.fuproc.2009.07.008.

- Pitoniak, E., C. Y. Wu, D. W. Mazyck, K. W. Powers, and W. Sigmund. 2005. "Adsorption enhancement mechanisms of silica-titania nanocomposites for elemental mercury vapor removal." *Environmental Science & Technology* no. 39 (5):1269-1274. doi: 10.1021/es049202b.
- Poschl, U. 2005. "Atmospheric aerosols: Composition, transformation, climate and health effects." *Angewandte Chemie-International Edition* no. 44 (46):7520-7540. doi: 10.1002/anie.200501122.
- Quann, R. J., M. Neville, M. Janghorbani, C. A. Mims, and A. F. Sarofim. 1982. "Mineral Matter and Trace-element Vaporization in a Laboratory-pulverized Coal Combustion System." *Environmental Science & Technology* no. 16 (11):776-781.
- Quann, R. J., and A. F. Sarofim. 1982. "Vaporization of refractory oxides during pulverized coal combustion." *Symposium (International) on Combustion* no. 19 (1):1429-1440.
- Ramanathan, V., P. J. Crutzen, J. T. Kiehl, and D. Rosenfeld. 2001. "Aerosols, Climate, and the Hydrological Cycle." *Science* no. 294 (5549):2119-2124. doi: 10.1126/science.1064034.
- Samet, J. M., F. Dominici, F. C. Curriero, I. Coursac, and S. L. Zeger. 2000. "Fine particulate air pollution and mortality in 20 US cities, 1987-1994." *New England journal of medicine* no. 343 (24):1742.
- Seinfeld, J. H., and S. N. Pandis. 2006. *Atmospheric Chemistry and Physics: From Air Pollution to Climate Change*.



Senior, C. L., and R. C. Flagan. 1982. "Ash Vaporization and Condensation During Combustion of a Suspended Coal Particle." *Aerosol Science and Technology* no. 1:371-383. doi: 10.1080/02786828208958602.

Senior, C. L., J. J. Helble, and A. F. Sarofim. 2000. "Emissions of mercury, trace elements, and fine particles from stationary combustion sources." *Fuel Processing Technology* no. 65:263-288. doi: 10.1016/s0378-3820(00)00082-5.

Senior, C. L., A. F. Sarofim, T. F. Zeng, J. J. Helble, and R. Mamani-Paco. 2000. "Gas-phase transformations of mercury in coal-fired power plants." *Fuel Processing Technology* no. 63 (2-3):197-213. doi: 10.1016/s0378-3820(99)00097-1.

Sheng, C., and Y. Li. 2008. "Experimental study of ash formation during pulverized coal combustion in O<sub>2</sub>/CO<sub>2</sub> mixtures." *Fuel* no. 87 (7):1297-1305. doi: 10.1016/j.fuel.2007.07.023.

Sheng, C., Y. Lu, X. Gao, and H. Yao. 2007. "Fine Ash Formation during Pulverized Coal Combustion--A Comparison of O<sub>2</sub>/CO<sub>2</sub> Combustion versus Air Combustion." *Energy & Fuels* no. 21:435-440.

Singh, D., P. Croiset, P. L. Douglas, and M. A. Douglas. 2003. "Techno-economic study of CO<sub>2</sub> capture from an existing coal-fired power plant: MEA scrubbing Vs. O<sub>2</sub>/CO<sub>2</sub> recycle combustion." *Energy Convers Manage* no. 44:3073-3091.

Sun, Y. L., Z. F. Wang, P. Q. Fu, T. Yang, Q. Jiang, H. B. Dong, J. Li, and J. J. Jia. 2013. "Aerosol composition, sources and processes during wintertime in Beijing, China." *Atmos. Chem. Phys.* no. 13 (9):4577-4592. doi: 10.5194/acp-13-4577-2013.

Suriyawong, A., M. Gamble, M.-H. Lee, R. Axelbaum, and P. Biswas. 2006. "Submicrometer Particle Formation and Mercury Speciation Under O<sub>2</sub>-CO<sub>2</sub> Coal Combustion." *Energy & Fuels* no. 20:2357-2363.

Suriyawong, A., C. J. Hogan Jr, J. Jiang, and P. Biswas. 2008. "Charged fraction and electrostatic collection of ultrafine and submicrometer particles formed during O<sub>2</sub>-CO<sub>2</sub> coal combustion." *Fuel* no. 87 (6):673-682. doi: 10.1016/j.fuel.2007.07.024.

Tan, Y., E. Croiset, M. A. Douglas, and K. V. Thambimuthu. 2006. "Combustion characteristics of coal in a mixture of oxygen and recycled flue gas." *Fuel* no. 85 (4):507-512. doi: 10.1016/j.fuel.2005.08.010.

Wang, X., B. J. Williams, Y. Tang, Y. Huang, L. Kong, X. Yang, and P. Biswas. 2013. "Characterization of organic aerosol produced during pulverized coal combustion in a drop tube furnace." *Atmos. Chem. Phys. Discuss.* no. 13 (2):3345-3377. doi: 10.5194/acpd-13-3345-2013.

Warnatz, J., U. Maas, and R. W. Dibble. 2006. *Combustion: Physical and Chemical Fundamentals, Modeling and Simulation, Experiments, Pollutant Formation*. 4 ed: Springer.

Wendt, J. O. L., and S. J. Lee. 2010. "High-temperature sorbents for Hg, Cd, Pb, and other trace metals: Mechanisms and applications." *Fuel* no. 89 (4):894-903. doi: 10.1016/j.fuel.2009.01.028.

Wu, C. Y., T. G. Lee, G. Tyree, E. Arar, and P. Biswas. 1998. "Capture of mercury in combustion systems by in situ-generated titania particles with UV irradiation." *Environmental Engineering Science* no. 15 (2):137-148. doi: 10.1089/ees.1998.15.137.

Yoo, J. I., T. Shinagawa, J. P. Wood, W. P. Linak, D. A. Santoianni, C. J. King, Y. C. Seo, and J. O. L. Wendt. 2005. "High-temperature sorption of cesium and strontium on dispersed kaolinite powders." *Environmental Science & Technology* no. 39 (13):5087-5094. doi: 10.1021/es048064n.

Zhang, Y., J. J. Schauer, Y. Zhang, L. Zeng, Y. Wei, Y. Liu, and M. Shao. 2008. "Characteristics of Particulate Carbon Emissions from Real-World Chinese Coal Combustion." *Environmental Science & Technology* no. 42 (14):5068-5073. doi: 10.1021/es7022576.

Zhao, Y. X., M. D. Mann, J. H. Pavlish, B. A. F. Mibeck, G. E. Dunham, and E. S. Olson. 2006. "Application of gold catalyst for mercury oxidation by chlorine." *Environmental Science & Technology* no. 40 (5):1603-1608. doi: 10.1021/es050165d.

Zhuang, Y., and P. Biswas. 2001. "Submicrometer Particle Formation and Control in a Bench-Scale Pulverized Coal Combustor." *Energy & Fuels* no. 15 (3):510-516. doi: 10.1021/ef000080s.

Zhuang, Y., and J. H. Pavlish. 2012. "Fate of Hazardous Air Pollutants in Oxygen-Fired Coal Combustion with Different Flue Gas Recycling." *Environmental Science & Technology* no. 46 (8):4657-4665. doi: 10.1021/es300143q.

Zhuang, Y., J. S. Thompson, C. J. Zygarlicke, and J. H. Pavlish. 2004. "Development of a mercury transformation model in coal combustion flue gas." *Environmental Science & Technology* no. 38 (21):5803-5808. doi: 10.1021/es030683t.

**CHAPTER 2. CHARACTERIZATION OF ORGANIC AND BLACK  
CARBON AEROSOLS FROM COAL COMBUSTION: AN  
EXPERIMENTAL STUDY IN A 1 MEGAWATT PILOT SCALE COAL  
COMBUSTOR**

## **Abstract**

Combustion is a main source of atmospheric aerosols, including organic carbon (OC) and black carbon (BC) aerosols. In this study, a pilot-scale coal combustor was used to investigate the formation of OC and BC aerosols under various combustion conditions. It was found that BC aerosol formation was extremely sensitive to the fuel-air equivalence ratio: its concentration decreased from  $236 \mu\text{g}/\text{m}^3$  to only  $2.4 \mu\text{g}/\text{m}^3$ , when the equivalence ratio was reduced from 0.92 to 0.80. However, the emissions of inorganic and OC aerosols were not as sensitive as BC aerosol. The formation of OC aerosols seemed to be enhanced by increasing the fuel-air equivalence ratio, which was opposite to the change of black carbon aerosol formation. Coal was also combusted in oxygen-rich environments. Inorganic submicrometer particle formation was greatly enhanced in oxygen-rich combustion mode, compared to conventional air firing. Significant concentrations of organic carbon aerosol were still present in the flue gas, while concentrations of black carbon aerosol were zero. The different trends of BC and OC aerosol formation strongly indicates formation pathway of OC aerosol is very different from BC aerosol formation.

## 2.1 Introduction

Atmospheric aerosols play a critical role in affecting radiative forcing and human health (Poschl 2005). Carbonaceous aerosols, including elemental (black) and organic carbon aerosols, draw much attention due to their unique properties of absorbing or scattering sun light and their potential hazards for human health (Hallquist et al. 2009, Kanakidou et al. 2005, Ramanathan and Carmichael 2008). It is well established that black carbon aerosols can absorb sunlight, thereby leading to positive radiative forcing. The recent IPCC report on climate change suggested that radiative forcing of black carbon aerosols was  $+0.64 \text{ W/m}^2$ , with uncertainty bounds of  $(+0.25, +1.08) \text{ W/m}^2$ , during the year from 1750 to 2011 (IPCC 2013). Bond et al. (2013) provides an estimate that direct radiative forcing of black carbon aerosols is  $+0.71 \text{ W/m}^2$ , with uncertainty bounds of  $(+0.08, +1.27) \text{ W/m}^2$  during the year from 1750 to 2005, and suggests that black carbon could be the second most important greenhouse agents from anthropogenic emissions. Organic carbon aerosols comprise 20% to 80% of the total fine aerosol mass (Hallquist et al. 2009). It is generally considered that organic aerosols affect radiative forcing mainly by scattering sunlight. However, many recent studies indicate that some organic aerosols, known as “brown organic aerosols” can also absorb sunlight (Andreae and Gelencsér 2006, Gustafsson et al. 2009) and may play an important role in climate change.

Coal combustion is a major type of fossil fuel combustion, which contributes a large share of electricity generation, ranging from 45% in the United States, to about 70% in India and China in 2009 (Biswas et al. 2011). Coal-fired power plants produce a significant fraction of carbonaceous aerosol (Olmez et al. 1988, Fisher et al. 1978, Mamane et al. 1986, Querol et al. 1996, Smith et al. 1979, Bond et al. 2004, Linak et al. 2007). Many studies have investigated formation of soot during coal combustion. Soot particles usually contain a main fraction of black

carbon and a very minor fraction of organic carbon. Veranth et al. (2000) studied unburned carbon in coal fly ash from a low-NO<sub>x</sub> pulverized coal burner and found the carbon was bimodally distributed: carbonaceous aerosols with submicrometer sizes were from soot, while other carbonaceous aerosols with supermicrometer sizes (usually larger than 10 μm) were from unburned char or soot aggregates mixed with the char. Brown and Fletcher (1998) proposed a model to describe soot formation during coal combustion. They assumed that tar is the precursor of soot. Tars are relative larger molecules. Under high temperature, they directly lose H, O and other atoms to form soot. Brown and Fletcher (1998) had built a model based on this assumption, and got a close result compared with the experiments. Chen et al. (2005) investigated morphologies of carbonaceous aerosol from coal combustion using electron microscopy; and found that the soot particles consists of chains of spherical nanoparticles, which contain several graphite layers inside the particles.

There are much fewer studies on formation of organic aerosols during coal combustion. In addition, pilot-scale data is strongly needed on how emission of carbonaceous aerosol responds to changes of coal combustion conditions. Therefore, this work reports a systematic study on the formation of aerosols, including both black carbon (BC) and organic carbon (OC) aerosols, in a 1 Megawatt pilot scale coal combustor under various combustion conditions.

## **2.2 Experimental Section**

### *2.2.1 Experimental Setup of Pulverized Coal Combustion in a 1 MW pilot-scale coal combustor*

The 1 MW pilot-scale coal combustor with a boiler is located in Advanced Coal and Energy Research Facility (ACERF, Website: <http://cccu.wustl.edu>) at Washington University in St. Louis. Figure 2.1 shows the schematic drawing of the coal combustion system. And a detailed

description of ACERF can be found in Appendix 4. West Elk coal was burned (West Elk coal is a low-sulfur, Colorado bituminous coal). The flue gas composition was monitored by a Horiba portable gas analyzer (Model PG-250). After the boiler, a slip stream (13 liter per min, LPM) of the flue gas was drawn to conduct the particle measurements. 5 LPM of flue gas was sent to an Aerodynamic particle sizer (APS, TSI Inc.). Another 8 LPM of flue gas passed through an impactor which was used to remove supermicrometer particles. Then the flue gas was dried by a diffusional dryer and connected to a scanning mobility particle sizer (SMPS, TSI Inc.) and a filter holder, which was used to collect particles from flue gas. Both Telfon filter and quartz filter were used. The collected aerosol samples were analysed for the elemental carbon/organic carbon (EC/OC) concentrations using a thermal/optical carbon analyzer (Model 2001, Atmoslytic Inc., Calabasas, CA for determining carbonaceous aerosol concentration in coal combustion flue gas; and X-ray fluorescence (XRF) analysis with a Panalytical Epsilon 5 energy dispersive XRF spectrometer for determining elemental compositions of aerosol mass.

### *2.2.2 Test plan*

The test plan is summarized in Table 2.1. The experiment set 1 was operated under conventional air-firing. The equivalence ratio (air-fuel ratio) was varied by changing input air flow rate. The experiment set 2 was operated under oxygen-rich conditions, which mixed air with different ratios of pure oxygen.



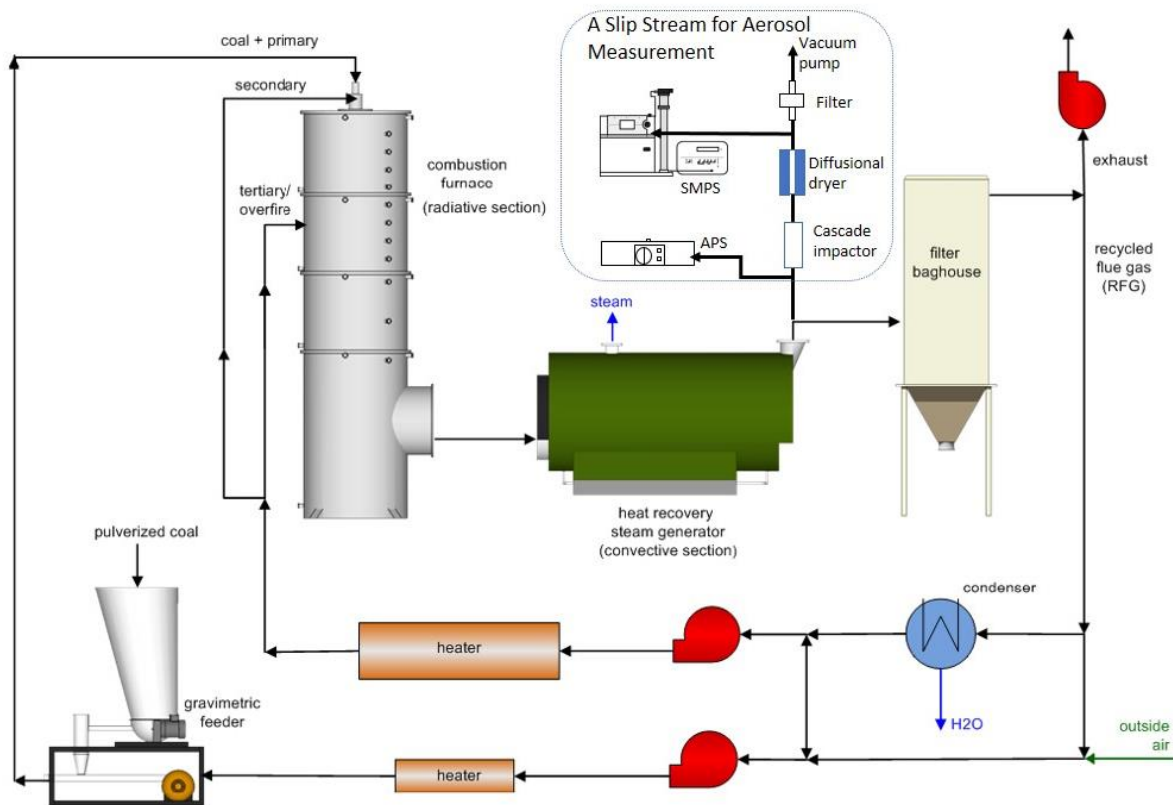


Figure 2.1 Schematic drawing of ACERF system (no recycled flue gas was used in this study)

Table 2.1 Test plan of experimental conditions in ACERF system

Experiment Set #	Test #	Coal Feeding Rate (kg/h)	O <sub>2</sub> Concentration in Flue Gas (%)	Fuel-air Equivalence Ratio	Oxygen Concentration for Input Gas (%)	Excess oxygen (%)	Air Flow Rate (kg/h)	Additional Oxygen Flow Rate (kg/h)
1. Air-firing	1	52	1.7	0.92	21	8	557	0
	2		4.16	0.80	21	20	648	0
	3		5.78	0.72	21	28	708	0
2. Oxygen-rich combustion	4	35	13	0.675	39	33	321	58
	5		18	0.64	49	37	227	86

## 2.3 Results and Discussion

### 2.3.1 Characterization of Organic Carbon (OC) Aerosol and Black Carbon (BC) Aerosol from Conventional Air Firing of Coal

As described in Table 2.1, Experiment Set #1 includes three tests performed under three different fuel-air ratios. Particle size distributions were measured. Figure 2.2 shows the size distributions from both SMPS and APS measurements. Generally, the particle size distribution did not change significantly when changing the fuel-air equivalence ratio. Thus, the total particulate emission was not sensitive to the change in fuel-air equivalence ratios.

It seems that smaller particles have a slightly higher sensitivity to the fuel-air ratios. Figure 2.2 shows that decreasing the fuel-air equivalence ratio led to a little increase in the number concentration for particles smaller than 100 nm. Moreover, the particle concentration for Test 1 (the fuel-air equivalence ratio = 0.92) in the size range from 100 to 400 nm is significantly higher than for the other two curves. This result may be due to formation of black carbon aerosol (soot) under high fuel-air equivalence ratio, because aerosol samples collected from this test was much darker than other tests (Fig. 2.3).

EC/OC (elemental carbon/organic carbon) analysis has been conducted for the aerosol samples shown in Fig. 2.3. EC is short for “elemental carbon”, which is the same with the term “black carbon” (BC). Figure 2.4 shows the concentrations of BC and OC aerosol in the flue gas. For Test 1, the equivalence ratio was 0.92. It is slightly higher than the normal operating condition of a typical pulverized coal boiler, which ranges from 0.87 to 0.83 (correspondence to 20 to 15% excess oxygen) (Babcock & Wilcox Company, 2010). But the CO concentration in flue gas was low (about 55 ppm) (Table 2.2), which indicates a proper combustion condition in this case. (In

most states in the US, the upper allowed limit for CO concentration in exhaust gas is from about 40 to 60 ppmv. Thus, the CO concentration in this test can meet the regulations in at least some states, such as Texas and Utah. Source: <http://www.emissionslimits.org/>). However, soot emission was significantly enhanced in Test 1. BC aerosol concentration in flue gas was  $236 \mu\text{g}/\text{m}^3$ , which accounts for about 29% of total fine particulate mass (particle size  $\leq 500 \text{ nm}$ ). When the equivalence ratio decreased to 0.80 (the  $\text{O}_2$  concentration in the flue gas was 4% in this case), the BC aerosol concentration dropped drastically to  $2.4 \mu\text{g}/\text{m}^3$ , which was about only 1% of the BC concentration from Test 1. And if the equivalence ratio was further decreased to 0.72, then no BC aerosol concentration could be detected. These results suggest that the emission of BC aerosols is extremely sensitive to changes in the fuel-air equivalence ratio.

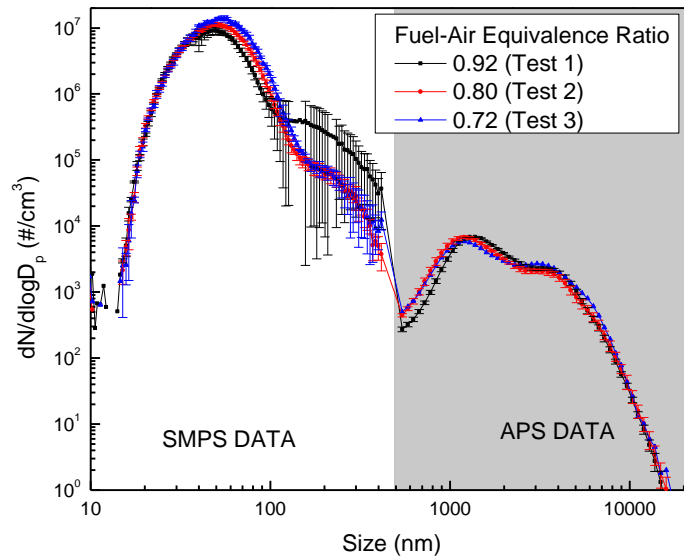


Figure 2.2 Size distributions of particles in coal combustion flue gas for Experiment Set #1 (At least 4 measurements had been done for each test. The error bars shows the standard deviation).

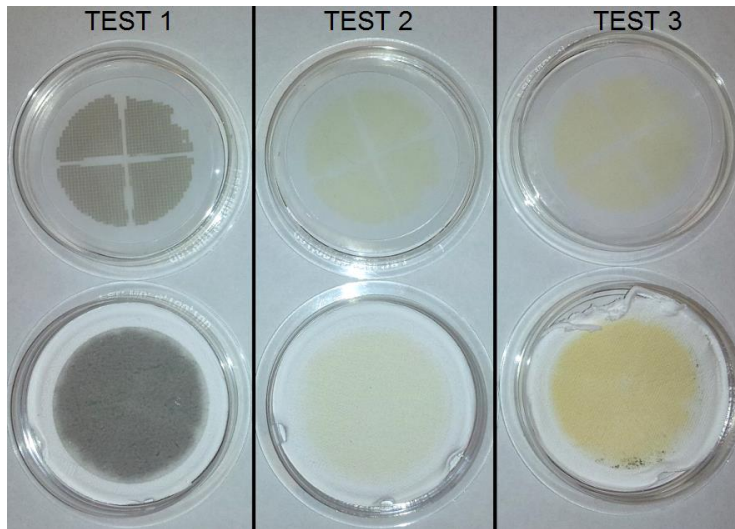


Figure 2.3 Pictures of aerosol samples collected on filters during the combustion for Experiment Set #1 (Top: Teflon filter; Bottom: Quartz filter).

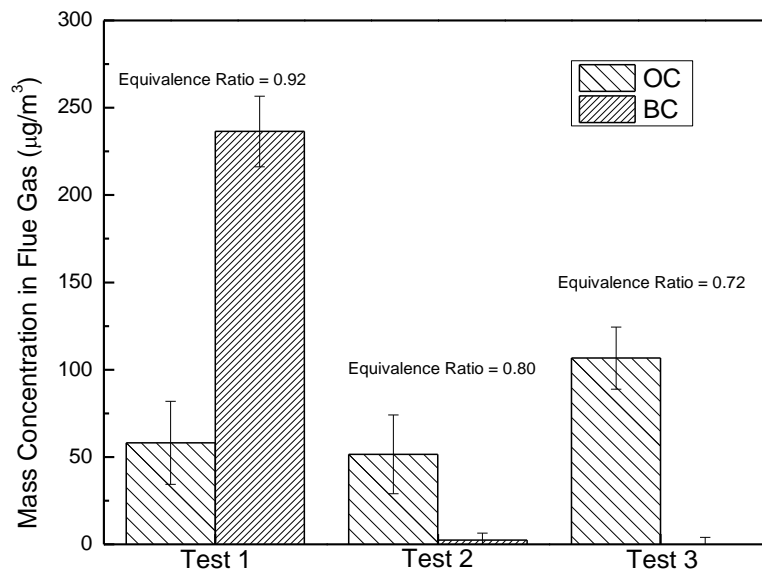


Figure 2.4 BC/OC emissions under different fuel-air equivalence ratios for Experiment Set #1 (the error bars show the uncertainty for the BC/OC measurement method).

Organic carbon aerosol concentration was not as sensitive as BC aerosol emission to the fuel-air equivalence ratio. Figure 2.4 shows that OC aerosol emission was actually enhanced at a lower fuel-air equivalence ratio. This phenomenon strongly indicates that the formation pathway of OC aerosol was very different from BC aerosol formation. Our previous work (shown in Chapter 3) observed a correlation between inorganic particle concentration and organic aerosol formation, and it proposed that inorganic particles play a critical role as carriers of organic aerosols (Wang, Williams, et al. 2013a). Figure 2.3 does show that the particle size distributions below 100 nm shifted to larger sizes when the fuel-air equivalence ratio was lowered. Thus, the enhancement of OC aerosol concentrations in this case may be due to higher inorganic particle concentrations in the flue gas.

Table 2.2 Flue gas composition for each experimental condition

Experiment Set #	Test #	O <sub>2</sub> (Vol. %)	CO <sub>2</sub> (Vol. %)	CO (Vol. PPM)	NO (Vol. PPM)
1. Air-firing	1	1.7	17.29	55	382
	2	4.16	14.42	9	685
	3	5.78	14.86	13	712
2. Oxygen-rich combustion	4	13	14.24	126	667
	5	18	17	86	729

Particle size distribution in coal combustion flue gas was also obtained using a Nano differential mobility analyzer (Nano DMA), which is able to measure extremely fine particles. Figure 2.5 shows that the concentrations of particles with sizes smaller than 10 nm were very low. One

possibility is that coal flue gas contains a high concentration of particles and other condensable gases, such as  $\text{SO}_3$  and  $\text{H}_2\text{O}$ . Thus, ultrafine particles in this range will quickly grow to larger particles.

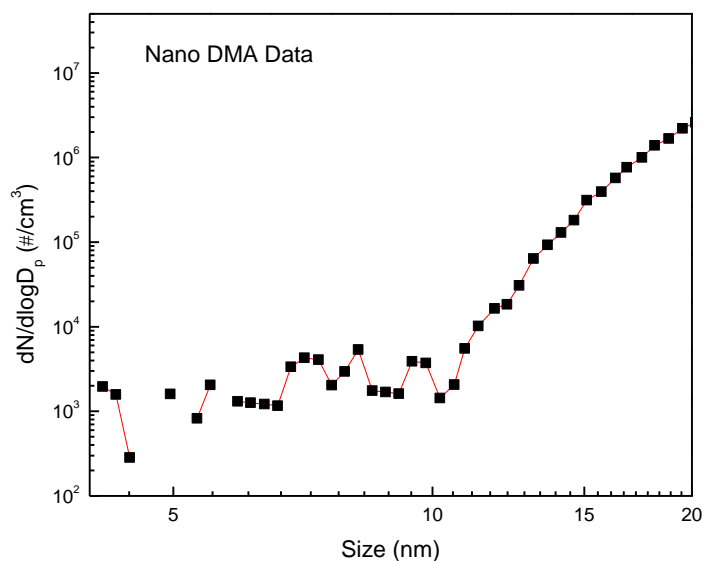


Figure 2.5 Size distribution (Nano DMA data) of ultrafine particles in coal combustion flue gas

### 2.3.2 Characterization of Organic Aerosol and Black Carbon Aerosol from Oxygen-rich Combustion

Oxy-coal combustion is a next generation coal combustion. It uses pure oxygen to burn coal particles and recycles flue gas back to furnace as a diluent, resulting in a higher concentration of carbon dioxide in the exhaust, which can facilitate  $\text{CO}_2$  capture or conversion (Abraham et al. 1982, Buhre, Elliott, et al. 2005, Croiset and Thambimuthu 1999). Oxy-coal combustion is usually operated in oxygen-rich environment. Thus, in this study, an oxygen-rich combustion

mode was also tested. Pure oxygen was mixed with air to increase the oxygen concentration in the input gas. Test 4 was performed under 39% (v/v) oxygen; and Test 5 was performed under 49% (v/v) oxygen. It is well known that increasing oxygen concentration can significantly enhance submicrometer inorganic particle formation. This is because submicrometer particle formation occurs via a vaporization-nucleation pathway (Quann et al. 1982, Haynes et al. 1982a, Zhuang and Biswas 2001, Suriyawong et al. 2006b, Wang, Michael Daukoru, et al. 2013): metal oxides in coal are reduced to metals or metal suboxides while coal particles are burning. These metals or metal suboxides usually have higher volatility; and some of them may be converted into vapors. The vapors can be quickly oxidized back to metal oxides by oxygen when they diffuse away from the coal particle surface. Then gas-to-particle conversion, including nucleation, condensation and coagulation, occurs to form submicrometer particles. Increasing oxygen concentration can increase the surface temperature of coal particles, thereby enhancing the evaporation of metal oxides. Then more submicrometer particles are formed. In this study, Figure 2.6 confirms this theory: the increasing of oxygen concentration resulted in a significant shift in particle size distribution to larger sizes for submicrometer particles. Figure 2.7 shows the elemental compositions of these submicrometer particles. The concentrations of most elements increase greatly with higher oxygen concentrations. It should be noted that the air firing case (Test 3) was performed at a higher coal feed rate (400 KW), while the oxygen-rich combustion cases (Test 4 and 5) were performed at a lower coal feed rate (270 KW) for safety concerns.

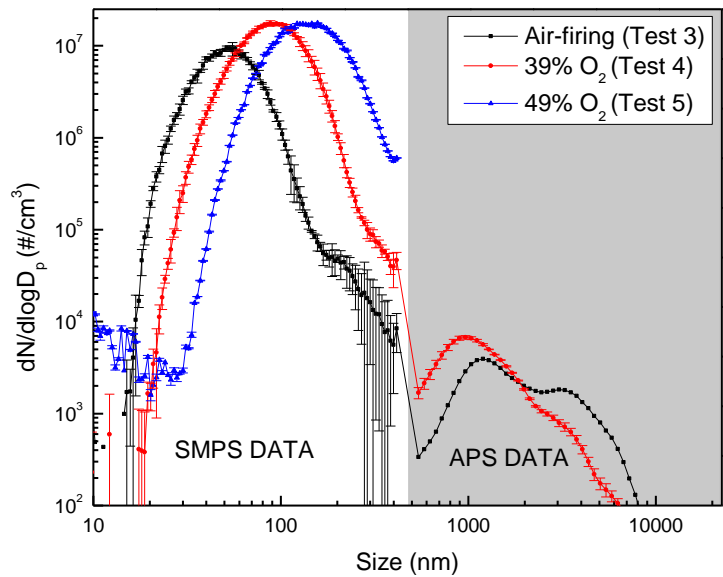


Figure 2.6 Size distributions of particles in coal combustion flue gas for Experiment Set #2 (The size distribution for Test 3 was normalized based on coal feed rate)

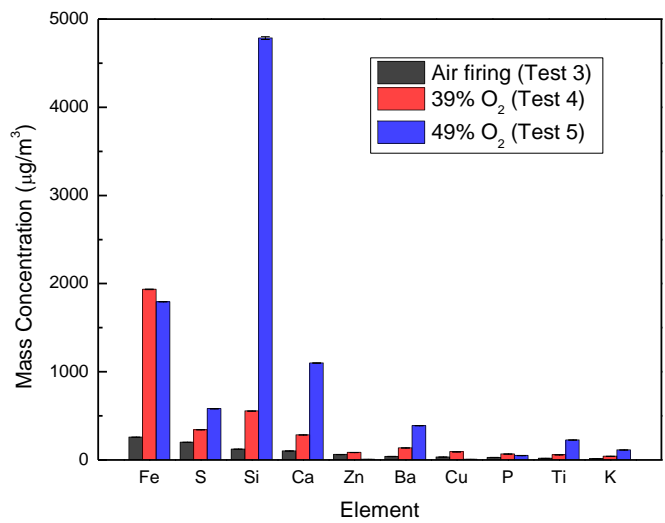




Figure 2.7 Elemental compositions of submicrometer particles in coal combustion flue gas for Experiment Set #2

Figure 2.8 compares the BC/OC aerosol concentration for two oxygen-rich combustion cases and 1 air-firing case. The BC aerosol concentrations are 0 for all three cases, since the fuel-air equivalence ratio was low, especially for oxygen-rich combustion cases. But surprisingly, there were still significant OC aerosol concentrations from oxygen-rich combustion flue gas. And more surprisingly, the OC concentration was even higher in Test 5 (49% O<sub>2</sub> case) than that in Test 4 (39% O<sub>2</sub> case), suggesting that the fuel-air equivalence ratio may not be a dominant factor affecting OC aerosol formation. Other factors, such as inorganic particle concentration, may play a critical role in OC aerosol formation.

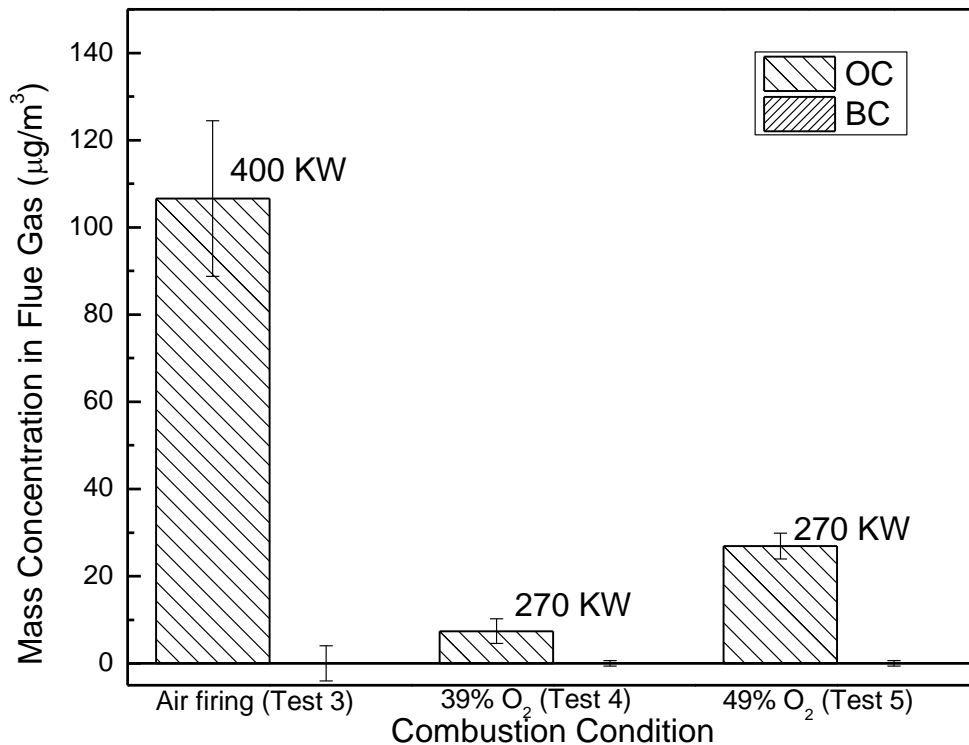


Figure 2.8 BC/OC aerosol concentrations under oxy-coal combustion (Experiment Set #2) (the error bars show the uncertainty for the BC/OC measurement method)

## 2.4 Conclusions

Pilot-scale experiments were conducted in a 1 MW coal combustor. It is shown that black carbon aerosol formation was extremely sensitive to the fuel-air equivalence ratio. The elemental (black) carbon aerosol concentration in flue gas decreased from 236  $\mu\text{g}/\text{m}^3$  to only 2.4  $\mu\text{g}/\text{m}^3$  when the fuel-air equivalence ratio was reduced from 0.92 to 0.80. (The  $\text{O}_2$  concentration in flue gas was changed from 1.7% to 4.16%). The emission of organic carbon aerosol was not as sensitive as black carbon aerosol. And the results suggested that organic carbon aerosol formation was enhanced by increasing the fuel-air equivalence ratio, which was opposite to the

change of black carbon aerosol formation. This phenomenon indicates that the formation mechanism of organic carbon aerosol should be very different from that of black carbon aerosol.

The coal combustor was also operated in oxygen-rich combustion mode. Pure oxygen was mixed with air to increase oxygen concentration in the input gas. Inorganic submicrometer particle formation was greatly enhanced in the oxy-coal combustion mode, compared to conventional air firing (peak size was shifted from 53 nm (air-firing) to 143 nm (oxygen-rich, Test 5)). Black carbon aerosol concentration was under the detection limit. However, surprisingly, there was still a significant concentration of organic carbon aerosol present in the flue gas, although the fuel-air equivalence ratio was very low in this mode, which may indicate that the fuel-air equivalence ratio is not a dominant factor affecting organic carbon aerosol formation.

## 2.5 References

- Abraham, B. M., J. G. Asbury, E. P. Lynch, and A. P. S. Teotia. 1982. "Coal-oxygen process provides carbon dioxide for enhanced recovery." *Oil Gas J* no. 80 (11):68-70.
- Andreae, M. O., and A. Gelencsér. 2006. "Black carbon or brown carbon? The nature of light-absorbing carbonaceous aerosols." *Atmos. Chem. Phys.* no. 6 (10):3131-3148. doi: 10.5194/acp-6-3131-2006.
- Babcock & Wilcox Company, 2010. "Steam: Its Generation and Use" Nabu Press, New York.
- Biswas, P., W. N. Wang, and W. J. An. 2011. "The energy-environment nexus: aerosol science and technology enabling solutions." *Frontiers of Environmental Science & Engineering in China* no. 5 (3):299-312. doi: 10.1007/s11783-011-0351-1.
- Bond, T. C., S. J. Doherty, D. W. Fahey, P. M. Forster, T. Berntsen, B. J. DeAngelo, M. G. Flanner, S. Ghan, B. Kärcher, D. Koch, S. Kinne, Y. Kondo, P. K. Quinn, M. C. Sarofim, M. G. Schultz, M. Schulz, C. Venkataraman, H. Zhang, S. Zhang, N. Bellouin, S. K. Guttikunda, P. K. Hopke, M. Z. Jacobson, J. W. Kaiser, Z. Klimont, U. Lohmann, J. P. Schwarz, D. Shindell, T. Storelvmo, S. G. Warren, and C. S. Zender. 2013. "Bounding the role of black carbon in the climate system: A scientific assessment." *Journal of Geophysical Research: Atmospheres* no. 118 (11):5380-5552. doi: 10.1002/jgrd.50171.
- Bond, T. C., D. G. Streets, K. F. Yarber, S. M. Nelson, J.-H. Woo, and Z. Klimont. 2004. "A technology-based global inventory of black and organic carbon emissions from combustion." *J. Geophys. Res.* no. 109 (D14):D14203. doi: 10.1029/2003jd003697.

Brown, A. L., and Fletcher, T. H. 1998. "Modeling Soot Derived from Pulverized Coal." *Energy & Fuels*, no. 12, 745-757, 10.1021/ef9702207,.

Buhre, B., L. Elliott, C. Sheng, R. P. Gupta, and T. F. Wall. 2005. "Oxy-fuel combustion technology for coal-fired power generation." *Progress in Energy and Combustion Science* no. 31 (4):283-307. doi: 10.1016/j.pecs.2005.07.001.

Chen, Y., Shah, N., Braun, A., Huggins, F. E., and Huffman, G. P. 2005. "Electron Microscopy Investigation of Carbonaceous Particulate Matter Generated by Combustion of Fossil Fuels." *Energy & Fuels*, no. 19, 1644-1651, 10.1021/ef049736y,.

Croiset, E., and K. Thambimuthu. 1999. "Coal combustion with flue gas recirculation for CO<sub>2</sub> recovery." In *Greenhouse gas technologies*, edited by P. Riemer, B. Eliasson and A. Wokaun, 581-6. Amsterdam: Elsevier Science.

Fisher, G. L., B. A. Prentice, D. Silberman, J. M. Ondov, A. H. Biermann, R. C. Ragaini, and A. R. McFarland. 1978. "Physical and morphological studies of size-classified coal fly ash." *Environmental Science & Technology* no. 12 (4):447-451. doi: 10.1021/es60140a008.

Gustafsson, Ö., M. Kruså, Z. Zencak, R. J. Sheesley, L. Granat, E. Engström, P. S. Praveen, P. S. P. Rao, C. Leck, and H. Rodhe. 2009. "Brown Clouds over South Asia: Biomass or Fossil Fuel Combustion?" *Science* no. 323 (5913):495-498. doi: 10.1126/science.1164857.

Hallquist, M., J. C. Wenger, U. Baltensperger, Y. Rudich, D. Simpson, M. Claeys, J. Dommen, N. M. Donahue, C. George, A. H. Goldstein, J. F. Hamilton, H. Herrmann, T. Hoffmann, Y. Iinuma, M. Jang, M. E. Jenkin, J. L. Jimenez, A. Kiendler-Scharr, W. Maenhaut, G. McFiggans, T. F. Mentel, A. Monod, A. S. H. Prvt, J. H. Seinfeld, J. D. Surratt, R. Szmigielski, and J. Wildt.

2009. "The formation, properties and impact of secondary organic aerosol: current and emerging issues." *Atmos. Chem. Phys.* no. 9 (14):5155-5236. doi: 10.5194/acp-9-5155-2009.

Haynes, B. S., M. Neville, R. J. Quann, and A. F. Sarofim. 1982. "Factors Governing the Surface Enrichment of Fly-ash in Volatile Trace Species." *Journal of Colloid and Interface Science* no. 87 (1):266-278.

IPCC. 2013. Climate Change 2013: The Physical Science Basis.

Kanakidou, M., J. H. Seinfeld, S. N. Pandis, I. Barnes, F. J. Dentener, M. C. Facchini, R. Van Dingenen, B. Ervens, A. Nenes, C. J. Nielsen, E. Swietlicki, J. P. Putaud, Y. Balkanski, S. Fuzzi, Horth, J., G. K. Moortgat, R. Winterhalter, C. E. L. Myhre, K. Tsigaridis, E. Vignati, E. G. Stephanou, and J. Wilson. 2005. "Organic aerosol and global climate modelling: a review." *Atmospheric Chemistry and Physics* no. 5:1053-1123.

Linak, W. P., J.-I. K. Yoo, S. J. Wasson, W. Zhu, J. O. L. Wendt, F. E. Huggins, Y. Chen, N. Shah, G. P. Huffman, and M. I. Gilmour. 2007. "Ultrafine ash aerosols from coal combustion: Characterization and health effects." *Proceedings of the Combustion Institute* no. 31:1929-1937. doi: 10.1016/j.proci.2006.08.086.

Mamane, Y., J. L. Miller, and T. G. Dzubay. 1986. "Characterization of individual fly ash particles emitted from coal- and oil-fired power plants." *Atmospheric Environment (1967)* no. 20 (11):2125-2135. doi: [http://dx.doi.org/10.1016/0004-6981\(86\)90306-9](http://dx.doi.org/10.1016/0004-6981(86)90306-9).

Olmez, I., A. E. Sheffield, G. E. Gordon, J. E. Houck, L. C. Pritchett, J. A. Cooper, T. G. Dzubay, and R. L. Bennett. 1988. "Compositions of Particles from Selected Sources in Philadelphia for

Receptor Modeling Applications." *Japca-the International Journal of Air Pollution Control and Hazardous Waste Management* no. 38 (11):1392-1402.

Poschl, U. 2005. "Atmospheric aerosols: Composition, transformation, climate and health effects." *Angewandte Chemie-International Edition* no. 44 (46):7520-7540. doi: 10.1002/anie.200501122.

Quann, R. J., M. Neville, M. Janghorbani, C. A. Mims, and A. F. Sarofim. 1982. "Mineral Matter and Trace-element Vaporization in a Laboratory-pulverized Coal Combustion System." *Environmental Science & Technology* no. 16 (11):776-781.

Querol, X., R. Juan, A. Lopez-Soler, J. Fernandez-Turiel, and C. R. Ruiz. 1996. "Mobility of trace elements from coal and combustion wastes." *Fuel* no. 75 (7):821-838. doi: 10.1016/0016-2361(96)00027-0.

Ramanathan, V., and G. Carmichael. 2008. "Global and regional climate changes due to black carbon." *Nature Geoscience* no. 1 (4):221-227.

Smith, R. D., J. A. Campbell, and K. K. Nielson. 1979. "Characterization and formation of submicron particles in coal-fired plants." *Atmospheric Environment* no. 13 (5):607-617. doi: [http://dx.doi.org/10.1016/0004-6981\(79\)90189-6](http://dx.doi.org/10.1016/0004-6981(79)90189-6).

Suriyawong, A., M. Gamble, M.-H. Lee, R. Axelbaum, and P. Biswas. 2006. "Submicrometer Particle Formation and Mercury Speciation Under O<sub>2</sub>-CO<sub>2</sub> Coal Combustion." *Energy & Fuels* no. 20 (6):2357-2363. doi: 10.1021/ef060178s.

Veranth, J. M., Fletcher, T. H., Pershing, D. W., and Sarofim, A. F. 2000. "Measurement of soot and char in pulverized coal fly ash." *Fuel*, no. 79, 1067-1075, 10.1016/s0016-2361(99)00250-1,.

Wang, X., S. Michael Daukoru, S. Torkamani, W.-N. Wang, and P. Biswas. 2013. "Role of exhaust gas recycle on submicrometer particle formation during oxy-coal combustion."

*Proceedings of the Combustion Institute* no. 34 (2):3479-3487. doi:

<http://dx.doi.org/10.1016/j.proci.2012.07.049>.

Wang, X., B. J. Williams, Y. Tang, Y. Huang, L. Kong, X. Yang, and P. Biswas. 2013.

"Characterization of organic aerosol produced during pulverized coal combustion in a drop tube furnace." *Atmos. Chem. Phys.* no. 13 (21):10919-10932. doi: 10.5194/acp-13-10919-2013.

Zhuang, Y., and P. Biswas. 2001. "Submicrometer Particle Formation and Control in a Bench-Scale Pulverized Coal Combustor." *Energy & Fuels* no. 15 (3):510-516. doi: 10.1021/ef000080s.



## **CHAPTER 3. CHARACTERIZATION OF ORGANIC AEROSOL PRODUCED FROM PULVERIZED COAL COMBUSTION IN A DROP- TUBE FURNACE**

*This results of this chapter has been published in Wang, X.; Williams, B. J.; Wang, X.; Tang, Y.; Yang, X.; Biswas, P., Characterization of Organic Aerosol Produced during Pulverized Coal Combustion in a Drop Tube Furnace. Atmospheric Chemistry and Physics, 2013, 13, 10919-10932*

*Supplementary figures and tables are available in Appendix 1*

## **Abstract**

The previous pilot-scale experiments (in Chapter 2) suggest that organic aerosol formation pathway is very different from soot formation. To study the detailed characteristics and formation mechanisms of organic aerosol emissions, controlled bench scale pulverized coal combustion studies were performed in a drop-tube furnace, showing a correlation between inorganic aerosol formation and organic aerosol formation. It is proposed that inorganic particles play a critical role as carriers of organic species. Aerosol mass spectrometry techniques were applied to characterize fine particle formation during coal combustion. The chemical composition of organic aerosol was a mixture of carboxylic acids, hydrocarbons and aromatic compounds.

### 3.1 Introduction

Coal combustion is a major source of atmospheric aerosol (Seinfeld and Pandis 2006), which adversely affects climate and human health (Poschl 2005). While the characterization and fate of the mineral matter component of coal during combustion has been well studied and understood (Biswas and Wu 1998, Linak and Wendt 1994, Zhuang and Biswas 2001), the characterization and fate of corresponding organic matter content has not yet been examined in detail. Although a few field studies have suggested that primary particulate organic carbon emission from some power plants is very low (Zaveri et al. 2010, Peltier et al. 2007), power plants with lower combustion efficiency may still produce a significant amount of carbonaceous aerosol, including both black carbon and organic aerosol (OA), particularly in some developing countries where particle control technology is not extensively used. Some studies (Huggins et al. 2004, Shoji et al. 2002) reported that particulate matter, emitted from coal combustion, contains a significant fraction (up to 13–16 % by mass) of carbonaceous matter. Recently, an ambient study reported that coal combustion sources contributed about 33% of total organic aerosol during the winter months in Beijing, China (Sun et al. 2013).

Soot particles may contain a minor fraction of organic matter. There are some studies which have investigated the formation mechanisms of soot particles from coal combustion. Brown and Fletcher (1998) proposed tar is the precursor to soot formation during coal combustion. Tar molecules have a relative larger molecular weight, which allows them to form soot by directly losing H, O and other atoms, without forming polycyclic aromatic hydrocarbons (PAHs). Rigby et al. (2000) found that soot yields decrease when flame temperature increases. And soot yields increase if the residence time of coal particles in the flame is increased, indicating that light-hydrocarbon may be incorporated into the soot while in the flame. Linak et al. (2007) reported

carbon content in ultrafine particles (diameter <500 nm) is produced from coal combustion. They also found that carbon content could be correlated with toxicity of particles.

Only a few studies have characterized emissions of particulate organic matter from pulverized coal combustion (Zhang et al. 2008, Linak et al. 2007). Zhang et al. (2008) measured emission factors of organic carbon (from 0.30 to 17.1 mg/kg of fuel depending on fuel types) for industrial coal boilers. They found 48-68% of particulate organic matter is organic acids. The main components also include polycyclic aromatic hydrocarbons (PAHs) and alkanes. Linak et al. (2007) combusted pulverized coal particles in a drop-tube furnace and reported that soot particles comprised a higher mass fraction of ultrafine particles (diameter <500 nm), according to their X-ray absorption near edge structure (XANES) spectra.

In developing countries, domestic coal combustion is used for household heating and cooking. Due to insufficient mixing of coal and air, much higher emissions of organic carbon have been found (Oros and Simoneit 2000, Simoneit et al. 1999) and Simoneit, 2000; Tian et al., 2008). Oros and Simoneit (2000) used a gas chromatography–mass spectrometry (GC-MS) to identify many organic compounds, including hydrocarbons, esters, ketones and other polar organic compounds. Tian et al. (2008) reported emission factors of hydrocarbon from coal combustion in a stove of 15.5 and 37.0 g/kg (of fuel) for anthracite coals and bituminous coals, respectively. Zhang et al. (2008) also measured the emission factors of organic carbon for domestic coal combustion, and reported the values to be 0.47 to 2.95 g/kg (of fuel) depending on coal types used.

In the past two decades, many advanced aerosol mass spectrometry techniques, such as thermal vaporization aerosol mass spectrometry and laser ablation single particle mass spectrometry,

have been developed and widely used to characterize atmospheric aerosols and help identify their sources (Gard et al. 1997, Jimenez et al. 2003). Mass spectrum measured directly from source is crucial to source apportionment of aerosols using these aerosol mass spectrometry methods. Several studies have determined the mass spectra of aerosols produced from many sources such as biomass-burning stoves, diesel-burning vehicles, and cook stoves (Silva and Prather 1997, Silva et al. 1999, Schneider et al. 2006, Mohr et al. 2009, Canagaratna et al. 2004). However, according to our knowledge, there are very few studies on organic aerosol characterization from coal combustion. For example, Healy et al. (2010) burned coal in an outdoor stove and measured its aerosol emission using a laser ablation single particle mass spectrometer. The obtained mass spectra were compared with ambient aerosol data; and a type of aerosols with similar mass spectra was identified from coal combustion. Similarly, Dall'Osto et al. (2012) obtained mass spectra of organic aerosols from a domestic peat and coal combustion experiment using a thermal vaporization aerosol mass spectrometer. They reported the mass spectra were similar to a type of organic aerosol; and concluded this type of organic aerosol originated from peat and coal combustion. Notably, all these studies focused on domestic coal combustion. Studies of organic aerosol emissions from pulverized coal combustion have not been conducted in detail using aerosol mass spectrometry techniques. This paper is an attempt to fill that information gap.

In this study, pulverized coal particles were combusted in a drop-tube furnace which were coupled with various aerosol instruments. A drop-tube furnace, a system commonly used to investigate pulverized coal combustion in the laboratory (Card and Jones 1995, Cloke et al. 2002, Visona and Stanmore 1999) due to its well-controlled temperature profile, gas composition and residence time, was used. Various mass spectrometry techniques such as thermal vaporization

aerosol mass spectrometry and gas chromatography–mass spectrometry were used to characterize and unravel the mechanistic details of the organic species' pathway during aerosol formation in coal combustors.

## **3.2 Experimental Section**

### *3.2.1 Experimental Setup and Test Plan of Bench-scale Pulverized Coal Combustion*

As shown in Fig. 3.1, the experimental setup consists of a drop-tube furnace (Lindberg/Blue M, Model HTF55342C, ThermoElectron Corp., USA) with an alumina tube (5.72 cm inner diameter and 121.92 cm long), a scanning mobility particle sizer (SMPS, TSI Inc., Shoreview, MN, USA), a high-resolution time-of-flight aerosol mass spectrometer (HR-Tof-AMS, Aerodyne Research Inc, MA, USA) and other supporting instruments. Pulverized Powder River Basin (PRB) sub-bituminous coal (coal particle diameter  $<50\ \mu\text{m}$ ) was fed using a coal feeder (design of the feeder has been published elsewhere (Quann et al. 1982)) into the drop-tube furnace at feed rates ranging from 1 to 3.5 g/hr. Total 3 liter/min (LPM) carrier gas (air or additional- $\text{N}_2$ /air mixture) was fed at the inlet to the furnace and passed through the alumina tube with coal particles. 1 LPM carrier gas was used in the coal feeder and carried coal particles into the furnace. Another 2 LPM carrier gas was introduced into the furnace directly. In this study, the wall temperature of the alumina tube was set at 1373 K. Coal particles can be combusted completely when they travel through the alumina tube. At the exit of the combustor, 5 LPM particle-free air was added as primary dilution. The diluted exhaust gas passed through a six-stage cascade impactor (Mark III, Pollution Control System Corp., Seattle, WA) to remove particles with a diameter larger than 500 nm. A slip stream with low flow rate was mixed with a high flow rate (details shown in Table 3.1) of particle-free air to achieve a secondary dilution after the impactor. A SMPS was

used to obtain the particle size distribution in the range 9–425 nm (at least 4 SMPS scans were conducted for each experimental condition). Particulate organic matter was characterized by a thermal vaporization aerosol mass spectrometer (AMS, Aerodyne Research Inc.). Fine particles were also collected by quartz filters for further analysis. All experimental conditions are summarized in Table 3.1. Coal feed rates and gas compositions were changed in order to investigate formation mechanisms of OA during coal combustion. The solids residence time in the furnace and the time-temperature history in the furnace can be found in Appendix 5.

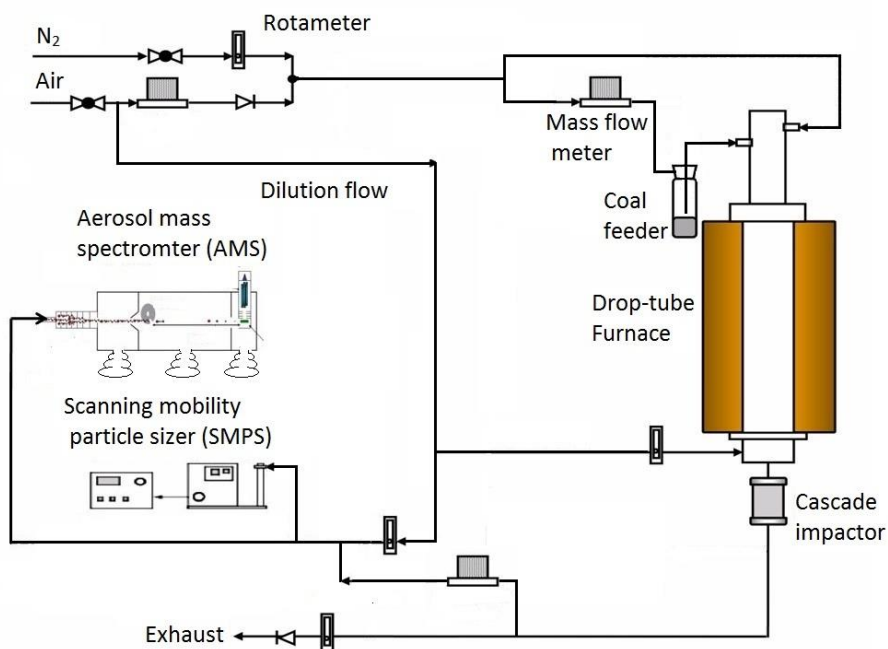


Figure 3.1 Schematic drawing of the laboratory-scale pulverized coal combustion system with measurement instruments identified.

Table 3.1 Summary of experimental conditions for drop-tube furnace study of pulverized coal combustion

Set	#	O <sub>2</sub> /Coal Ratio (mol/mol)	Coal Feed Rate (g/hr)	Air Flow Rate (lpm)	Additional N <sub>2</sub> Flow Rate (lpm)	Air/Additional-N <sub>2</sub> Ratio	Sampling Dilution Ratio	Fuel-Air Equivalence ratio	Objective
I	1	30.1	1	3	0	-	100.7	0.033	Organic aerosol formation under different O <sub>2</sub> /Coal ratios
	2	20.1	1.5	3	0	-		0.05	
	3	15.0	2	3	0	-		0.067	
	4	12.0	2.5	3	0	-		0.083	
	5	10.0	3	3	0	-		0.1	
	6	8.6	3.5	3	0	-		0.12	
II	1	27.1	1	2.7	0.3	90/10	50.4	0.037	Organic aerosol formation under different gas compositions at lower coal feed rate (1 g/hr)
	2	24.1	1	2.4	0.6	80/20		0.041	
	3	18.1	1	1.8	1.2	60/40		0.069	
III	4	9.0	3	2.7	0.3	90/10	100.7	0.11	Organic aerosol formation under different gas compositions at higher coal feed rate (3 g/hr)
	5	8.0	3	2.4	0.6	80/20		0.13	
	6	6.0	3	1.8	1.2	60/40		0.17	



### *3.2.2 High-Resolution Time-of-Flight Aerosol Mass Spectrometer (HR-ToF-AMS)*

The Aerodyne quadrupole Aerosol Mass Spectrometer (Q-AMS) was described in detail by (Canagaratna et al. 2007, Allan et al. 2003, Jimenez et al. 2003). HR-ToF-AMS is a newer version of AMS and has better mass-to-charge ratio ( $m/z$ ) resolution and faster response than the Q-AMS. The HR-ToF-AMS has been described in detail by DeCarlo et al. (2006). Briefly, aerosol particles are introduced into the AMS via the aerodynamic lens, which focuses the particles into a narrow beam. Particle size is resolved based on particle velocity across a time of flight chamber at the exit of the aerodynamic lens. Next, particles are impacted on a vaporizer where the non-refractory fraction is vaporized and immediately ionized using electron impact ionization. Finally, these ions are analyzed by a time-of-flight mass spectrometer. The vaporizer temperature was set to 600 °C. Coal combustion produces CO<sub>2</sub>, which will also contribute to some organic peaks like  $m/z$  28 and 44. A set of control experiments were conducted to determine and subtract the contribution of organic signal from background CO<sub>2</sub>. For each experimental condition, the AMS was running under the V-mode and the sampling time was about 15 min. And filtered, particle-free exhaust gas measured by AMS was used as the baseline. By using high-resolution mass spectra, the exact molecular formula of each organic peak (e.g. C<sub>x</sub>H<sub>y</sub>O<sub>z</sub>) was obtained, and overall elemental ratios for the entire mass spectrum was calculated. The method of elemental ratio calculation has been described by Aiken et al. (2007).

### *3.2.3 Analysis of Filter Samples Using Total Organic Carbon (TOC) Analyzer and Gas Chromatography–Mass Spectrometer (GC-MS)*

Particles (with diameters <500 nm) generated from the drop-tube furnace were collected on quartz filters and then analyzed with a total organic carbon analyzer (TOC-LCPH, Shimadzu Co.)

for their total carbon content. These particles were then examined with a thermal/optical carbon analyzer (Model 2001, Atmoslytic Inc., Calabasas, CA) for the ratio of elemental carbon/organic carbon. Particles on a quartz filter were also extracted with 30 ml mixture of dichloromethane and methanol (3:1 in volume). Then the extract was filtered and concentrated to about 5 ml in a vacuum evaporator. A stream of ultrapure nitrogen was used to further concentrate the extract. Finally the extract was derivatized with BSTFA (BSTFA/TMCS, 99:1, Sigma-Aldrich Co.) and introduced into a GC-MS (Thermo ISQ GC-MS, Thermo Fisher Scientific Inc.) for analysis.

### **3.3 Results and Discussion**

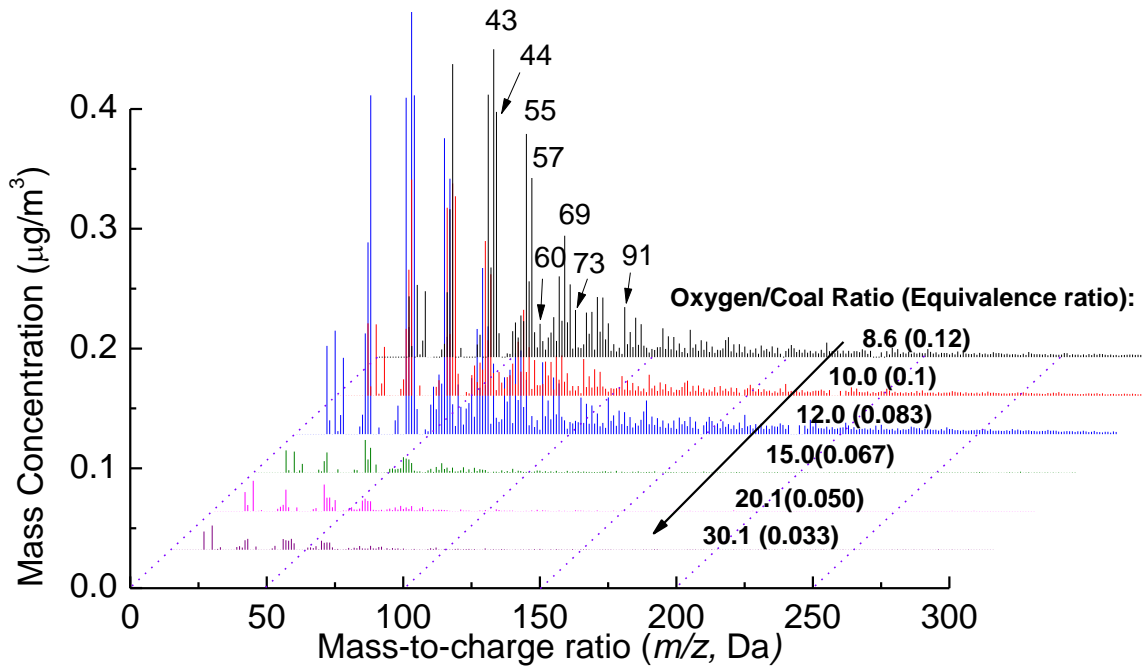
The overall study examined the understanding of the pathways of organic aerosol formation by performing systematic experiments in a drop tube combustor. Using this information, the mechanism of organic aerosol formation during coal combustion was investigated.

#### *3.3.1 Characterization of Organic Aerosol from Coal Combustion in a Drop-tube Furnace*

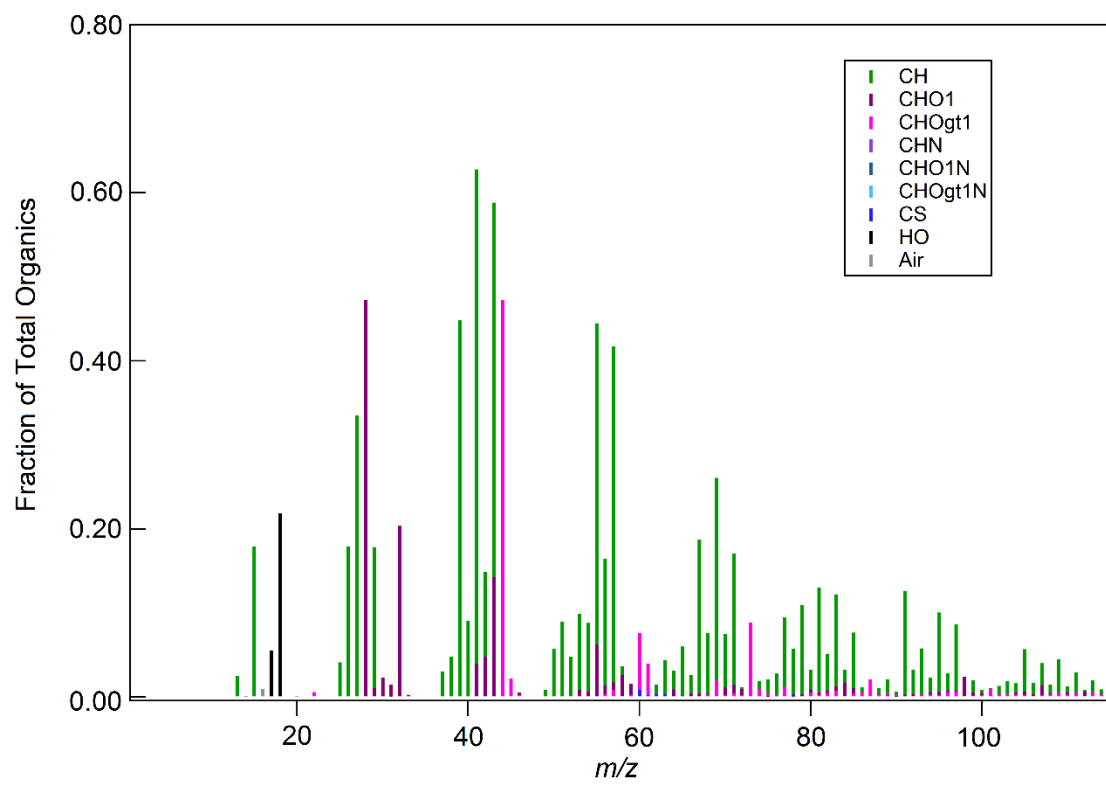
The average AMS organic mass spectra of aerosol from the drop tube coal combustor under various oxygen/coal ratios are shown in Fig. 3.2. Many significant organic peaks (such as  $m/z$  43, 44, 55, 57, 60, 69, 73, 91) are observed, confirming that pulverized coal combustion produces organic aerosols, even at the high oxygen/coal ratios in this efficient combustion system. The oxygen/coal ratio is defined as “feed rate of  $O_2$  in moles per hour / feed rate of carbon in moles per hour” and it ranged from 8.6 to 30.1 (In a full scale coal-fired power plant, a typical oxygen/coal ratio is 1.2). In combustion science, the equivalence ratio is commonly used, which is defined as the ratio of the fuel-to-oxidizer ratio to the stoichiometric fuel-to-oxidizer ratio; here the equivalence ratios ranged from 0.12 to 0.033. However, the fraction of organic matter to total fine particle mass is small. Inorganic compounds, such as  $SiO_2$ ,  $CaO$  and  $Al_2O_3$ ,

are dominant species in coal combustion aerosol (Linak and Wendt 1994). Figure A1.1 (shown in appendix) shows particle size distributions from the coal combustor, which indicates that changing oxygen/coal ratio from 30.1 to 8.6 slightly increased particle concentrations.

A.



B.



C.

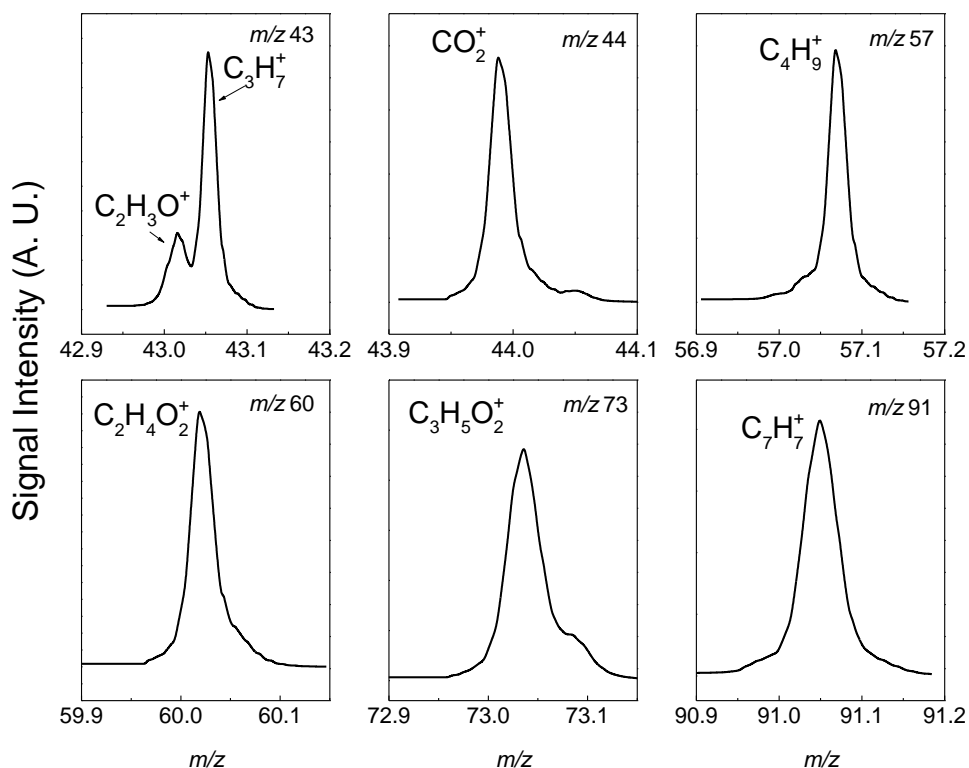
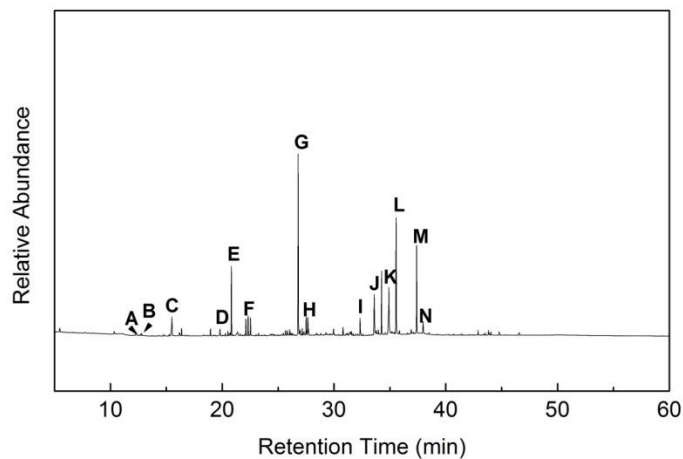


Figure 3.2. (A) Average organic mass spectra for fine particulate matter from pulverized coal combustion under different oxygen/coal ratios. Each mass spectrum corresponds to one oxygen/coal ratio. The mass spectra were obtained by an Aerodyne Aerosol Mass Spectrometer (AMS); (B) High resolution AMS spectrum and (C) Some important high resolution peak patterns for fine particulate matter from pulverized coal combustion under the oxygen/coal ratio at 12.0. CHOgt1 represents a group of high resolution ions, including  $CO_2^{+2}$ ,  $CO_2^+$ ,  $^{13}CO_2^+$ ,  $CH_2O_2^+$ ,  $C_3O_2^+$ ,  $C_8H_5O_3^+$ ,  $C_8H_7O_4^+$ ,  $C_{16}H_{23}O_4^+$  (Combustion condition: Wall temperature: 1376 K, Air flow rate 3 LPM, Coal feed rate: 2.5 gram/hr, Fuel-air equivalence ratio: 0.083)

High-resolution (HR) aerosol mass spectrum can provide more detailed information on molecular formula for each ion. Figure 3.2B shows the HR spectrum for coal combustion aerosols at the oxygen/coal ratio at 12.0. It shows that  $C_xH_y^+$ ,  $C_xH_yO^+$  and  $C_xH_yO_z^+$  are the main ion series, and sulfur or nitrogen containing organic species do not contribute a significant fraction to the total organics. Some unit mass peaks, such as  $m/z$  43, 44, 57, 60, and 73 are considered as tracers of hydrocarbon organic aerosol (HOA), oxygenated organic aerosol (OOA), or biomass burning organic aerosol (BBOA) (Canagaratna et al. 2007). Thus, it is important to examine their HR peak patterns. Figure 3.2C shows the patterns for those peaks. The unit mass peak at  $m/z$  43 is actually consisted of two ions:  $C_2H_3O^+$  ( $m/z$  43.018391) and  $C_3H_7^+$  ( $m/z$  43.054779). The peak of  $C_3H_7^+$  is much higher than  $C_2H_3O^+$ . The ratio of these two ions can be considered as an indicator of the extent of oxygenation (Mohr et al. 2009). A higher  $C_3H_7^+/C_2H_3O^+$  ratio suggests lower extent of oxygenation. Fig. 3.2B also shows a pronounced peak at  $m/z$  44, which is an important indicator for OOA. Figure 3.2C shows the unit mass peak at  $m/z$  44 is solely consisted of the ion  $CO_2^+$  ( $m/z$  43.989830). It is formed via the thermal decarboxylation of carboxylic acids (Aiken et al. 2007). The fraction of  $m/z$  44 to the total organic signal,  $f_{44}$ , is 7.5%. And  $f_{43}$  is 9.3%. According to Ng et al. (2011), the combination of these two values suggests that the organic compounds in this mass spectrum are semi-volatile OOAs, which are highly oxygenated. Similar to  $m/z$  43, the unit mass peak at  $m/z$  57 is dominantly composed of the ion  $C_4H_9^+$  ( $m/z$  57.070431); and the ion  $C_3H_5O^+$  ( $m/z$  57.034039) does not contribute a significant fraction for  $m/z$  57.  $C_3H_5O^+$  ion is also an indicator for oxygenated species. The discrepancy between what is observed for HR analysis of  $m/z$  43 and 57 being dominated by hydrocarbon fractions compared to the observed  $m/z$  43 to 44 ratio may

suggest that most of the oxygenated species in coal combustion aerosol are carboxylic acids. Other oxygenated organic species, such as alcohol, ketone and aldehyde may not contribute a large fraction of total organic matter. One HR-AMS study (Aiken et al. 2007) has shown that pure oleic acid aerosol also produced higher  $C_3H_7^+$  and  $C_4H_9^+$  peaks but lower  $C_2H_3O^+$  and  $C_3H_5O^+$  peaks. In addition, the peak at  $m/z$  91 should originate from aromatic compounds. The HR data (Fig. 3.2C) shows this peak mainly consists of the ion  $C_7H_7^+$  ( $m/z$  91.054771), which contains a benzene ring.

A.



B.

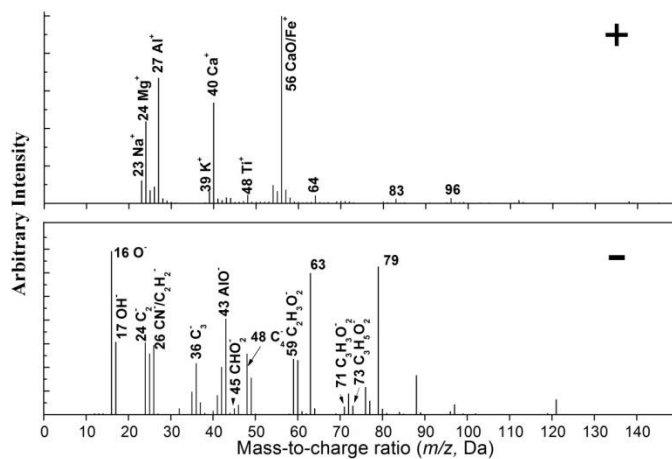


Figure 3.3. (A) GC-MS measurements of extracts from coal combustion particles. Different chemical compounds were separated depending on their retention time in GC column. Major compounds were identified according to their mass spectra: A. *Benzaldehyde, 3-methoxy-4-[(trimethylsilyl)oxy]-,O-methyloxime*; B. *3-Hydroxybutyric acid, t-butyl ester*; C. *Benzaldehyde,*



*2-methyl-*; D. *1,3-Benzenediol,o-(4-methylbenzoyl)-o-(2-methoxybenzoyl)-*; E. *Benzene, 1,3-bis(1,1-dimethylethyl)-*; F. *2-Isopropyl-5-methyl-1-heptanol*; G. *Phenol,2,4-bis(1,1-dimethylethyl)-*; H. *Benzoic acid,3,5-bis(1,1-dimethylethyl)-4-hydroxy-,ethyl ester*; I. *13-Docosen-1-ol,(Z)-*; J. *Hexadecanoic acid, methyl ester*; K. *n-Hexadecanoic acid*; L. *14-Pentadecenoic acid*; M. *Oxtadecanoic acid, methyl ester*; N. *Oxtadecanoic acid*. The presence of some esters may be due to the derivatization of acids with BSTFA; **(B)** Positive and negative mass spectra for extract of fine particulate matter from pulverized coal combustion. The mass spectra were obtained by an Aerosol Time-of-flight Mass Spectrometer (ATOFMS) (Combustion condition: Wall temperature: 1376 K, Air flow rate 3 LPM, Coal feed rate: 2.5 gram/hr, Fuel-air equivalence ratio: 0.083)

The mass spectra in Fig. 3.2A are similar to those from biomass burning aerosols that were reported by Schneider et al. (2006). Noticeably, the combustion condition from Schneider et al.'s study was not well controlled: biomass was burned in an open furnace; and they did not report the fuel-air equivalence ratio and temperature. Particularly, peaks at  $m/z$  60 and 73 are generally considered as important biomass burning particle tracers. Figure 3.2C shows the HR peak pattern for  $m/z$  60 and 73. The main ion that contributes to  $m/z$  60 is  $C_2H_4O_2^+$  and is traditionally considered to result from fragmentation of levoglucosan, which is one of the major compounds emitted from biomass burning (Schneider et al. 2006, Weimer et al. 2008). The fraction of  $m/z$  60 to the total organic signal,  $f_{60}$ , is 1.1% for Fig. 3.2B. Weimer et al. (2008) reports that  $f_{60}$  of wood combustion aerosol is from 0.6 to 6.7%. Thus, this fraction is higher than the lower end of  $f_{60}$  for wood combustion aerosols. Therefore, coal combustion aerosol

cannot be distinguished from wood combustion aerosol just based on  $f_{60}$ . Similarly,  $f_{73}$  for Fig. 2B is 1.6%, while  $f_{73}$  for wood combustion aerosol is from 0.3 to 2.0% (Weimer et al., 2008). Figure 2C also shows that  $C_3H_5O_2^+$  is the main ion for the peak at  $m/z$  73. To further characterize the organics, fine particulate matter from the coal combustor was collected on a quartz filter. The organics were extracted by a mixture of methanol and dichloromethane; derivatized with BSTFA and analysed by gas chromatography–mass spectrometry (GC/MS). No levoglucosan was detected (Fig. 3.3A), which implies that other detected compounds (e.g., some carboxylic acids) most likely contributed to the observed  $m/z$  60 and 73. These masses have been previously observed with carboxylic acid samples in the AMS (Aiken et al. 2007). This observation implies that an ambient mass spectral signature with elevated  $m/z$  60 and 73 could have biomass burning or coal combustion origins, and further supporting information is required to determine the major contributing source.

In the drop-tube coal combustion experiments, collected particles were also extracted with deionized water (18 M $\Omega$ ), then atomized and measured by an Aerosol Time-of-flight Mass Spectrometer (ATOFMS), which can analyse single aerosol particles by laser desorption/ionization (Gard et al. 1997). The ATOFMS mass spectrum (Fig. 3.3B) contains many inorganic peaks, such as Ca, Na and K. However, the K peak is comparatively low. This observation, however, is not consistent with the study by Suess et al. (2002) in which they observed larger K peaks in ATOFMS spectra for coal combustion particles in an in situ measurement (i.e., freshly emitted particles were directly introduced into ATOFMS and measured). The reason for the low K peak in this study is that K has high mineral affinity (elements associated with aluminosilicates, carbonates and other minerals in coal ash), and only about 1% of K in fly ash from coal combustion can be extracted by water (Querol et al. 1996).

Peaks at  $m/z$  of -45, -59 and -73 in ATOFMS spectra are usually considered as the fragments of levoglucosan (Silva et al. 1999). These peaks detected in Fig. 3C are not from levoglucosan in this study; hence they are not unique biomass burning tracers for particles in the atmosphere. The similarity of the organic species in aerosol formed during coal combustion and biomass burning is due to the fact that coal has its origins from biomass and was formed via coalification, which is a process that reduces hydrogen and oxygen content of biomass (with cellulose, lignin, hemicellulose being the major components) and increases the fraction of carbon content (Haenel 1992).

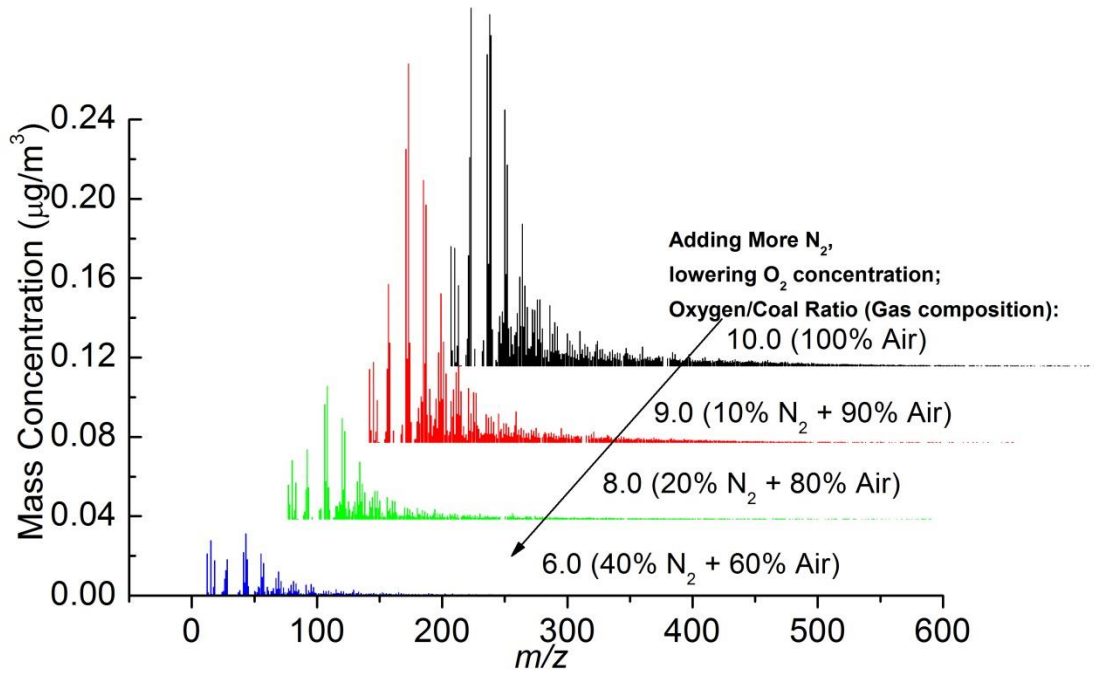
### *3.3.2 Formation Mechanisms of Organic Aerosol from Coal Combustion*

OA formation is affected by oxygen/coal ratios. To examine this, the coal feed rate was changed while the air flow rate remained fixed. Figure 3.2 contrasts mass spectra between higher oxygen/coal ratios (15.0–30.1) and lower oxygen/coal ratios (8.6–12.0). When the oxygen/coal ratio is lower than 12.0, the peak of  $\text{CO}_2^+$  at  $m/z$  44 becomes one of the dominant peaks in the mass spectrum, suggesting that OOA is a major component of particulate organic matter. High-resolution AMS has the capability to determine elemental composition of organics (Aiken et al. 2008). At a lower oxygen/coal ratio, the O/C molar ratios of the organic matter are around 0.25 (Fig. A1.2), which is similar to some fresh secondary organic aerosols generated in chamber experiments (Ng, Canagaratna, Zhang, et al. 2010). Larger char particles were removed by the impactor as they have particle diameters larger than 1  $\mu\text{m}$ . Therefore, the oxygenated organic matter should be formed from tar, which is composed of volatile products of coal pyrolysis. GC/MS measurement shows that the composition of the organics is mainly comprised of oxidized aromatic compounds and some fatty acids (Fig. 3.2B), which could be the oxidized tar

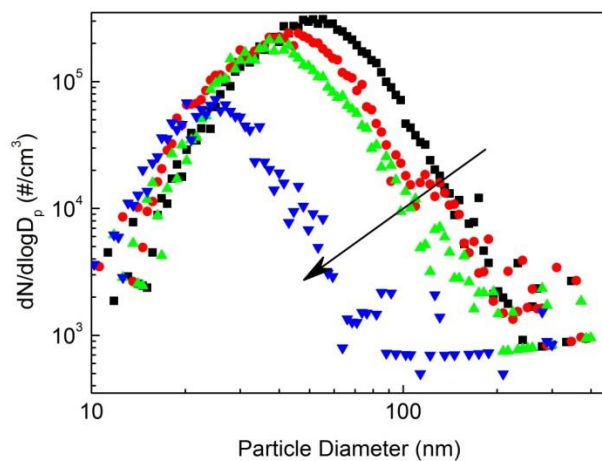
compounds. At higher oxygen/coal ratio ( $>15.0$ ), abundance of the organic peaks is much lower, indicating OA formation is favored at lower oxygen/coal ratios.

Organic matter is typically fully oxidized (to gaseous  $\text{CO}_2$  and  $\text{CO}$ ) in air at high combustion temperatures. Thus, the organic matter detected in the particles was probably prevented from oxidation by unknown mechanisms in the combustor. A conjecture is proposed: the organic vapors are adsorbed by inorganic particles during coal combustion. After adsorption of organic vapors, inorganic particles may continue to grow, thereby covering and protecting organic matter from further oxidation. To test this hypothesis, different amounts of pure  $\text{N}_2$  were added into the coal combustor to suppress inorganic particle formation (a mechanism explained in our research group's previous study (Suriyawong et al. 2006b)). Formation of OA particles should be favored under lower air-fuel equivalence ratios, which would be the case when more  $\text{N}_2$  is added into the system as the oxygen/coal ratio is lowered. However, as shown in Fig. 3.4A, when more  $\text{N}_2$  was added at a fixed coal feed rate of 3.0 g/hr, organic peaks became significantly lower compared to the air case (lower nitrogen concentrations). Both the total particle number concentration and size became smaller, resulting in lower inorganic ash particle concentrations (Suriyawong et al., 2006). At the reduced overall inorganic particle concentrations, the surface area available for adsorption of organic vapor was also reduced (Fig. 3.4B). The similar phenomenon (Fig. A1.3) was also observed for an experiment with a lower coal feed rate (1.0 g/hr).

A.



B.



C.

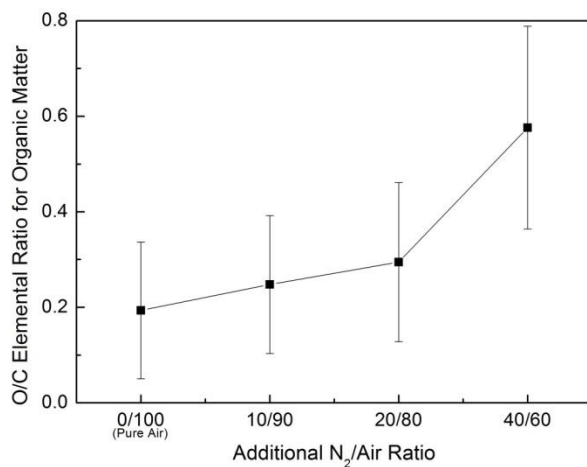


Figure 3.4. (A) Average organic mass spectra and (B) Size distributions for different additional-N<sub>2</sub>/Air ratios while coal feed rate was fixed at 3.0 g/hr. The mass spectra were obtained by AMS, while the size distributions were measured by SMPS. Each color of mass spectrum or size distribution corresponds to certain additional-N<sub>2</sub>/Air ratios: (Blank: Air; Red: 10% N<sub>2</sub> + 90%

Air; Green: 20% N<sub>2</sub> + 80% Air; Blue: 40% N<sub>2</sub> + 60% Air); (C) Oxygen/Carbon (O/C) elemental ratios with error bars of organic matter for different additional-N<sub>2</sub>/Air ratios.

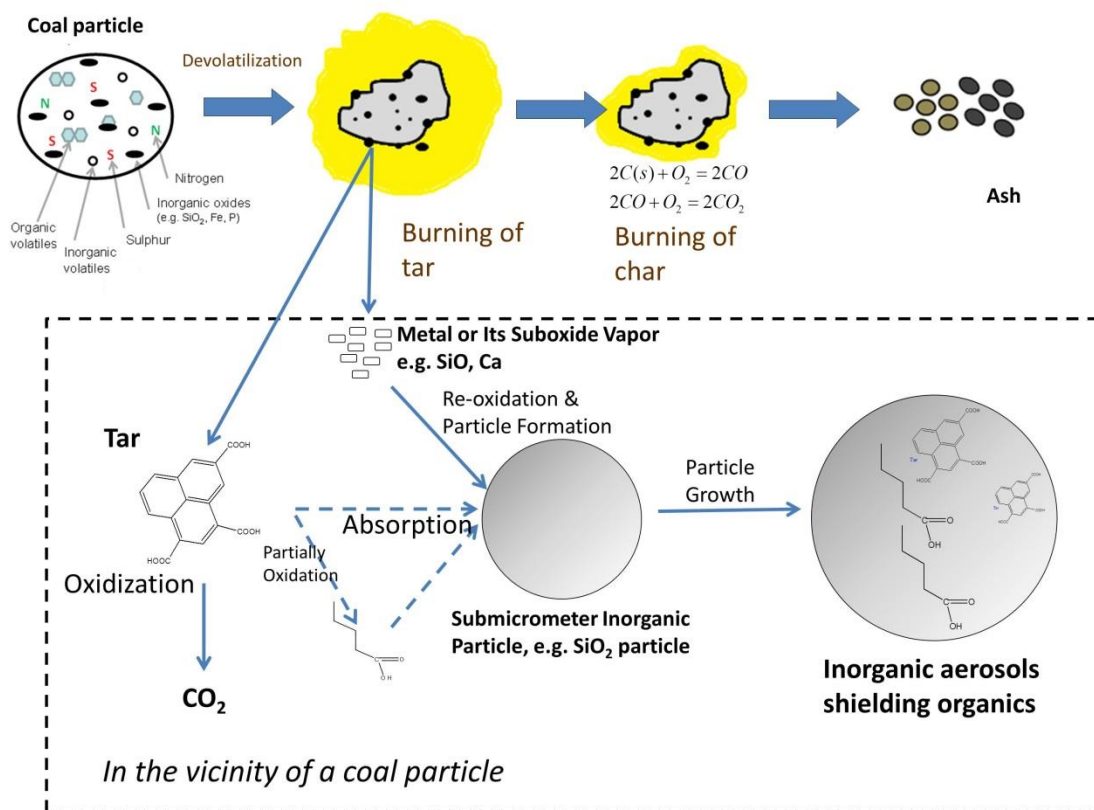


Figure 3.5. Proposed formation mechanisms of OA from coal combustion.

It could be hypothesized that decreased oxygen content suppressed the oxidation of tar and thus suppressed formation of the OA mass; however, Fig. 3.4C shows that the O/C ratio of particulate organic matter actually increases when the N<sub>2</sub>/Air ratio increases, providing further support for the proposed mechanism where inorganic aerosol is protecting OA mass from further oxidation. Notably, the error bars shown in Fig. 3.4C are large. A t-test was applied: The p-value between

pure air (0/100) and 40% N<sub>2</sub> addition (40/60) was less than 0.0001, which is considered to be extremely statistically significant. The p-values between (0/100) and (10/90), (10/90) and (20/80), (20/80) and (40/60) were 0.27, 0.50 and 0.04, respectively. The Van Krevelen diagram was designed to show change of elemental compositions during coal evolution (Van Krevelen 1950). This diagram has been used more recently for the evolution of organic aerosol in the atmosphere (Heald et al. 2010). Here, the Van Krevelen diagram of organic aerosols produced from coal combustion under the different N<sub>2</sub>/Air ratios is shown in Fig. A1.4. The slope of the trend line is -0.24, which is between 0 and -1, suggesting that the oxidation process may produce more carboxylic acids and alcohol/peroxides (Heald et al. 2010). As previously mentioned, alcohol species may not contribute a significant fraction to coal combustion organic aerosol. Thus the oxidation process may largely produce more carboxylic acids and organic peroxides. Thus, generally the trend is significant: O/C ratio increased, when more N<sub>2</sub> was added into the system. Under lower additional-N<sub>2</sub>/Air ratio, higher concentrations of inorganic particles are formed during coal combustion. With increased surface area, they adsorb more organic species, and prevent their further oxidation. Thus, the O/C ratio in the particulate matter is lower even under higher oxygen concentration (lower N<sub>2</sub>/Air ratio), which is consistent with observations in Fig. 3.4C. In addition, size distributions of particles from coal combustion result in a maximum peak diameter of about 50 nm (Fig. A1.1). However organic mass size distributions peak at about 100 nm (Fig. A1.5), indicating organic matter is associated with the larger particles that have a higher absolute surface area and provide better protection against oxidation.

Figure 3.5 summarizes the proposed formation mechanisms of OA during pulverized coal combustion: Molecules in coal usually contain aromatic clusters which are connected by hydrocarbon bridges and loops (Haenel 1992). The bond strength of aromatic rings is much



greater than those of the hydrocarbon bridges and loops. When coal particles are combusted in the furnace, bridges and loops break apart first. Tar, a group of compounds with smaller molecular weights, are released. In the furnace, most of gas-phase tar is quickly oxidized and fully combusted. However, some of the tar species are adsorbed by the inorganic ash particles with chemical composition such as  $\text{SiO}_2$ ,  $\text{Al}_2\text{O}_3$ ,  $\text{CaO}$  and sulfate. These particles can protect tar from further oxidation. Therefore, particulate organic matter survives the highly oxidizing environment and may potentially be emitted to the atmosphere.

### **3.4 Conclusions**

Coal combustion produces fine particles with a fraction of carbonaceous matter (~13% of total mass in this study), including both black carbon and organic carbon. It is shown from controlled bench scale pulverized coal combustion studies that inorganic aerosols play a critical role as carrier of organic species. Using some commonly-used aerosol mass spectrometry techniques (Aerodyne AMS, GC-MS, and TSI ATOFMS), fine particulate matter from coal combustion was characterized in detail. The main OA components include oxidized aromatic matter and carboxylic acids. It was found that these organic species have similar mass spectra as those from biomass combustion aerosols. For atmospheric aerosol studies, due to the similarity of organic signals between coal combustion and biomass burning measured by both AMS and ATOFMS, some biomass burning aerosol tracers may not be reliable in certain locations.

### 3.5 References

Aiken, A. C., P. F. DeCarlo, and J. L. Jimenez. 2007. "Elemental analysis of organic species with electron ionization high-resolution mass spectrometry." *Analytical Chemistry* no. 79 (21):8350-8358. doi: 10.1021/ac071150w.

Aiken, A. C., P. F. Decarlo, J. H. Kroll, D. R. Worsnop, J. A. Huffman, K. S. Docherty, I. M. Ulbrich, C. Mohr, J. R. Kimmel, D. Sueper, Y. Sun, Q. Zhang, A. Trimborn, M. Northway, P. J. Ziemann, M. R. Canagaratna, T. B. Onasch, M. R. Alfarra, A. S. H. Prevot, J. Dommen, J. Duplissy, A. Metzger, U. Baltensperger, and J. L. Jimenez. 2008. "O/C and OM/OC ratios of primary, secondary, and ambient organic aerosols with high-resolution time-of-flight aerosol mass spectrometry." *Environmental Science & Technology* no. 42 (12):4478-4485. doi: 10.1021/es703009q.

Allan, J. D., J. L. Jimenez, P. I. Williams, M. R. Alfarra, K. N. Bower, J. T. Jayne, H. Coe, and D. R. Worsnop. 2003. "Quantitative sampling using an Aerodyne aerosol mass spectrometer 1. Techniques of data interpretation and error analysis." *J. Geophys. Res.* no. 108 (D3):4090. doi: 10.1029/2002jd002358.

Biswas, P., and C. Y. Wu. 1998. "Control of toxic metal emissions from combustors using sorbents: A review." *Journal of the Air & Waste Management Association* no. 48 (2):113-127.

Bond, T. C., D. G. Streets, K. F. Yarber, S. M. Nelson, J.-H. Woo, and Z. Klimont. 2004. "A technology-based global inventory of black and organic carbon emissions from combustion." *J. Geophys. Res.* no. 109 (D14):D14203. doi: 10.1029/2003jd003697.

Brown, A. L., and T. H. Fletcher. 1998. "Modeling Soot Derived from Pulverized Coal." *Energy & Fuels* no. 12 (4):745-757. doi: 10.1021/ef9702207.

Canagaratna, M. R., J. T. Jayne, D. A. Ghertner, S. Herndon, Q. Shi, J. L. Jimenez, P. J. Silva, P. Williams, T. Lanni, F. Drewnick, K. L. Demerjian, C. E. Kolb, and D. R. Worsnop. 2004.

"Chase Studies of Particulate Emissions from in-use New York City Vehicles." *Aerosol Science and Technology* no. 38 (6):555-573. doi: 10.1080/02786820490465504.

Canagaratna, M. R., J. T. Jayne, J. L. Jimenez, J. D. Allan, M. R. Alfarra, Q. Zhang, T. B.

Onasch, F. Drewnick, H. Coe, A. Middlebrook, A. Delia, L. R. Williams, A. M. Trimborn, M. J. Northway, P. F. DeCarlo, C. E. Kolb, P. Davidovits, and D. R. Worsnop. 2007. "Chemical and microphysical characterization of ambient aerosols with the aerodyne aerosol mass spectrometer." *Mass Spectrometry Reviews* no. 26 (2):185-222. doi: 10.1002/mas.20115.

Card, J. B. A., and A. R. Jones. 1995. "A Drop Tube Furnace Study of Coal Combustion and Unburned Carbon Content Using Optical Techniques." *Combustion and Flame* no. 101 (4):539-547. doi: 10.1016/0010-2180(94)00237-m.

Cloke, M., E. Lester, and A. W. Thompson. 2002. "Combustion characteristics of coals using a drop-tube furnace." *Fuel* no. 81 (6):727-735. doi: Pii s0016-2361(01)00199-5

10.1016/s0016-2361(01)00199-5.

Dall'Osto, M., J. Ovadnevaite, D. Ceburnis, D. Martin, R. M. Healy, I. P. O'Connor, J. R. Sodeau, J. C. Wenger, and C. O'Dowd. 2012. "Characterization of urban aerosol in Cork City (Ireland) using aerosol mass spectrometry." *Atmos. Chem. Phys. Discuss.* no. 12 (11):29657-29704. doi: 10.5194/acpd-12-29657-2012.

DeCarlo, P. F., J. R. Kimmel, A. Trimborn, M. J. Northway, J. T. Jayne, A. C. Aiken, M. Gonin, K. Fuhrer, T. Horvath, K. S. Docherty, D. R. Worsnop, and J. L. Jimenez. 2006. "Field-

Deployable, High-Resolution, Time-of-Flight Aerosol Mass Spectrometer." *Analytical Chemistry* no. 78 (24):8281-8289. doi: 10.1021/ac061249n.

Gard, E., J. E. Mayer, B. D. Morrical, T. Dienes, D. P. Fergenson, and K. A. Prather. 1997. "Real-time analysis of individual atmospheric aerosol particles: Design and performance of a portable ATOFMS." *Analytical Chemistry* no. 69 (20):4083-4091. doi: 10.1021/ac970540n.

Haenel, M. W. 1992. "Recent progress in coal structure research." *Fuel* no. 71 (11):1211-1223. doi: 10.1016/0016-2361(92)90046-q.

Heald, C. L., J. H. Kroll, J. L. Jimenez, K. S. Docherty, P. F. DeCarlo, A. C. Aiken, Q. Chen, S. T. Martin, D. K. Farmer, and P. Artaxo. 2010. "A simplified description of the evolution of organic aerosol composition in the atmosphere." *Geophysical Research Letters* no. 37 (8):L08803. doi: 10.1029/2010GL042737.

Healy, R. M., S. Hellebust, I. Kourtchev, A. Allanic, I. P. O'Connor, J. M. Bell, J. R. Sodeau, and J. C. Wenger. 2010. "Source apportionment of PM<sub>2.5</sub> in Cork Harbour, Ireland using a combination of single particle mass spectrometry and quantitative semi-continuous measurements." *Atmos. Chem. Phys. Discuss.* no. 10 (1):1035-1082. doi: 10.5194/acpd-10-1035-2010.

Huggins, F. E., G. P. Huffman, W. P. Linak, and C. A. Miller. 2004. "Quantifying hazardous species in particulate matter derived from fossil-fuel combustion." *Environmental Science & Technology* no. 38 (6):1836-1842. doi: 10.1021/es0348748.

Jimenez, J. L., J. T. Jayne, Q. Shi, C. E. Kolb, D. R. Worsnop, I. Yourshaw, J. H. Seinfeld, R. C. Flagan, X. Zhang, K. A. Smith, J. W. Morris, and P. Davidovits. 2003. "Ambient aerosol

sampling using the Aerodyne Aerosol Mass Spectrometer." *J. Geophys. Res.* no. 108 (D7):8425.  
doi: 10.1029/2001jd001213.

Linak, W. P., and J. O. L. Wendt. 1994. "Trace metal transformation mechanisms during coal combustion." *Fuel Processing Technology* no. 39 (1-3):173-198.

Linak, W. P., J.-I. K. Yoo, S. J. Wasson, W. Zhu, J. O. L. Wendt, F. E. Huggins, Y. Chen, N. Shah, G. P. Huffman, and M. I. Gilmour. 2007. "Ultrafine ash aerosols from coal combustion: Characterization and health effects." *Proceedings of the Combustion Institute* no. 31:1929-1937.  
doi: 10.1016/j.proci.2006.08.086.

Mohr, C., J. A. Huffman, M. J. Cubison, A. C. Aiken, K. S. Docherty, J. R. Kimmel, I. M. Ulbrich, M. Hannigan, and J. L. Jimenez. 2009. "Characterization of Primary Organic Aerosol Emissions from Meat Cooking, Trash Burning, and Motor Vehicles with High-Resolution Aerosol Mass Spectrometry and Comparison with Ambient and Chamber Observations." *Environmental Science & Technology* no. 43 (7):2443-2449. doi: 10.1021/es8011518.

Ng, N. L., M. R. Canagaratna, J. L. Jimenez, P. S. Chhabra, J. H. Seinfeld, and D. R. Worsnop. 2011. "Changes in organic aerosol composition with aging inferred from aerosol mass spectra." *Atmos. Chem. Phys. Discuss.* no. 11 (3):7095-7112. doi: 10.5194/acpd-11-7095-2011.

Ng, N. L., M. R. Canagaratna, Q. Zhang, J. L. Jimenez, J. Tian, I. M. Ulbrich, J. H. Kroll, K. S. Docherty, P. S. Chhabra, R. Bahreini, S. M. Murphy, J. H. Seinfeld, L. Hildebrandt, N. M. Donahue, P. F. DeCarlo, V. A. Lanz, A. S. H. Prevot, E. Dinar, Y. Rudich, and D. R. Worsnop. 2010. "Organic aerosol components observed in Northern Hemispheric datasets from Aerosol

Mass Spectrometry." *Atmospheric Chemistry and Physics* no. 10 (10):4625-4641. doi: 10.5194/acp-10-4625-2010.

Oros, D. R., and B. R. T. Simoneit. 2000. "Identification and emission rates of molecular tracers in coal smoke particulate matter." *Fuel* no. 79 (5):515-536. doi: 10.1016/s0016-2361(99)00153-2.

Peltier, R. E., A. P. Sullivan, R. J. Weber, A. G. Wollny, J. S. Holloway, C. A. Brock, J. A. de Gouw, and E. L. Atlas. 2007. "No evidence for acid-catalyzed secondary organic aerosol formation in power plant plumes over metropolitan Atlanta, Georgia." *Geophys. Res. Lett.* no. 34 (6):L06801. doi: 10.1029/2006gl028780.

Poschl, U. 2005. "Atmospheric aerosols: Composition, transformation, climate and health effects." *Angewandte Chemie-International Edition* no. 44 (46):7520-7540. doi: 10.1002/anie.200501122.

Quann, R. J., M. Neville, M. Janghorbani, C. A. Mims, and A. F. Sarofim. 1982. "Mineral Matter and Trace-element Vaporization in a Laboratory-pulverized Coal Combustion System." *Environmental Science & Technology* no. 16 (11):776-781.

Querol, X., R. Juan, A. Lopez-Soler, J. Fernandez-Turiel, and C. R. Ruiz. 1996. "Mobility of trace elements from coal and combustion wastes." *Fuel* no. 75 (7):821-838. doi: 10.1016/0016-2361(96)00027-0.

Rigby, J., J. Ma, B. W. Webb, and T. H. Fletcher. 2000. "Transformations of Coal-Derived Soot at Elevated Temperature." *Energy & Fuels* no. 15 (1):52-59. doi: 10.1021/ef000111j.

Schneider, J., S. Weimer, F. Drewnick, S. Borrmann, G. Helas, P. Gwaze, O. Schmid, M. O. Andreae, and U. Kirchner. 2006. "Mass spectrometric analysis and aerodynamic properties of various types of combustion-related aerosol particles." *International Journal of Mass Spectrometry* no. 258 (1-3):37-49. doi: 10.1016/j.ijms.2006.07.008.

Seinfeld, J. H., and S. N. Pandis. 2006. *Atmospheric Chemistry and Physics: From Air Pollution to Climate Change*.

Shoji, T., F. E. Huggins, G. P. Huffman, W. P. Linak, and C. A. Miller. 2002. "XAFS spectroscopy analysis of selected elements in fine particulate matter derived from coal combustion." *Energy & Fuels* no. 16 (2):325-329. doi: 10.1021/ef010200b.

Silva, P. J., D. Y. Liu, C. A. Noble, and K. A. Prather. 1999. "Size and chemical characterization of individual particles resulting from biomass burning of local Southern California species." *Environmental Science & Technology* no. 33 (18):3068-3076. doi: 10.1021/es980544p.

Silva, P. J., and K. A. Prather. 1997. "On-line characterization of individual particles from automobile emissions." *Environmental Science & Technology* no. 31 (11):3074-3080. doi: 10.1021/es961063d.

Simoneit, B. R. T., J. J. Schauer, C. G. Nolte, D. R. Oros, V. O. Elias, M. P. Fraser, W. F. Rogge, and G. R. Cass. 1999. "Levoglucosan, a tracer for cellulose in biomass burning and atmospheric particles." *Atmospheric Environment* no. 33 (2):173-182. doi: 10.1016/S1352-2310(98)00145-9.

Suess, D. T. 2002. *Single Particle Mass Spectrometry Combustion Source Characterization and Atmospheric Apportionment of Vehicular, Coal and Biofuel Exhaust Emissions*, Chemistry, University of California, Riverside, Riverside.

- Sun, Y. L., Z. F. Wang, P. Q. Fu, T. Yang, Q. Jiang, H. B. Dong, J. Li, and J. J. Jia. 2013. "Aerosol composition, sources and processes during wintertime in Beijing, China." *Atmos. Chem. Phys.* no. 13 (9):4577-4592. doi: 10.5194/acp-13-4577-2013.
- Suriyawong, A., M. Gamble, M.-H. Lee, R. Axelbaum, and P. Biswas. 2006. "Submicrometer Particle Formation and Mercury Speciation Under O<sub>2</sub>-CO<sub>2</sub> Coal Combustion." *Energy & Fuels* no. 20 (6):2357-2363. doi: 10.1021/ef060178s.
- Tian, L., D. Lucas, S. L. Fischer, S. C. Lee, S. K. Hammond, and C. P. Koshland. 2008. "Particle and Gas Emissions from a Simulated Coal-Burning Household Fire Pit." *Environmental Science & Technology* no. 42 (7):2503-2508. doi: 10.1021/es0716610.
- Van Krevelen, D. W. 1950. "Graphical-statistical method for the study of structure and reaction processes of coal." *Fuel* no. 24:269-284.
- Visona, S. P., and B. R. Stanmore. 1999. "Modeling nitric oxide formation in a drop tube furnace burning pulverized coal." *Combustion and Flame* no. 118 (1-2):61-75. doi: 10.1016/s0010-2180(98)00140-0.
- Weimer, S., M. R. Alfarra, D. Schreiber, M. Mohr, A. S. H. Prevot, and U. Baltensperger. 2008. "Organic aerosol mass spectral signatures from wood-burning emissions: influence of burning conditions and wood type." *Journal of Geophysical Research - Part D - Atmospheres*:D10304 (10 pp.). doi: 10.1029/2007jd009309.
- Zaveri, R. A., C. M. Berkowitz, F. J. Brechtel, M. K. Gilles, J. M. Hubbe, J. T. Jayne, L. I. Kleinman, A. Laskin, S. Madronich, T. B. Onasch, M. S. Pekour, S. R. Springston, J. A. Thornton, A. V. Tivanski, and D. R. Worsnop. 2010. "Nighttime chemical evolution of aerosol



and trace gases in a power plant plume: Implications for secondary organic nitrate and organosulfate aerosol formation, NO<sub>3</sub> radical chemistry, and N<sub>2</sub>O<sub>5</sub> heterogeneous hydrolysis." *J. Geophys. Res.* no. 115 (D12):D12304. doi: 10.1029/2009jd013250.

Zhang, Y., J. J. Schauer, Y. Zhang, L. Zeng, Y. Wei, Y. Liu, and M. Shao. 2008. "Characteristics of Particulate Carbon Emissions from Real-World Chinese Coal Combustion." *Environmental Science & Technology* no. 42 (14):5068-5073. doi: 10.1021/es7022576.

Zhuang, Y., and P. Biswas. 2001. "Submicrometer Particle Formation and Control in a Bench-Scale Pulverized Coal Combustor." *Energy & Fuels* no. 15 (3):510-516. doi: 10.1021/ef000080s.

## **CHAPTER 4. FORMATION MECHANISM OF ORGANIC AEROSOL DURING COAL COMBUSTION: ROLES OF PYROLYSIS**

*The results of this chapter has been compiled as a paper, which was selected for oral presentation at the 35th International Symposium on Combustion. It has also been submitted to Proceedings of the Combustion Institute.*

*Supplementary figures and tables are available in Appendix 2*

## **Abstract**

Coal combustion is one of the major emission source of atmospheric organic aerosols, especially in developing countries. However, the formation mechanisms of organic aerosols during coal combustion have not been adequately studied. This study presents a detailed comparison of the chemical compositions between organic aerosol emissions from coal combustion and organic tars from coal pyrolysis, which is an early stage of coal combustion. Two coals, PRB coal and ILL#6 coal, were combusted in a laboratory drop-tube furnace coal combustor; and pyrolyzed in a flat-flame system, which is used as a fast pyrolysis device. The compositions of organic constituents of the combustion aerosols and pyrolysis products were measured by an aerosol mass spectrometer (AMS) and a thermal desorption aerosol gas chromatography–mass spectrometer (TAG). The chemical composition of major species for both combustion organic aerosols and pyrolysis products are non-aromatic hydrocarbons, carboxylic acids and aromatic compounds. A list of specific organic compounds has been identified. The similarities of the chemical compositions strongly suggest that the coal pyrolysis products are the precursors of the organic aerosols. In addition, more carboxylic acids/oxygenated organic compounds were found in the combustion aerosols, indicating that many pyrolysis products are oxidized before final emissions of organic aerosols. Thermal gravimetric analysis (TGA) was also conducted to study the pyrolysis process of the two coals. The activation energy distributions were calculated from their TGA results using a distributed activation energy model (DAEM).

#### **4.1 Introduction**

Coal combustion is a major source of air pollutants, including particulate matter (Seinfeld and Pandis 2006). The chemical composition of particulate matter (aerosol) from coal combustion consists of inorganic minerals, sulfates, elemental carbon and organic matter. Fractions of each component vary under different combustion conditions, especially for carbon content. Previous studies analyzing PM<sub>2.5</sub> emissions from several coal-fired power plants found that the fractions of element carbon and organic carbon ranges from 0.39% to 2.8%, and 1.9% to 17.1% (Zhang et al. 2008). In developed countries, coal combustion does not seem to be significant source of atmospheric organic aerosol (Zaveri et al. 2010, Peltier et al. 2007), due to the strict regulation of particulate matter emissions. However, in developing countries, such as China, coal combustion is considered to be a major source of organic aerosol emission. For instance, Sun et al. (2013) reported that coal combustion may contribute about 33% of total atmospheric organic aerosol in Beijing during the winter.

There are very few studies that focus on organic aerosol formation during coal combustion, while inorganic aerosol formation during coal combustion has been well studied: the formation of submicrometer particles occurs via metal-oxide vaporization-nucleation pathways while the formation of supermicrometer particles is through fragmentation of remaining char particles after complete combustion (Haynes et al. 1982a, Damle et al. 1982a, Suriyawong et al. 2006b). For organic aerosols from coal combustion, Zhang et al. (2008) reported that 48-68% of particulate organic matter from coal combustion aerosols is found in the form of organic acids. Other major compounds identified include polycyclic aromatic hydrocarbons (PAHs) and alkanes. Our previous study (2013b) has characterized organic aerosol formation during pulverized coal combustion in a drop-tube furnace and demonstrated that the inorganic matter prevented the

complete oxidation of the organic species, resulting in their eventual emission. In addition, Brown and Fletcher (1998) proposed that the tar released during coal pyrolysis is the precursor for soot, which is a mixture of elemental carbon and organic matter.

The coal combustion process occurs in three steps: 1) pyrolysis of coal; 2) burning of tar and 3) burning of char (Williams et al. 2001, Warnatz et al. 2006). The first step of coal combustion, pyrolysis produces large quantities of organic volatiles. It is very likely that these organic volatiles are also the precursors of organic aerosols. In order to understand organic aerosol formation during coal combustion, this study presents a detailed comparison of the chemical compositions of organic aerosols and pyrolysis products from coal combustion. Pulverized coal particles were combusted in a drop-tube furnace, while fast pyrolysis experiments were conducted in a flat-flame burner system. An aerosol mass spectrometer and a thermal desorption aerosol gas chromatograph, two advanced mass spectrometry technologies, were employed to analyze the organic compounds in the organic aerosol and pyrolysis products. The distributed activation energy model was also applied to obtain kinetic devolatilization parameters for the pyrolysis of coal.

## **4.2 Experimental Section**

### *4.2.1 Experimental Set-up for Coal Combustion*

Figure 4.1a shows the experimental set-up for coal combustion. The system consists of a Lindberg/Blue M Model HTF55342C drop-tube furnace (ThermoElectron Corp., USA) with a 5.72 cm inner diameter and 121.92 cm long alumina tube connected to a scanning mobility particle sizer (SMPS, TSI Inc., Shoreview MN, USA), and a high-resolution time-of-flight

aerosol mass spectrometer (HR-Tof-AMS, Aerodyne Research, MA, USA), as well as other supporting instruments. Both Powder River Basin (PRB) and Illinois No. 6 (ILL#6) coals were combusted. The proximate and ultimate analyses of the PRB coal and ILL#6 coal used in this study can be found in our previous study (Daukoru 2010). Pulverized coal with coal particle diameters  $<50\ \mu\text{m}$  was introduced into the furnace using a coal feeder (design from Quann et al., (1982)). The coal entered the furnace at a feed rate of 2.5 g/hr. A total of 3 liter/min (LPM) of air was fed into the furnace and passed through the alumina tube with the coal particles. 0.5 LPM of air was used in the coal feeder to carry the coal particles into the furnace, and the remaining 2.5 LPM of air was directly introduced into the furnace. The wall temperature of the alumina tube was held at 1373 K. The fuel-air equivalence ratio was 0.083 for all the combustion experiment. 5 LPM of particle-free air was added as primary dilution at the exit of the combustor. In order to remove the particles with diameters larger than 500 nm, the diluted exhaust gas was passed through a six-stage particle cascade impactor (Mark III, Pollution Control System Corp, Seattle, WA). After passing through the impactor, a slip-stream with low flow rate of 0.5 LPM was mixed with a flow rate (3.8 LPM) of particle-free air to achieve secondary dilution. The diluted exhaust was passed through a thermal vaporization aerosol mass spectrometer (AMS, Aerodyne Research Inc.) in order to characterize the particulate organic matter. Fine particles from the exhaust were also collected on quartz filters for further analysis with thermal desorption aerosol gas chromatography (TAG).

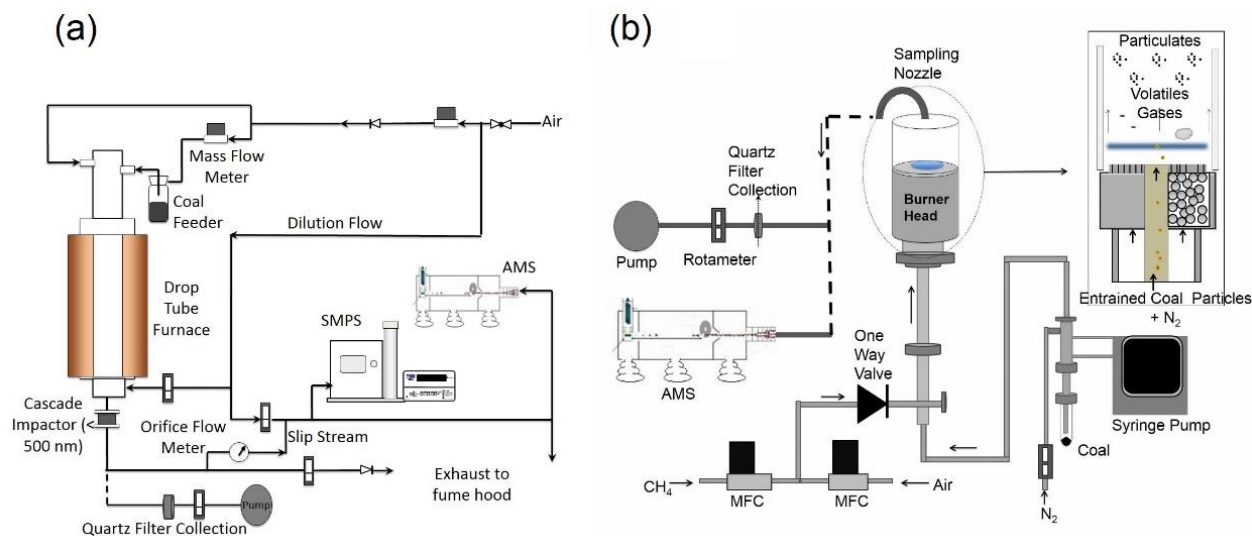


Figure 4.1. Schematic drawing of the experimental setup: (a) Drop-tube furnace system; (b) Flat-flame system

#### 4.2.2 Experimental Set-up for Coal Pyrolysis

A premixed methane-air flat flame reactor (Fig. 4.1b) was used to study the pyrolysis of coal. A honeycomb burner nozzle with 207 separate 0.8 mm diameter holes was used as a flow stabilizer. 0.12 LPM of methane and 2.4 LPM of air were used, controlled by mass flow controllers. The coal feeder was used to feed the coal particles into the burner, where they were entrained with 1 LPM of nitrogen flow. The coal particles and nitrogen gas were then fed axially into the methane-air flat flame by a feeding tube at the center of the flame at a rate of 1 g/hr. Coal particles underwent very fast pyrolysis and their high molecular weight pyrolysis products formed a mist of aerosols above the flame. These aerosols were collected 120 mm above the flat flame and characterized using an AMS. Fine particles were also collected on quartz filters for TAG chromatography.

#### *4.2.3 High Resolution Time-of-flight Aerosol Mass Spectrometer (HR-ToF-AMS)*

The HR-ToF-AMS is described in detail in some literatures reports. Particles are introduced into the device using an aerodynamic lens that focuses them into a narrow beam. The velocity of the particles across a chamber at the exit of the aerodynamic lens is used to determine the particle size. The particles are then impacted onto a vaporizer (600 °C) and immediately ionized through electron impact ionization where the ions are then analyzed by time-of-flight mass spectrometry.

#### *4.2.4 Thermal Desorption Aerosol Gas Chromatograph Mass Spectrometer (TAG)*

The TAG system was designed to identify particulate organic compounds. Williams et al., (2006) provides an in depth description of the TAG system. In this experiment, a small square from the quartz filter containing particulates from either coal combustion or pyrolysis was inserted directly into the thermal desorption chamber. The sample was then thermally desorbed onto a gas chromatograph (GC) column to separate the compounds for detection. Compounds were detected using quadrupole mass spectrometry.

#### *4.2.5 Thermogravimetric Analysis (TGA) Experiment and Distributed Activation Energy Model (DAEM)*

In order to examine and model the pyrolysis reactions, a TA Instruments Q5000 IR Thermogravimetric Analyzer (TGA) was used. The coal sample weight was continuously monitored while high purity nitrogen was purged through the chamber. The temperature of the sample chamber was first increased to 105 °C with a 10 K min<sup>-1</sup> heating rate, and temperature was maintained for an hour to remove all moisture content. Next, with a heating rate of either 5, 10, or 20 K min<sup>-1</sup>, the sample was heated to 800°C. This temperature was maintained for two hours. TGA experiments were performed for both PRB and ILL#6 coals with each of the three aforementioned heating rates.



The Distributed Activation Energy Model (DAEM) is often used to model complex reactions such as coal pyrolysis. It assumes many parallel, irreversible, first-order reactions take place simultaneously. The rate constant,  $k$ , for each reaction is represented by Arrhenius' form:  $k = k_0 \exp(-E/RT)$ , where  $E$  is activation energy,  $R$  is gas constant,  $T$  is temperature and  $k_0$  is pre-exponential factor. A method for estimating the normalized distribution of the activation energy,  $f(E)$ , and  $k_0$  proposed by Miura and Maki (1998) was used to determine the reaction parameters for pulverized PRB and ILL#6 coal. The amount of volatiles released,  $V$ , at a time,  $t$ , is given by the following equations:

$$1 - \frac{V}{V^*} = \int_0^{\infty} \exp\left(-k_0 \int_0^t e^{-\frac{E}{RT}} dt\right) f(E) dE \quad (1)$$

where  $V^*$  is the total effective volatile content of coal. For a certain  $V/V^*$ ,  $E$  and  $k_0$  can be calculated from a simplified equation (eq.2) by plotting  $\ln(a/T^2)$  versus  $1/T$  at the 3 different heating rates,  $a$ :

$$\ln\left(\frac{a}{T^2}\right) = \ln\left(\frac{k_0 R}{E}\right) + 0.6075 - \frac{E}{RT} \quad (2)$$

Using this process, a curve relating  $V/V^*$  and  $E$  is obtained, and  $f(E)$  is the derivative of this curve. The details and derivations of this model can be found in the paper (Miura and Maki 1998).

#### *4.6 Summary of the Experimental Test Plan*

Both PRB coal and ILL#6 coal were combusted in the drop-tube furnace, and devolatilized in the flat flame system. Their emissions were analyzed by AMS and TAG. TGA experiments were performed for both PRB and ILL#6 coals with three heating rates (5, 10, and 20 K min<sup>-1</sup>), and DAEM was used to obtain the kinetic parameters for the coal pyrolysis from the TGA results.

### 4.3 Results and Discussion

#### *4.3.1 Does organic aerosol originate from pyrolysis products? -- Comparisons of chemical compositions of organic aerosols from combustion and products from pyrolysis of PRB coal*

Pulverized PRB coal was sent through the flat flame system and underwent fast pyrolysis. The pyrolysis products were measured by an AMS (Fig. 4.2a). A series of peaks at  $m/z$  27, 29, 41, 43, 44, 51, 55, 57, 67, 69, 81, 83, 91, 107 and 115 were detected. The peaks at  $m/z$  27, 29, 41, 43, 55, 57, 69, and 83 were due to the fragmentation of non-aromatic hydrocarbons (Canagaratna et al. 2007). The peak at  $m/z$  44 indicated the presence of carboxylic acids (Canagaratna et al. 2007). The peaks at  $m/z$  77 and 91 resulted from aromatic compounds (Ng, Canagaratna, Jimenez, et al. 2010, McLafferty and Tureek 1993). Therefore, the pyrolysis products were comprised of a mixture of non-aromatic hydrocarbons, carboxylic acids and aromatic compounds.

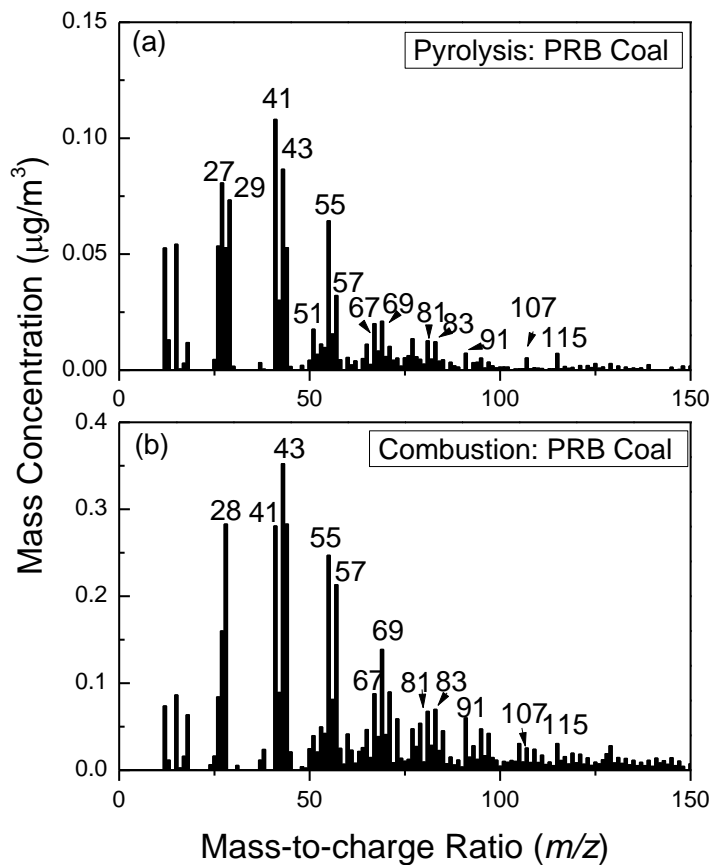


Figure 4.2. AMS spectrum of (a) organic products from pyrolysis of PRB coal and (b) organic aerosols from combustion of PRB coal

A large number of organic species were detected when pulverized PRB coal was combusted in the drop tube furnace. Figure 4.2b shows the AMS spectrum for organic aerosols formed during the combustion of pulverized PRB coal. Comparisons between Figures 4.2a and 4.2b indicated similar peaks present at  $m/z$  41, 43, 44, 51, 55, 57, 67, 69, 81, 83, 91, 107 and 115, suggesting that the organic aerosols again consist of non-aromatic hydrocarbons, carboxylic acids and aromatic compounds. The similarity between the AMS spectra for both cases provides a strong

evidence that the organic aerosol produced from coal combustion originates from the products of coal pyrolysis.

The peak at  $m/z$  44 ( $\text{CO}_2^+$ ) is an important tracer of oxygenated organic compounds, which are mainly carboxylic acids (Canagaratna et al. 2007). In addition, fraction of  $\text{CO}_2^+$  to total organic matter ( $f_{44}$ ) is a value that indicates the extent of oxidation (Ng, Canagaratna, Jimenez, et al. 2010). The values of  $f_{44}$  are 0.067 and 0.075 for the pyrolysis products and organic aerosols from combustion, respectively. Thus, the organic aerosols from combustion are more oxygenated than pyrolysis products. This result suggests oxidative transformation of the pyrolysis products.

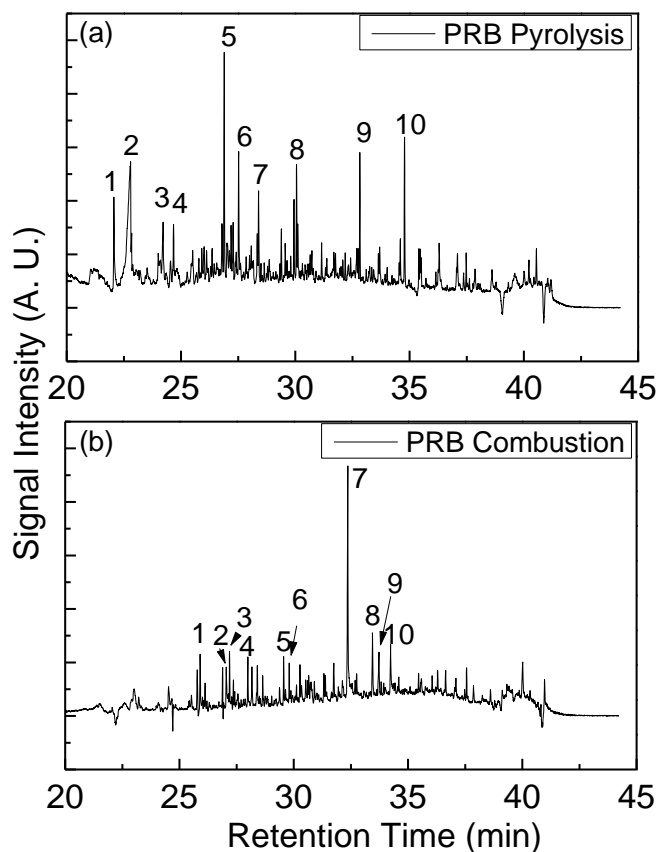


Figure 4.3. TAG chromatography of (a) organic aerosol from combustion of PRB coal; and (b) organic products from pyrolysis of PRB coal

The AMS is able to quantitatively measure almost any organic compound. However, due to the fragmentation of organic compounds under electron ionization, it is difficult to determine the exact molecular structure. To overcome this drawback, a TAG system was used. Figure 4.3a shows the TAG chromatograph of organic products from the pyrolysis of PRB coal, with the highest peaks labeled and identified in Table A2.1 (a complete list of compounds can be found in Table A2.3). 43% of all of the compounds formed during pyrolysis were also found in combustion emissions, and 57% of the compounds found in combustion emissions were also

found in pyrolysis products. A major peak found in both emissions was 1-tetradecene (Peak No. 1 in Fig. 4.3a, 4 in 4.3b).

The TAG results also show that there are many more aromatic compounds in pyrolysis products, and more oxygenated compounds in combustion emissions. Model coal structures exhibit hexagonal carbon arrangements, which leads to the high number of aromatic compounds after the structure begins to dissociate during pyrolysis. These aromatic compounds include benzoic acid (Peak No. 2 in Fig. 4.3b), 1,2,3,4-tetramethylnaphthalene (Peak No. 8 in Fig. 4.3b), 2-ethyl-2,4,8,8-tetramethyl-perhydrophenanthrene (Peak No. 9 in Fig. 4.3b), and 1-methyl-7-(1-methylethyl)-phenanthrene (Peak No. 10 in Fig. 4.3b). During the combustion process, many of these compounds are oxidized to form acidic compounds, such as hexadecanoic acid (Peak No. 7 in Fig. 4.3a), the largest organic peak found in the PRB combustion emissions, and octadecanoic acid (Peak No. 10 in Fig. 4.3a).

The TAG results confirm the findings from the AMS results. Similarities between chemical compositions from the organic aerosols in coal combustion and the products from coal pyrolysis strongly suggest that the products from coal pyrolysis are precursors to organic aerosols. Furthermore, many pyrolysis products are oxidized prior to final organic aerosol emissions. This process is summarized in Fig. 4.4. First, coal particles undergo pyrolysis and produce a large amount of organic volatiles. Most of the volatiles are combusted completely to form CO<sub>2</sub> and H<sub>2</sub>O, but a small fraction of organic compounds are partially oxidized or not oxidized, resulting in the presence of organic aerosol in the exhaust.

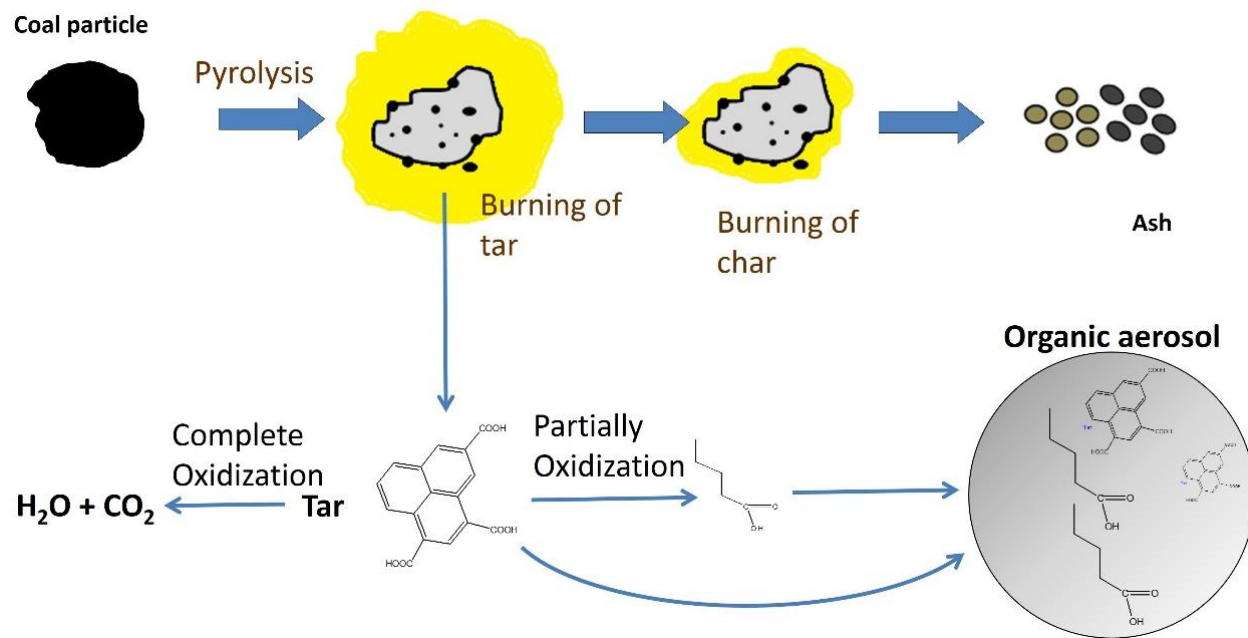


Figure 4.4. Summary of organic aerosol formation during coal combustion

#### 4.3.2 Comparison of PRB coal and ILL#6 coal

Figure 4.5a shows the AMS spectrum of organic products from pyrolysis of ILL#6 coal. This spectrum is similar to Fig. 4.2a. Peaks at  $m/z$  27, 29, 41, 43, 44, 55, 57, 69, 77, 91 and 115 are present. This indicates that the chemical composition of these organic products are non-aromatic hydrocarbons, carboxylic acids and some aromatic compounds, similar to PRB coal. Figure 4.5b shows the AMS spectrum of the organic aerosol from the combustion of ILL#6 coal. There are significant peaks at  $m/z$  42 and 44. However, the peaks at  $m/z$  55, 57, 69 are much lower than those in Fig. 4.5a, indicating much lower non-aromatic hydrocarbon content. The peak at  $m/z$  44 is the indicator for carboxylic acids (Canagaratna et al. 2007). Thus, it seems that the most of the organic aerosols generated from ILL#6 coal combustion were oxygenated organic compounds. The identified compounds were very different from aerosols generated from PRB coal

combustion (Fig. 4.2b), which contained a significant amount of non-aromatic hydrocarbons. Although the reason for this is not clear, it is hypothesized that the difference of chemical composition between the two coals is a factor. ILL#6 coal is a high sulfur content coal. During combustion, more  $\text{SO}_3$  was formed. And after the flue gas was cooled down, it may react with water vapor to form sulfuric acid, which can act as strong oxidizers. These compounds may play a role in the oxidation of organic aerosols.

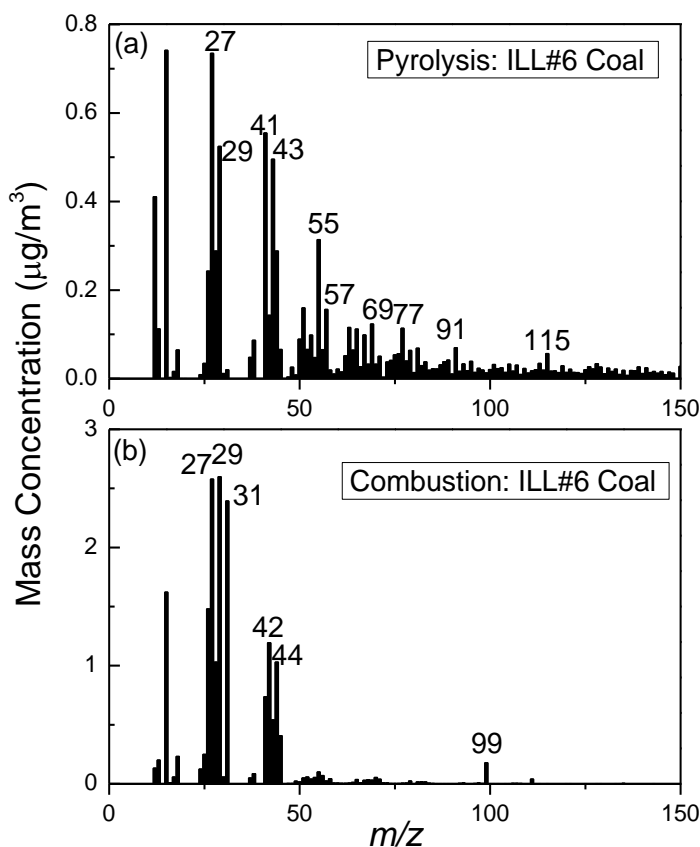


Figure 4.5. AMS spectrum of (a) organic aerosols from combustion of ILL#6 coal; and (b) organic products from pyrolysis of ILL#6 coal.



The TAG results for ILL#6 coal (the gas chromatography is shown in Fig. 4.6; the major compound list is shown in Table A2.2; and a complete compound list is shown in Table A2.4) shows a relatively similar trends to the emissions of PRB coal, though different compounds were identified. Many more aromatic compounds were found in both the pyrolysis and combustion emissions of ILL#6. Significant aromatic peaks in the pyrolysis products include benzoic acid (Peak No. 1 in Fig. 4.6a), 2-methoxy-4-vinylphenol (No. 2 in Fig. 4.6a), N-benzyl-n-ethyl-p-isopropylbenzamide (No. 4 in Fig. 4.6a), nonyl-benzene (No. 6 in Fig. 4.6a), 1-phenyl-naphthalene (No. 9 in Fig. 4.6a), and 2-ethyl-2,4,8,8-tetramethyl-perhydrophenanthrene (No. 11 in Fig. 4.6a). There were many alkenes found in the ILL#6 pyrolysis chromatography (significant peaks identified as alkenes include 1-tetradecene (No. 3 in Fig. 4.6a), 3-hexadecene (No. 5 in Fig. 4.6a), 3-eicosene (No. 8 in Fig. 4.6a).), while there were many alkanes found in the combustion chromatography (significant alkanes include tetradecane (No. 3 in Fig. 4.6b), 2,6,10-trimethyl dodecane (No. 6 in Fig. 4.6b), pentadecane (No. 5 in Fig. 4.6b), hexadecane (No. 7 in Fig. 4.6b), 2,6,10,14-tetramethyl pentadecane (No. 8 in Fig. 4.6b), and octadecane (No. 9 in Fig. 4.6b). It seems that aromatic compounds are relatively more stable than alkenes during the formation of organic aerosols, because more aromatic compounds were found in both the pyrolysis and combustion emissions. Less alkenes found in organic aerosols may suggest that the alkenes produced from the coal pyrolysis undergo oxidation reactions to form more oxygenated organic compounds; or addition reactions to form alkanes in the furnace.

Fewer oxygenated organic compounds were found in the combustion emissions of ILL#6 than in the PRB coal, which is not consistent with the AMS results. As previously mentioned, Figure 4.5b shows that the major components of organic aerosols were oxygenated organic compounds.

The AMS is able to detect any kind of organics. Therefore, the reason that the TAG did not find these oxygenated organic compounds is that many of these compounds could not be completely eluted through the GC column, which is used in the TAG for the separation of different chemical species (Williams et al. 2006). The combustion of ILL#6 coal may produce many of these highly oxygenated organics which may not be detected in the TAG. There were many compound matches seen between the pyrolysis emissions of the two coals. The significant peaks found in both pyrolysis emissions include benzoic acid (No. 2 in Fig 4.3a, 1 in 4.5a), tetradecene (No. 4 in Fig. 3.3a, 3 in 3.5a), and 2-ethyl-2,4,8,8-tetramethyl-perhydrophenanthrene (No. 9 in Fig 4.3a, 11 in 4.5a). In addition, the pyrolysis of ILL#6 coal produced more aromatic compounds than the pyrolysis of PRB coal, which may suggest that ILL#6 coal has higher fraction of aromatic rings in its coal structure.

Very few of the same compounds were found in the combustion emissions of both ILL#6 coal and PRB coal. Many non-aromatic hydrocarbons were found in both combustion chromatography results, however there were more alkenes in the PRB combustion emissions and more alkanes in the ILL#6 combustion emissions. This could be due to the presence of carbon-carbon double bonds in alkenes from ILL#6 coal combustion may be oxidized by sulfuric acid or sulfate to form highly oxygenated compounds which are difficult to detect in the TAG.

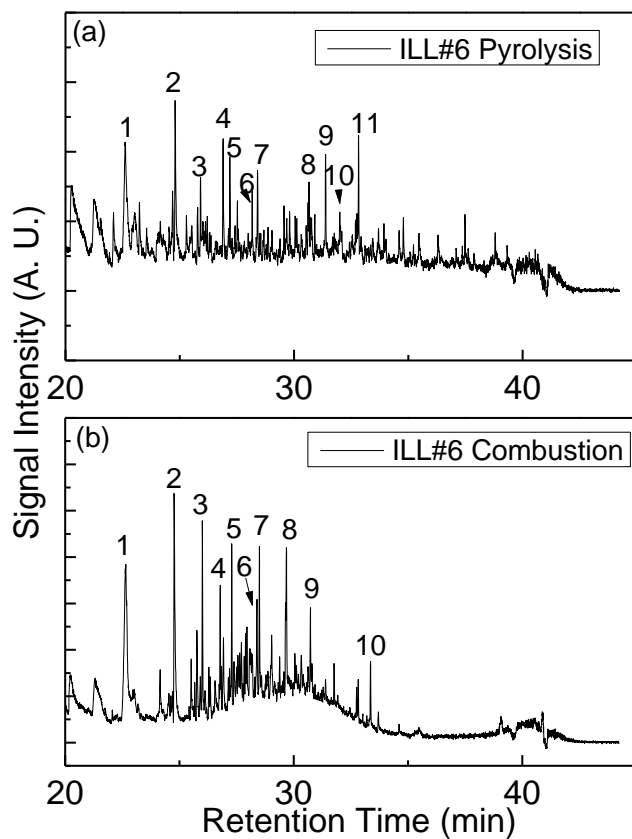


Figure 4.6. TAG chromatography of (a) organic aerosol from combustion of ILL#6; and (b) organic products from pyrolysis of ILL#6 coal .

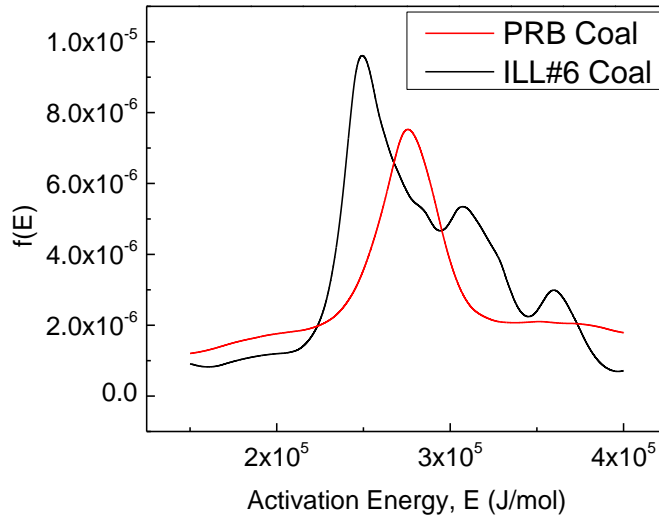


Figure 4.7. Activation energy distributions for PRB coal and ILL#6 coal obtained by DAEM model.

#### 4.3.3 Modeling of coal pyrolysis

Pyrolysis can be viewed as a combination of multiple parallel first order reactions. In order to determine the kinetic parameters for those reactions, such as activation energy distribution ( $f(E)$ ), a distributed activation energy model, developed by Miura and Maki (1998), was applied to the results from TGA of coals. Noticeably, it is well known that there is a large difference between the TGA experiment and the actual coal pyrolysis happened in coal combustion, especially in heating rate. Higher heating rate may result in releasing more organic volatiles. The method (Miura and Maki, 1998) that we used here has been widely used for estimating kinetic parameters for coal pyrolysis. Although the heating rate in the TGA is much lower, the kinetic data obtained from this method can still provide us some information about coal pyrolysis.

Figure A2.1a and A2.1b show the TGA curves of PRB coal and ILL#6 coal at three different heating rates: 5, 10 and 20 K/min. The temperature range is from 378 to 1073 K. Temperatures below 378K are not shown, because only moisture is released in this stage. Figure 4.7 shows the  $f(E)$  curves while Fig. A2.1c shows the corresponding pre-exponential factors ( $k_0$ ) for each activation energy ( $E$ ). The curve for PRB coal has a unimodal distribution which peaks at around 280 kJ. There are several peaks in the  $f(E)$  curve for ILL#6 coal. The highest peak occurs at 250 kJ, which is lower than for PRB coal. However, the other two peaks have significant higher activation energies when compared to PRB coal. These additional peaks may originate from pyrolysis of aromatic compounds, which have higher bond energies than carbon-carbon single or double bond. This is consistent with the TAG results, which show that the pyrolysis of ILL#6 coal produced more aromatic compounds.

#### **4.4 Conclusions**

This study presents a detailed comparison of the chemical compositions of organic aerosols generated from coal combustion and organic tars from coal pyrolysis. Two pulverized coals, PRB coal and ILL#6 coal, were combusted in a drop-tube furnace and produced organic aerosols, whose chemical compositions were then analyzed using an aerosol mass spectrometer (AMS) and a thermal desorption aerosol gas chromatograph (TAG). These two coals were also sent through a flat-flame system, and the composition of the resultant products of the fast pyrolysis process were measured using AMS and TAG. The major chemical components for both combustion organic aerosols and pyrolysis products were identified to be non-aromatic hydrocarbons, carboxylic acids and aromatic compounds. The similarities strongly suggest that the coal pyrolysis products are the precursors of organic aerosols. Several additional

carboxylic acids/oxygenated organic compounds were found in the pyrolysis products, indicating that many pyrolysis products are oxidized before final emissions of organic aerosols.

The distributed activation energy model (DAEM) was applied to obtain the kinetic parameters of the pyrolysis of coal. The activation energy distribution,  $f(E)$ , for PRB coal pyrolysis peaks at around 280 kJ, while the  $f(E)$  curve for ILL#6 coal has three peaks: at 250 kJ, 310 kJ, and 360 kJ, from highest to lowest. The second and third peaks at higher activation energies may originate from pyrolysis of aromatic compounds. This is consistent with the TAG results, which show that the pyrolysis of ILL#6 coal produced more aromatic compounds.

#### 4.5 Reference

Allan, J. D., J. L. Jimenez, P. I. Williams, M. R. Alfarra, K. N. Bower, J. T. Jayne, H. Coe, and D. R. Worsnop. 2003. "Quantitative sampling using an Aerodyne aerosol mass spectrometer 1. Techniques of data interpretation and error analysis." *J. Geophys. Res.* no. 108 (D3):4090. doi: 10.1029/2002jd002358.

Brown, A. L., and T. H. Fletcher. 1998. "Modeling Soot Derived from Pulverized Coal." *Energy & Fuels* no. 12 (4):745-757. doi: 10.1021/ef9702207.

Canagaratna, M. R., J. T. Jayne, J. L. Jimenez, J. D. Allan, M. R. Alfarra, Q. Zhang, T. B. Onasch, F. Drewnick, H. Coe, A. Middlebrook, A. Delia, L. R. Williams, A. M. Trimborn, M. J. Northway, P. F. DeCarlo, C. E. Kolb, P. Davidovits, and D. R. Worsnop. 2007. "Chemical and microphysical characterization of ambient aerosols with the aerodyne aerosol mass spectrometer." *Mass Spectrometry Reviews* no. 26 (2):185-222. doi: 10.1002/mas.20115.

Coggon, M. M., A. Sorooshian, Z. Wang, A. R. Metcalf, A. A. Frossard, J. J. Lin, J. S. Craven, A. Nenes, H. H. Jonsson, L. M. Russell, R. C. Flagan, and J. H. Seinfeld. 2012. "Ship impacts on the marine atmosphere: insights into the contribution of shipping emissions to the properties of marine aerosol and clouds." *Atmos. Chem. Phys.* no. 12 (18):8439-8458. doi: 10.5194/acp-12-8439-2012.

Damle, A. S., D. S. Ensor, and M. B. Ranade. 1982. "Coal Combustion Aerosol Formation Mechanisms - A Review." *Aerosol Science and Technology* no. 1 (1):119-133.

Daukoru, S. 2010. *The Role of Flue-Gas Recycle in Submicrometer Particle Formation during Oxy-Combustion of American and Chinese Coals*, Department of Energy, Environmental & Chemical Engineering, Washington University in St. Louis.

DeCarlo, P. F., J. R. Kimmel, A. Trimborn, M. J. Northway, J. T. Jayne, A. C. Aiken, M. Gonin, K. Fuhrer, T. Horvath, K. S. Docherty, D. R. Worsnop, and J. L. Jimenez. 2006. "Field-Deployable, High-Resolution, Time-of-Flight Aerosol Mass Spectrometer." *Analytical Chemistry* no. 78 (24):8281-8289. doi: 10.1021/ac061249n.

Haynes, B. S., M. Neville, R. J. Quann, and A. F. Sarofim. 1982. "Factors Governing the Surface Enrichment of Fly-ash in Volatile Trace Species." *Journal of Colloid and Interface Science* no. 87 (1):266-278.

Jimenez, J. L., J. T. Jayne, Q. Shi, C. E. Kolb, D. R. Worsnop, I. Yourshaw, J. H. Seinfeld, R. C. Flagan, X. Zhang, K. A. Smith, J. W. Morris, and P. Davidovits. 2003. "Ambient aerosol sampling using the Aerodyne Aerosol Mass Spectrometer." *J. Geophys. Res.* no. 108 (D7):8425. doi: 10.1029/2001jd001213.

McLafferty, F. W., and F. Tureek. 1993. *Interpretation of Mass Spectra*. Sausalito: Univ Science Books.

Miura, K., and T. Maki. 1998. "A simple method for estimating  $f(E)$  and  $k(0)(E)$  in the distributed activation energy model." *Energy & Fuels* no. 12 (5):864-869. doi: 10.1021/ef970212q.



Ng, N. L., M. R. Canagaratna, J. L. Jimenez, Q. Zhang, I. M. Ulbrich, and D. R. Worsnop. 2010. "Real-Time Methods for Estimating Organic Component Mass Concentrations from Aerosol Mass Spectrometer Data." *Environmental Science & Technology* no. 45 (3):910-916. doi: 10.1021/es102951k.

Peltier, R. E., A. P. Sullivan, R. J. Weber, A. G. Wollny, J. S. Holloway, C. A. Brock, J. A. de Gouw, and E. L. Atlas. 2007. "No evidence for acid-catalyzed secondary organic aerosol formation in power plant plumes over metropolitan Atlanta, Georgia." *Geophys. Res. Lett.* no. 34 (6):L06801. doi: 10.1029/2006gl028780.

Quann, R. J., M. Neville, M. Janghorbani, C. A. Mims, and A. F. Sarofim. 1982. "Mineral Matter and Trace-element Vaporization in a Laboratory-pulverized Coal Combustion System." *Environmental Science & Technology* no. 16 (11):776-781.

Seinfeld, J. H., and S. N. Pandis. 2006. *Atmospheric Chemistry and Physics: From Air Pollution to Climate Change*.

Sun, Y. L., Z. F. Wang, P. Q. Fu, T. Yang, Q. Jiang, H. B. Dong, J. Li, and J. J. Jia. 2013. "Aerosol composition, sources and processes during wintertime in Beijing, China." *Atmos. Chem. Phys.* no. 13 (9):4577-4592. doi: 10.5194/acp-13-4577-2013.

Skeen, S. A., B. M. Kumfer, R. L. Axelbaum. 2010. " Nitric Oxide Emissions during Coal and Coal/Biomass Combustion under Air-Fired and Oxy-fuel Conditions." *Energy & Fuels.* no. 24 :4414-4152. doi: 10.1021/ef100299n.

Suriyawong, A., M. Gamble, M.-H. Lee, R. Axelbaum, and P. Biswas. 2006. "Submicrometer Particle Formation and Mercury Speciation Under O<sub>2</sub>-CO<sub>2</sub> Coal Combustion." *Energy & Fuels* no. 20 (6):2357-2363. doi: 10.1021/ef060178s.

Wang, X., B. J. Williams, Y. Tang, Y. Huang, L. Kong, X. Yang, and P. Biswas. 2013. "Characterization of organic aerosol produced during pulverized coal combustion in a drop tube furnace." *Atmos. Chem. Phys. Discuss.* no. 13 (2):3345-3377. doi: 10.5194/acpd-13-3345-2013.

Warnatz, J., U. Maas, and R. W. Dibble. 2006. *Combustion: Physical and Chemical Fundamentals, Modeling and Simulation, Experiments, Pollutant Formation*. 4 ed: Springer.

Williams, A., M. Pourkashanian, and J. M. Jones. 2001. "Combustion of pulverised coal and biomass." *Progress in Energy and Combustion Science* no. 27 (6):587-610. doi: Doi: 10.1016/s0360-1285(01)00004-1.

Williams, B. J., A. H. Goldstein, N. M. Kreisberg, and S. V. Hering. 2006. "An In-Situ Instrument for Speciated Organic Composition of Atmospheric Aerosols: Thermal Desorption Aerosol GC/MS-FID (TAG)." *Aerosol Science and Technology* no. 40 (8):627-638. doi: 10.1080/02786820600754631.

Zaveri, R. A., C. M. Berkowitz, F. J. Brechtel, M. K. Gilles, J. M. Hubbe, J. T. Jayne, L. I. Kleinman, A. Laskin, S. Madronich, T. B. Onasch, M. S. Pekour, S. R. Springston, J. A. Thornton, A. V. Tivanski, and D. R. Worsnop. 2010. "Nighttime chemical evolution of aerosol and trace gases in a power plant plume: Implications for secondary organic nitrate and

organosulfate aerosol formation, NO<sub>3</sub> radical chemistry, and N<sub>2</sub>O<sub>5</sub> heterogeneous hydrolysis." *J. Geophys. Res.* no. 115 (D12):D12304. doi: 10.1029/2009jd013250.

Zhang, Y., J. J. Schauer, Y. Zhang, L. Zeng, Y. Wei, Y. Liu, and M. Shao. 2008. "Characteristics of Particulate Carbon Emissions from Real-World Chinese Coal Combustion." *Environmental Science & Technology* no. 42 (14):5068-5073. doi: 10.1021/es7022576.

## **CHAPTER 5. EFFECT OF SULFUR CONTENT IN COAL ON ORGANIC AEROSOL FORMATION DURING COAL COMBUSTION**

*The results of this chapter has been compiled as a paper: Wang, X.; Wang, H.; Huang, Y.; Jing, H.; Wang, W.N.; Cui, W.; Williams, B. J.; Gross, M. L.; Yang, X.; and Biswas, P., Evidence for A New Source of Nitrogen-Containing Organic Aerosol: Combustion of High Sulfur Content Coal. Submitted to Environmental Science & Technology Letters.*

*Supplementary figures and tables are available in Appendix 3*

## **Abstract**

The previous chapter proposed a mechanism that links organic aerosol formation with inorganic aerosol formation during coal combustion. This work shows that organic aerosol formation was significantly enhanced when higher sulfur content coal was burning. A strong correlation between organic aerosol mass and particulate sulfate concentration had been determined, which confirmed the link between organic aerosol formation and inorganic aerosol formation during coal combustion. In addition, this work also found that combustion of high sulphur content coal produces large fractions of nitrogen-containing organic aerosols. It is proposed that coal pyrolysis produces many nitrogen-containing organic volatiles, and acidic particulate sulfate can absorb these volatiles to the particle phase via neutralization reactions.

## 5.1 Introduction

Atmospheric aerosols play a crucial role in radiative forcing and climate change (Seinfeld and Pandis 2006). Organic aerosol (OA) comprises about 20-80% of the total fine particulate mass (Hallquist et al. 2009). Significant fractions of particulate organic matter are nitrogen-containing organic compounds (NOC), which may contribute up to 18% of the total fine aerosol mass (Aiken et al. 2009, Zhang et al. 2002). NOCs also account for a major fraction of the total nitrogen in atmospheric aerosols (Cornell et al. 2001, Mace et al. 2003). The deposition of nitrogen-containing organic aerosol is an essential part of the nitrogen-cycle in the ecosystem (Cornell et al. 1995). The major identified sources for nitrogen-containing OA include biomass burning (Laskin et al. 2009), partitioning of atmospheric amine species (Ge et al. 2011a, b) and other secondary organic aerosol formation processes (Alfarra et al. 2006). However, due to the complexity of NOCs in atmospheric aerosols, their sources/formation processes have yet to be fully explored.

Pulverized coal combustion is the main source for electricity or heat generation. But it is also a major source of particulate matter in the atmosphere, particularly in developing countries (Wang, Williams, et al. 2013b). The main component of aerosols produced from a well-operated coal-fired boiler is inorganic matter (Linak and Wendt 1994). However, organic matter may also contain certain fraction of fine aerosol mass, particularly from boilers with low combustion efficiency and inefficient particle capture device (Zhang et al. 2008). In some developing countries, such as China, coal combustion has been identified as one of the major source of atmospheric organic aerosol (Sun et al. 2013, Hu et al. 2013, Wang, Williams, et al. 2013b). This work, surprisingly, shows that nitrogen-containing organic matter comprises a large fraction

of total organic aerosol emissions from the combustion of high sulfur content coal, which is widely used in developing countries.

## 5.2 Experimental Section

### 5.2.1 Experimental Set-up

Figure 5.1 shows the experimental set-up for coal combustion, which consists of a Lindberg/Blue M Model HTF55342C drop-tube furnace (ThermoElectron Corp., USA) with a 5.72 cm inner diameter and 121.92 cm long alumina tube connected to many aerosol instruments, including a high-resolution time-of-flight aerosol mass spectrometer (HR-ToF-AMS, Aerodyne Research, MA, USA), and a scanning mobility particle sizer (SMPS, TSI Inc., Shoreview MN, USA), etc. Illinois No. 6 (ILL#6) coals or PRB coal mixed with different ratios of elemental sulfur particles were combusted. The proximate and ultimate analyses of the PRB coal and ILL#6 coal used in this study can be found in Table 5.1. Pulverized coal particles (diameters  $<50\ \mu\text{m}$ ) was introduced into the drop-tube furnace using a self-made coal feeder (1982). The coal feed rate was fixed at 2.5 g/hr. A total of 3 liter/min (LPM) of air was fed into the furnace: 0.5 LPM of air went through the coal feeder to carry coal particles, and another 2.5 LPM of air was directly fed into the drop-tube furnace. Thus, the fuel-air equivalence ratio was 0.083. The temperature on the wall of the alumina tube was set at 1373 K. The detailed description, including residence time, temperature profile, of the drop-tube system can be found in Appendix 5. At the exit of the drop-tube, the exhaust gas was diluted by a 5 LPM of particle-free air. Then, the diluted exhaust gas was passed through a six-stage particle cascade impactor (Mark III, Pollution Control System Corp, Seattle, WA) to remove aerosols with particle diameter larger than 500 nm. After the impactor, a 0.5 LPM slip-stream was mixed with a 3.8 LPM of particle-free air to achieve secondary dilution. A HR-TOF-AMS and a SMPS were used to characterize chemical

compositions and size distribution of fine particles in the diluted exhaust gas. Fine particles from coal combustion exhaust gas were also collected on Teflon filters for further offline analysis with by (1) an high-performance liquid chromatography coupled with electrospray ion source and ultrahigh resolution time-of-flight mass spectrometer (UPLC/ESI-UHRTOFMS) and (2) an X-ray fluorescence spectroscopy (XRF, Panalytical Epsilon 5 energy dispersive XRF spectrometer, Almelo, Netherlands).

Table 5.1. Proximate and ultimate analysis of coals

	<b>ILL#6 Coal</b>	<b>PRB Coal*</b>
Proximate Analysis (% wt)		
Volatile Matter <sup>a</sup>	42	48.3
Fixed Carbon <sup>a</sup>	48	42.9
Ash <sup>a</sup>	10	8.0
Moisture <sup>b</sup>	13.5	27.7
Lower Heating Value <sup>a</sup> (MJ/kg)	29.6	28.0
Ultimate Analysis (% wt) <sup>a</sup>		
Carbon	71	67.3
Nitrogen	1.3	0.96
Hydrogen	5	4.58
Oxygen	9.13	19.9
<u>Sulfur</u>	<u>3.47</u>	<u>0.57</u>
Chlorine	0.11	0.01
Fluorine		0.796



\*Source: (Daukoru 2010)

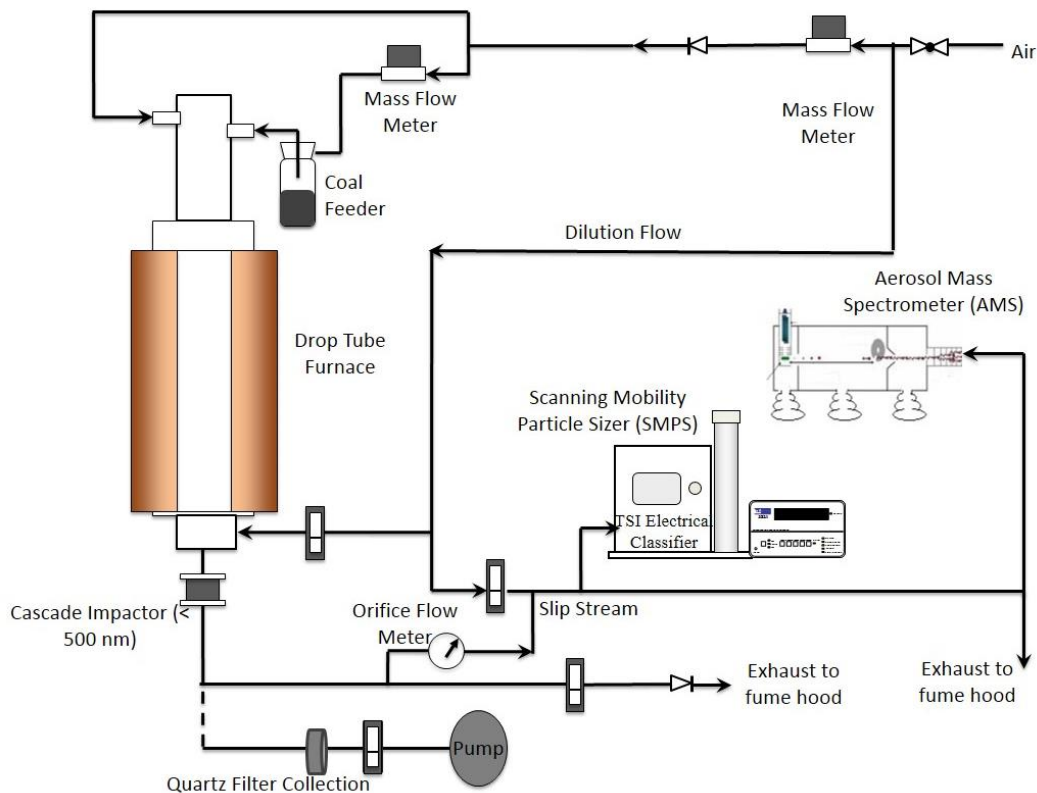


Figure 5.1. Schematic diagram of the experimental set-up .

#### 5.4.2 High Resolution Time-of-flight Aerosol Mass Spectrometer (HR-ToF-AMS)

The literatures (Canagaratna et al. (2007), Allan et al. (2003), Jimenez et al. (2003), DeCarlo et al. (2006)) provides a detailed description of HR-ToF-AMS. Briefly, aerosol particles passed through an aerodynamic focusing lens which makes most of the particles move in a narrow beam. Particle size can be obtained by measuring the velocity of the particles at the exit of the aerodynamic lens. The particles are then collected on a hot vaporizer (600 °C). Organic matter and some inorganic matter are evaporated and then immediately ionized by electron impact. The produced ions are introduced to time-of-flight mass spectrometry, which can accurately determine the mass-to-charge ratios for these ions.

### 5.2.3 Analysis using HPLC/ESI-UHR-TOFMS

Aerosol samples were collected on Teflon filters (PALL Life Sciences, 47 mm diameter, 1.0  $\mu$ m pore size, Teflo membrane). The filter samples were extracted in 5 mL of methanol by 40 min of sonication. The extract was blown dry under a gentle N<sub>2</sub> stream (without added heat) to 0.5 ml solution, which was then analyzed by a high-performance liquid chromatography (HPLC) coupled with electrospray ion source and ultrahigh resolution time-of-flight mass spectrometer (HPLC/ESI-UHR-TOFMS).

10  $\mu$ L sample in methanol was dissolved in 90  $\mu$ L H<sub>2</sub>O and injected onto Phenomene RP C18 Column (150\*2.00 mm, 4 micron) manually. The sample was then eluted and separated from this column via an Agilent 1200 HPLC (Santa Clara, CA) with a gradient operated at 200  $\mu$ L/min flow rate, and injected into a Maxis (Bruker, Bremen, Germany) quadrupole time-of-flight (QTOF) mass spectrometer via ESI. The following settings was used for the ESI-UHR-TOFMS: capillary voltage was 3.8 kV; pressure of nebulizer gas was 1.0 bar; drying gas flow rate and temperature were 8.0 L/min and 200 °C, respectively. The following settings was used for the HPLC: Solvent A was water containing 0.1% formic acid, and solvent B was 80% acetonitrile, 20% water containing 0.1% formic acid. The gradient settings were 2–15% solvent B in 15 min, 15–20% solvent B in 10 min, 20–25% solvent B in 10 min, 25–50% solvent B in 10 min, 50–80% solvent B in 15 min, 80–90% solvent B in 5 min, and isocratic flow at 100% solvent B for 2 min and then returned to 2% solvent B in 13 min.

## 5.3 Results and Discussion

Illinois No. 6 (ILL#6) coal is a high sulfur content coal; its sulfur content is 3.47% (its proximate and ultimate analysis is shown in Table 5.1). We combusted it in a drop-tube furnace, which is

widely used as a laboratory-scale coal combustor (Card and Jones 1995, Cloke et al. 2002). A high-resolution aerosol mass spectrometer (HR-AMS) and a scanning mobility particle sizer were deployed to analyze the chemical characterization and size distributions of fine aerosol emissions ( $PM_{10}$ ) from coal combustion (Fig. 4.1). A high concentration of submicrometer particles were formed in the flue gas (Fig. 4.2). Aerosol samples, collected on Teflon filters, were extracted by methanol and analyzed by a high-performance liquid chromatography coupled with an electrospray ion source and an ultrahigh resolution time-of-flight mass spectrometer (HPLC/ESI-UHRTOFMS). Figure 5.3 shows the AMS organic mass spectrum for fine particulate matter from ILL#6 coal combustion. A large number of peaks, such as  $m/z$  30, 42, 43, and 44, belongs to the CHN ( $C_xH_yN_z^+$ ) group, clearly demonstrating the presence of nitrogen-containing organic species. Low signal intensities of  $m/z$  55 and 57 indicate the low concentration of hydrocarbons. To verify the molecular formulas of these important peaks, the high resolution peak patterns are shown in Fig. 5.3B. The unit mass resolution (UMR) peak at  $m/z$  30 is actually composed of two peaks:  $CH_2O^+$  and  $CH_4N^+$ .  $C_2H_6^+$  may not contribute much to this UMR peak, since  $C_2H_6^+$  ( $m/z$  30.047) is away from the center of the peak. The UMR peak at  $m/z$  42 is composed of  $C_2H_2O^+$ ,  $C_2H_4N^+$  and  $C_3H_6^+$ .  $C_2H_4N^+$  should contribute the largest fraction, because the exact mass of  $C_2H_4N^+$  is located at the center of the UMR peak at  $m/z$  42. Similarly, the UMR peak at  $m/z$  43 is composed of  $C_2H_3O^+$ ,  $C_2H_5N^+$  and  $C_3H_7^+$ .  $C_2H_4N^+$  should be the main peak. The peak at  $m/z$  44 is usually considered to be  $CO_2^+$ , which is an indicator of oxygenated organic aerosol (Canagaratna et al. 2007). But, surprisingly, Fig. 5.3B shows that  $m/z$  44 is composed of  $CO_2^+$ ,  $C_2H_4O^+$ ,  $C_2H_6N^+$  and  $C_3H_8^+$ , among which  $C_2H_6N^+$  is a dominant peak at  $m/z$  44.  $CO_2^+$  has a much smaller contribution to this UMR peak. The contributions from  $C_2H_4O^+$  and  $C_3H_8^+$  are not significant, because both of them are away

from the centers of the two peaks at  $m/z$  44. Elemental ratios are listed in Fig. 5.4. The N/C ratio is about 0.048, which is much higher than biomass burning aerosols (He et al. 2010).

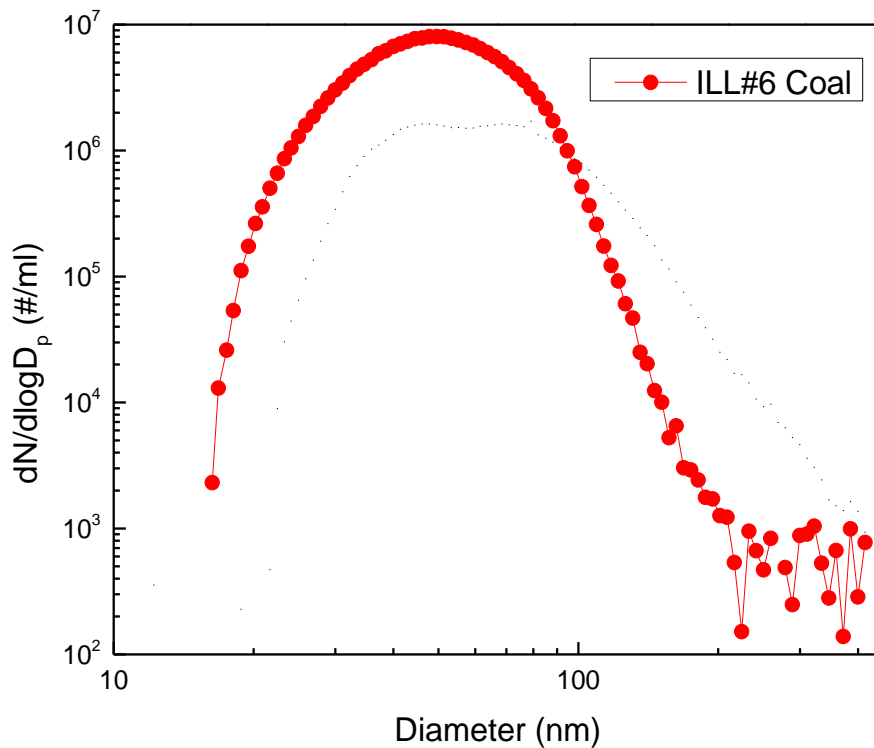
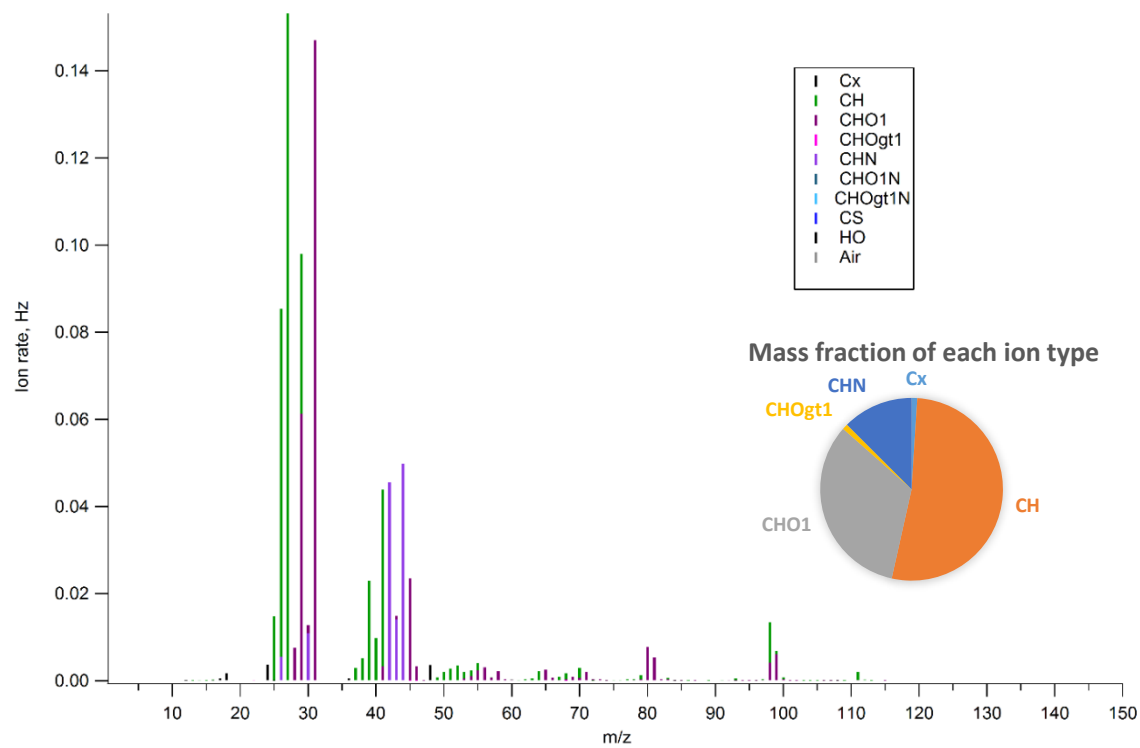


Figure 5.2. Size distribution of submicrometer particles from the combustion of ILL#6 coal (Combustion condition: temperature: 1376 K, air flow rate: 3 LPM, fuel-air equivalence ratio: 0.083)

(A)



(B)

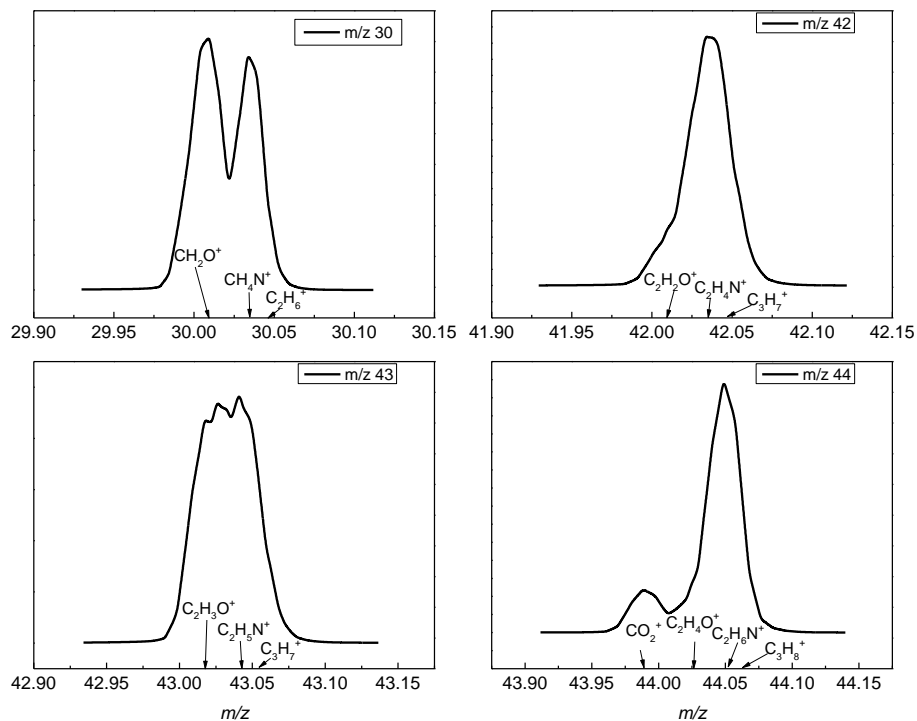


Figure 5.3 (A) AMS mass spectrum; and (B) High resolution peak patterns for fine organic particulate matter from combustion of ILL#6 coal, a high sulfur content coal. CHOgt1 represents a group of high resolution ions, including CHOgt1, which represents a group of high resolution ions, including  $\text{CO}_2^{+2}$ ,  $\text{CO}_2^+$ ,  $^{13}\text{CO}_2^+$ ,  $\text{CH}_2\text{O}_2^+$ ,  $\text{C}_3\text{O}_2^+$ ,  $\text{C}_8\text{H}_5\text{O}_3^+$ ,  $\text{C}_8\text{H}_7\text{O}_4^+$ ,  $\text{C}_{16}\text{H}_{23}\text{O}_4^+$  (Combustion condition: temperature: 1376 K, air flow rate: 3 LPM, fuel-air equivalence ratio: 0.083)

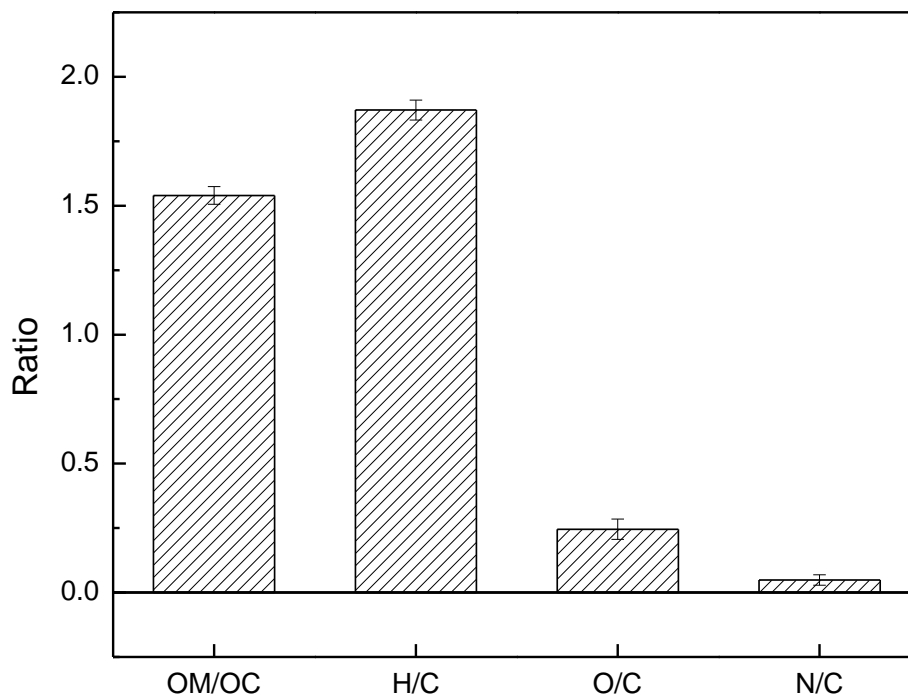


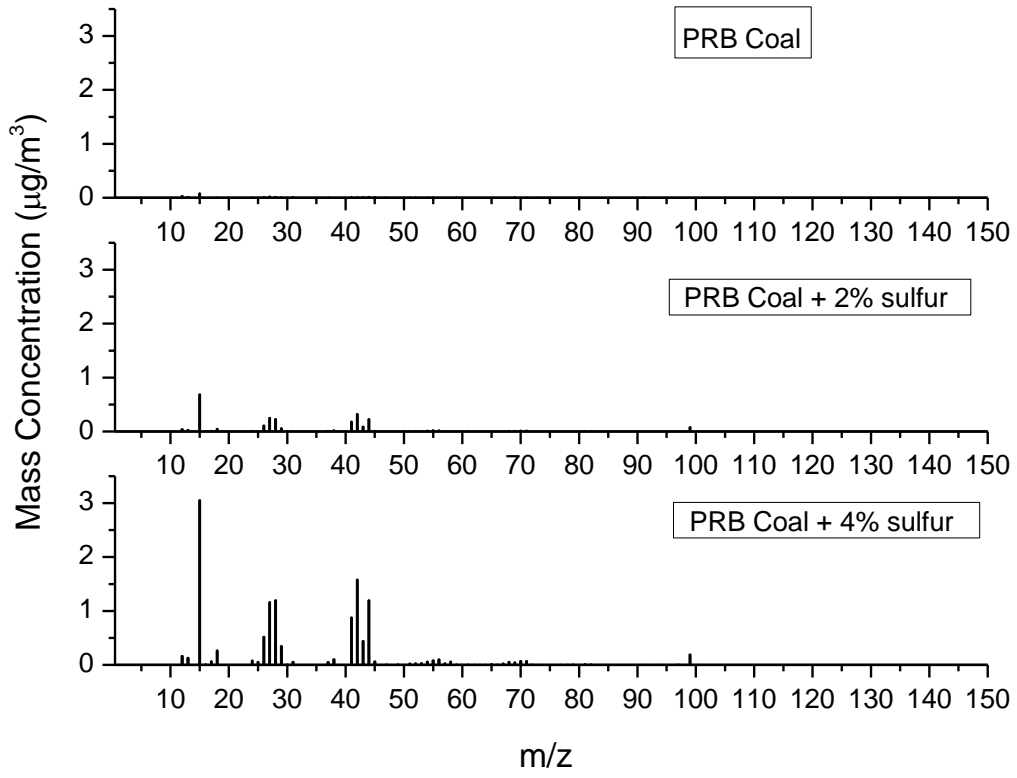
Figure 5.4 Elemental ratios for fine organic particulate matter from the combustion of ILL#6 coal, a high sulfur content coal. OM means “organic matter”. And OC means “organic carbon”. OM/OC means the ratio between the mass of total organic matter and the mass of organic carbon. (Combustion condition: temperature: 1376 K, air flow rate: 3 LPM, fuel-air equivalence ratio: 0.083).

Our previous study has reported that the AMS organic mass spectrum for fine particulate matter from the combustion of PRB coal, a low sulfur content coal (its sulfur content is 0.57%, Table 5.1), does not show any significant nitrogen-containing organic peaks (Wang, Williams, et al. 2013b). Therefore, a key question is asked: why are the organic aerosol emissions from high sulfur content coal combustion so different from low sulfur content coal combustion? To bridge

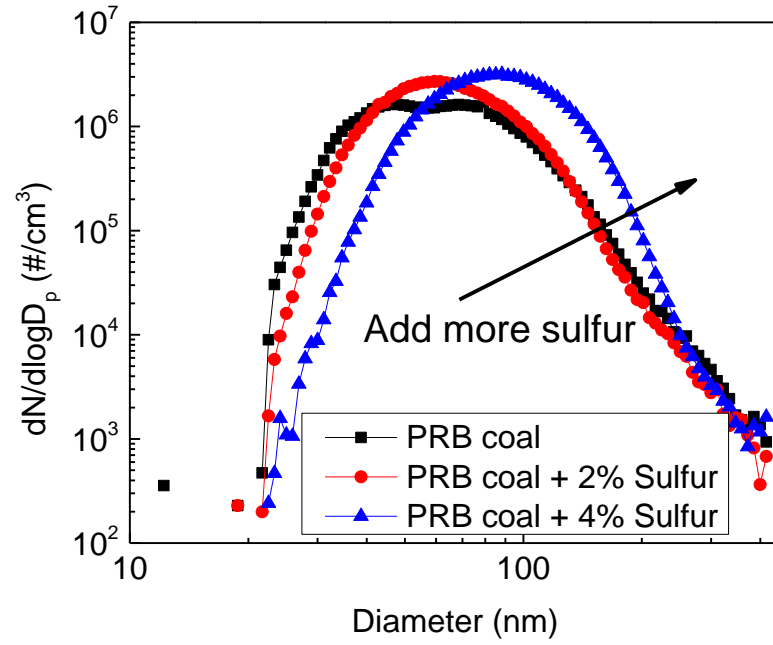
the low and the high sulfur content coals, sulfur was mixed with PRB coal to change its sulfur content gradually from low to high. Then the coal mixtures were combusted in the drop-tube furnace. Figure 5.5 shows the characteristics of submicrometer particles from the combustion of PRB coals mixed with different contents of sulfur (0, 2% and 4%, respectively). When the sulfur content in coal is increased, the formation of organic aerosol was significantly enhanced (Fig. 5.5A), which suggests that sulfur content does play a role in organic aerosol formation. Similar to the ILL#6 coal combustion, the high resolution AMS spectrum from the combustion of PRB coal plus 4% sulfur also shows the presence of a large amount of nitrogen-containing organic peaks (Fig. 5.6). It is a very surprising finding that nitrogen-containing organic aerosol formation actually relates to the sulfur content in coal.



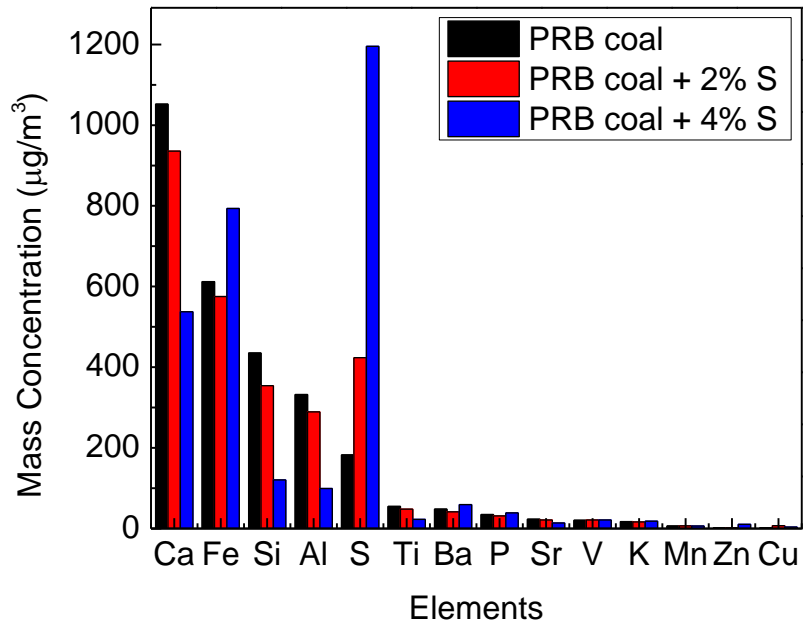
(A)



(B)



(C)



(D)

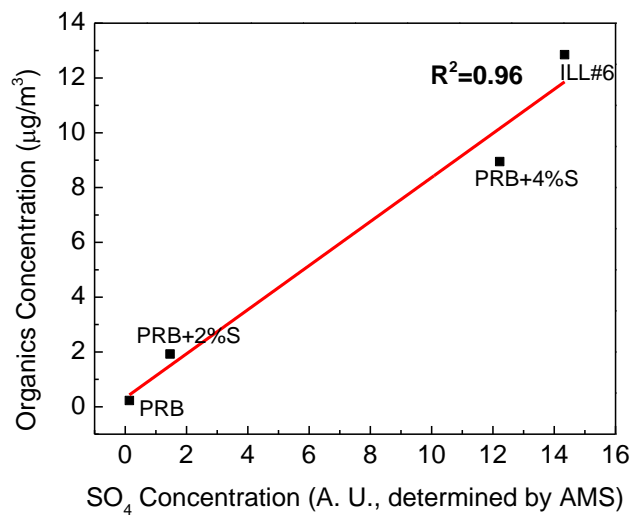


Figure 5.5 (A) AMS organic spectrum; (B) Size distributions; (C) Elemental compositions; and (D) Correlation of concentration between SO<sub>4</sub> species and the organic matter of submicrometer particles from the combustion of PRB coals mixed with different contents of elemental sulfur particles (Combustion condition: temperature: 1376 K, air flow rate: 3 LPM, air-fuel equivalence ratio: 10)

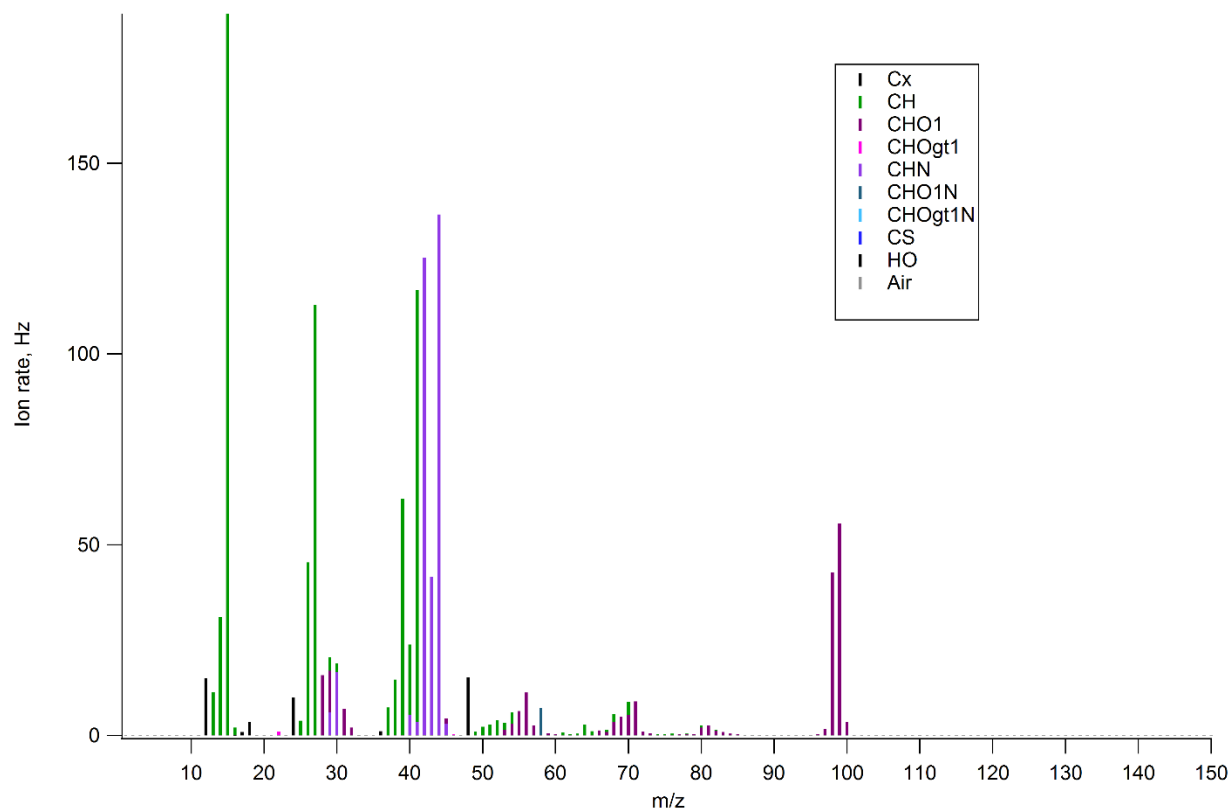


Figure 5.6 High resolution organic AMS spectrum of submicrometer particles from the combustion of PRB coals mixed with 4% elemental sulfur particles (Combustion condition: temperature: 1376 K, air flow rate: 3 LPM, fuel-air equivalence ratio: 0.083)

Our previous study reported that organic aerosol formation was associated with inorganic aerosol during coal combustion. Sulfur content can greatly affect inorganic aerosol formation. The particle size distributions show that higher concentrations of submicrometer particles were produced when the sulfur content in coal was increased (Fig. 5.5B). And the submicrometer particles from the combustion of higher sulfur content contain more sulfur (Fig. 5.5C). The reason has been well studied: combustion of higher sulfur content coal results in higher concentrations of  $\text{SO}_2$  in flue gas. A certain fraction of  $\text{SO}_2$  is converted into  $\text{SO}_3$ , which may

react with metal oxides to form sulfates and enter the particle phase. Thus, higher sulfur content coal combustion produces higher concentrations of submicrometer particles.

A strong correlation,  $R^2 = 0.96$ , between organic aerosol and  $\text{SO}_4$  (from sulfate) concentration has been found, see Fig. 5.5D, in which AMS can only provide a qualitative value for metal sulfate concentration. Figure A3.1 also shows a strong correlation between organic aerosol and particulate sulfur that was quantitatively determined by XRF. It demonstrates that sulfate particles play a critical role in organic aerosol formation. And a large fraction of these particulate organic compounds are nitrogen-containing species. Our previous study proposed the formation mechanism of organic aerosol during coal combustion: coal pyrolysis produces a large amount of organic volatiles, most of which is completely oxidized to  $\text{CO}_2$  and  $\text{H}_2\text{O}$ . Small fraction of these organic volatiles may be trapped by inorganic particles, which may protect them from complete oxidation; and finally form particulate organic emissions. All coals contain certain amounts of fuel nitrogen. For example, fuel nitrogen accounts for 1.0% and 1.3% of total coal dry mass for PRB coal and ILL#6 coal, respectively. It is well known that these nitrogen atoms are connected with aromatic clusters in coal with C-N bond (Haenel 1992, Wang et al. 2012). Coal pyrolysis can produce many nitrogen-containing organic volatiles (Kelemen et al. 1994, Kelemen et al. 1998). Pyrrolic, pyridinic and quaternary nitrogen typically accounts for 50-80, 20-40% and 0-20% of total nitrogen mass in coal, respectively (Mitrakirtley et al., 1993; Mullins et al., 1993). In addition, aromatic amine may also contribute a small fraction of coal nitrogen. For ILL#6 coal, pyrrolic, pyridinic and quaternary nitrogen accounts for 62, 26 and 12% of total nitrogen, respectively (Castro-Marcano 2011). During the coal devolatilization process, fuel nitrogen can either be released as organic volatiles or remain in char particles. The ratio is depending on the coal type and temperature (Glarborg et al., 2003). Almost all the

nitrogen-containing organic volatiles are the aromatic compounds (Chen et al., 1992). Some sulfate particles are acidic, such as iron sulfate; and the C-N groups are basic. These sulfate particles may help trap nitrogen-containing organic volatiles via acid-base neutralization reactions. Therefore, the nitrogen-containing organic compounds identified in this study are probably organic salts. Figure 5.7 summarizes the formation mechanism of the nitrogen-containing particulate organic compounds during combustion of high sulfur content coal. Noticeably, in this study, elemental sulfur was added to the coal. However, the natural forms of sulfur in coal are not elemental sulfur. The forms of sulfur present in coal include (1) pyrites ( $\text{FeS}_2$ ), (2) organic sulfur and (3) some minor fraction of sulfate. It is generally considered that organic sulfur in coal is present in four forms: (1) mercaptan or thiol, (2) sulfide or thio-ether, (3) disulfide and (4) aromatic systems containing the thiophene ring. Gluskoter and Simon (1968) reported that a mean ratio of pyritic to organic sulphur is about 1.56 for Illinois coal. For Illinois #6 coal, organic sulfur ranges from 0.4 to 3% of total coal mass (Gluskoter and Simon, 1968). During the coal burning, almost all the sulfur is oxidized to  $\text{SO}_2$ . And then some of  $\text{SO}_2$  is finally converted to sulfate particles. It is acidic sulfate particles that can enhance organic aerosol formation, according to the proposed mechanism (Fig. 3). Thus, the form of sulfur in coal may not be important to the formation of organic aerosol. The comparisons between Fig.5.2 and Fig.5.6 also strongly support this viewpoint: the high resolution AMS organic spectra from combustion of ILL#6 coal and combustion of PRB coal + 4% sulfur are very similar to each other, although their forms of sulfur are different. Both spectra contain large fractions of nitrogen-containing organic species.

To identify the molecular formula of organic compounds, fine particulate matter from the combustion of PRB coal plus 4% sulfur was collected on a Telfon filter. Then it was extracted

by methanol. The extract was analyzed by an HPLC/ESI-UHR-TOFMS. Figure A3.2 shows the total ion chromatography under ESI positive mode. Most of the signals came out after 40 min, indicating those compounds are very hydrophobic. The major peaks in Fig. A3.2 are listed in Table 5.2. Using accurate mass and isotopic patterns, the ion formula for each peak has been calculated. All major peaks have been identified as nitrogen-containing organic ions, which confirms the finding from the AMS results. Most of them also contain at least one O atom, suggesting they are oxygenated organic compounds.

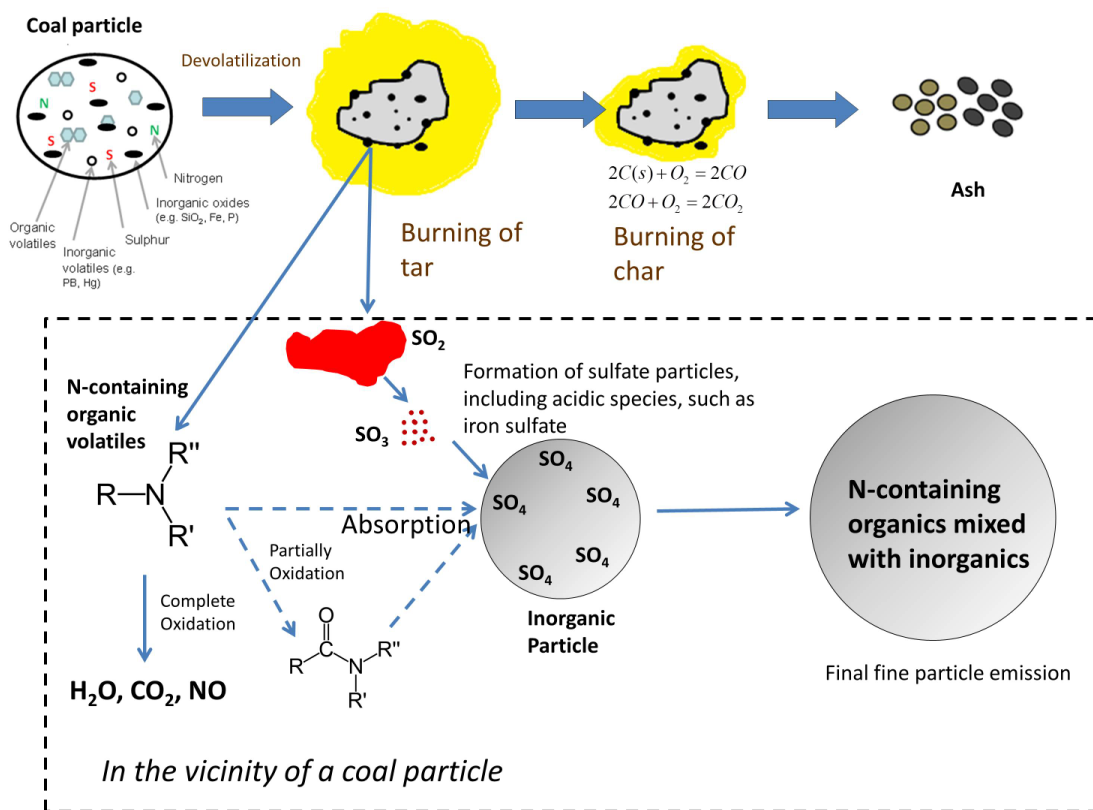


Figure 5.7 Formation mechanism of particulate nitrogen-containing organic matter during combustion high sulfur content coal.

Table 5.2. Identified Organic Compounds of the Methanol Extract from Submicrometer Particles Collected from the Combustion of PRB Coal Mixing with 4% Sulfur (by UPLC/ESI(+)/UHR-TOFMS)

Retention Time (min)	Major Peaks (m/z)	Calculated Ion Formula	Actual Mass of Calculated Formula	Error (ppm)
1.1	110.0089	C <sub>2</sub> H <sub>3</sub> N <sub>2</sub> O <sub>2</sub> Na	110.00922	2.927
44.8	156.1022	C <sub>8</sub> H <sub>14</sub> NO <sub>2</sub>	156.10245	1.625
	188.1285	C <sub>9</sub> H <sub>18</sub> NO <sub>3</sub>	188.12867	0.895
	210.1105	C <sub>9</sub> H <sub>17</sub> NO <sub>3</sub> Na	210.11061	0.528
47.6	170.1180	C <sub>9</sub> H <sub>16</sub> NO <sub>2</sub>	170.11810	0.61
	202.1444	C <sub>10</sub> H <sub>20</sub> NO <sub>3</sub>	202.14432	0.403
	224.1262	C <sub>10</sub> H <sub>19</sub> NO <sub>3</sub> Na	224.12626	0.282
49.6	184.1335	C <sub>10</sub> H <sub>18</sub> NO <sub>2</sub>	184.13375	1.378
	216.1598	C <sub>11</sub> H <sub>22</sub> NO <sub>3</sub>	216.15997	0.78
	238.1417	C <sub>11</sub> H <sub>21</sub> NO <sub>3</sub> Na	238.14191	0.895
50.9	230.1753	C <sub>12</sub> H <sub>24</sub> NO <sub>3</sub>	230.17562	1.384
	296.2586	C <sub>18</sub> H <sub>34</sub> NO <sub>2</sub>	296.25895	1.196
51.2	296.2588	C <sub>18</sub> H <sub>34</sub> NO <sub>2</sub>	296.25895	0.521
53.8	298.2744	C <sub>18</sub> H <sub>36</sub> NO <sub>2</sub>	298.27460	0.685
	316.2852	C <sub>18</sub> H <sub>38</sub> NO <sub>3</sub>	316.28517	0.098
54.1	284.2379	C <sub>20</sub> H <sub>30</sub> N	284.23782	0.264
54.4	310.2385	C <sub>18</sub> H <sub>32</sub> NO <sub>3</sub>	310.23822	0.584
54.8	310.2384	C <sub>18</sub> H <sub>32</sub> NO <sub>3</sub>	310.23822	0.906
55.5	380.3321	C <sub>27</sub> H <sub>42</sub> N	380.33173	0.985
56.3	280.2643	C <sub>18</sub> H <sub>34</sub> NO	280.26404	0.929
56.9	280.2641	C <sub>18</sub> H <sub>34</sub> NO	280.26404	0.215



57.1	280.2641	C <sub>18</sub> H <sub>34</sub> NO	280.26404	0.215
57.3	280.2640	C <sub>18</sub> H <sub>34</sub> NO	280.26404	0.142
	296.2589	C <sub>18</sub> H <sub>34</sub> NO <sub>2</sub>	296.25895	0.183
	328.2851	C <sub>19</sub> H <sub>38</sub> NO <sub>3</sub>	328.28517	0.21
	350.2671	C <sub>19</sub> H <sub>37</sub> NO <sub>3</sub> Na	350.26711	0.039

## 5.4 References

- Aiken, A. C., D. Salcedo, M. J. Cubison, J. A. Huffman, P. F. DeCarlo, I. M. Ulbrich, K. S. Docherty, D. Sueper, J. R. Kimmel, D. R. Worsnop, A. Trimborn, M. Northway, E. A. Stone, J. J. Schauer, R. M. Volkamer, E. Fortner, B. de Foy, J. Wang, A. Laskin, V. Shutthanandan, J. Zheng, R. Zhang, J. Gaffney, N. A. Marley, G. Paredes-Miranda, W. P. Arnott, L. T. Molina, G. Sosa, and J. L. Jimenez. 2009. "Mexico City aerosol analysis during MILAGRO using high resolution aerosol mass spectrometry at the urban supersite (T0) - Part 1: Fine particle composition and organic source apportionment." *Atmospheric Chemistry and Physics* no. 9 (17):6633-6653.
- Alfarra, M. R., D. Paulsen, M. Gysel, A. A. Garforth, J. Dommen, A. S. H. Prévôt, D. R. Worsnop, U. Baltensperger, and H. Coe. 2006. "A mass spectrometric study of secondary organic aerosols formed from the photooxidation of anthropogenic and biogenic precursors in a reaction chamber." *Atmos. Chem. Phys.* no. 6 (12):5279-5293. doi: 10.5194/acp-6-5279-2006.
- Allan, J. D., J. L. Jimenez, P. I. Williams, M. R. Alfarra, K. N. Bower, J. T. Jayne, H. Coe, and D. R. Worsnop. 2003. "Quantitative sampling using an Aerodyne aerosol mass spectrometer 1. Techniques of data interpretation and error analysis." *J. Geophys. Res.* no. 108 (D3):4090. doi: 10.1029/2002jd002358.
- Canagaratna, M. R., J. T. Jayne, J. L. Jimenez, J. D. Allan, M. R. Alfarra, Q. Zhang, T. B. Onasch, F. Drewnick, H. Coe, A. Middlebrook, A. Delia, L. R. Williams, A. M. Trimborn, M. J. Northway, P. F. DeCarlo, C. E. Kolb, P. Davidovits, and D. R. Worsnop. 2007. "Chemical and microphysical characterization of ambient aerosols with the aerodyne aerosol mass spectrometer." *Mass Spectrometry Reviews* no. 26 (2):185-222. doi: 10.1002/mas.20115.

Card, J. B. A., and A. R. Jones. 1995. "A Drop Tube Furnace Study of Coal Combustion and Unburned Carbon Content Using Optical Techniques." *Combustion and Flame* no. 101 (4):539-547. doi: 10.1016/0010-2180(94)00237-m.

Castro-Marcano, F.; Mathews, J. P., Constitution of Illinois No. 6 Argonne Premium Coal: A Review. *Energy Fuels* 2011, 25, (3), 845-853.

Chen, J. C.; Niksa, S., Coal Devolatilization during Rapid Transient Heating.1. Primary Devolatilization. *Energy Fuels* 1992, 6, (3), 254-264.

Cloke, M., E. Lester, and A. W. Thompson. 2002. "Combustion characteristics of coals using a drop-tube furnace." *Fuel* no. 81 (6):727-735. doi: Pii s0016-2361(01)00199-5  
10.1016/s0016-2361(01)00199-5.

Cornell, S., K. Mace, S. Coeppicus, R. Duce, B. Huebert, T. Jickells, and L. Z. Zhuang. 2001. "Organic nitrogen in Hawaiian rain and aerosol." *Journal of Geophysical Research: Atmospheres* no. 106 (D8):7973-7983. doi: 10.1029/2000jd900655.

Cornell, S., A. Randell, and T. Jickells. 1995. "Atmospheric inputs of dissolved organic nitrogen to the oceans." *Nature* no. 376 (6537):243-246.

Daukoru, S. 2010. *The Role of Flue-Gas Recycle in Submicrometer Particle Formation during Oxy-Combustion of American and Chinese Coals*, Department of Energy, Environmental & Chemical Engineering, Washington University in St. Louis.

DeCarlo, P. F., J. R. Kimmel, A. Trimborn, M. J. Northway, J. T. Jayne, A. C. Aiken, M. Gonin, K. Fuhrer, T. Horvath, K. S. Docherty, D. R. Worsnop, and J. L. Jimenez. 2006. "Field-

Deployable, High-Resolution, Time-of-Flight Aerosol Mass Spectrometer." *Analytical Chemistry* no. 78 (24):8281-8289. doi: 10.1021/ac061249n.

Ge, X., A. S. Wexler, and S. L. Clegg. 2011a. "Atmospheric amines – Part I. A review." *Atmospheric Environment* no. 45 (3):524-546. doi: 10.1016/j.atmosenv.2010.10.012.

Ge, X., A. S. Wexler, and S. L. Clegg. 2011b. "Atmospheric amines – Part II. Thermodynamic properties and gas/particle partitioning." *Atmospheric Environment* no. 45 (3):561-577. doi: 10.1016/j.atmosenv.2010.10.013.

Glarborg, P.; Jensen, A. D.; Johnsson, J. E., Fuel nitrogen conversion in solid fuel fired systems. *Prog. Energy Combust. Sci.* 2003, 29, (2), 89-113.

Gluskoter, H. I.; Simon, J. A., Sulfur in Illious Coals. In Illious State Geology Survey: 1968; Vol. 432.

Haenel, M. W. 1992. "Recent progress in coal structure research." *Fuel* no. 71 (11):1211-1223. doi: 10.1016/0016-2361(92)90046-q.

Hallquist, M., J. C. Wenger, U. Baltensperger, Y. Rudich, D. Simpson, M. Claeys, J. Dommen, N. M. Donahue, C. George, A. H. Goldstein, J. F. Hamilton, H. Herrmann, T. Hoffmann, Y. Iinuma, M. Jang, M. E. Jenkin, J. L. Jimenez, A. Kiendler-Scharr, W. Maenhaut, G. McFiggans, T. F. Mentel, A. Monod, A. S. H. Prvt, J. H. Seinfeld, J. D. Surratt, R. Szmigielski, and J. Wildt. 2009. "The formation, properties and impact of secondary organic aerosol: current and emerging issues." *Atmos. Chem. Phys.* no. 9 (14):5155-5236. doi: 10.5194/acp-9-5155-2009.

- He, L. Y., Y. Lin, X. F. Huang, S. Guo, L. Xue, Q. Su, M. Hu, S. J. Luan, and Y. H. Zhang. 2010. "Characterization of high-resolution aerosol mass spectra of primary organic aerosol emissions from Chinese cooking and biomass burning." *Atmos. Chem. Phys.* no. 10 (23):11535-11543. doi: 10.5194/acp-10-11535-2010.
- Hu, W. W., M. Hu, B. Yuan, J. L. Jimenez, Q. Tang, J. F. Peng, W. Hu, M. Shao, M. Wang, L. M. Zeng, Y. S. Wu, Z. H. Gong, X. F. Huang, and L. Y. He. 2013. "Insights on organic aerosol aging and the influence of coal combustion at a regional receptor site of central eastern China." *Atmos. Chem. Phys.* no. 13 (19):10095-10112. doi: 10.5194/acp-13-10095-2013.
- Jimenez, J. L., J. T. Jayne, Q. Shi, C. E. Kolb, D. R. Worsnop, I. Yourshaw, J. H. Seinfeld, R. C. Flagan, X. Zhang, K. A. Smith, J. W. Morris, and P. Davidovits. 2003. "Ambient aerosol sampling using the Aerodyne Aerosol Mass Spectrometer." *J. Geophys. Res.* no. 108 (D7):8425. doi: 10.1029/2001jd001213.
- Kelemen, S. R., M. L. Gorbaty, and P. J. Kwiatek. 1994. "QUANTIFICATION OF NITROGEN FORMS IN ARGONNE PREMIUM COALS." *Energy & Fuels* no. 8 (4):896-906. doi: 10.1021/ef00046a013.
- Kelemen, S. R., M. L. Gorbaty, P. J. Kwiatek, T. H. Fletcher, M. Watt, M. S. Solum, and R. J. Pugmire. 1998. "Nitrogen transformations in coal during pyrolysis." *Energy & Fuels* no. 12 (1):159-173. doi: 10.1021/ef9701246.
- Laskin, A., J. S. Smith, and J. Laskin. 2009. "Molecular Characterization of Nitrogen-Containing Organic Compounds in Biomass Burning Aerosols Using High-Resolution Mass Spectrometry." *Environmental Science & Technology* no. 43 (10):3764-3771. doi: 10.1021/es803456n.

Linak, W. P., and J. O. L. Wendt. 1994. "Trace metal transformation mechanisms during coal combustion." *Fuel Processing Technology* no. 39 (1-3):173-198.

Mace, K. A., P. Artaxo, and R. A. Duce. 2003. "Water-soluble organic nitrogen in Amazon Basin aerosols during the dry (biomass burning) and wet seasons." *Journal of Geophysical Research: Atmospheres* no. 108 (D16):4512. doi: 10.1029/2003jd003557.

Mitrakirtley, S.; Mullins, O. C.; Branthaver, J. F.; Cramer, S. P., Nitrogen Chemistry of Kerogens and Bitumens from X-ray-absorbtion Near-Edge Structure Spectroscopy. *Energy Fuels* 1993, 7, (6), 1128-1134.

Mullins, O. C.; Mitrakirtley, S.; Vanelp, J.; Cramer, S. P., Molecular-structure of Nitrogen in Coal from XANES Spectroscopy. *Appl. Spectrosc.* 1993, 47, (8), 1268-1275.

Quann, R. J., M. Neville, M. Janghorbani, C. A. Mims, and A. F. Sarofim. 1982. "Mineral Matter and Trace-element Vaporization in a Laboratory-pulverized Coal Combustion System." *Environmental Science & Technology* no. 16 (11):776-781.

Seinfeld, J. H., and S. N. Pandis. 2006. *Atmospheric Chemistry and Physics: From Air Pollution to Climate Change*.

Sun, Y. L., Z. F. Wang, P. Q. Fu, T. Yang, Q. Jiang, H. B. Dong, J. Li, and J. J. Jia. 2013.

"Aerosol composition, sources and processes during wintertime in Beijing, China." *Atmos. Chem. Phys.* no. 13 (9):4577-4592. doi: 10.5194/acp-13-4577-2013.

Wang, X., B. J. Williams, Y. Tang, Y. Huang, L. Kong, X. Yang, and P. Biswas. 2013.

"Characterization of organic aerosol produced during pulverized coal combustion in a drop tube furnace." *Atmos. Chem. Phys. Discuss.* no. 13 (2):3345-3377. doi: 10.5194/acpd-13-3345-2013.

Wang, Z., J. Zhang, Y. Zhao, and C. Zheng. 2012. "Relationship between nitrogenous species in coals and volatile nitrogen-containing yields during pyrolysis." *Asia-Pacific Journal of Chemical Engineering* no. 7 (1):124-130. doi: 10.1002/apj.501.

Zhang, Q., C. Anastasio, and M. Jimenez-Cruz. 2002. "Water-soluble organic nitrogen in atmospheric fine particles (PM<sub>2.5</sub>) from northern California." *Journal of Geophysical Research: Atmospheres* no. 107 (D11):AAC 3-1-AAC 3-9. doi: 10.1029/2001jd000870.

Zhang, Y., J. J. Schauer, Y. Zhang, L. Zeng, Y. Wei, Y. Liu, and M. Shao. 2008. "Characteristics of Particulate Carbon Emissions from Real-World Chinese Coal Combustion." *Environmental Science & Technology* no. 42 (14):5068-5073. doi: 10.1021/es7022576.

## **CHAPTER 6. MERCURY REMOVAL DURING COAL COMBUSTION BY INJECTION OF VANADIUM PENTOXIDE ( $V_2O_5$ )**

*The results of this chapter has been compiled as a paper: Wang, X.; Li, S.; Wang, W.N.; and Biswas, P., Mercury Removal during Coal Combustion by Injection of Vanadium Pentoxide ( $V_2O_5$ ). Submitted to Environmental Engineering Science.*



## **Abstract**

Novel method that can control Hg emission efficiently and economically from various coal combustors is strongly needed. High temperature sorbent injection is an efficient method for metallic species oxidation and capture during combustion. This study examines the performance of this method on Hg oxidation from pulverized coal combustion in a drop-tube furnace.  $V_2O_5$  was tested as sorbent and demonstrated good performance on  $Hg^0$  oxidation. The results also showed that  $V_2O_5$  addition did not significantly affect particulate matter (fly ash) formation. The effective performance of  $V_2O_5$  results from the formation of ultrafine  $V_2O_5$  particles during the combustion process. In addition, the effect of chlorine (Cl) concentration in coal on  $Hg^0$  oxidation was also examined. The result shows that Cl can help  $Hg^0$  oxidation on  $V_2O_5$  surface. A simple techno-economic analysis shows that the cost of the  $V_2O_5$  injection method is competitive with existing Hg control technologies.

## 6.1 Introduction

In United States, coal combustion emits approximately 50 tons of mercury (about 1/3 of total anthropogenic emission), a toxic pollutant, into the atmosphere every year (Senior, Helble, et al. 2000, Senior, Sarofim, et al. 2000, Pavlish et al. 2003). Hence, US Environmental Protection Agency (EPA) recently finalized the Mercury and Air Toxics Standard (MATS), which strictly regulates emissions of Hg and other pollutants from coal combustion.

Coal contains trace amounts of Hg (Pavlish et al. 2003). During coal combustion, Hg is released from coal as its elemental form  $\text{Hg}^0(\text{g})$ . In post combustion environment where the temperature is decreasing, some of  $\text{Hg}^0(\text{g})$  may be oxidized to  $\text{Hg}^{2+}$  compounds. HCl and  $\text{Cl}_2$  are considered as the main oxidants of the reactions.  $\text{Hg}^{2+}$  compounds can absorb onto particulate matter in flue gas and form Hg(p) (Galbreath and Zygarlicke 2000, Senior, Helble, et al. 2000, Senior, Sarofim, et al. 2000). Thus, there are 3 forms of Hg in exhaust gas of coal combustion: 1)  $\text{Hg}^0(\text{g})$ ; 2)  $\text{Hg}^{2+}(\text{g})$ ; and 3) Hg(p).  $\text{Hg}^{2+}(\text{g})$  is water-soluble and can be readily removed by wet flue gas desulfurization (WFGD) systems (Zhuang et al. 2004). Hg(p) can also be easily removed by particulate matter control device such as fabric filter (FF) baghouse and electrostatic precipitator (ESP). But  $\text{Hg}^0(\text{g})$  is relatively difficult to be captured and it is reported that the elemental form is the main form of Hg emission from coal combustion (Pavlish et al. 2003).

Several technologies have been proposed to capture Hg in combustion exhaust. The most established method is activated carbon injection. Powdered activated carbon is injected into flue gas ductwork and absorbs  $\text{Hg}^0$ . Then particulate control device can remove it with fly ash. It is a simple and efficient method. But there are some disadvantages. Firstly, the cost is significant (Jones et al. 2007). Secondly, activated carbon will mix with fly ash and affect its flammability

and solubility (Pflughoeft-Hassett et al. 2009). Thus, a low cost non-carbon technology is desired for mercury capture from coal combustion.

One general approach for non-carbon method is promoting the oxidation of  $\text{Hg}^0$  to  $\text{Hg}^{2+}$ , a mercury form that can be easily captured. Many halogen species are oxidizers of  $\text{Hg}^0(\text{g})$ . Chlorine is major halogen specie in coal and plays key roles in Hg oxidation (Senior, Sarofim, et al. 2000). Liu et al. (2007) found addition of bromine gas can greatly enhance  $\text{Hg}^0(\text{g})$  oxidation. Cao et al. (2007) found HBr can also enhance  $\text{Hg}^0(\text{g})$  oxidation. Moreover, Li et al. (2009) also showed that KI has capability to oxidize  $\text{Hg}^0(\text{g})$ .

Many metals/metal oxides can catalyze  $\text{Hg}^0(\text{g})$  oxidation, such as  $\text{Fe}_2\text{O}_3$ , CuO, and some precious metals (gold, silver and palladium) (Galbreath et al. 2005, Ghorishi et al. 2005, Zhao et al. 2006). Besides these metals/metal oxides, selective catalytic reduction (SCR) catalysts have been studied extensively, because they have been already widely installed for  $\text{NO}_x$  reduction and are also shown to have the capability of oxidation of  $\text{Hg}^0$  (Cao, Chen, et al. 2007, Cao et al. 2008, Presto and Granite 2006). SCR catalyst is typically consist of  $\text{V}_2\text{O}_5$ ,  $\text{WO}_3$  or zeolite supported on various carriers such as  $\text{TiO}_2$ . It can help reduce  $\text{NO}_x$  with  $\text{NH}_3$  to  $\text{N}_2$ . Many studies have reported that SCR catalysts can also oxidize  $\text{Hg}^0(\text{g})$ , particularly in the presence of halogen species (Cao, Chen, et al. 2007). There are several factors that can affect the performance of SCR catalysts, such as concentrations of hydrogen chloride and sulfur oxides in flue gas (Cao, Chen, et al. 2007, Senior 2006, Eswaran and Stenger 2005).

Another general approach is sorbent injection into combustion zone (high temperature sorbent) (Biswas and Zachariah 1997, Biswas and Wu 1998, Lee et al. 2001, Gale and Wendt 2002, 2003, Jeong et al. 2007, Lee et al. 2005, Gale and Wendt 2005, Suriyawong et al. 2009, Suriyawong et

al. 2010, Wendt and Lee 2010). In high temperature combustion environment, metallic species are released to gas phase and form vapors. At the exit of combustor, when temperature drops, these vapors will undergo homogeneous nucleation or heterogeneous condensation and form submicrometer aerosols. When sorbent particles are injected into combustor, metallic vapors can be captured. Therefore, these metallic species are associated with sorbent particles which usually have larger particle size and can be easily removed by particulate matter control devices (Owens and Biswas 1996). This methodology can be applied to Hg removal. For instance,  $\text{TiO}_2$  is a well-studied photocatalyst which can help oxidize  $\text{Hg}^0(\text{g})$  (Li, Li, et al. 2011a, Li et al. 2012). Wu et al. reported a method using  $\text{TiO}_2$  sorbent (Wu et al. 1998): the sorbent precursor was added into the combustor. Then the precursor was oxidized to form  $\text{TiO}_2$  agglomerate with large surface area, which can efficiently capture  $\text{Hg}^0(\text{g})$ . They also showed that using UV radiation can further improve binding of Hg with  $\text{TiO}_2$  sorbent particles, thereby enhancing Hg capture. Suriyawong et al. have demonstrated the effectiveness of this method on a pilot scale (Suriyawong et al. 2009). In addition, calcium- and iron-based sorbents are shown to have similar capability of Hg removal (Zhuang et al. 2007, Pavlish et al. 2003).

Both SCR catalysts and sorbent injection into combustion zone (high temperature sorbent) have good performance on Hg oxidation and capture. The combination of these two technologies may be an effective methodology for Hg control.  $\text{V}_2\text{O}_5$ , which is one of most active component in SCR catalysts and a relatively low-cost material, as a high temperature sorbent to oxidize and capture Hg. This study examines the performance of this new method from pulverized coal combustion in a drop-tube furnace. Its effects on particulate matter formation have been investigated. In addition, the effects of chlorine and sulfur contents in coal have also been studied, since they may have significant influences on this method.

## 6.2 Experimental Section

The experimental setup shown in Fig. 6.1 consists of a coal feeding system, a drop-tube furnace (Lindberg/Blue M, Model HTF55342C, ThermoElectron Corp., USA) with an alumina reactor tube (5.7 cm inner diameter, and 122 cm long), a cascade impactor, and various sampling and measuring systems. Pulverized Powder River Basin (PRB) sub-bituminous coal (coal particle diameter  $\leq 50 \mu\text{m}$ ; supplied by Ameren UE, St. Louis, MO) was introduced into the electrically heated alumina tube in the drop-tube furnace by a self-made coal feeder (design of the feeder can be found in the literature (Quann et al. 1982)) at 1.5 g/h. For all experiments, a total gas flow rate of 1.0 liter-per-minute (LPM) was fixed. Thus, the fuel-air equivalence ratio was 0.15. At the exit of the combustor, 7 LPM particle-free air was added as primary dilution, and then a six-stage cascade impactor (Mark III, Pollution Control System Corp., Seattle, WA) was used to remove particles with diameter larger than 600 nm in the diluted exhaust gas. The downstream of the impactor was then drawn to a real time scanning mobility particle sizer (SMPS, TSI Inc., Shoreview, MN) to determine the particle size distribution ranging from 9 to 425 nm. The submicrometer particles were also collected on Teflon filters for elemental analysis by an X-ray fluorescence spectroscopy (XRF, Panalytical Epsilon 5 energy dispersive XRF spectrometer, Almelo, Netherlands), crystal determination by X-ray diffraction (XRD, Rigaku Geigerflex D-MAX/A diffractometer) and morphology examination using an FEI Nova NanoSEM 230 Scanning Electron Microscope (SEM).

For mercury concentration measurements, a 0.47 LPM flue gas was drawn from the exhaust gas (before the primary dilution) and passed through a mercury sampling train to determine oxidized and elemental mercury concentrations (the dilution gas was turned off during Hg sampling). The sampling train and technique used for gaseous mercury collection and measurement are based on

the method developed by Hedrick et al. (2001). The sampling train consists of five impingers. The following solutions were used to collect gaseous mercury: two impingers of 1.0 M tris-buffer and EDTA for oxidized mercury capture, one impinger of 10% hydrogen peroxide and 2% nitric acid for oxidizing and capturing of elemental mercury, and two impingers of 0.05 M potassium iodide and 2% hydrochloric acid for elemental mercury capture. The impinger solutions with captured mercury content were then analyzed by direct mercury analyzer (DMA-80, Milestone S.r.l., Italy) to determine the elemental and oxidized fractions of mercury in the exhaust gas.

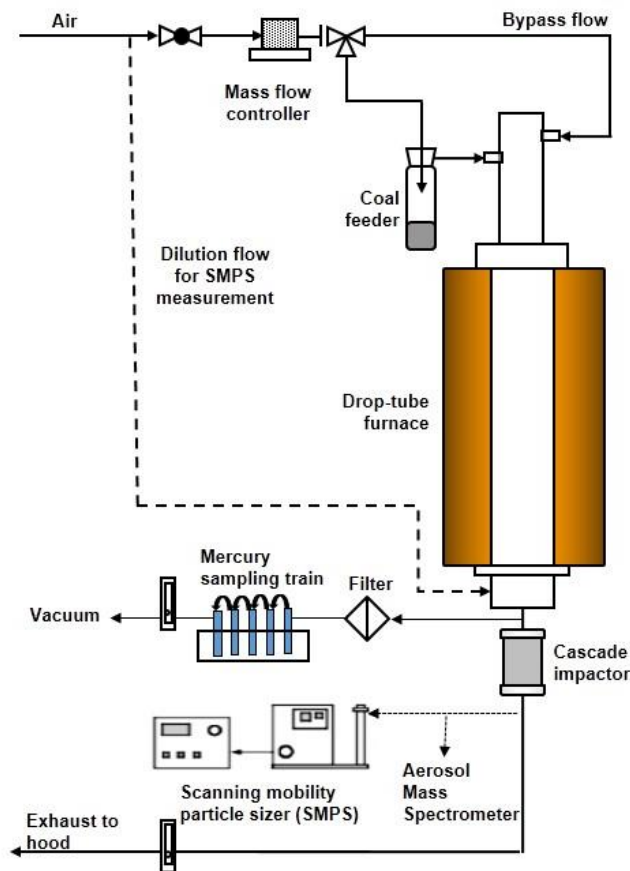


Figure 6.1. Schematic diagram of the experimental set-up

The overall test plan is summarized in Table 6.1. First, the baseline elemental mercury concentration from PRB coal combustion was determined. Then elemental mercury oxidation efficiency of using  $V_2O_5$  (purity  $\geq 98\%$ , particle size: 325 mesh) was measured. Set II experiments were designed to study the effects of varying mixing ratio of  $V_2O_5$  on mercury oxidation efficiency.  $V_2O_5$  concentrations of 50, 100, 300, and 500 ppm were tested. The objects of Set III experiments were to determine the effects of chlorine content in coal on mercury oxidation efficiency.

Table 6.1. Experimental test plan for this study

Set	#	Sorbent Material	Mixing Ratio of Sorbent (ppm <sub>w</sub> )	NaCl Addition (ppm <sub>w</sub> )	Objectives
I	1	N/A	N/A	0	To determine baseline $Hg^0$ concentration from PRB combustion and $Hg^0$ oxidation efficiency using $V_2O_5$ as sorbent
	2	$V_2O_5$	100	0	
II	1	$V_2O_5$	50	0	To determine the effect of $V_2O_5$ mixing ratio on $Hg^0$ oxidation
	2		100	20	
	3		300	40	
	4		500	60	
III	1	$V_2O_5$	100	100	To determine the effect of chlorine concentration on $Hg^0$ oxidation
	2			300	
	3			500	

### 6.3 Results and Discussion

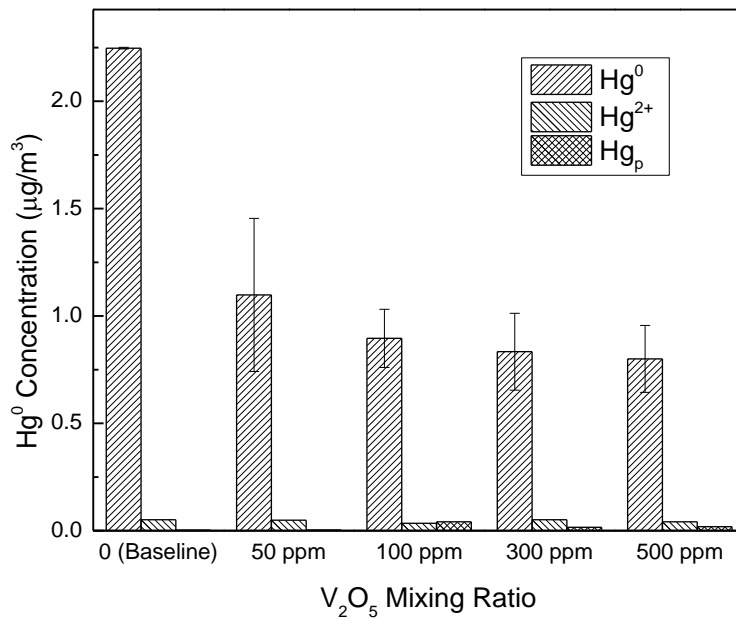
The overall study examined the performance of injecting  $V_2O_5$  as high temperature sorbent on Hg oxidation from pulverized coal combustion in a drop-tube furnace at various conditions. Particulate matter formation and the effects of chlorine in coal on Hg oxidation have also been studied.

#### 6.3.1 Oxidizing $Hg^0$ by mixing $V_2O_5$ with coal

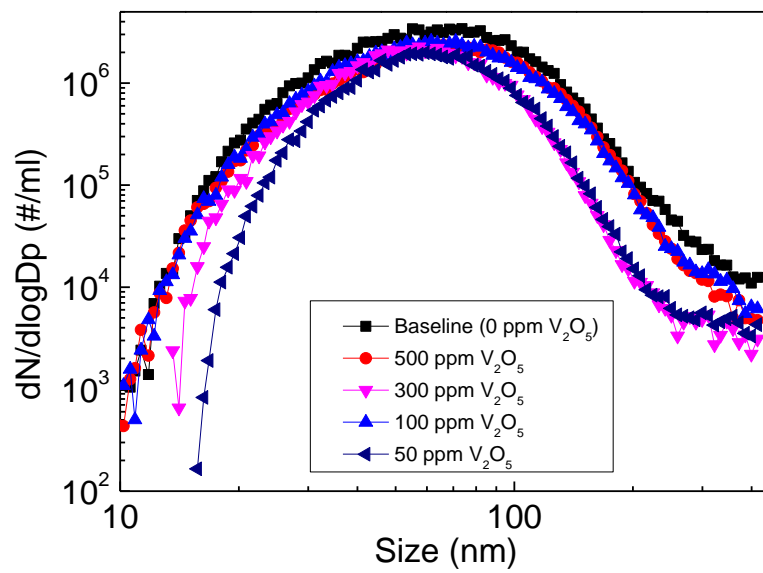
As shown in Fig. 6.2a,  $V_2O_5$  particles were mixed with PRB coal at different ratios (Experiment Set 1). Without adding  $V_2O_5$ , the  $Hg^0$  concentration (the baseline concentration) in the flue gas was  $2.25 \mu\text{g}/\text{m}^3$ , typically for system using PRB coal. When  $V_2O_5$  was mixed with coal, the  $Hg^0$  concentration decreased significantly. For example, when the mixing ratio was 50 ppm, the  $Hg^0$  concentration was  $1.09 \mu\text{g}/\text{m}^3$ , and the  $Hg^0$  oxidation efficiency ( $= 1 - \frac{Hg^0 \text{ Concentration}}{\text{Baseline } Hg^0 \text{ Concentration}}$ ) was about 51.2%. Experimental results show that  $Hg^0$  concentration decreases with increases in  $V_2O_5$  mixing ratio, the  $Hg^0$  concentration was decreasing, and the best oxidation efficiency, 64.4%, can be achieved when the mixing ratio was 500 ppm. These results demonstrate that  $V_2O_5$  has good performance on  $Hg^0$  oxidation. In our previous study (Li, Daukoru, et al. 2009), potassium iodine (KI) was used as high temperature sorbent. The  $Hg^0$  removal efficiencies were 30%, 53% and 61%, when KI mixing ratios were 235, 389 and 777 ppm, respectively, lower than the performance of  $V_2O_5$ . Therefore,  $V_2O_5$  has a superior performance as high temperature sorbent.



(a)



(b)



(c)

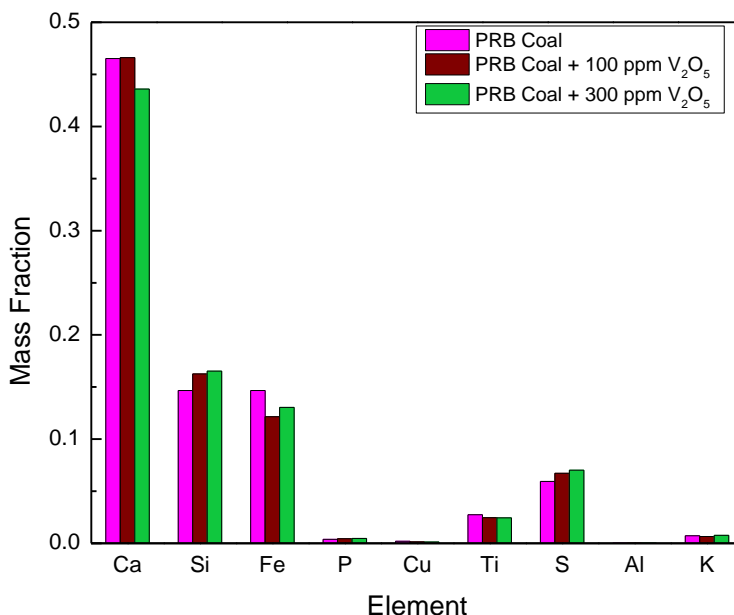


Figure 6.2. Combustion of PRB coal mixed with V<sub>2</sub>O<sub>5</sub> at different ratios: (a) Mercury concentrations in the flue gas; (b) Fine particle size distribution; and (c) Elemental compositions of fine particulate matter

Figure 6.2a shows that the Hg<sup>0</sup> oxidation efficiency did not increase significantly while keeping increasing V<sub>2</sub>O<sub>5</sub> mixing ratio above 100 ppm. This finding suggests that V<sub>2</sub>O<sub>5</sub> was not the limiting factor in those cases. The mechanism of Hg<sup>0</sup> oxidation by V<sub>2</sub>O<sub>5</sub> is the catalytic oxidation of Hg<sup>0</sup> on V<sub>2</sub>O<sub>5</sub> surface (Presto and Granite 2006, Cao, Chen, et al. 2007, Li, Li, et al. 2011a). Hg<sup>2+</sup> should be formed after this process. According to mass balance, the concentration of Hg<sup>2+</sup> in the flue gas should be equal to the value of the baseline concentration of Hg<sup>0</sup> minus the concentration of Hg<sup>0</sup> in the flue gas. However, Fig. 6.2a shows that Hg<sup>2+</sup> concentrations

were very low for all experiments. This can be explained by the fact that  $\text{Hg}^{2+}$  (such as  $\text{HgO}$  and  $\text{HgCl}_2$ ) has much lower vapor pressure than  $\text{Hg}^0$  (Johnson et al. 1966, Lamoreaux et al. 1987). The temperature of flue gas dropped to the room temperature very quickly in our system. This resulted in the conversion to the particulate phase or condensation of  $\text{Hg}^{2+}$  on existing particles or tubing surfaces. Our previous research also shows the similar result (Li, Daukoru, et al. 2009). In a full scale system, high concentration of fine particles provide very large surface area on which  $\text{Hg}^{2+}$  can condensate. But in the bench-scale system used in this study, fine particles did not provide significant surface area ( $\sim 1 \times 10^{-4} \text{ cm}^2/\text{cm}^3$ , calculated from particle size distribution showed in Fig. 6.2b), comparing the surface area from the tubing. Therefore, most of  $\text{Hg}^{2+}$  may condensate on tubing's inside surface, rather than on particle surface. The low Hg concentrations found in particulate matter (shown in Fig. 6.2a) also confirms it. But this should not be an issue in a full scale system, where has much higher surface area from fly ash particles.

$\text{V}_2\text{O}_5$  addition could have effects on particulate matter (fly ash) formation: adding sorbent particles could provide extra surface for condensation of metallic species during coal combustion, thereby shifting particle size distribution to larger sizes (Biswas and Wu 1998). Figure 6.2b shows the size distributions of fine particles from the experiment set 1. However there is no obvious difference among those size distributions, indicating such low  $\text{V}_2\text{O}_5$  mixing ratio does not have significant influence on particle formation. Generally, all size distributions peak at about 60 nm. Elemental compositions for those particles are shown in Fig. 6.2c. Again, no significant difference is found. Calcium (Ca) is one of the dominant species in particulate matter, since PRB coal has high calcium content (Wang, Michael Daukoru, et al. 2013). Other major species include silicon (Si), iron (Fe), sulfur (S), titanium (Ti) and potassium (K). It is interesting to note that sulfur concentration in particulate matter slightly increase when more

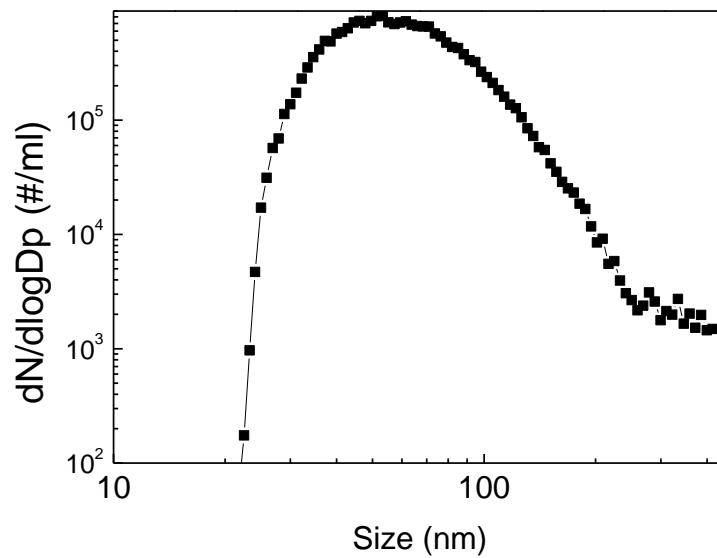
V<sub>2</sub>O<sub>5</sub> was mixed with coal. The increase may be due to the oxidation of SO<sub>2</sub> to SO<sub>3</sub> on V<sub>2</sub>O<sub>5</sub> surface, because V<sub>2</sub>O<sub>5</sub> is an efficient catalyst of SO<sub>2</sub> oxidation (Kamata et al. 2001). SO<sub>3</sub> is a strong acidic gas. It may react with some metal oxides, such as CaO, to form sulfate and enter the particle phase.

### 6.3.2 Transformation of V<sub>2</sub>O<sub>5</sub> during coal combustion

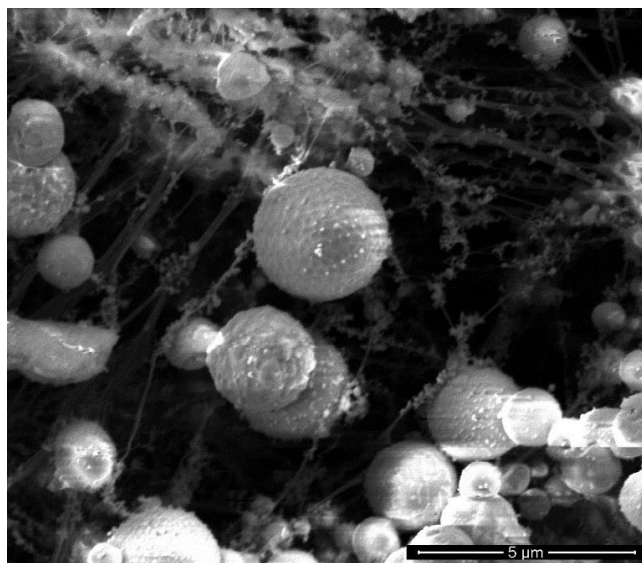
The previous part demonstrates that adding V<sub>2</sub>O<sub>5</sub> to coal can efficiently reduce Hg<sup>0</sup> concentration in flue gas. The role that V<sub>2</sub>O<sub>5</sub> plays in Hg<sup>0</sup> oxidation needs to be further investigated. Pure V<sub>2</sub>O<sub>5</sub> particles were sent into the drop-tube furnace. Particle size distribution has been measured at the outlet of the drop-tube furnace (Fig. 6.3a), which shows the presence of high concentration of ultrafine particles. In the SEM image (Fig. 6.3b) of the pure V<sub>2</sub>O<sub>5</sub> particle that was collected on a Teflon filter from the outlet of the drop-tube furnace, there are some micrometer size particles and large amount of nanoparticles, which are attached to the fibers of the filter. Almost all particles have spherical shape. Figure 6.3c shows the original shape of V<sub>2</sub>O<sub>5</sub> particles, most of which are rod; and their sizes are much larger (~100 to 200 μm in length). The change of size and shape strongly indicates a gas-to-particle conversion process that the V<sub>2</sub>O<sub>5</sub> particles were undergoing in the furnace (Widiyastuti et al. 2009). The melting point of V<sub>2</sub>O<sub>5</sub> is 963 K. And the temperature inside the drop-tube furnace was around 1376 K. Therefore, V<sub>2</sub>O<sub>5</sub> particles would quickly become liquid droplet in the furnace. Some liquid may be evaporated and form V<sub>2</sub>O<sub>5</sub> vapor. When the gas is leaving from the furnace and its temperature drops below 963 K. V<sub>2</sub>O<sub>5</sub> vapor would start nucleation process, which produce high concentration of V<sub>2</sub>O<sub>5</sub> ultrafine particles. The ultrafine V<sub>2</sub>O<sub>5</sub> particles provide large surface area, which can greatly facilitate the oxidation of Hg<sup>0</sup>. Fine V<sub>2</sub>O<sub>5</sub> particles had been also collected for the analysis of X-ray Diffraction (XRD) (Fig. 6.3d). No significant peak has been found in the

spectrum, suggesting that ultrafine  $V_2O_5$  particles are in amorphous phase. Figure 6.4 summarizes this whole process.

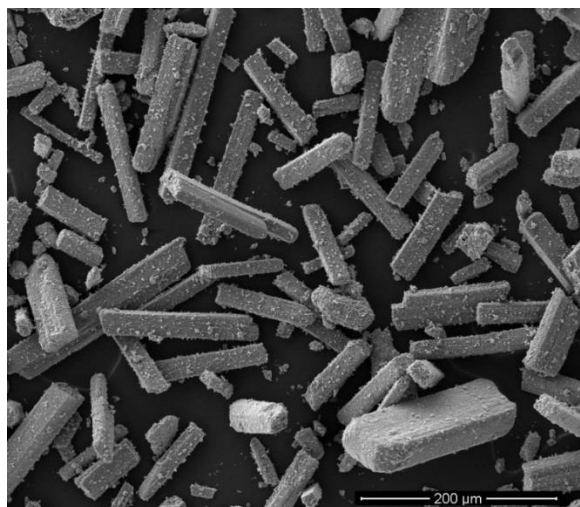
(a)



(b)



(c)



(d)

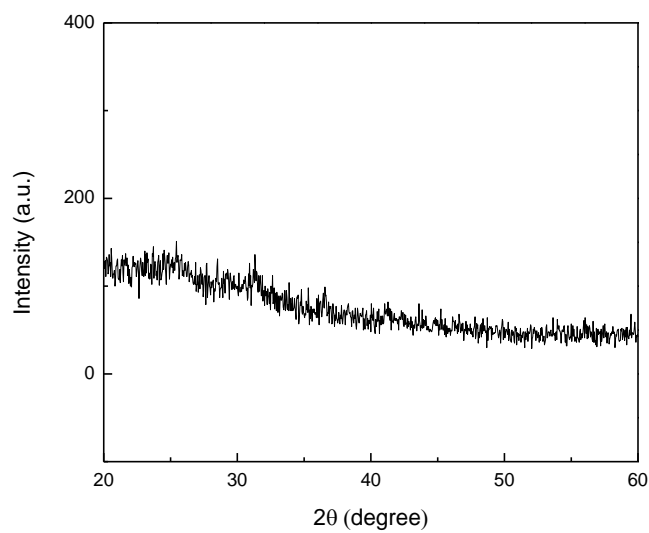


Figure 6.3. (a) Particle size distribution from pure V<sub>2</sub>O<sub>5</sub> experiment; (b) SEM image of V<sub>2</sub>O<sub>5</sub> particles collected from the outlet of the drop-tube furnace; (c) SEM image of original V<sub>2</sub>O<sub>5</sub> particles; and (d) X-ray Diffraction (XRD) spectrum of the collected particles from pure V<sub>2</sub>O<sub>5</sub> experiment.

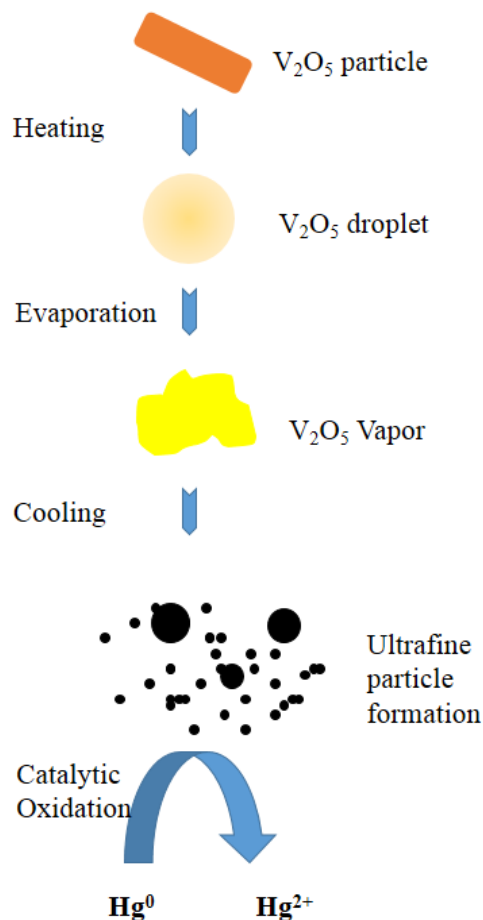


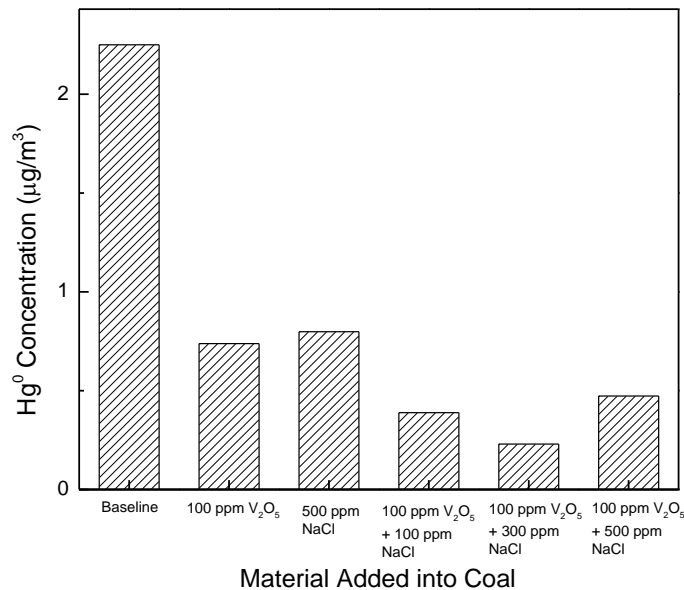
Figure 6.4. Illustration of ultrafine  $V_2O_5$  particles formation .

### 6.3.3 Effect of chlorine (Cl) concentration in coal on $Hg^0$ oxidation

Coal contains trace amount of chlorine. During coal combustion, chlorine in coal is released into the gas phase, which is the main oxidizer for  $Hg^0$  oxidation (Senior, Sarofim, et al. 2000, Zhuang et al. 2007). By adding different mixing ratio of NaCl into the mixture of PRB coal and 100ppm  $V_2O_5$ , Cl concentrations were changed (shown in Experiment Set 2 in Table 6.1); and its effect on  $Hg^0$  oxidation has been investigated. Figure 6.5a shows that  $Hg^0$  concentration decreased

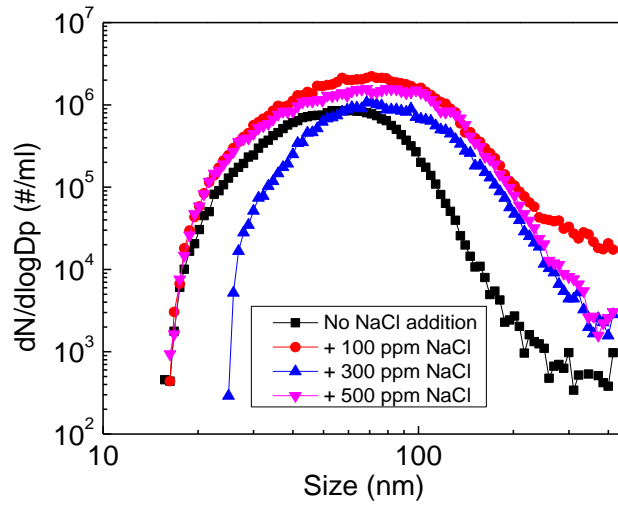
when Cl was added to coal, suggesting that Cl did help oxidize  $\text{Hg}^0$ . This result is consistent with previous studies, which report that adding Cl into coal can promote the oxidations of  $\text{Hg}^0$  in both gas phase and particle surface (Zhuang et al. 2007, Galbreath et al. 2005). Moreover, Fig. 6.5a also shows that adding 500ppm NaCl and 100ppm  $\text{V}_2\text{O}_5$  has higher  $\text{Hg}^0$  oxidation efficiency than adding 500ppm NaCl alone (without adding  $\text{V}_2\text{O}_5$ ), which indicates adding Cl probably enhanced  $\text{Hg}^0$ 's oxidation on  $\text{V}_2\text{O}_5$  surface. Thus adding Cl is an effective way to enhance  $\text{Hg}^0$  oxidation. But in practice, although the halogen injection method can efficiently remove Hg from flue gas, it could have some undesired effects, such as causing serious corrosion in power plant (Zhuang et al. 2009).

(a)



(b)





(c)

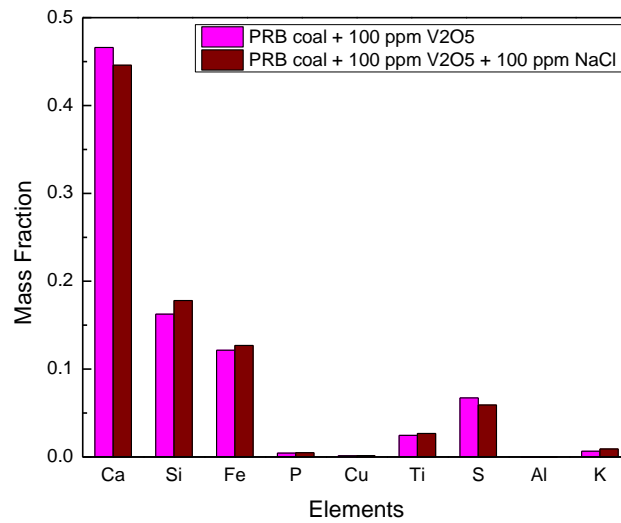


Figure 6.5. Effect of chlorine content in coal on mercury concentrations in the flue gas: (a) Mercury concentrations in the flue gas; (b) Fine particle size distribution; and (c) Elemental compositions of fine particulate matter.

Particulate formation was also studied. The size distribution of fine particles shifted to larger particle size when more NaCl was added (Fig. 6.5b). This is because NaCl is a relative volatile substance (melting point: 1074 K). During coal combustion, NaCl is evaporated into gas phase due to high temperature. At the exit of the drop-tube furnace, the temperature drops and the sodium vapor may condensate on particles, thereby increasing particle sizes. This process may affect Hg oxidation by  $V_2O_5$ , since it can block some active sites on  $V_2O_5$  particles. Thus the process may account for the decreased performance of  $V_2O_5$  when 500 ppm NaCl was added. Elemental compositions for the fine particles are shown in Fig. 6.5c. No significant difference is found.

#### 6.3.4 Techno-economic analysis

Cost is one of the most important factors to be considered for a new technology. The  $V_2O_5$  injecting method reported here has unique advantage in terms of cost. Firstly, this method does not require a complex injection equipment like activated carbon injection.  $V_2O_5$  can be added into coal before the coal pulverizer, which can mix  $V_2O_5$  with coal well. Secondly, the cost of  $V_2O_5$  is low. In December, 2012, the price for  $V_2O_5$  (purity 98%) was around 5.9 \$/lb (Bloomberge 2012). Figure 6.6 compared the material cost of  $V_2O_5$  with activated carbon injection and bromine-impregnated activated carbon injection when Hg oxidation efficiency is around 70% for these three methods.

The cost of  $V_2O_5$  was calculated based on the performance of mixing 100 ppm  $V_2O_5$  with PRB coal in this study:

$$\text{Cost} = \text{“Price of } V_2O_5\text{”} \times \text{“Mass of } V_2O_5 \text{ needed”}$$

Where “Mass of V<sub>2</sub>O<sub>5</sub> needed”=“Mass of Hg removed”/ (“Hg removal efficiency” × “Hg Concentration in coal”)×100×10<sup>-6</sup>;

The average costs of the activated carbon injection for 70% Hg capture were taken from a paper (Jones et al., 2007). It shows that the cost of V<sub>2</sub>O<sub>5</sub> injection method is lower than activated carbon injection. However, the above cost analysis is based on the laboratory-scale study. For example, cooling rate of the flue gas plays an important role in Hg oxidation. In the drop-tube system, the cooling rate of the flue gas was about 180 K/s (from 1000K to 500K, calculated from the temperature profile in Appendix 5), which was lower than a typical full scale system. Senior et al., (2000) reports that lower cooling rate leads to a higher conversion of elemental mercury. Thus, the Hg oxidation using this method in a full scale system may be lower than our drop tube result. In a full-scale power plant, many conditions may be different from this study. Therefore, to confirm its high performance cost ratio, pilot-scale and full-scale tests will be needed.

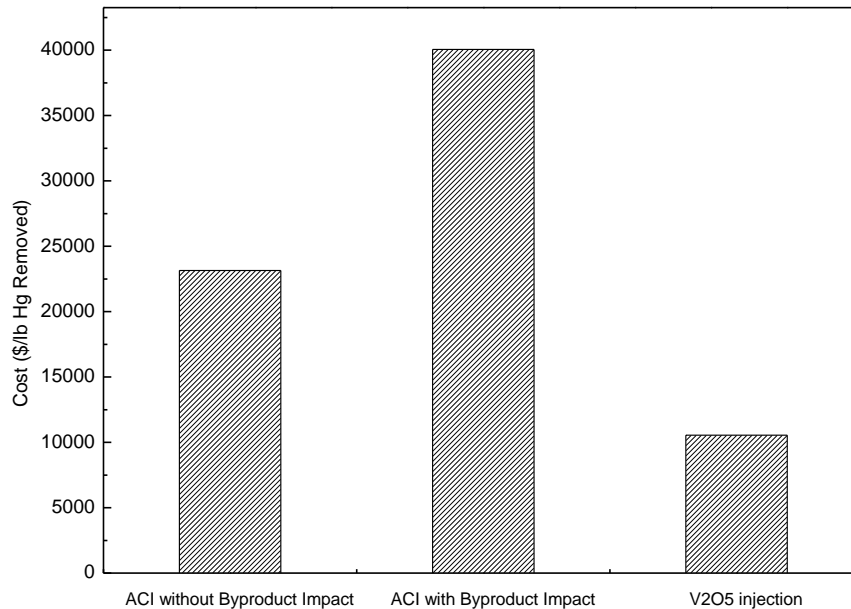


Figure 6.6. Comparison of material cost among the V<sub>2</sub>O<sub>5</sub> injection, activated carbon injection for about 70% mercury removal

#### 6.4 Conclusions

This study examines the performance of injecting V<sub>2</sub>O<sub>5</sub> as sorbent on Hg oxidation during pulverized coal combustion in a drop-tube furnace. It shows exceptional performance on Hg<sup>0</sup> oxidation using this method: about 60 to 70% of elemental mercury was oxidized while only 100 to 500 ppm of V<sub>2</sub>O<sub>5</sub> were mixed with PRB coal. It is proposed that the injected V<sub>2</sub>O<sub>5</sub> particles catalyzed Hg<sup>0</sup> oxidation on their surfaces. Hg<sup>2+</sup>, the oxidation product, may condense on fly ash particle surfaces or tubing surfaces, thereby being removed from the flue gas.

High concentrations of ultrafine V<sub>2</sub>O<sub>5</sub> particles were found to be formed in the coal combustor. By comparing morphology of V<sub>2</sub>O<sub>5</sub> particles before and after going through the combustor, the

formation pathway was proposed in this study: solid  $V_2O_5$  particles are quickly converted to liquid droplets in the combustor. Liquid may evaporate and produces  $V_2O_5$  vapor in the high temperature environment. When the gas is cooling down,  $V_2O_5$  vapor starts nucleation process. High concentrations of  $V_2O_5$  ultrafine particles are produced. These ultrafine  $V_2O_5$  particles provide large surface areas, which can greatly facilitate the oxidation of  $Hg^0$ .

Particulate matter (fly ash) formation was not significantly affected by  $V_2O_5$  injection, in terms of particle size distributions and chemical compositions. In addition, the experimental results show that chlorine content in coal can enhance  $Hg^0$  oxidation on  $V_2O_5$  surface. A simple techno-economic analysis shows that the cost of the  $V_2O_5$  injection method is much lower than activated carbon injection, which has been widely used in industry.

## 6.5 References

Biswas, P., and C. Y. Wu. 1998. "Control of toxic metal emissions from combustors using sorbents: A review." *Journal of the Air & Waste Management Association* no. 48 (2):113-127.

Biswas, P., and M. R. Zachariah. 1997. "In Situ Immobilization of Lead Species in Combustion Environments by Injection of Gas Phase Silica Sorbent Precursors." *Environmental Science & Technology* no. 31 (9):2455-2463. doi: 10.1021/es9700663.

Bloomberge. *Vanadium Ore (pentoxide)Min 98% Europe \$ per lb V2O5* 2012. Available from <http://www.bloomberg.com/quote/MBVAV2O5:IND>.

Cao, Y., B. Chen, J. Wu, H. Cui, J. Smith, C. K. Chen, P. Chu, and W. P. Pan. 2007. "Study of mercury oxidation by a selective catalytic reduction catalyst in a pilot-scale slipstream reactor at a utility boiler burning bituminous coal." *Energy & Fuels* no. 21 (1):145-156. doi: 10.1021/ef0602426.

Cao, Y., Z. Gao, J. Zhu, Q. Wang, Y. Huang, C. Chiu, B. Parker, P. Chu, and W.-P. Pan. 2008. "Impacts of halogen additions on mercury oxidation, in a slipstream selective catalyst reduction (SCR), reactor when burning sub-bituminous coal." *Environmental Science & Technology* no. 42 (1):256-261. doi: 10.1021/es071281e.

Cao, Y., Q. Wang, C.-w. Chen, B. Chen, M. Cohron, Y.-c. Tseng, C.-c. Chiu, P. Chu, and W.-P. Pan. 2007. "Investigation of mercury transformation by HBr addition in a slipstream facility with real flue gas atmospheres of bituminous coal and powder river basin." *Energy & Fuels* no. 21 (5):2719-2730. doi: 10.1021/ef060547k.

Eswaran, S., and H. G. Stenger. 2005. "Understanding mercury conversion in selective catalytic reduction (SCR) catalysts." *Energy & Fuels* no. 19 (6):2328-2334. doi: 10.1021/ef050087f.

Galbreath, K. C., and C. J. Zygarlicke. 2000. "Mercury transformations in coal combustion flue gas." *Fuel Processing Technology* no. 65:289-310. doi: 10.1016/s0378-3820(99)00102-2.

Galbreath, K. C., C. J. Zygarlicke, J. E. Tibbetts, R. L. Schulz, and G. E. Dunham. 2005. "Effects of NO<sub>x</sub>, alpha-Fe<sub>2</sub>O<sub>3</sub>, gamma-Fe<sub>2</sub>O<sub>3</sub>, and HCl on mercury transformations in a 7-kW coal combustion system." *Fuel Processing Technology* no. 86 (4):429-448. doi: 10.1016/j.fuproc.2004.03.003.

Gale, T. K., and J. O. L. Wendt. 2002. "High-temperature interactions between multiple-metals and kaolinite." *Combustion and Flame* no. 131 (3):299-307. doi: Pii s0010-2180(02)00404-2  
10.1016/s0010-2180(02)00404-2.

Gale, T. K., and J. O. L. Wendt. 2003. "Mechanisms and models describing sodium and lead scavenging by a kaolinite aerosol at high temperatures." *Aerosol Science and Technology* no. 37 (11):865-876. doi: 10.1080/02786820390225808.

Gale, T. K., and J. O. L. Wendt. 2005. "In-furnace capture of cadmium and other semi-volatile metals by sorbents." *Proceedings of the Combustion Institute* no. 30:2999-3007. doi: 10.1016/j.proci.2004.08.197.

Ghorishi, S. B., C. W. Lee, W. S. Jozewicz, and J. D. Kilgroe. 2005. "Effects of fly ash transition metal content and flue gas HCl/SO<sub>2</sub> ratio on mercury speciation in waste combustion." *Environmental Engineering Science* no. 22 (2):221-231. doi: 10.1089/ees.2005.22.221.

Hedrick, E., T. G. Lee, P. Biswas, and Y. Zhuang. 2001. "The development of iodine based impinger solutions for the efficient capture of Hg<sup>0</sup> using direct injection nebulization—inductively coupled plasma mass spectrometry analysis." *Environmental Science & Technology* no. 35 (18):3764-3773. doi: 10.1021/es010648r.

Hoffmann, J., and J. Ratafia-Brown. 2003. Preliminary Cost Estimate of Activated Carbon Injection for Controlling Mercury Emissions from an Un-Scrubbed 500 MW Coal-Fired Power Plant. Science Applications International Corporation.

Jeong, S. K., S. B. Kim, S. S. Kim, X. Chen, and P. Biswas. 2007. "Simultaneous removal of Cd and Pb from flue gases using in-situ generated nano-sized sorbents." *Journal of Industrial and Engineering Chemistry* no. 13 (7):1154-1161.

Johnson, J. W., W. J. Silva, and D. Cubicciotti. 1966. "The vapor pressure and enthalpy of vaporization of molten mercuric chloride to the critical point." *Journal of Physical Chemistry* no. 70 (9):2985-2988. doi: 10.1021/j100881a044.

Jones, A. P., J. W. Hoffmann, D. N. Smith, T. J. Feeley, and J. T. Murphy. 2007. "DOE/NETL's phase II mercury control technology field testing program: Preliminary economic analysis of activated carbon injection." *Environmental Science & Technology* no. 41 (4):1365-1371. doi: 10.1021/es0617340.

Kamata, H., H. Ohara, K. Takahashi, A. Yukimura, and Y. Seo. 2001. "SO<sub>2</sub> oxidation over the V<sub>2</sub>O<sub>5</sub>/TiO<sub>2</sub> SCR catalyst." *Catalysis Letters* no. 73 (1):79-83. doi: 10.1023/a:1009065030750.



- Lamoreaux, R. H., D. L. Hildenbrand, and L. Brewer. 1987. "High-temperature Vaporization Behavior of Oxides. 2. Oxides of Be, Mg, Sr, Ba, B, Al, Ga, In, Tl, Si, Ge, Sn, Pb, Zn, Cd, and Hg." *Journal of Physical and Chemical Reference Data* no. 16 (3):419-443.
- Lee, M.-H., K. Cho, A. P. Shah, and P. Biswas. 2005. "Nanostructured Sorbents for Capture of Cadmium Species in Combustion Environments." *Environmental Science & Technology* no. 39 (21):8481-8489. doi: 10.1021/es0506713.
- Lee, T. G., P. Biswas, and E. Hedrick. 2001. "Comparison of Hg<sup>0</sup> capture efficiencies of three in situ generated sorbents." *AIChE Journal* no. 47 (4):954-961. doi: 10.1002/aic.690470418.
- Li, H., Y. Li, C.-Y. Wu, and J. Zhang. 2011. "Oxidation and capture of elemental mercury over SiO<sub>2</sub>-TiO<sub>2</sub>-V<sub>2</sub>O<sub>5</sub> catalysts in simulated low-rank coal combustion flue gas." *Chemical Engineering Journal (Lausanne)* no. 169 (1-3):186-193. doi:10.1016/j.cej.2011.03.003.
- Li, H., C.-Y. Wu, Y. Li, and J. Zhang. 2012. "Superior activity of MnO<sub>x</sub>-CeO<sub>2</sub>/TiO<sub>2</sub> catalyst for catalytic oxidation of elemental mercury at low flue gas temperatures." *Applied Catalysis B-Environmental* no. 111:381-388. doi: 10.1016/j.apcatb.2011.10.021.
- Li, Y., M. Daukoru, A. Suriyawong, and P. Biswas. 2009. "Mercury Emissions Control in Coal Combustion Systems Using Potassium Iodide: Bench-Scale and Pilot-Scale Studies." *Energy & Fuels* no. 23 (1):236-243. doi: 10.1021/ef800656v.
- Liu, S.-H., N.-Q. Yan, Z.-R. Liu, Z. Qu, P. Wang, S.-G. Chang, and C. Miller. 2007. "Using bromine gas to enhance mercury removal from flue gas of coal-fired power plants." *Environmental Science & Technology* no. 41 (4):1405-1412. doi: 10.1021/es061705p.

Nelson, S., Landreth, R., Zhou, Q., Miller, J. 2004. Accumulated Power-Plant Mercury-Removal Experience with Brominated PAC Injection. Sorbent Technologies Corporation.

Owens, T. M., and P. Biswas. 1996. "Vapor Phase Sorbent Precursors for Toxic Metal Emissions Control from Combustors." *Industrial & Engineering Chemistry Research* no. 35 (3):792-798. doi: 10.1021/ie9502446.

Pavlish, J. H., E. A. Sondreal, M. D. Mann, E. S. Olson, K. C. Galbreath, D. L. Laudal, and S. A. Benson. 2003. "State review of mercury control options for coal-fired power plants." *Fuel Processing Technology* no. 82 (2-3):89-165. doi: 10.1016/s0378-3820(03)00059-6.

Pflughoeft-Hassett, D. F., D. J. Hassett, T. D. Buckley, L. V. Heebink, and J. H. Pavlish. 2009. "Activated carbon for mercury control: Implications for fly ash management." *Fuel Processing Technology* no. 90 (11):1430-1434. doi: 10.1016/j.fuproc.2009.07.008.

Presto, A. A., and E. J. Granite. 2006. "Survey of catalysts for oxidation of mercury in flue gas." *Environmental Science & Technology* no. 40 (18):5601-5609. doi: 10.1021/es060504i.

Quann, R. J., M. Neville, M. Janghorbani, C. A. Mims, and A. F. Sarofim. 1982. "Mineral Matter and Trace-element Vaporization in a Laboratory-pulverized Coal Combustion System." *Environmental Science & Technology* no. 16 (11):776-781.

Senior, C. L. 2006. "Oxidation of mercury across selective catalytic reduction catalysts in coal-fired power plants." *Journal of the Air & Waste Management Association* no. 56 (1):23-31.

Senior, C. L., J. J. Helble, and A. F. Sarofim. 2000. "Emissions of mercury, trace elements, and fine particles from stationary combustion sources." *Fuel Processing Technology* no. 65:263-288. doi: 10.1016/s0378-3820(00)00082-5.

Senior, C. L., A. F. Sarofim, T. F. Zeng, J. J. Helble, and R. Mamani-Paco. 2000. "Gas-phase transformations of mercury in coal-fired power plants." *Fuel Processing Technology* no. 63 (2-3):197-213. doi: 10.1016/s0378-3820(99)00097-1.

Suriyawong, A., X. Chen, and P. Biswas. 2010. "Nano-Structured Sorbent Injection Strategies for Heavy Metal Capture in Combustion Exhausts." *Aerosol Science and Technology* no. 44 (8):676-691. doi: 10.1080/02786826.2010.485589.

Suriyawong, A., M. Smallwood, Y. Li, Y. Zhuang, and P. Biswas. 2009. "Mercury Capture by Nano-structured Titanium Dioxide Sorbent during Coal Combustion: Lab-scale to Pilot-scale Studies." *Aerosol and Air Quality Research* no. 9 (4):394-403. doi: 10.4209/aaqr.2009.02.0012.

Wang, X., S. Michael Daukoru, S. Torkamani, W.-N. Wang, and P. Biswas. 2013. "Role of exhaust gas recycle on submicrometer particle formation during oxy-coal combustion." *Proceedings of the Combustion Institute* no. 34 (2):3479-3487. doi:10.1016/j.proci.2012.07.049.

Wendt, J. O. L., and S. J. Lee. 2010. "High-temperature sorbents for Hg, Cd, Pb, and other trace metals: Mechanisms and applications." *Fuel* no. 89 (4):894-903. doi: 10.1016/j.fuel.2009.01.028.

Widiyastuti, W., A. Purwanto, W.-N. Wang, F. Iskandar, H. Setyawan, and K. Okuyama. 2009. "Nanoparticle formation through solid-fed flame synthesis: Experiment and modeling." *AICHE Journal* no. 55 (4):885-895. doi: 10.1002/aic.11695.

Wu, C. Y., T. G. Lee, G. Tyree, E. Arar, and P. Biswas. 1998. "Capture of mercury in combustion systems by in situ-generated titania particles with UV irradiation." *Environmental Engineering Science* no. 15 (2):137-148. doi: 10.1089/ees.1998.15.137.

Zhao, Y. X., M. D. Mann, J. H. Pavlish, B. A. F. Mibeck, G. E. Dunham, and E. S. Olson. 2006. "Application of gold catalyst for mercury oxidation by chlorine." *Environmental Science & Technology* no. 40 (5):1603-1608. doi: 10.1021/es050165d.

Zhuang, Y., C. Chen, R. Timpe, and J. Pavlish. 2009. "Investigations on bromine corrosion associated with mercury control technologies in coal flue gas." *Fuel* no. 88 (9):1692-1697. doi: 10.1016/j.fuel.2009.01.013.

Zhuang, Y., J. S. Thompson, C. J. Zygarlicke, and J. H. Pavlish. 2004. "Development of a mercury transformation model in coal combustion flue gas." *Environmental Science & Technology* no. 38 (21):5803-5808. doi: 10.1021/es030683t.

Zhuang, Y., J. S. Thompson, C. J. Zygarlicke, and J. H. Pavlish. 2007. "Impact of calcium chloride addition on mercury transformations and control in coal flue gas." *Fuel* no. 86 (15):2351-2359. doi: 10.1016/j.fuel.2007.02.016.

**CHAPTER 7. ROLE OF EXHAUST GAS RECYCLE ON  
SUBMICROMETER PARTICLE FORMATION DURING OXY-COAL  
COMBUSTION**

*The results of this chapter has been published in Wang, X.; Daukoru, S. M.; Torkamani, S.; Wang, W. N.; Biswas, P., Role of Flue Gas Recycle on Submicrometer Particle Formation during Oxy-Coal Combustion. Proceedings of the Combustion Institute 2013, 34(2): 3479-3487.*

## **Abstract**

During oxy-coal combustion, recycled exhaust gas is used as a diluent to replace nitrogen in pulverized coal-fired boilers to moderate boiler temperatures. The effect of recycle (up to recycle ratios of 60%) on combustion of Powder River Basin (PRB) coal related submicrometer particle formation was investigated in a drop-tube furnace system. The recycled exhaust gas containing lower O<sub>2</sub> concentration and higher CO<sub>2</sub> concentration suppressed submicrometer particle formation. However, it was found that water vapor in recycled exhaust gas greatly enhanced the formation of submicrometer particles. The gas composition changes that result with exhaust-gas recycle significantly affected the size distribution of submicrometer particles at the exit of the combustor. Differences in the particle size distribution with and without filtration of recycled exhaust gas was insignificant. The composition of the resultant particles in oxy-coal combustion and conventional coal-air combustion as determined by X-ray diffraction was similar.

## 7.1 Introduction

Coal combustion is the largest single contributor to global anthropogenic CO<sub>2</sub> emissions, contributing 42% of total CO<sub>2</sub> emissions and 73% of the CO<sub>2</sub> emissions associated with electricity and heat use (IEA 2009, Baumert et al. 2005). Oxy-coal combustion replaces the air with oxygen and uses recycled flue gas (RFG) as a diluent, resulting in a higher concentration (>98%) of carbon dioxide in the exhaust that promotes control, capture and possible conversion of CO<sub>2</sub> (Abraham et al. 1982, Buhre, Elliott, et al. 2005, Croiset and Thambimuthu 1999). Such a concept for boiler design has ancillary advantages of reduced NO<sub>x</sub> emissions (Okazaki and Ando 1997, Hu et al. 2001, 2003), reduced flue gas volume (Buhre, Elliott, et al. 2005), and heat transfer characteristics replicating those of existing, conventional pulverized-coal boilers (Tan et al. 2006). This combustion modality has the potential to be cheaper than post-combustion capture techniques (Singh et al. 2003, Beér 2007). However, the relationship between oxy-coal boiler design and emissions require detailed study, due to the impacts of such emissions on human health and the environment (Samet et al. 2000, Ramanathan et al. 2001) and on downstream processes such as compression and sequestration.

While many of the studies have investigated the effects of recycled exhaust gas on boiler performance, combustion efficiency, and gaseous pollutant emissions, only a few have focused on submicrometer particle formation (Suriyawong et al. 2006a, Sheng et al. 2007, Quann et al. 1990, Quann and Sarofim 1982), and none have done so at the laboratory scale with actual (rather than simulated) recycled exhaust gas. The formation of submicrometer particles bears continued relevance due to their penetration through conventional particle control devices (Li, Suriyawong, et al. 2009, Suriyawong et al. 2008) and concerns about their harmful effects on

human health should emissions occur (Samet et al. 2000). Understanding the formation mechanisms of submicrometer particles under various combustion modalities, including oxy-coal combustion with exhaust gas recycle, is therefore an important step in increasing the efficiency of particle control devices and systems. Using the same drop-tube furnace setup as used in this study, but without real recycle, Suriyawong *et al.* (2006a) studied submicrometer particle formation mechanisms during oxy-coal combustion and found surface temperature of burning char is a key parameter affecting the formation of submicrometer metal-oxide particles and their enrichment in trace metals, since it can affect metal-oxide vaporization rates as well as vaporization rates for volatile metals. Sheng and co-worker (Sheng et al. 2007, Sheng and Li 2008) studied submicrometer particle formation during oxy-coal combustion of a low-rank Chinese coal using a drop-tube furnace and confirmed CO<sub>2</sub> suppression of submicrometer particle formation via the vaporization-nucleation pathway. They also found that, in comparison to conventional O<sub>2</sub>-N<sub>2</sub> systems, oxy-coal combustion in O<sub>2</sub>-CO<sub>2</sub> did not affect the mineral phases detected but affected the relative amounts in which those phases were present in the total residual ash.

All of these laboratory-scale studies were performed using single pass flow-through drop-tube furnace studies that did not include exhaust gas recycling, an important aspect of oxy-coal combustion systems. This is a particularly important consideration as the exhaust gas usually contains high concentrations of aerosols and moisture. Recycle of the exhaust gas will introduce these back into the combustion chamber, and this may affect the resultant particle formation processes during coal combustion. The objective of this study is to investigate the role of exhaust gas recycle in submicrometer particle formation during oxy-coal combustion. The effect



of filtering and de-humidifying the recycled exhaust gas under different combustion conditions, such as different recycle ratios, coal feed rates and oxygen/carbon dioxide ( $O_2/CO_2$ ) ratios is established.

## **7.2 Experimental section**

The experimental system shown in Fig. 7.1a consists of a drop-tube furnace (Lindberg/Blue, ThermoElectron Corp., USA), containing an alumina tube (5.7-cm inner diameter and 121.9-cm long), and various sampling and measurement devices. Pulverized PRB sub-bituminous coal (supplied by Ameren UE, St. Louis, MO) was fed using a coal feeder (Quann et al. 1982) into the electrically-heated alumina tube in the drop-tube furnace at the rate of 0.5 or 2.5 g/hr. A total gas flow rate of 3.0 liter-per-minute (lpm) was maintained for all experiments conducted in this study to maintain a fixed residence time of 9 seconds, sufficient to achieve complete char burnout for all experiments.

The exhaust gas passed through a cascade impactor (Mark III, Pollution Control System Corp., Seattle, WA), removing ash particles larger than 500 nm. Certain fractions of exhaust gas were recycled back to the furnace. Before it entered the furnace, different treatments for the recycled exhaust gas were used to establish the impact on submicrometer aerosol formation (Table 7.1). The exhaust-gas recycle ratio is defined as the ratio of the volumetric flow rate ( $Q_1$ ) of recycled exhaust gas to the total volumetric gas flow rate ( $Q_1+Q_2$ ) through the furnace (Fig. 7.1a). The recycle ratio is a typical parameter applied to describe systems that include recycled flows such as engines with exhaust gas recirculation.

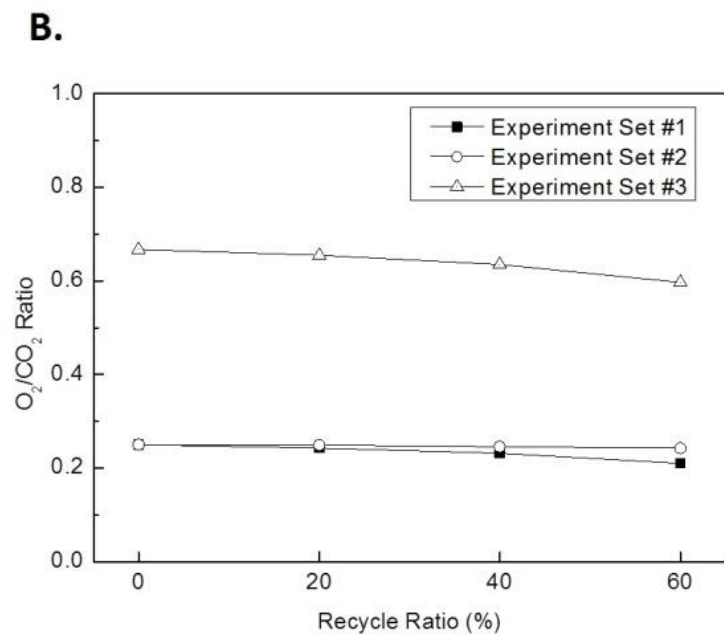
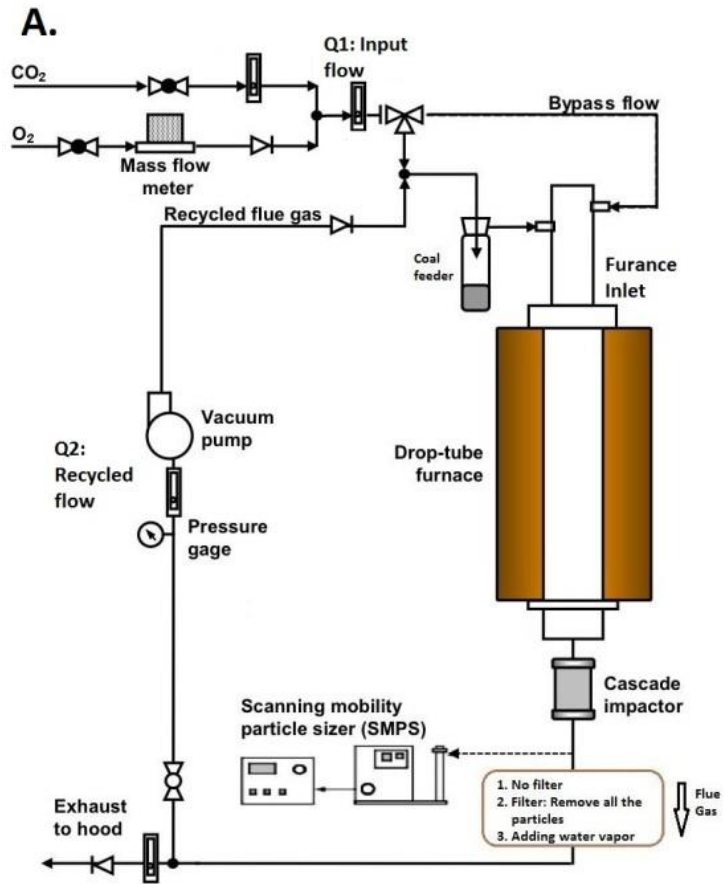


Figure 7.1. **a)** Schematic diagram of drop-tube furnace system for oxy-combustion studies with exhaust gas recycle; **b)**  $\text{O}_2/\text{CO}_2$  ratios at the furnace inlet under different recycle ratios .

Table 7.1. Summary of oxy-coal combustion test conditions (Q1 and Q2 are indicated in Fig. 7.1a).

Set	#	Coal Type	Coal Feed Rate (g/hr)	Input Flowrate, Q1 (lpm)	Recycle Flowrate, Q2 (lpm)	Recycle Ratio, (vol.%)	Input O <sub>2</sub> / CO <sub>2</sub> Ratio (v/v)	O <sub>2</sub> / CO <sub>2</sub> Ratio (v/v) at the Furnace Inlet	Fuel-air equivalence ratio	Treatment of Recycled Exhaust Gas
I	1	PRB	2.5	3.0	0	0	20/80 (=0.250)	0.250	0.087	N/A
	2			2.4	0.6	20		0.243	0.11	1. No filter; 2. With filter; 3. Adding humidity
	3			1.8	1.2	40		0.232	0.15	1. No filter; 2. With filter; 3. Adding humidity
	4			1.2	1.8	60		0.210	0.22	1. No filter; 2. With filter; 3. Adding humidity
II	1	PRB	0.5	3.0	0	0	20/80 (=0.250)	0.250	0.017	N/A
	2			2.4	0.6	20		0.249	0.022	1. No filter; 2. With filter
	3			1.8	1.2	40		0.246	0.03	1. No filter; 2. With filter
	4			1.2	1.8	60		0.242	0.044	1. No filter; 2. With filter
III	1	PRB	2.5	3.0	0	0	40/60 (=0.667)	0.667	0.044	N/A
	2			2.4	0.6	20		0.655	0.055	1. No filter; 2. With filter
	3			1.8	1.2	40		0.635	0.075	1. No filter; 2. With filter
	4			1.2	1.8	60		0.597	0.11	1. No filter; 2. With filter

Real-time submicrometer particle sampling was performed by drawing a 0.3-lpm slip-stream into a scanning mobility particle sizer (SMPS, TSI Inc., Shoreview, MN) to obtain the particle size distribution in the range of 9 ~ 425 nm. The overall experimental test plan is summarized in Table 7.1. The objective of the experiments is to compare particle formation during oxy-coal combustion using different treatments of recycled exhaust gas: 1) no treatment; 2) with filtration of particles (Millipore glass fiber filter, Type: APFA, all particles were removed); 3) with addition of moisture (Recycled flue gas was slowly passing through a glass impinger filled with water, which saturated the gas with water vapor. The relative humidity of the gas was achieving 100%. Then the gas mixed with dry input flow at the furnace inlet. The relative humidity at the furnace inlet was just equal to the recycle ratio at the room temperature. For example, the relative humidity at the furnace inlet is 40% when the recycle ratio is 40%. Therefore, if the

recycle ratio increases, the water vapor pressure will be higher in the furnace). There are 3 sets of experiments with different feed rates and O<sub>2</sub>/CO<sub>2</sub> ratios, in order to study effects of treatments under various conditions.

## **7.3 Results and discussion**

### *7.3.1. Effect of Filtered Exhaust Gas Recycle*

One of the most salient effects of exhaust gas recycle during oxy-coal combustion is on the gas composition in the furnace, since exhaust gas contains higher concentration of CO<sub>2</sub>. If some exhaust gas is recycled back to the furnace, the inlet gas composition will change and O<sub>2</sub>/CO<sub>2</sub> ratio will be lowered with an increase in the recycle ratio (Table 7.1, Fig. 7.1b). Changes in the inlet gas composition may affect submicrometer particle formation (Fig. 7.2) (Shaddix 2007), which is investigated here. To just study the impact of the change in inlet gas composition and to exclude the possible effect of particles in recycled exhaust gas, all particles in the recycled exhaust gas were removed by filtration.

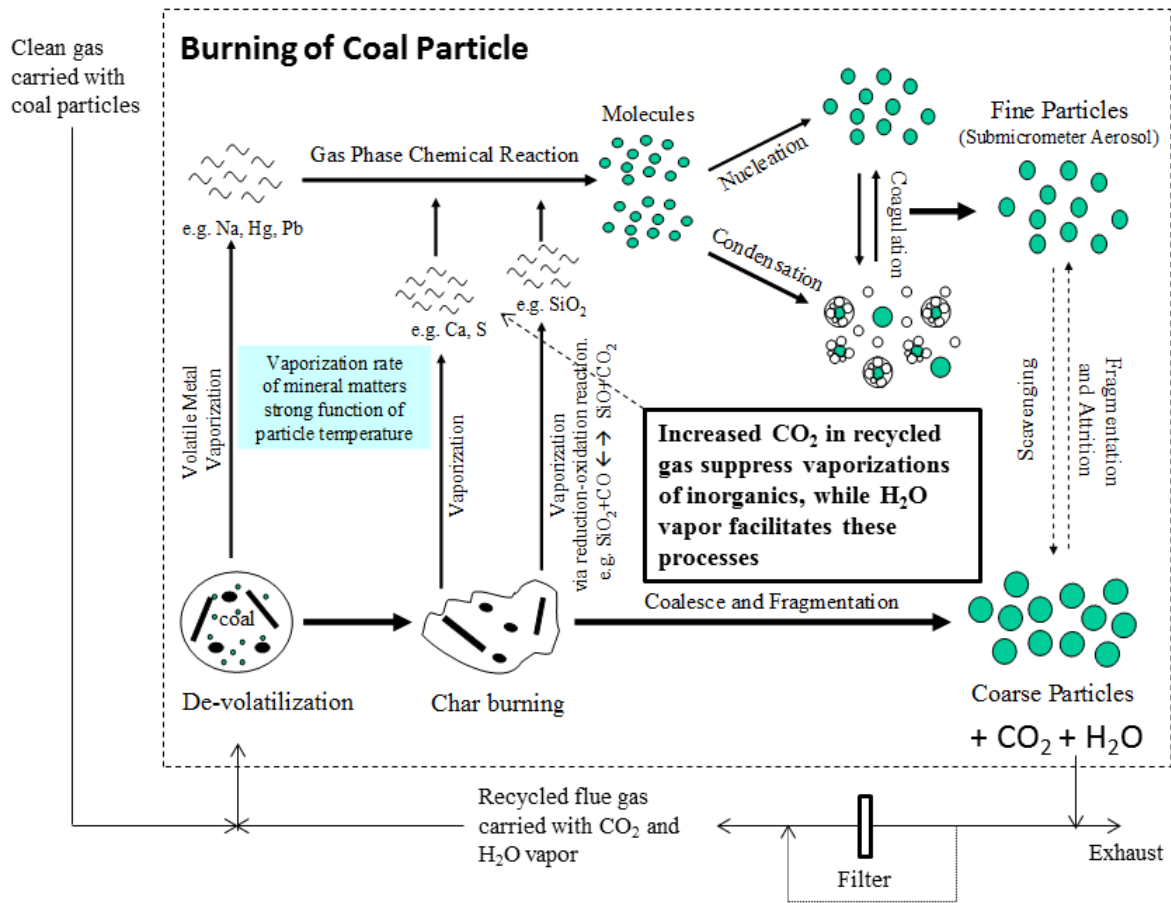


Figure 7.2. Ash particle formation pathways during oxy-coal combustion; adapted from Suriyawong et al. (2006a). Illustrated is the impact of recycle exhaust gas.

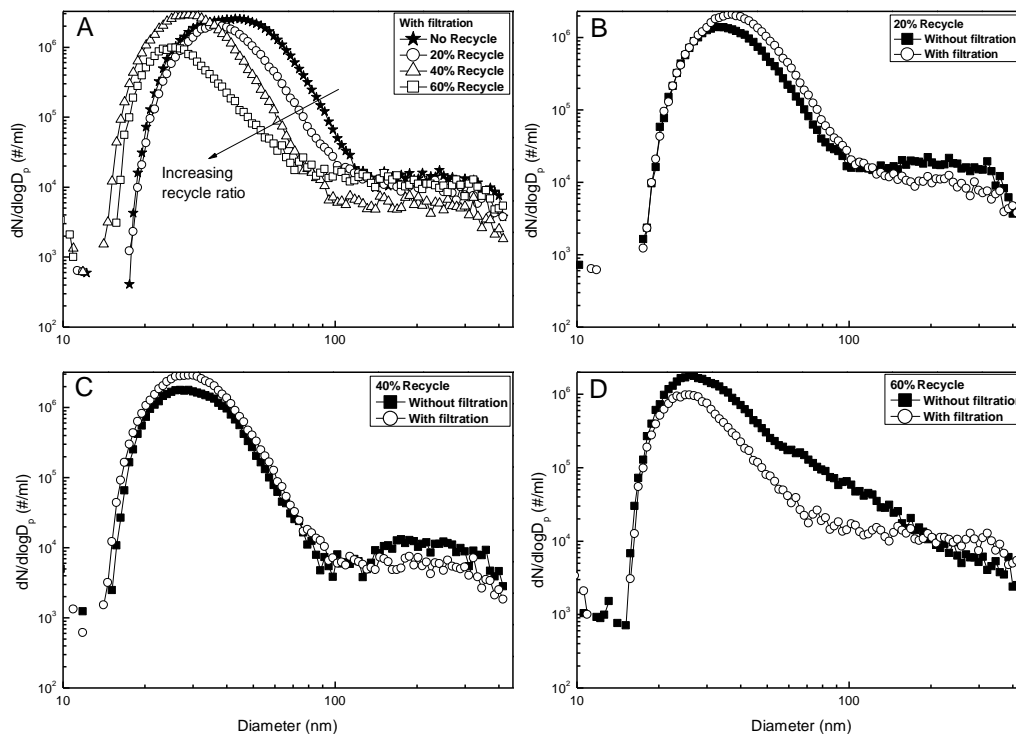


Figure 7.3. Combustion of PRB coal (Experiment Set #1): **a**) Particle size distributions under different recycle ratios with filtration of recycled exhaust gas; Comparisons of size distributions between with filtration and without filtration of recycled exhaust gas under recycle ratio: **b**) 20%; **c**) 40%; **d**) 60% .

Submicrometer particle size distributions comparing oxy-coal combustion without recycle to oxy-coal combustion with recycle at three recycle ratios are shown in Fig. 7.3a. The furnace temperature (1100 °C) and gas residence time were fixed for all experiments in the Experiment Set #1. Increasing exhaust-gas recycle ratios from 0 to 60%-recycle implied a 16% decrease in the O<sub>2</sub>/CO<sub>2</sub> ratio at the furnace inlet (Table 7.1). According to Fig. 7.3a, increasing recycle ratio

resulted in a leftward-shift of the particle size distribution, i.e. particle size tended to be smaller under higher recycle ratio conditions. This observation is explained by examining formation mechanisms of submicrometer particles during coal combustion.

The formation of submicrometer particles is depicted in Fig. 7.2 (Haynes et al. 1982b, Damle et al. 1982b, Suriyawong et al. 2006a). Several studies have established that the metal-oxide vaporization-nucleation pathway accounts for most of the submicrometer particle mass (Damle et al. 1982b). This pathway involves: 1) metal-oxide reduction at the char surface to produce relatively volatile sub-oxides; 2) sub-oxide vaporization and rapid re-oxidation to form stable metal-oxide nuclei, and 3) subsequent growth by coagulation and condensation. Assuming that the reduction of metal oxides by carbon monoxide takes place at equilibrium at the char surface, the partial pressure of respective sub-oxide vapors ( $P_{SiO}$ ) can be expressed a function of bulk  $O_2$ - $CO_2$  concentrations ( $P_{CO}$ ,  $P_{CO_2}$ ) as well as the temperature( $T$ )-dependent equilibrium constants ( $K$ ) and the activity coefficient ( $\alpha_{SiO}$ ) (Suriyawong et al. 2006a, Senior, Panagiotou, et al. 2000):  $P_{SiO} = \alpha_{SiO} \times K(T) \times P_{CO} / P_{CO_2}$ . Therefore, the bulk gas composition has both direct and indirect effects on the vapor equilibrium of volatile sub-oxides: directly via the partial pressures of bulk  $O_2$  and  $CO_2$ , and indirectly via the vaporization temperature, which is also dependent on the bulk gas composition, since  $CO_2$  has larger heat capacity than  $O_2$ . Higher concentration of  $CO_2$  leads to a lower flame temperature (Suriyawong et al. 2006a). The higher fraction of recycled exhaust gas mixed with the inlet gas led to lower resultant  $O_2/CO_2$  ratios in the combustor. Due to the reasons elucidated earlier, the lower  $O_2/CO_2$  ratio results in the shift of particle size distribution to smaller sizes (as illustrated in Fig. 7.3a).

X-ray diffraction was also used to identify the major metal-oxide species present in collected submicrometer ash samples for three combustion conditions: (a) coal-air, (b) oxy-coal without exhaust gas recycle, and (c) oxy-coal with a 40% filtered exhaust-gas recycle ratio (Fig. 7.4). Figure 7.4 shows that the most prominent peaks result from silica (S), which is the major ash constituent. Not much difference was observed in terms of silica peak intensity, and none of the identified silica peaks appeared to be altered by exhaust gas recycle. This observation is consistent with the results of Sheng and Li (2008). The same conclusions could be drawn for alumina (A) peaks (at around 26 and 52°), where no noticeable changes were observed in terms of peak intensity. Slightly diminishing strength of calcium oxide (C) peak at around 31° was found when comparing oxy-coal without recycle to oxy-coal with 40% recycle. However, major differences were observed for hematite ( $\text{Fe}_2\text{O}_3$ , H). The strongest  $\text{Fe}_2\text{O}_3$  peak (~33°) diminished in strength under oxy-combustion conditions, while the same peak did not appear to be affected by exhaust-gas recycle. The reduction is possibly due to the longer retention time of particles in the furnace when recycle was applied. Thus,  $\text{Fe}_2\text{O}_3$  had more time to react with CaO or other metal oxides to form ferrites.



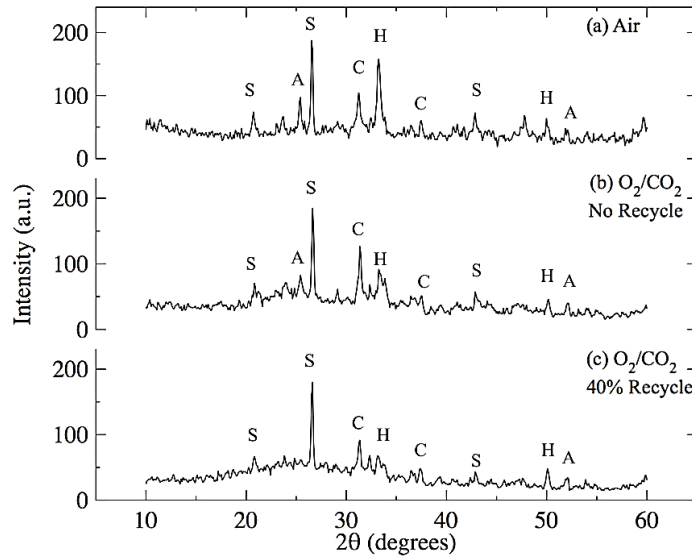


Figure 7.4. X-ray diffractograms of submicrometer ash particles, comparing conventional coal-air with oxy-coal combustion without recycle and oxy-coal combustion with recycle (S: SiO<sub>2</sub>, A: Al<sub>2</sub>O<sub>3</sub>, C: CaO, H: Fe<sub>2</sub>O<sub>3</sub>).

### 7.3.2. Effect of Exhaust Gas Recycle Without Filtration

Exhaust gas contains high concentration of submicrometer particles. If recycled exhaust gas was directly sent back to the furnace without filtration, the particles in the recycled exhaust gas may affect particle formation during the coal combustion. For example, when the particles in recycled exhaust gas enter the furnace, they can act as nuclei on which metal/metal suboxide vapor would condense, thereby suppressing new particle formation (nucleation) and leading to a shift of particle size distributions to larger sizes. Figure 7.3b-7.3d shows the comparisons of particle size distributions with/without filtration of recycled exhaust gas at different recycle ratios. No significant differences were observed. One of the possible reasons for this is that particles entering the furnace may re-evaporate in the high temperatures zone, such as the region where volatiles, released from coal pyrolysis, are oxidized. The presence of H<sub>2</sub> formed during

coal pyrolysis (Solomon et al. 1988) can provide a reducing environment for enhanced vaporization of the metal oxides that enter the combustion zone with the recycled exhaust gas. The other reason could be that the submicrometer particles in the recycled gas are lost by other mechanisms such as deposition and scavenging by the unburned coal particles. Results from these studies indicate that the submicrometer particles introduced into the combustion chamber therefore do not have a significant effect on altering the size distribution of the resultant particles. The primary reason for the shift in the distributions is due to the alteration of the gas composition as described earlier.

### *7.3.3 Effect of Humidification of Recycled Exhaust Gas*

Coal has a certain amount of moisture content, and hydrogen in its matrix. When it is combusted, moisture is released as water vapor and hydrogen atoms also form water vapor via oxidation. Recycle of the unconditioned exhaust gas would result in water vapor being introduced into the combustor. As illustrated in many previous studies, water vapor plays an important role in submicrometer particle formation. It can greatly enhance the growth rate of nuclei (Kulmala and Laaksonen 1990, Kulmala et al. 2000), by a lowering of the energy barrier to convert vapors into submicrometer particles, thereby significantly enhancing particle nucleation and subsequent growth rate (Kulmala and Laaksonen 1990). In addition, water vapor is a catalyst for CO oxidation (Sundaresan and Amundson 1980). It may also enhance the CO oxidation rate around the char particle, thereby increasing its surface temperature, leading to faster vaporization of inorganic minerals and enhancement of aerosol formation.

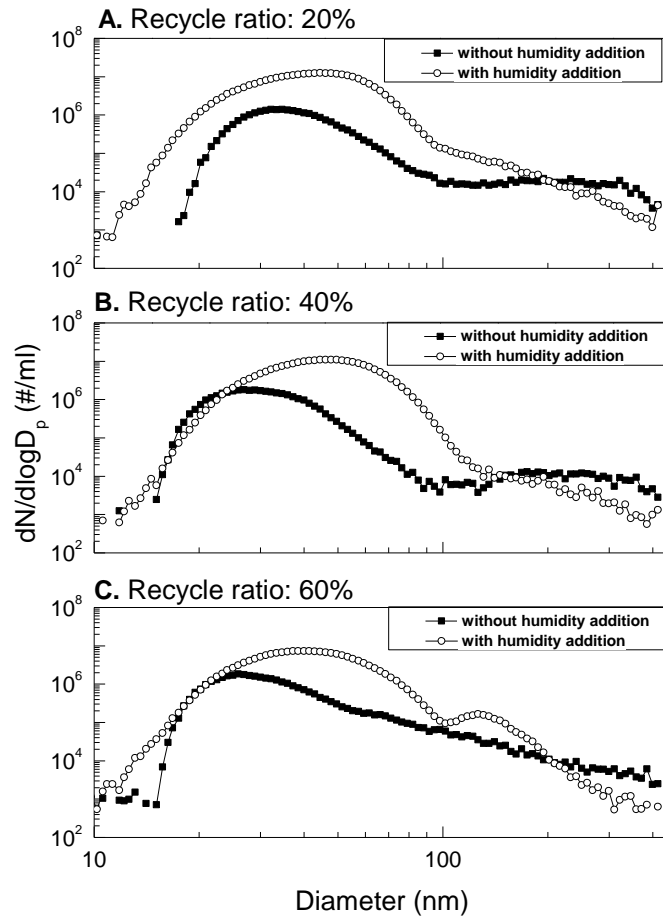


Figure 7.5. Comparisons of size distributions between with and without moisture addition of recycled exhaust gas under recycle ratio: **a)** 20%; **b)** 40%; **c)** 60% .

The effect of humidification of the recycled exhaust gas on particle formation is shown in Fig. 7.5. The recycled exhaust gas was saturated with water vapor before it was re-introduced into the furnace. This resulted in a significant increase in aerosol concentration, particularly in the size range from 30 ~ 100 nm (Fig. 7.5). For example, the increase was as high as two orders of magnitude in the size range around 60 nm at a recycle ratio of 40%. In addition, the size

distributions shifted to the large particle size significantly during humidification. The effect of hygroscopicity of particles may also account for this phenomenon. Particles from coal combustion contain large fraction of inorganic species (e.g. CaO and MgO) (Buhre, Hinkley, et al. 2005), which can absorb water vapor and grow to larger size (Seinfeld and Pandis 2006). Moreover, the particle size in the 60%-recycle case has a bimodal distribution. The larger mode may result from particle coagulation via collisions among smaller particles whose concentrations are greatly enhanced by humidification. The detailed mechanisms need further investigation. Based on this result, removal of moisture of recycled exhaust gas is strongly recommended in oxy-coal combustion systems to ensure no increase of submicrometer particle formation in the combustor.

#### *7.3.4 Effect of Coal Feed Rate*

In order to compare the effect of feed rate on submicrometer particle formation, the coal feed rate was changed to 0.5 g/hr while other conditions were kept the same as in Experiment Set #1. Figure 7.6a shows the particle size distributions under different recycle ratios with filtration of recycled exhaust gas. When recycle ratio was equal to 0, both the particle number concentration and mean particle size were significantly lower and smaller than that in the Experimental Set #1, since smaller amount of coal produced lower concentrations of submicrometer particles. However, there is no perceptible change among the various particle size distributions at different recycle ratios. Table 7.1 shows that at the lower coal feed rate (0.5 g/hr), O<sub>2</sub>/CO<sub>2</sub> ratio did not change too much when the recycle ratio was increased (the O<sub>2</sub>/CO<sub>2</sub> ratio had a 3% decrease). Thus the particle size distribution also did not change significantly. Figure 7.6b-7.6c shows the comparison between the runs with filtrated recycled exhaust gas and those without filtration at different recycle ratios. As in the previous experiments, the results further confirm that removal

of particles in recycled exhaust gas did not affect submicrometer particle formation during coal combustion.

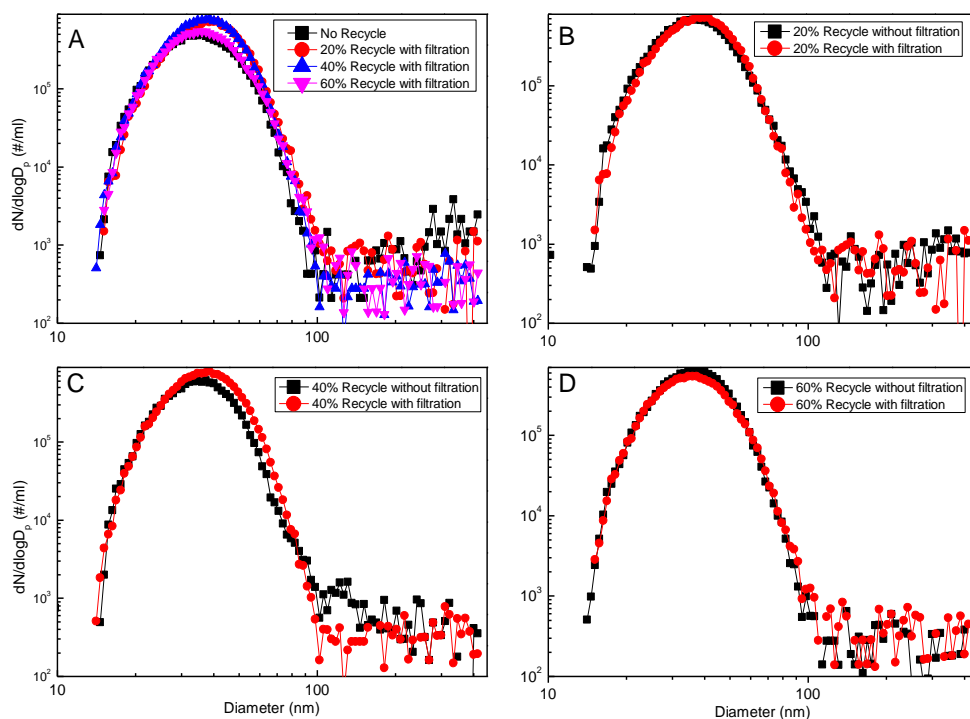


Figure 7.6. Combustion of PRB coal at the lower feed rate (Experiment Set #2): **A**) Particle size distributions under different recycle ratios with filtration of recycled exhaust gas; Comparisons of size distributions between with filtration and without filtration of recycled flue gas under recycle ratio: **B**) 20%; **C**) 40%; **D**) 60% .

### 7.3.5 Effect of $O_2/CO_2$ Ratio

As previously illustrated, the gas composition plays a critical role in influencing particle formation during coal combustion. Figure 7.7 shows the results from Experiment Set #3, which

used the same conditions as the Experiment Set #1 except for a higher O<sub>2</sub>/CO<sub>2</sub> Ratio (40/60). Higher O<sub>2</sub> concentration leads to higher char surface temperature (Caram and Amundson 1977), which results in higher vaporization rate of inorganic minerals and enhancement of submicrometer particle formation. Compared with Fig. 7.3a, the size distributions in Fig. 7.7a were much higher and broader, confirming that particle formation was enhanced for conditions in Experiment Set #3. Moreover, the size distributions shifted slightly to the left when recycle ratio was increased. This is because while recycle ratio varied from 0 to 60%, the O<sub>2</sub>/CO<sub>2</sub> ratio changed by about 10.5%, which is smaller than that in the Experimental Set #1 (~ 16%). Similar to the results of Experimental Set #1 & 2, Figure 6.7b-6.7d also shows no difference in the size distributions where the exhaust gas was filtered compared to that without filtration, at different recycle ratios. Notably, the particle concentrations were much higher in Experimental Set #3 tests as the recycled exhaust gas contained higher concentration of submicrometer particles. However, this higher concentration still did not significantly affect the particle size distributions in the coal combustor.

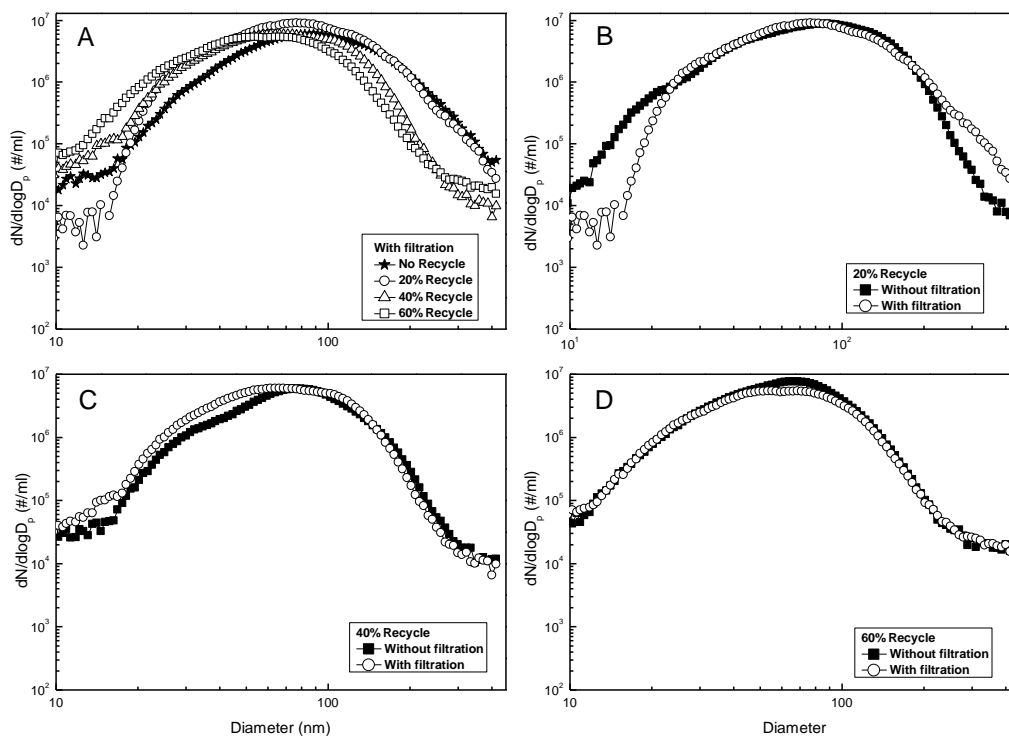


Figure 7.7. Combustion of PRB coal at higher  $O_2/CO_2$  ratio (Experiment Set #3): **a)** Particle size distributions under different recycle ratios with filtration of recycled exhaust gas; Comparisons of size distributions between with filtration and without filtration of recycled exhaust gas under recycle ratio: **b)** 20%; **c)** 40%; **d)** 60% .

#### 7.4 Conclusions

The role of exhaust gas recycle (up to a ratio of 60%) during oxy-coal combustion of PRB coal on submicrometer aerosol formation was investigated. The primary reason for alteration of the size distribution of the particles formed in the combustor was due to the alteration of the gas composition during exhaust gas recycle. The increase in the concentration of carbon dioxide in

the combustor due to the recycling of exhaust gases suppressed submicrometer particle formation. No major difference in the crystal structure of the mineral matter was observed as a result of the recycling of exhaust gases. Difference in the particle size distribution for oxy-combustion with and without filtration of recycled exhaust gas was insignificant, indicating that the existing particles in recycled gases do not impact formation of particles during oxy-coal combustion.

Water vapor in the recycled exhaust gas however was shown to increase the growth rate of submicrometer particles. This was attributed to enhancement of particle nucleation and catalytic CO oxidation on the surface of the char particle by increased water vapor in the combustor. The effect of hygroscopicity of particles may also account for the growth of submicrometer particles. The results indicate that removal of moisture prior to recycling of exhaust gases may be an important consideration.



## 7.5 References

- Abraham, B. M., J. G. Asbury, E. P. Lynch, and A. P. S. Teotia. 1982. "Coal-oxygen process provides carbon dioxide for enhanced recovery." *Oil Gas J* no. 80 (11):68-70.
- Baumert, K. A., T. Herzog, and J. Pershing. 2005. *Navigating the Numbers: Greenhouse Gas Data and International Climate Policy*. World Resources Institute.
- Beér, J. M. 2007. "High efficiency electric power generation: The environmental role." *Progress in Energy and Combustion Science* no. 33 (2):107-134. doi: 10.1016/j.pecs.2006.08.002.
- Buhre, B., L. Elliott, C. Sheng, R. P. Gupta, and T. F. Wall. 2005. "Oxy-fuel combustion technology for coal-fired power generation." *Progress in Energy and Combustion Science* no. 31 (4):283-307. doi: 10.1016/j.pecs.2005.07.001.
- Buhre, B. J. P., J. T. Hinkley, R. P. Gupta, T. F. Wall, and P. F. Nelson. 2005. "Submicron ash formation from coal combustion." *Fuel* no. 84 (10):1206-1214. doi: 10.1016/j.fuel.2004.08.025.
- Caram, H. S., and N. R. Amundson. 1977. "Diffusion and Reaction in a Stagnant Boundary Layer about a Carbon Particle." *Industrial & Engineering Chemistry Fundamentals* no. 16 (2):171-181. doi: 10.1021/i160062a001.
- Croiset, E., and K. Thambimuthu. 1999. "Coal combustion with flue gas recirculation for CO<sub>2</sub> recovery." In *Greenhouse gas technologies*, edited by P. Riemer, B. Eliasson and A. Wokaun, 581-6. Amsterdam: Elsevier Science.

Damle, A. S., D. S. Ensor, and M. B. Ranade. 1982. "Coal Combustion Aerosol Formation Mechanisms: A Review." *Aerosol Sc. & Tech.* no. 1 (1):119-133. doi: 10.1080/02786828208958582.

Haynes, B. S., M. N. Neville, R. J. Quann, and A. F. Sarofim. 1982. "Factors governing the surface enrichment of fly ash in volatile trace species." *Journal of Colloid and Interface Science* no. 87 (1):266-278.

Hu, Y. Q., N. Kobayashi, and M. Hasatani. 2001. "The reduction of recycled-NO<sub>x</sub> in coal combustion with O<sub>2</sub>/recycled flue gas under low recycling ratio." *Fuel* no. 80 (13):1851-1855.

Hu, Y. Q., N. Kobayashi, and M. Hasatani. 2003. "Effects of coal properties on recycled-NO<sub>x</sub> reduction in coal combustion with O<sub>2</sub>/recycled flue gas." *Energy Conversion and Management* no. 44 (14):2331-2340.

IEA. 2009. CO<sub>2</sub> Emissions from Fuel Combustion Highlights.

Kulmala, M., and A. Laaksonen. 1990. "Binary Nucleation of Water Sulfuric-acid System - Comparison of Classical-Theories With Different H<sub>2</sub>SO<sub>4</sub> Saturation Vapor-Pressures." *Journal of Chemical Physics* no. 93 (1):696-701.

Kulmala, M., U. Pirjola, and J. M. Makela. 2000. "Stable sulphate clusters as a source of new atmospheric particles." *Nature* no. 404 (6773):66-69.

Li, Y., A. Suriyawong, M. Daukoru, Y. Zhuang, and P. Biswas. 2009. "Measurement and Capture of Fine and Ultrafine Particles from a Pilot-Scale Pulverized Coal Combustor with an

Electrostatic Precipitator." *J. Air & Waste Manage. Assoc.* no. 59 (5):553-9. doi: [10.3155/1047-3289.59.3.1](https://doi.org/10.3155/1047-3289.59.3.1).

Okazaki, K., and T. Ando. 1997. "NO<sub>x</sub> reduction mechanism in coal combustion with recycled CO<sub>2</sub>." *Energy* no. 22 (2/3).

Quann, R. J., M. Neville, M. Janghorbani, C. A. Mims, and A. F. Sarofim. 1982. "Mineral Matter and Trace-element Vaporization in a Laboratory-pulverized Coal Combustion System." *Environmental Science & Technology* no. 16 (11):776-781.

Quann, R. J., M. Neville, and A. F. Sarofim. 1990. "A Laboratory Study of the Effect of Coal Selection on the Amount and Composition of Combustion Generated Submicron Particles." *Combustion Sc. & Tech.* no. 74 (1):245-265.

Quann, R. J., and A. F. Sarofim. 1982. "Vaporization of refractory oxides during pulverized coal combustion." *Symposium (International) on Combustion* no. 19 (1):1429-1440.

Ramanathan, V., P. J. Crutzen, J. T. Kiehl, and D. Rosenfeld. 2001. "Aerosols, Climate, and the Hydrological Cycle." *Science* no. 294 (5549):2119-2124. doi: [10.1126/science.1064034](https://doi.org/10.1126/science.1064034).

Samet, J. M., F. Dominici, F. C. Curriero, I. Coursac, and S. L. Zeger. 2000. "Fine particulate air pollution and mortality in 20 US cities, 1987-1994." *New England journal of medicine* no. 343 (24):1742.

Seinfeld, J. H., and S. N. Pandis. 2006. *Atmospheric Chemistry and Physics: From Air pollution to Climate Change*. 2 ed. New York: Wiley-Interscience.

Senior, C. L., T. Panagiotou, A. F. Sarofim, and J. J. Helble. 2000. Formation of Ultrafine Particulate Matter from Pulverized Coal Combustion. In *219th American Chemical Society National Conference*. San Francisco, CA: American Chemical Society.

Shaddix, C. 2007. Coal Particle Ignition, Devolatilisation & Char Combustion Kinetics During Oxy-Combustion. In *Intl. Oxy-Combustion Research Network*. Windsor, CT: IEA Greenhouse Gas R&D Programme.

Sheng, C., and Y. Li. 2008. "Experimental study of ash formation during pulverized coal combustion in O<sub>2</sub>/CO<sub>2</sub> mixtures." *Fuel* no. 87 (7):1297-1305. doi: 10.1016/j.fuel.2007.07.023.

Sheng, C., Y. Lu, X. Gao, and H. Yao. 2007. "Fine Ash Formation during Pulverized Coal Combustion--A Comparison of O<sub>2</sub>/CO<sub>2</sub> Combustion versus Air Combustion." *Energy & Fuels* no. 21:435-440.

Singh, D., P. Croiset, P. L. Douglas, and M. A. Douglas. 2003. "Techno-economic study of CO<sub>2</sub> capture from an existing coal-fired power plant: MEA scrubbing Vs. O<sub>2</sub>/CO<sub>2</sub> recycle combustion." *Energy Convers Manage* no. 44:3073-3091.

Solomon, P. R., D. G. Hamblen, R. M. Carangelo, M. A. Serio, and G. V. Deshpande. 1988. "General model of coal devolatilization." *Energy & Fuels* no. 2 (4):405-422. doi: 10.1021/ef00010a006.

Sundaresan, S., and N. R. Amundson. 1980. "Diffusion and Reaction in a Stagnant Boundary Layer about a Carbon Particle. 6. Effect of Water Vapor on the Pseudo-Steady-State Structure." *Industrial & Engineering Chemistry Fundamentals* no. 19 (4):351-357. doi: 10.1021/i160076a005.

Suriyawong, A., M. Gamble, M.-H. Lee, R. Axelbaum, and P. Biswas. 2006. "Submicrometer Particle Formation and Mercury Speciation Under O<sub>2</sub>-CO<sub>2</sub> Coal Combustion." *Energy & Fuels* no. 20:2357-2363.

Suriyawong, A., C. J. Hogan Jr, J. Jiang, and P. Biswas. 2008. "Charged fraction and electrostatic collection of ultrafine and submicrometer particles formed during O<sub>2</sub>-CO<sub>2</sub> coal combustion." *Fuel* no. 87 (6):673-682. doi: 10.1016/j.fuel.2007.07.024.

Tan, Y., E. Croiset, M. A. Douglas, and K. V. Thambimuthu. 2006. "Combustion characteristics of coal in a mixture of oxygen and recycled flue gas." *Fuel* no. 85 (4):507-512. doi: 10.1016/j.fuel.2005.08.010.

## **CHAPTER 8. CONCLUSIONS**

This chapter summarizes the major findings of this study.

### **8.1 Organic aerosol formation during coal combustion (Chapter 2, 3, 4 and 5)**

The first part of this dissertation unraveled the formation mechanism of organic aerosol during coal combustion. In this part of study, a set of experiments was conducted in a 1 MW pilot-scale coal combustor to investigate the sensitivities of organic carbon aerosol and black carbon aerosol to combustion conditions. It is shown that black carbon aerosol formation was extremely sensitive to the fuel-air equivalence ratio. The elemental (black) carbon aerosol concentration in flue gas decreased drastically from 236  $\mu\text{g}/\text{m}^3$  to 2.4  $\mu\text{g}/\text{m}^3$  when the fuel-air equivalence ratio was only slightly reduced, from 0.92 to 0.80. However, the emission of organic carbon aerosol was not as sensitive as black carbon aerosol. And surprisingly, organic carbon aerosol formation was enhanced by increasing the fuel-air equivalence ratio, which trend was opposite to that of black carbon aerosol formation. Coal was also combusted in an oxygen-rich environment. The formation of inorganic submicrometer particle was greatly enhanced in this mode, compared to conventional air firing. Significant concentrations of organic carbon aerosol were still present in the flue gas, while concentrations of black carbon aerosol were zero. This finding strongly indicates the difference between organic carbon aerosol formation and black carbon aerosol formation.

Detailed organic aerosol formation mechanisms have been studied in a lab-scale system. Aerosol mass spectrometry techniques were applied to characterize coal combustion aerosols from a drop-tube coal combustor and coal pyrolysis products from a flat-flame coal pyrolyzer. The chemical composition of major species for both combustion organic aerosols and pyrolysis products are hydrocarbons, carboxylic acids and aromatic compounds. The similarities of the chemical compositions demonstrate that the products from coal pyrolysis, the initial step of coal

combustion, are the precursors of organic aerosols. More carboxylic acids and oxygenated organic compounds were found in the combustion aerosols, indicating that many pyrolysis products are oxidized before conversion to organic aerosols.

A strong correlation between inorganic and organic aerosol formations has been found in this work, demonstrating that inorganic particles play a critical role as carriers of organic species. Sulfate species in inorganic aerosols play a particularly important role in organic aerosol formation. Enhanced organic aerosol formation during the combustion of high sulfur content coal has been observed for the first time. High resolution mass spectra analysis shows the presence of amine-like organics in aerosols. The correlation between particulate sulfate and organics suggests that acidic sulfate species may convert basic amine-like organics, a major type of coal pyrolysis products, from the gas phase to the particle phase through acid-base neutralization reactions.

## **8.2 Mercury removal during coal combustion by injection of Vanadium Pentoxide ( $V_2O_5$ ) (Chapter 6)**

The second part examines the performance of this method on Hg capture from pulverized coal combustion in a drop-tube furnace.  $V_2O_5$  was tested as a sorbent and demonstrated good performance on elemental mercury capture. The effective performance of  $V_2O_5$  results from the formation of ultrafine  $V_2O_5$  particles during the combustion process. It is proposed that the ultrafine  $V_2O_5$  particles catalyzed  $Hg^0$  oxidation on their large surfaces.  $Hg^{2+}$ , the oxidation product, may condense on fly ash particle surfaces or on tubing surfaces, thereby being removed from the flue gas.



### **8.3 Submicrometer particle formation during oxy-coal combustion (Chapter 7)**

This part of the dissertation investigates the effects of recycle (up to recycle ratios of 60%) on the combustion of Powder River Basin (PRB) coal-related submicrometer particle formation in a drop-tube furnace system. The recycled exhaust gas containing a lower O<sub>2</sub> concentration and a higher CO<sub>2</sub> concentration suppressed submicrometer particle formation. However, it was found that water vapor in recycled exhaust gas greatly enhanced the formation of submicrometer particles. The gas composition changes that result from exhaust-gas recycle significantly affected the size distribution of submicrometer particles at the exit of the combustor. Differences in the particle size distribution with and without the filtration of recycled exhaust gas were insignificant. The composition of the resultant particles in oxy-coal combustion and conventional coal-air combustion as determined by X-ray diffraction was similar.

### **8.4 Implications for “Real World”**

- Coal combustion aerosol may be a major source of atmospheric aerosols, especially in developing countries, due to ineffective use of emission control systems. Source apportionment for atmospheric aerosols is key information for government to make policies to reduce aerosol pollutions in the air. Chapter 3 characterized organic aerosol from coal combustion in great detail. We detected many specific organic signals, which can be used as tracers for coal combustion aerosols. Atmospheric scientists could use this information to identify the contribution from coal combustion to total atmospheric aerosols.
- Chapter 3 and 4 investigated the formation mechanisms of organic aerosol during coal combustion. They are fundamental researches, which identified the important roles of coal pyrolysis and inorganic aerosols on formation of organic aerosols.

- Chapter 5 reported a new source of nitrogen-containing organic aerosol: combustion of high sulfur content coal. This work shows that nitrogen-containing organic matter comprises a large fraction of total organic aerosol emission from combustion of high sulfur content coal. These organic species could be very toxic, since their structure may be similar to aromatic amines, a type of known toxic substances. Many developing countries are still using high sulfur content coal. For example, about 8% of coal used in China has a sulfur content larger than 3%. Therefore, combustion of high sulfur content coal may produce a large amount of these nitrogen-containing organic aerosols in the atmosphere, especially in developing countries.
- Chapter 6 reported a new method to do the Hg control from coal combustion: High temperature sorbent injection using  $V_2O_5$  as sorbent. This method has a relatively high Hg capture efficiency and it is simple and inexpensive.
- Chapter 7 examined the effect of flue gas recycle on submicrometer particle formation during oxy-coal combustion. The obtained information can be used to understand particle formation in future oxy-coal boilers.

## **CHAPTER 9. FUTURE WORK**

## **9.1 Further elucidation of formation pathways of organic aerosols during coal combustion**

This dissertation presents strong evidence for a proposed mechanism of organic aerosol formation during coal combustion: when coal particles are combusted in the furnace, tars are released. In the furnace, most of gas-phase tar is quickly oxidized and fully combusted. However, some of the tar species are adsorbed by the inorganic ash particles with chemical composition such as  $\text{SiO}_2$ ,  $\text{Al}_2\text{O}_3$ ,  $\text{CaO}$  and sulfate. These particles can protect tar from further oxidation. Particulate organic matter can survive in the highly oxidizing environment and get emitted to the atmosphere. In addition, this dissertation reports a strong correlation of concentrations between sulfate particles and organic aerosols. It is proposed that some acidic sulfate particles may help trap nitrogen-containing tars via acid-base neutralization reactions. Although many experimental evidences strongly support the proposed formation pathways of organic aerosols, there are still some problems that need to be elucidated:

- (1) How are organics mixed with inorganic matter during initial stage of combustion?
- (2) Is oxidation of organic aerosol really retarded by mixing with inorganic matter?
- (3) Can acidic sulfate particles really absorb amine species from gas phase to particle phase?
- (4) What are the forms of sulfate in coal combustion aerosols?
- (5) Do other inorganic components play a similar role in the formation of organic aerosol with sulfur?
- (6) Can char particles still release trace amounts of organic volatiles?

Thus, to answer these questions, a list of future work is suggested:

### *9.1.1 How are organics mixed with inorganic matter?*

It is proposed that tar species are adsorbed by the inorganic ash particles, which may retard the oxidation of absorbed tar species. How the organics are mixed with inorganics directly affects

retardation of organics oxidation. Thus, it is very important to know how the organics are mixed with inorganic matter in a coal combustion aerosol. There are three possible ways of mixing: 1) organics are present on the surface of inorganic particles, 2) they are mixed homogeneously with inorganic matter, and 3) organics are present in the core of inorganic particles. And obviously, the latter two ways of mixing are more likely to retard oxidation of organics.

To answer this question, coal combustion aerosols produced from different combustion conditions may be collected on Transmission electron microscopy (TEM) grids. High-resolution TEM can be used to observe how organics are mixed with inorganic matter. It is also very interesting to see how sulfur content affects the mixing of organics and inorganics.

#### *9.1.2 Is oxidation of organic aerosol really retarded by mixing with inorganic matter?*

To answer this question, a very controlled experimental study is needed and proposed here:

Coal tars will be intentionally mixed with inorganic particles, such as  $\text{SiO}_2$ , to simulate coal combustion aerosols, which are mixtures of inorganics and organics. Then, the artificial mixtures will be placed in a TGA; and then be exposed to a high temperature environment in the presence of oxygen. A GC will be used to monitor the exhaust gas composition to calculate reaction rates. For example, the reaction rate for oxidation of organics can be calculated from temporal profiles of  $\text{CO}_2$  concentration. And reaction rate for pyrolysis of organics can be calculated from temporal profiles of  $\text{H}_2$  or  $\text{CH}_4$  concentrations.

One of the challenges of this proposed study is to make the mixtures of organics and inorganics in a certain mixing way. It is very difficult to make such mixtures in a submicrometer particle. Thus, at first, mixtures in larger particles can be made and tested to see whether the retardation of oxidation of organics could occur; and to obtain the kinetic parameters for the oxidations of

organics. Then the obtained kinetic parameters can be used to estimate reaction rates for submicrometer particles.

In addition, actual coal combustion aerosols can also be collected and tested in TGA. This experiment can provide the minimum time that is required to completely oxidize the organics in coal combustion aerosol under certain conditions (at certain temperature, and oxygen concentration).

### *9.1.3 Can acidic sulfate particles really absorb amine species from gas phase to particle phase?*

An experimental study is proposed here to study this question. Iron sulfate is a major acidic sulfate species in fly ash particles. An experiment is designed to figure out whether iron sulfate particles can absorb basic amine vapors and form nitrogen-containing organic aerosols under certain conditions (temperature, gas composition): Certain concentrations of iron sulfate will be dissolved in water. The solution will be atomized then dried in a diffusional drier to form iron sulfate particles. These particles will be carried by air or a mixture of oxygen and nitrogen and be introduced into a tubular furnace, where the temperature will be precisely controlled. Another stream of air or a mixture of oxygen and nitrogen will carry amine vapors and then be mixed with the stream that contains iron sulfate particles before entering the furnace. A high resolution AMS will be connected to the downstream of the furnace. Thus, if iron sulfate particles can absorb amine vapors to form organic aerosols, the AMS can measure the concentrations of the organic aerosols. Using the high-resolution mass spectrum, more detailed chemical characterization can be done for these organic aerosols.

Effect of temperature and gas compositions can be investigated for this experiment. Other than iron sulfate, aluminum sulfate can be also tested, since it is also a major sulfate species in coal combustion aerosols.

#### *9.1.4 What are the forms of sulfate in coal combustion aerosols?*

Sulfate in coal combustion aerosols may be present in several forms, such as calcium sulfate, iron sulfate, and aluminum sulfate. When temperature of the exhaust gas is below than 500K, sulfuric acid may also be produced; and it either condenses on the existing aerosols or forms a mist of ultrafine particles. An experimental work is proposed to distinguish the forms of sulfate in coal combustion aerosols.

First, submicrometer aerosols from coal combustion will be collected on a Teflon filter. The total sulfur concentration in these aerosols will be determined using XRF.

Second, submicrometer aerosols from coal combustion will be collected on a quartz filter. Then the filter sample will be placed in a tubular furnace and heated to 600 K. Thus, all sulfuric acid will be evaporated. A stream of pure nitrogen will pass through the tubular furnace and bring the sulfuric acid out. After leaving the furnace, the temperature will go down. Thus, sulfuric acid will form a mist of aerosols again. Then, an AMS will be used to measure the concentration of the sulfuric acid aerosols. Finally, the concentration of sulfuric acid in coal combustion aerosols can be calculated.

Third, the total sulfate concentration can also be calculated by subtracting the sulfur concentration in sulfuric acid from total sulfur concentration.

Fourth, submicrometer aerosols from coal combustion will be collected on a quartz filter. Then XRD will be used to quantitatively determine the fraction of each sulfate species, such as calcium sulfate, iron sulfate and aluminum sulfate.

### *9.1.5 Do other inorganic components play a similar role with sulfur in the formation of organic aerosols?*

To study this question, an experimental work is proposed. The strategy will be similar to the sulfur work in Chapter 5. Coal will be mixed with a small ratios of metal oxide to enhance formation of inorganic particles. Then an AMS will be used to observe how organic aerosol formation will be changed.

Specially, a small ratios of calcium oxide, sodium oxide or magnesium oxide will be mixed with PRB coal particles. The mixtures will be sent to the drop-tube furnace. A SMPS will be connected to the exhaust gas line to measure the particle size distributions. And an AMS will be used to analyze characterizations of organic aerosols. Correlation between inorganic particle formation and organic particle formation will be investigated. The high resolution AMS spectrum will provide detailed information on chemical speciation of organic aerosols. The chemical compositions of these organic aerosols will be compared to the organic aerosols produced from the combustion of high sulfur content coal.

### *9.1.6 Can hot char particles still release trace amounts of organic volatiles?*

According to the AMS results for the coal combustion in the drop-tube furnace, the concentration of organic aerosol were about 10 ~ 100  $\mu\text{g}/\text{m}^3$  (without dilution) in the flue gas. Thus, only small amounts of tars are needed to produce these concentrations of organic aerosols. It is well known that the devolatilization process completes in less than 100ms after coal particle is heated up. But it is still possible that a char particle may continue to release some trace amount of organic volatiles after the completion of devolatilization. These organic volatiles may be too little to affect any combustion process. But if they can be released at the end of the drop tube, they may contribute to the formation of organic aerosols.



To test this idea only requires a few simple experimental works. A fast pyrolyzer will be used to convert coal particles to char particles. Then the char particles will be placed in a TGA. Only pure nitrogen will be flow through the TGA chamber. The temperature of the coal particles will be quickly ramped up to 1100 K and then keep constant. If there is a loss on the weight of char particles, then it suggests that some volatiles are being released. A GC-MS may be used to identify whether these volatiles are organics or not.

#### *9.1.7 Modeling of organic aerosol emission from coal combustion*

After all these questions getting answered, detailed information on organic aerosol formation should be obtained. It will make the modeling work possible. Combustion model will be coupled with aerosol dynamics model. The combustion model will include coal devolatilization model and shrink core model for char burning. Coal devolatilization model can provide the releasing rate of tar. The shrink core model for char burning coupled with aerosol dynamics model will calculate size distributions for inorganic particles. Partitioning of organics can be simply calculated. The oxidation of organic aerosol will be estimated using the kinetic parameters which will be obtained from the proposed experimental works. Finally, the concentration of organic aerosol in flue gas will be determined. The data from modeling will be compared to the results from the drop-tube experiments. The modeling work could provide emission factors for organic aerosols under various combustion conditions. The information could be used to accurately estimate total organic aerosol emission from coal combustion.

## **9.2 Atmospheric aging of coal combustion aerosols**

Coal combustion aerosol could be a major source of atmospheric aerosol, especially in developing countries. Coal combustion aerosol may react with other atmospheric trace gases and keep changing in terms of chemical compositions and morphologies in the atmosphere.

Specifically, inorganic matter and organic matter in coal combustion aerosols may be oxidized in the atmosphere. It is important to know the oxidation kinetics and products of coal combustion aerosols from reaction with O<sub>3</sub>, OH radical, NO<sub>3</sub> radical and H<sub>2</sub>O<sub>2</sub>.

This is a suggested future work: aerosols generated from coal combustors (either the drop-tube furnace or ACERF pilot-scale coal combustor) can be introduced into a flow tube reactor. Then they will be mixed with some important oxidants (in separate experiments), such as ozone, OH radicals, H<sub>2</sub>O<sub>2</sub> and NO<sub>3</sub> radicals, in the reactor. Their exposure will be controlled to be equivalent to several days or weeks' oxidation in the troposphere. The products will be analyzed by SMPS, AMS, TAG and gas analyzer. Offline LC-ESI-MS may be used as needed for complementary chemical observations. The oxidation kinetics and products from reactions between coal combustion aerosols and O<sub>3</sub>, OH radical, NO<sub>3</sub> radical and H<sub>2</sub>O<sub>2</sub> will be elucidated.

### **9.3 Mercury oxidation in electrostatic precipitator (ESP)**

For mercury research, future studies may focus on testing other photo-catalytic sorbent materials coupled with particulate matter control devices, such as electrostatic precipitator (ESP). Sorbent particles can deposit on the inner walls of ESP. The radiation emitted by corona discharge may induce the photo-catalytic oxidation of mercury on the surfaces of some sorbent particles. The catalytic oxidation may significantly help remove mercury from coal combustion flue gas.

### **9.4 Formation of organic carbon and black carbon aerosols during oxy-coal combustion**

For submicrometer particle formation during oxy-coal combustion, there is still little knowledge on carbonaceous aerosol formation under oxy-coal combustion conditions. Future work may focus on black and organic aerosol formation during oxy-coal combustion. Aerosol produced from oxy-coal combustion will be characterized by many advanced techniques, such as AMS, TAG and LC-ESI-MS. Similar to this work, some important tests can be done in the pilot-scale

coal combustion system. More detailed study can be done in a lab-scale system, such as in a drop-tube furnace.

## APPENDIX I. SUPPORTING MATERIALS FOR CHAPTER 3.

-- Characterization of organic aerosol produced from pulverized coal combustion  
in a drop-tube furnace

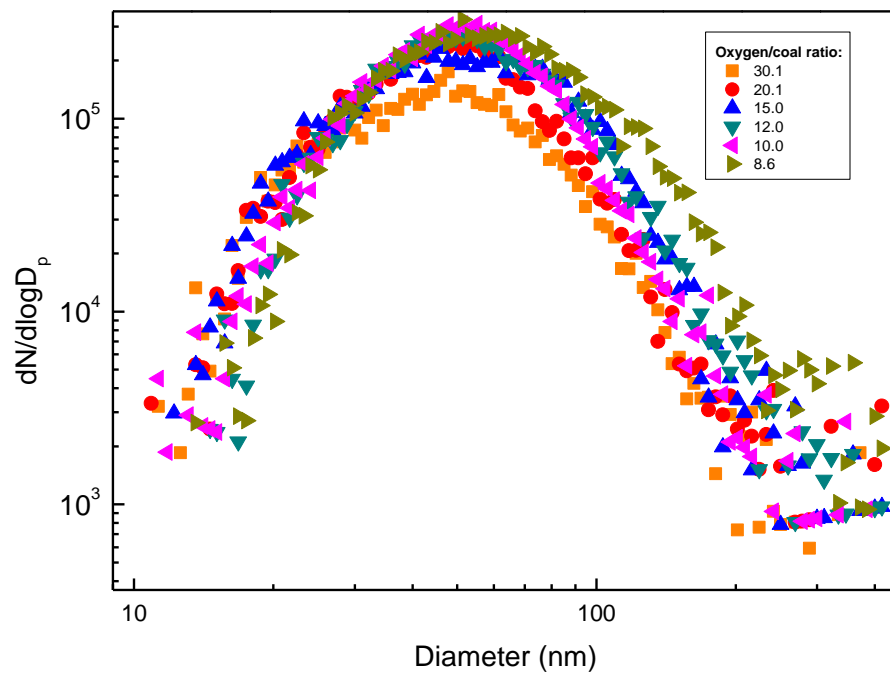


Figure A1.1. Size distribution of particles from coal combustion under various oxygen/coal ratios

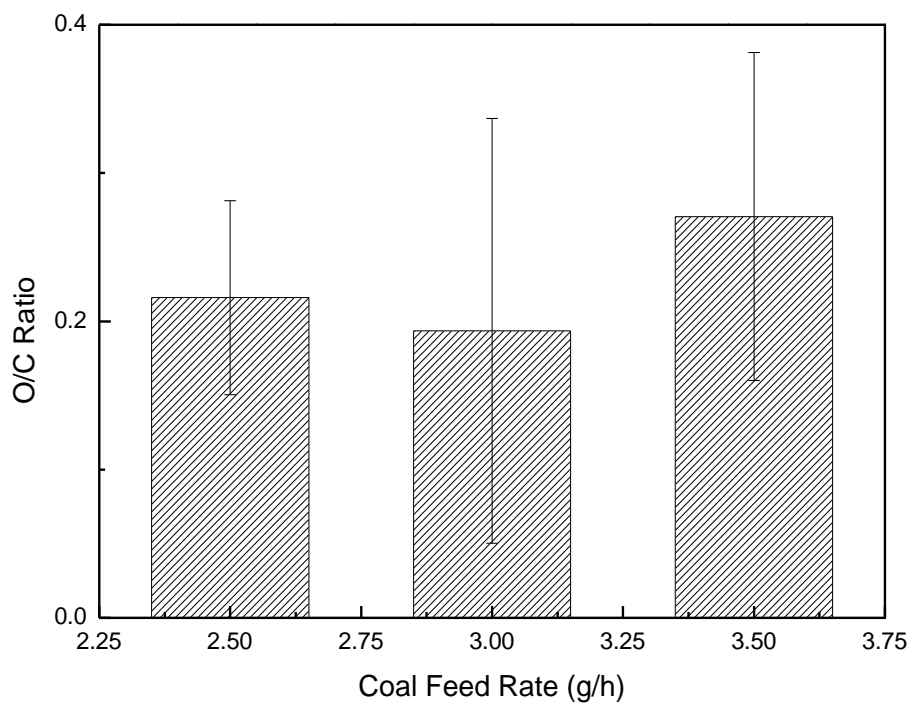
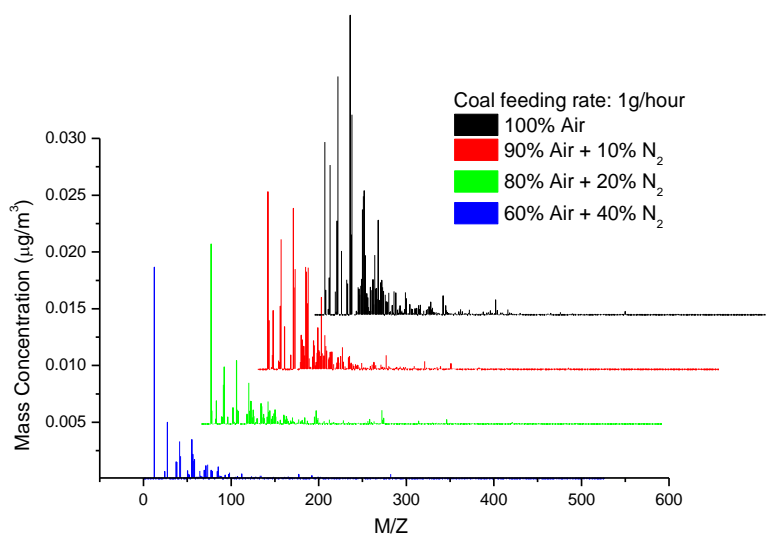


Figure A1.2. O/C elemental ratios for particulate organic matter from coal combustion at larger coal feed rates (the MS signal is too low to calculate O/C ratio for coal feed rate at 1, 1.5 and 2 g/hr).

A.



B.

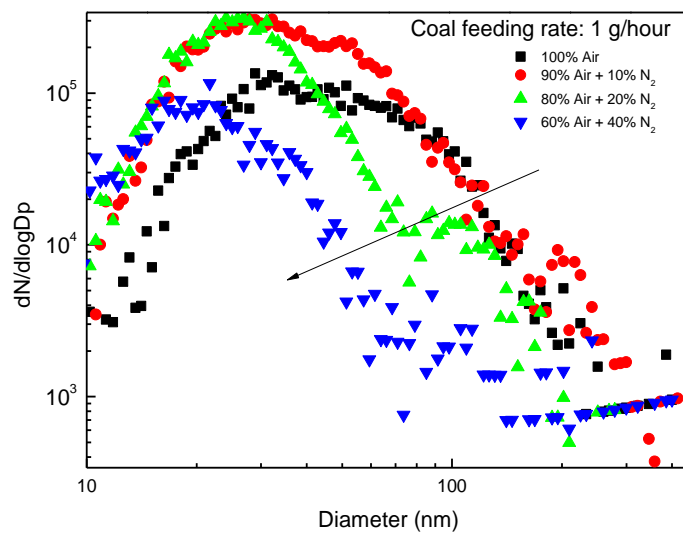


Figure A1.3. (A) Average AMS organic mass spectra and (B) size distributions (from SMPS) for different air/nitrogen ratios at a lower coal feed rate (1.0 g/h).

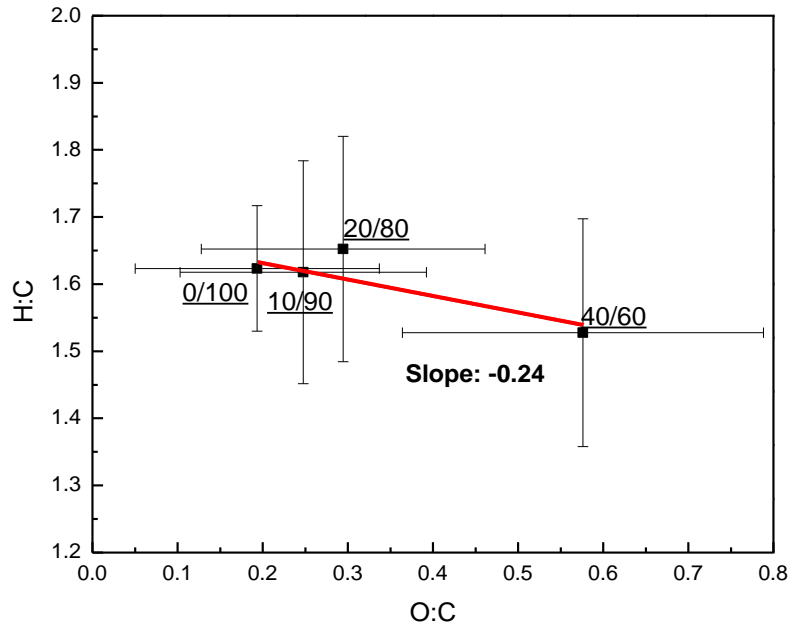


Figure A1.4. Van Krevelen diagram of organic aerosols produced from coal combustion under the different  $N_2/Air$  ratios (the ratios marked with underline).

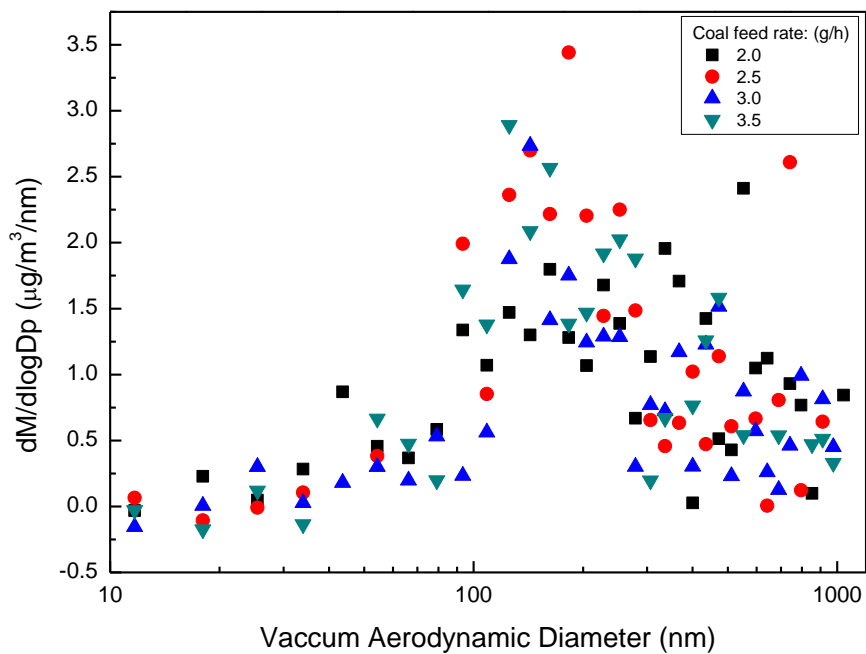


Figure A1.5. Mass size distribution of particulate organic matter from coal combustion at different coal feed rates (the MS signal is too low to mass size distribution for coal feed rate at 1 and 1.5 g/hr): The aerosol mass spectrometer used in this study is able to measure mass size distribution of organic matters in aerosol particles. .



## APPENDIX II. SUPPORTING MATERIALS FOR CHAPTER 4.

-- Formation mechanism of organic aerosol during coal combustion: roles of pyrolysis

Table A2.1. List of identified major organic compounds from combustion and pyrolysis of PRB coal

Retention Time	Compound	Molecular Formula	Major Ions in Mass Spectrum	Peak No. (See Fig. 3)	In Both Pyrolysis and Combustion
<i>Organic Aerosols from PRB Combustion</i>					
25.909	1-Tetradecene	C14H28	41, 55, 69, 83, 97	1	Y
26.898	Pentasiloxane, dodecamethyl-	C12H36O4Si5	73, 147, 281	2	Y
27.195	3-Hexadecene, (Z)-	C16H32	41, 55, 69, 83	3	Y
28.001	Cyclopentene, 1-octyl-	C13H24	67, 82	4	N
29.563	1-Heptadecene	C17H34	43, 57, 69, 83, 97	5	Y
29.801	Tetradecanal	C14H28O	41, 55, 67, 81, 96	6	Y
32.363	Hexadecanoic acid	C16H32O2	43, 60, 73	7	N
33.449	3-(1-Methylpropyl)-2-hydroxy-2-cyclopenten-1-one	C9H14O2	125	8	N
33.73	Hexadecanenitrile	C16H31N	43, 57, 97, 110	9	N
34.238	Octadecanoic acid (CAS)	C18H36O2	43, 57, 73	10	N
<i>PRB Pyrolysis Products</i>					
22.07	Cyclopentasiloxane, decamethyl	C10H30O5Si5	71, 26, 355	1	N
22.8	Benzoic Acid	C7H6O2	77, 105, 122	2	N
24.216	Nonanoic acid	C9H18O2	41, 60, 73	3	N
24.541	1-tetradecene	C14H28	41, 55, 69, 83, 97	4	Y

26.892	Ethyl 2-[(1-hydroxy-2-isopropyl-5-methyl)cyclohexyl]hexanoate	C18H34O3	213, 281	5	Y
27.524	1,1,4,5,6-pentamethyl-2,3-dihydriodene	C14H20	173	6	N
29.946	1-undecene, 8-methyl-	C12H24	43, 55, 69, 84	7	N
30.059	1,2,3,4-tetramethylnaphthalene	C14H16	169, 184	8	N
32.827	2-ethyl-2,4,8,8-tetramethyl-perhydrophenanthrene	C20H36	123, 163, 191, 247	9	N
34.783	Phenanthrene, 1-methyl-7-(1-methylethyl)-	C18H18	219, 234	10	N

Table A2.2. List of identified major organic compounds from the combustion and pyrolysis of ILL#6 coal

Retention Time	Compound	Molecular Formula	Major Ions in Mass Spectrum	Peak No. (See Figure 6)	In Both Pyrolysis and Combustion
<i>Organic Aerosol from ILL#6 Combustion</i>					
22.653	Benzoic Acid	C7H6O2	77, 195, 122	1	Y
24.766	Phthalic anhydride	C8H4O3	76, 104	2	N
26.004	Tetradecane	C14H30	43, 57, 71, 85	3	N
26.782	Dodacane, 2,6,10-trimethyl	C25H22	43, 57, 71, 85	4	N
27.29	Pentadecane	C15H32	43, 57, 71, 85	5	Y
28.393	Napthalene, 1,4,6-trimethyl	C13H14	155, 170	6	N
28.495	Hexadecane	C16H34	43, 57, 71, 85	7	Y
29.679	Pentadecane, 2,6,10, 14-tetramethyl	C19H40	43, 57, 71	8	Y
30.733	Octadecane	C18H38	43, 57, 71, 85	9	N

33.36	Sulfur, mol. (S8)	S8	64	10	N
<i>ILL#6 Pyrolysis Products</i>					
22.611	Benzoic Acid	C7H6O2	51, 77, 105, 122	1	Y
24.8	2-methoxy-4-vinylphenol	C9H10O2	107, 135	2	N
25.908	Tetradecene	C14H28	43, 55, 69, 83	3	Y
26.897	N-Benzyl-N-ethyl-p-isopropylbenzamide	C19H23NO	147, 281	4	N
27.194	3-Hexadecene, (Z)	C16H32	41, 55, 69, 83	5	N
28.173	Benzene, nonyl	C15H24	92	6	N
28.405	1-tetradecene	C14H28	43, 55, 70, 83	7	N
30.654	3-Eicosene, (E)	C20H40	43, 57, 69, 83	8	N
31.383	Napthalene, 1-phenyl-	C16H12	204	9	N
32	Hexadecanoic acid, methyl ester	C17H34O2	43, 74, 87	10	N
32.826	2-ethyl-2,4,8,8-tetramethyl-perhydrophenanthrene	C20H36	123, 163, 191, 247	11	Y

Table A2.3. Complete List of Organic Compounds Identified for the Combustion Aerosol and Pyrolysis Products from PRB Coal

Retenti on time	Compound	Molecular Formula	Maj or Ions	Alternative Name(s)
<i>PRB Combustion</i>				
23.028	Azulene (CAS)	C10H8	128	Cyclopentacycloheptene, Bicyclo [5.3.0]decapentaene
24.525	1-Tridecene (CAS)	C13H26	43, 55, 69, 83, 97	n-Tridec-1-ene, alpha-tridecene, 1-C13H26

24.698	Cyclohexasiloxane, dodecamethyl-	C <sub>12</sub> H <sub>36</sub> O <sub>6</sub> Si <sub>6</sub>	73, 341, 429	dodecamethylcyclohexasiloxane
25.779	1,1'-Biphenyl (CAS)	C <sub>12</sub> H <sub>10</sub>	154	Biphenyl, Diphenyl, Bibenzene, 1,1'-diphenyl
25.909	1-Tetradecene	C <sub>14</sub> H <sub>28</sub>	43, 55, 69, 83, 97	n-Tetradec-1-ene, alpha-tetradecene, neodene 14
26.131	Dodecanal (CAS)	C <sub>12</sub> H <sub>24</sub> O	41, 57, 67, 82	n-dodecenal, 1-dodecenal, Lauraldehyde, Aldehyde C-12
26.898	Pentasiloxane, dodecamethyl-	C <sub>19</sub> H <sub>23</sub> NO	73, 147, 281	
27.049	Pyridine, 3-(1-methyl-1H-pyrrol-2-yl)-	C <sub>10</sub> H <sub>10</sub> N <sub>2</sub>	158	Pyridine, 3-(1-methylpyrrol-2-yl)
27.195	1-Tridecene	C <sub>13</sub> H <sub>26</sub>	55, 69, 83, 97	
28.001	Cyclopentene, 1-octyl-	C <sub>13</sub> H <sub>24</sub>	67, 82	1-Octyl-1-cyclopentene
28.174	Benzene, nonyl-	C <sub>15</sub> H <sub>24</sub>	92	
28.412	1-Hexadecene (CAS)	C <sub>16</sub> H <sub>32</sub>	43, 55, 69, 83, 97	Cetene, 1-Cetene, n-Hexadec-1-ene
28.644	Z-2-Dodecenol	C <sub>12</sub> H <sub>24</sub> O	43, 57, 68, 82, 96	
29.557	1-Heptadecene	C <sub>17</sub> H <sub>34</sub>	43, 57, 69, 83, 97	
29.801	Tetradecanal	C <sub>14</sub> H <sub>28</sub> O	43, 60, 73	Myristaldehyde, Myristylaldehyde, Tetradecylaldehyde
30.276	Tetradecanoic acid (CAS)	C <sub>14</sub> H <sub>28</sub> O <sub>2</sub>	43, 60, 73	Myristic acid, Myristinic acid
30.53	Benzene, undecyl- (CAS)	C <sub>17</sub> H <sub>28</sub>	92	Undecylbenzene, 1-Phenylundecane
30.66	5-Octadecene, (E)-	C <sub>18</sub> H <sub>36</sub>	43, 55,	(5E)-5-Octadecene

			69, 83, 97	
30.902	Oxirane, heptadecyl-	C19H38O	43, 55, 71, 82, 96	1,2-Epoxy-nonadecane, 2-Heptadecyloxirane
31.325	Pentadecanoic acid	C15H30O2	43, 60, 73	Pentadecylic acid, n-Pentadecanoic acid
31.384	Naphthalene, 1-phenyl-	C16H12	204	1-Phenylnaphthalene
31.757	Nonadecane	C19H40	43, 57, 71, 85	
32.363	Hexadecanoic acid (CAS)	C16H32O2	43, 60, 73	Palmitic acid, Palmitinic acid, n-hexadecanoic acid
32.687	Cycloeicosane	C20H40	43, 55, 69, 83, 97	Cycloeicosane
33.449	3-(1-Methylpropyl)-2-hydroxy-2-cyclopenten-1-one	C9H14O2	125	
33.73	Hexadecanenitrile	C16H31N	43, 57, 97, 110	
34.238	Octadecanoic acid (CAS)	C18H36O2	43, 57, 73	Stearic acid, n-octadecanoic acid, PD 185
35.471	Eicosane	C20H42	43, 57, 71, 85	n-Eicosane, Icosane
36.06	1-Propene, 3-(2-cyclopentenyl)-2-methyl-1,1-diphenyl-	C21H22	129, 207	
36.303	Tetracosane (CAS)	C24H50	43, 57, 71, 85	n-tetracosane
36.649	Benzenepropanoic acid, 2-methoxy-, methyl ester	C11H14O3	91	
37.097	Heptacosane	C27H56	43, 57, 71, 85	

37.865	Docosane (CAS)	C22H46	43, 57, 71, 85	n-docosane, C22H46 STANDARD, Normal- docosane
38.616	Pentacosane	C25H52	43, 57, 71, 85	n-Pentacosane
40.016	Cholesta-3,5-diene (CAS)	C27H44	43, 57	Cholesterilene, Delta 3- 5-Cholestadiene
40.346	Quaterphenyl-	C24H18	306	
40.973	(-)-(S)-(Cyclopentylidenemethyl)-N-methyl-S- phenylsulfoximine	C13H17NOS	155	
<i>PRB Pyrolysis</i>				
22.07	Cyclopentasiloxane, decamethyl	C10H30O5Si 5	71, 26, 355	
22.8	Benzoic Acid	C7H6O2	77, 105, 122	Retarder BA, Retardex, HA 1, Tenn-Plas
22.828	Octanoic acid	C8H16O2	41, 60, 73	Caprylic acid, neo-fat 8, Octylic acid
24.216	Nonanoic acid	C9H18O2	41, 60, 73	
24.541	1-tetradecene	C14H28	41, 55, 69, 83, 97	
24.676	Cyclohexasiloxane, dodecamethyl-	C12H36O6Si 6	73, 341, 429	
25.514	n-decanoic acid	C10H20O2	41, 60, 73	
25.778	1,1'-biphenyl	C12H10	154	Diphenyl, bibenzene
25.784	Napthalene, 2-ethenyl	C12H10	154	2-vinylphthalene
25.913	1-tetradecene	C14H28	43, 55, 69, 83, 97	Neodene 14
26.011	1-isobenzofurandione, 4-methyl	C9H6O3	90, 118, 162	Phthalic anhydride, 3- methyl
26.119	Z-2-dodecenol	C12H24O	43, 57, 68, 82	

26.368	Napthalene, 2,7-dimethyl	C12H12	141, 156	
26.892	Ethyl 2-[(1-hydroxy-2-isopropyl-5-methyl)cyclohexyl]hexoate	C18H34O3	213, 281	
27.043	Pyridine, 2-(10methyl-1H-pyrrol)-	C10H10N2	158	
27.195	1-pentadecene	C15H30	43, 55, 69, 83, 97	
27.281	3-ethyl-4,4-dimethyl-2-(2-methylpropenyl)cyclohex-2-enone	C14H22O	177, 191, 206	
27.524	1,1,4,5,6-pentamethyl-2,3-dihydrindene	C14H20	173	
27.849	alpha-calacorene	C15H20	142, 157	
28.005	Undecanoic acid	C11H22O2	60, 73	
28.173	Benzene, nonyl	C15H24	91, 133	
28.335	Diethyl phthalate	C12H14O4	149	
28.4	Napthalene, 2,3,6-trimethyl	C13H14	155, 170	
29.389	Napthalene, 1,6-dimethyl-4-(1-methylethyl)-	C15H18	183, 198	
29.557	E-14-hexadecenal	C16H30O	45, 55, 69, 83, 87	
29.8	Tetradecanal \$\$ Myristaldehyde \$\$ Myristylaldehyde \$\$ Tetradecylaldehyde	C14H28O	43, 57, 82	
29.946	1-undecene, 8-methyl-	C12H24	43, 55, 69, 84	
30.059	1,2,3,4-tetramethylnapthalene	C14H16	169, 184	
30.113	Isobutyl laurate	C16H32O2	56, 183	
30.535	Benzene, undecyl-	C17H28	92	
30.659	E-15-heptadecenal	C17H32O	43,	

			55, 69, 83, 97	
30.729	Pentadecane	C15H32	43, 57, 71, 85	
31.156	2-pentadecanone, 6,10,14-trimethyl	C18H36O	43, 58, 71	
31.378	Napthalene, 1-phenyl	C16H12	204	
31.383	Cyclobuta(1",2":3,4;3",4":3'4'_dicyclobuta(1,2:1',2:1',2')dibenzene, 4b,4c,8b,8c	C16H12	203	
31.692	1-nonadecene	C19H38	43, 55, 69, 83, 97	
31.762	Hexadecane	C16H34	43, 57, 71, 85	Cetane
32.691	1-octadecene	C18H36	43, 57, 83, 97	
32.751	Octadecane	C18H38	43, 57, 71, 85	
32.827	2-ethyl-2,4,8,8-tetramethyl-perhydrophenanthrene	C20H36	123, 163, 191, 247	
33.697	Heneicosane	C21H44	43, 57, 71, 85	
34.599	Docosane	C22H46	43, 57, 71, 85	
34.783	Phenanthrene, 1-methyl-7-(1-methylethyl)-	C18H18	219, 234	
35.41	1H-Indene, 1-(2,3-dihydro-1H-inden-1-ylidene)-2,3-dihydro-	C18H16	117, 203, 217, 232	
35.464	Tricosane	C23H48	43,	



			57, 71, 85	
35.507	Abieta-8,11,13-trien-7-one	C <sub>20</sub> H <sub>28</sub> O	199, 269	
36.302	Tetracosane	C <sub>24</sub> H <sub>50</sub>	43, 57, 71, 85	
37.097	Pentacosane	C <sub>25</sub> H <sub>52</sub>	43, 57, 71, 85	
37.48	2-benzylindole	C <sub>15</sub> H <sub>13</sub> N	130, 207	
37.87	Docosane	C <sub>22</sub> H <sub>46</sub>	43, 57, 71, 85	
39.323	Octacosane	C <sub>28</sub> H <sub>58</sub>	43, 57, 71, 85	
39.605	Tetracosamethyl-cyclododecasiloxane	C <sub>24</sub> H <sub>72</sub> O <sub>12</sub> Si <sub>12</sub>	73, 147, 221, 355, 429	
40.015	Heptacosane	C <sub>27</sub> H <sub>56</sub>	43, 57, 71, 85	

Table A2.4. Complete List of Organic Compounds Identified for the Combustion Aerosol and Pyrolysis Products from ILL#6 Coal

Retention Time	Compound	Formula	Major Ions	Alternative Names
<i>ILL#6 Combustion</i>				
22.653	Benzoic Acid	C7H6O2	77, 195, 122	Retardex, Retarder BA
24.155	Nonoic Acid	C9H18O2	41, 60, 73	
24.539	Octadecanoic acid, ethy ester	C20H40O2	88, 101	Ethyl stearate
24.625	Tridecane	C13H28	43, 57, 71	
24.701	Cyclohexasiloxane, dodecamethyl-	C12H36O6Si6	73, 341	Dodecamethylcyclohexasiloxane
24.766	Phthalic anhydride	C8H4O3	76, 104	1,3-Isobenzofurandione, ESEN, Phthalandione
25.517	Decanoic acid	C10H20O2	60, 73, 129	Capric acid, Decoic acid, Decyclic Acid
25.76	1,1'-biphenyl	C12H10	154	Biphenyl, diphenyl, bibenzene, 1,1'-diphenyl
26.004	Tetradecane	C14H30	43, 57, 71, 85	
26.29	Naphalene, 1,7-dimethyl-	C12H12	141, 156	1,7-dimethylnapthalene
26.344	Napthalene, 1,6-dimethyl-	C12H12	141, 156	1,8-dimethylnapthalene
26.782	Dodacane, 2,6,10-trimethyl	C25H22	43, 57, 71, 85	Farmesan, farmesane, 2,6,20-trimethyldodecane
26.928	Dodecane, 1-chloro	C12H25Cl	43, 57, 91	Dodecane, 1-chloro-
27.144	1,4a-dimethyl-2-oxo-7-isopropyltetrahydronapthalene	C15H20O	173, 201, 216	
27.29	Pentadecane	C15H32	43, 57, 71, 85	
27.382	2,5-Dimethyl-1,6-methano-10-annilene	C13H14	155, 170	
27.512	1,1,5,6-tetramethyl-tetralin1,2,3,4-tetrahydro-1,1,5,6-tetramethyl-n	C14H20	173	

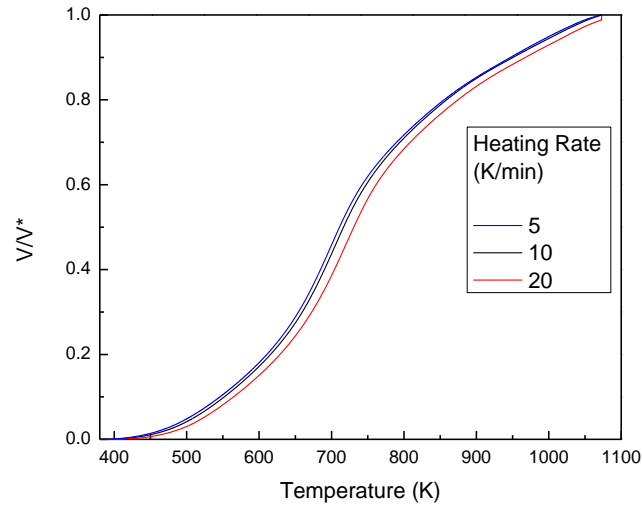
27.56	Dibenzofuran	C <sub>12</sub> H <sub>8</sub> O	168	
27.636	Napthalene, 1,4,6-trimethyl-	C <sub>13</sub> H <sub>14</sub>	155, 170	1,4,6-trimethylnapthalene
27.706	Napthalene, 2,3,6-trimethyl	C <sub>13</sub> H <sub>14</sub>	155, 170	2,3,6-trimethylnapthalene
27.89	1,4,6-Trimethylnapthalene?			
28.393	Napthalene, 1,4,6-trimethyl	C <sub>13</sub> H <sub>14</sub>	155, 170	1,6,7-trimethylnapthalene
28.495	Hexadecane	C <sub>16</sub> H <sub>34</sub>	43, 57, 71, 85	
29.036	Tridecane, 2-methyl	C <sub>14</sub> H <sub>30</sub>	43, 57, 71, 85	2-methyltridecane
29.382	Azulene, 1,4-dimethyl-7(1-methylethyl)-	C <sub>15</sub> H <sub>18</sub>	183, 198	
29.679	Pentadecane, 2,6,10, 14-tetramethyl	C <sub>19</sub> H <sub>40</sub>	43, 57, 71	Pristane
30.052	Azulene, 7-ethyl,1,4-dimethyl	C <sub>14</sub> H <sub>16</sub>	169, 184	Ba 2784, Camazulene, Chamazulen
30.63	Phenanthrene	C <sub>14</sub> H <sub>10</sub>	178	
30.733	Octadecane	C <sub>18</sub> H <sub>38</sub>	43, 57, 71, 85	
31.398	Anthracene, 9-ethenyl	C <sub>16</sub> H <sub>12</sub>	101, 203	
31.765	Nonadecane	C <sub>19</sub> H <sub>40</sub>	43, 57, 71, 85	n-nonadecane
32.749	Eicosane	C <sub>20</sub> H <sub>42</sub>	43, 57, 71, 85	Icosane
32.825	2-ethyl-2,4,8,8-tetramethyl-perhydrophenanthrene	C <sub>20</sub> H <sub>36</sub>	123, 163, 247	
33.36	Sulfur, mol. (S <sub>8</sub> )	S <sub>8</sub>	64	Octa-sulfur, Octathiocane
34.608	Heneicosane	C <sub>21</sub> H <sub>44</sub>	43, 57, 71, 85	
39.068	Cyclononsiloxane, octadecamethyl-	C <sub>18</sub> H <sub>54</sub> O <sub>9</sub> Si <sub>9</sub>	73, 147, 221, 429	
<i>ILL#6 Pyrolysis</i>				
20.27	2-Pyrrolidinone, 1-methyl	C <sub>5</sub> H <sub>9</sub> NO	44, 99	
21.243	Phenol, 2-methoxy	C <sub>7</sub> H <sub>8</sub> O <sub>2</sub>	81, 109, 124	Guiacol
22.103	Cyclopentasiloxane, decamethyl-	C <sub>10</sub> H <sub>30</sub> O <sub>5</sub> Si <sub>5</sub>	73, 267, 355	
22.611	Benzoic Acid	C <sub>7</sub> H <sub>6</sub> O <sub>2</sub>	51, 77, 105, 122	Retardex, HA 1, Tenn Plas, Retarder BA

23.232	Decanal	C10H20O	42, 47	Decyl aldehyde
24.155	Nonoic Acid	C9H18O2	41, 60, 73	
24.53	1-Undecene	C11H22	43, 55, 70, 83	
24.686	Cyclohexasiloxane, ddecamethyl	C12H36O6Si6	73, 341	
24.8	2-methoxy-4-vinylphenol	C9H10O2	107, 135	
25.297	Phenol, 2,6-dimethoxy-	C8H10O3	154	Pyrogallol 1,2-dimethyl ether, Syringol
25.784	Biphenyl	C12H10	154	
25.908	Tetradecene	C14H28	43, 55, 69, 83	4-tetradecene, trans-4-tetradecene
26.011	1,3-Isobenzofurandione, 4-methyl-	C9H6O3	90, 118, 162	
26.205	3-tetradecene	C14H28	43, 55, 69, 83	
26.897	N-Benzyl-N-ethyl-p-isopropylbenzamide	C19H23NO	147, 281	
27.194	3-Hexadecene, (Z)	C16H32	41, 55, 69, 83	
27.292	Undecane	C12H26	43, 57 71	
27.524	1,1,4,5,6-Pentamethyl-2,3-dihydroindene	C14H20	173	
27.562	Dibenzofuran	C12H8O	139, 168	
28.173	Benzene, nonyl	C15H24	92	
28.405	1-tetradecene	C14H28	43, 55, 70, 83	Neodene 14, alpha-tetradecene
28.297	Hexadecane	C16H34	43, 57, 71, 85	
29.038	Bezene, 1-nonenyl	C15H22	104, 117	
29.681	Tetradecane	C14H30	43, 57, 71, 85	
29.562	Chloroacetic acid, pentadecyl ester	C17H33ClO2	43, 55, 69, 83	Pentadecyl chloroacetate
29.805	Cyclododecene, 1-methyl-	C13H24	41, 55, 67, 81, 96	
30.054	Azulene, 7-ethyl,1,4-dimethyl	C14H16	169, 184	
30.124	Acridine, 9,10-dihydro	C13H11N	180	Acridane, Carbazine
30.616	Anthracene	C14H10	178	Anthracin, Green Oil, Paranaphthalene, Tetra Olive N2G

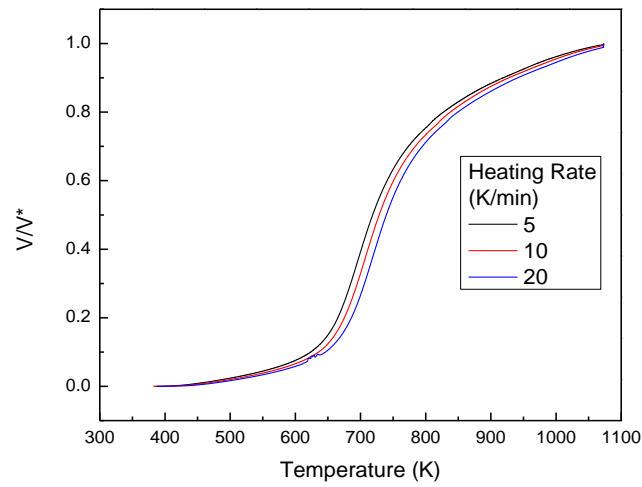
30.654	3-Eicosene, (E)	C <sub>20</sub> H <sub>40</sub>	43, 57, 69 83	
30.729	Tridecane	C <sub>13</sub> H <sub>28</sub>	43, 57 71, 85	
30.908	1-Pentadecene	C <sub>15</sub> H <sub>30</sub>	43, 55, 69, 83	
31.383	Napthalene, 1-phenyl-	C <sub>16</sub> H <sub>12</sub>	204	Alpha-phenylnapthalene
32	Hexadecanoic acid, methyl ester	C <sub>17</sub> H <sub>34</sub> O <sub>2</sub>	43, 74, 87	
32.826	2-ethyl-2,4,8,8-tetramethyl- perhydrophenanthrene	C <sub>20</sub> H <sub>36</sub>	123, 163, 191, 247	
33.697	Nonadecane	C <sub>19</sub> H <sub>40</sub>	43, 57 71, 85	
34.599	Eicosane	C <sub>20</sub> H <sub>42</sub>	43, 57 71, 85	

Figure A2.1. Thermogravimetric mass curves comparing a) PRB coal and b) ILL#6 coal at different heating rates: 5, 10 and 20 K/min; c)  $k_0$  vs.  $E$  Relationship for PRB Coal and ILL#6 Coal.

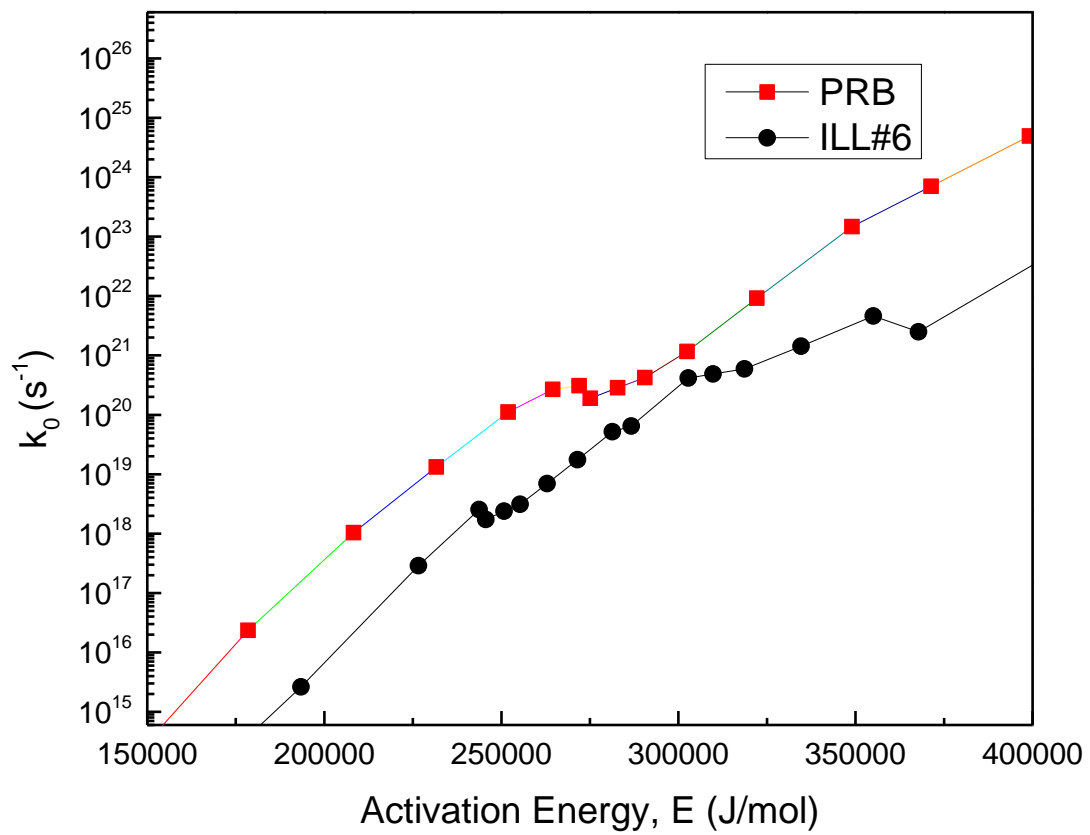
(a)



(b)



(c)



### APPENDIX III. SUPPORTING MATERIALS FOR CHAPTER 5.

-- Effect of sulfur content in coal on organic aerosol formation during coal combustion

Figure A3.1. Correlation of concentration between sulfur (determined by XRF) and organic matter of submicrometer particles from the combustion of PRB coals mixing with different content of sulfur .

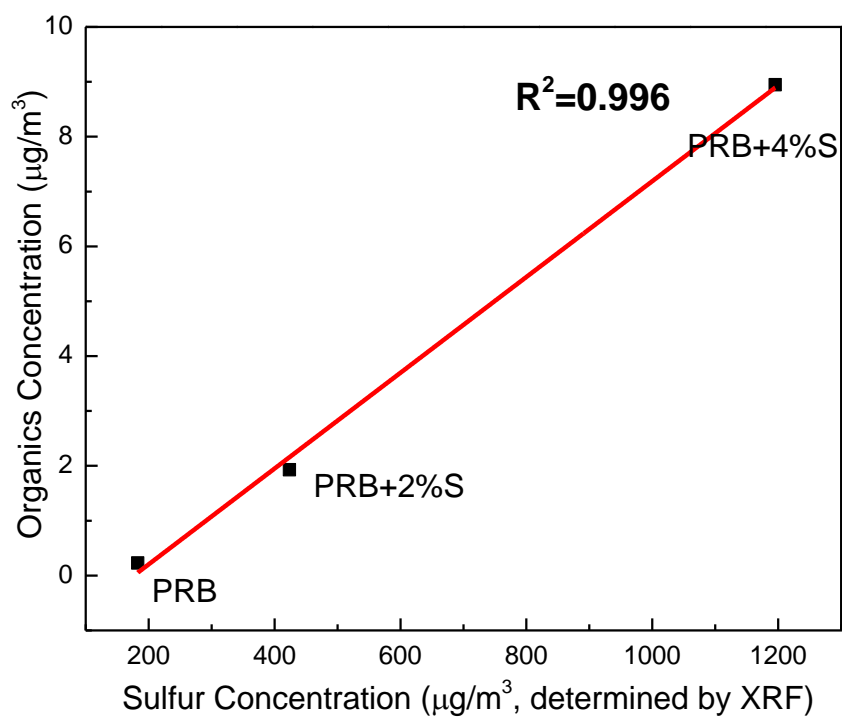




Figure A3.2. Total ion chromatography (LC-ESI(+)-TOFMS) of the methanol extract from submicrometer particles collected from the combustion of PRB coals mixing with 4% sulfur.

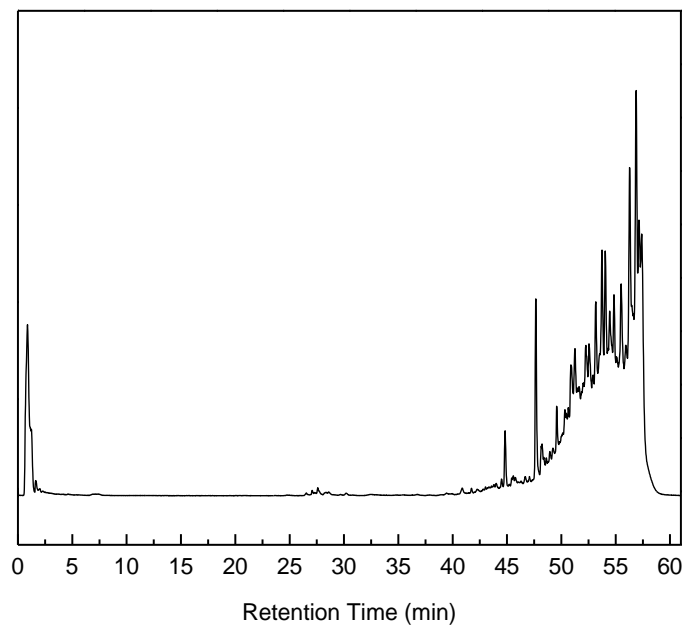
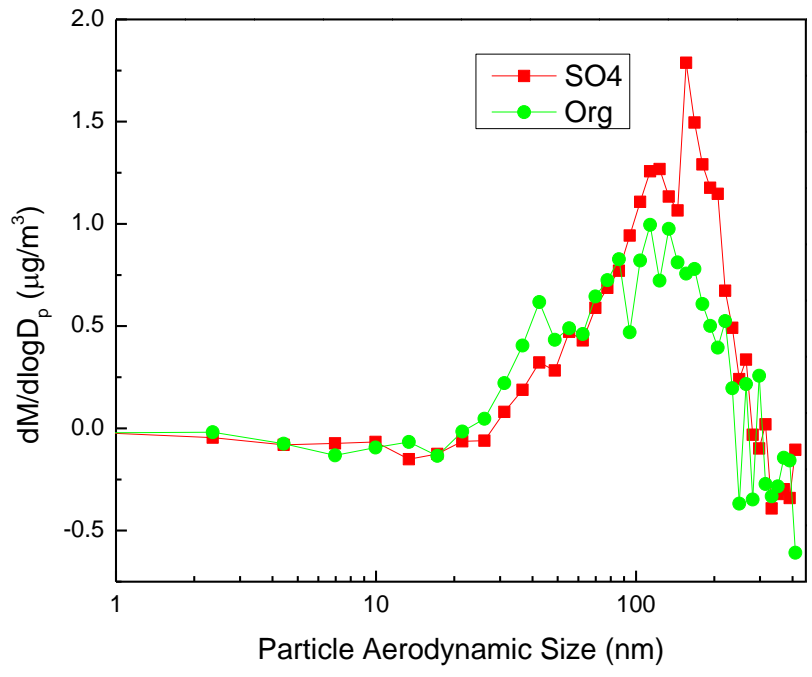


Figure A3.3. Mass size distribution of SO<sub>4</sub> and organic species from the combustion of PRB coal plus 4% sulfur.



## APPENDIX IV. DESCRIPTION OF ACERF TEST FACILITY

\* Adapted from an internal report written by Bhupesh Dhungel

The schematic diagram of the ACEFF test facility is shown in [Figure A4.1](#): pulverized coal particles are fed into the furnace using a gravimetric feeder. Input gas (air, oxygen enriched air or oxygen enriched recycled flue gas) is supplied via the primary and secondary fans. The coal particles are carried by the primary stream of gas, which is “primary oxidizer”. The secondary oxidizer is further split into two streams: the tangential and axial streams, which are referred as secondary and tertiary streams respectively. After burning in the down-fired combustor, the hot flue gas is cooled in a separated heat recovery steam generator. Then it enters the fabric filter, where the ash in the flue gas is removed. A part of flue gas can be recycled back to the furnace to investigate oxy-coal combustion.

The cylindrical furnace is shown in [Figure A4.2](#), which is down-fired combustor with an inner diameter (ID) of 1.1m and a total length of 6.1m. It has many access ports, which are spaced with a distance of approximately of 0.28m. We can use these ports to do gas or solid sampling. The down-fired burner is shown in [Figure A4.3](#), which is capable of burning natural gas as well as pulverized solid fuels. The center tube of the burner is for delivering natural gas only. Burning natural gas is mainly to maintain a high furnace temperature before conducting coal experiments. Coal particles and primary oxidizer are supplied by the concentric tube outside the natural gas tube. The axial (tertiary) and tangential (secondary) streams are delivered through the outermost tube. The axial steam passes through a honeycomb flow straightener and then exit the burner.

The coal used in this facility is West Elk coal, which is a low - sulfur, Colorado bituminous coal.

Its proximate and ultimate analysis are shown below:

**Proximate Analysis for West Elk Coal (% , as received):**

Moisture	10.43
Ash	8.51
Sulfur	0.47
BTU	11,486
MAF BTU	14,079
Pounds SO <sub>2</sub> /MM BTU	0.74
Pounds Ash/MM BTU	6.91
Ash to Sulfur Ratio	18.28
% Volatile Matter	34.85
% Fixed Carbon	46.02

**Ultimate Analysis for West Elk Coal (% , dry basis):**

Ash	27.50
Hydrogen	5.08
Carbon	74.12
Sulfur	0.52
Oxygen	9.27
Nitrogen	1.53
Chlorine	0.012

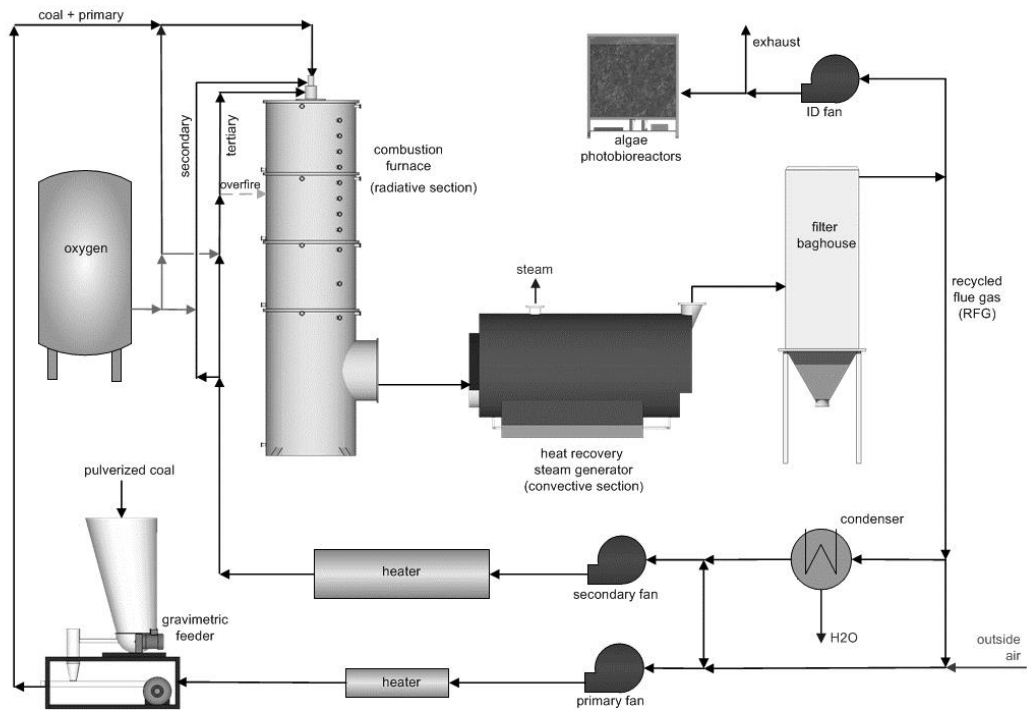


Figure A4.1; Process flow diagram of the test facility

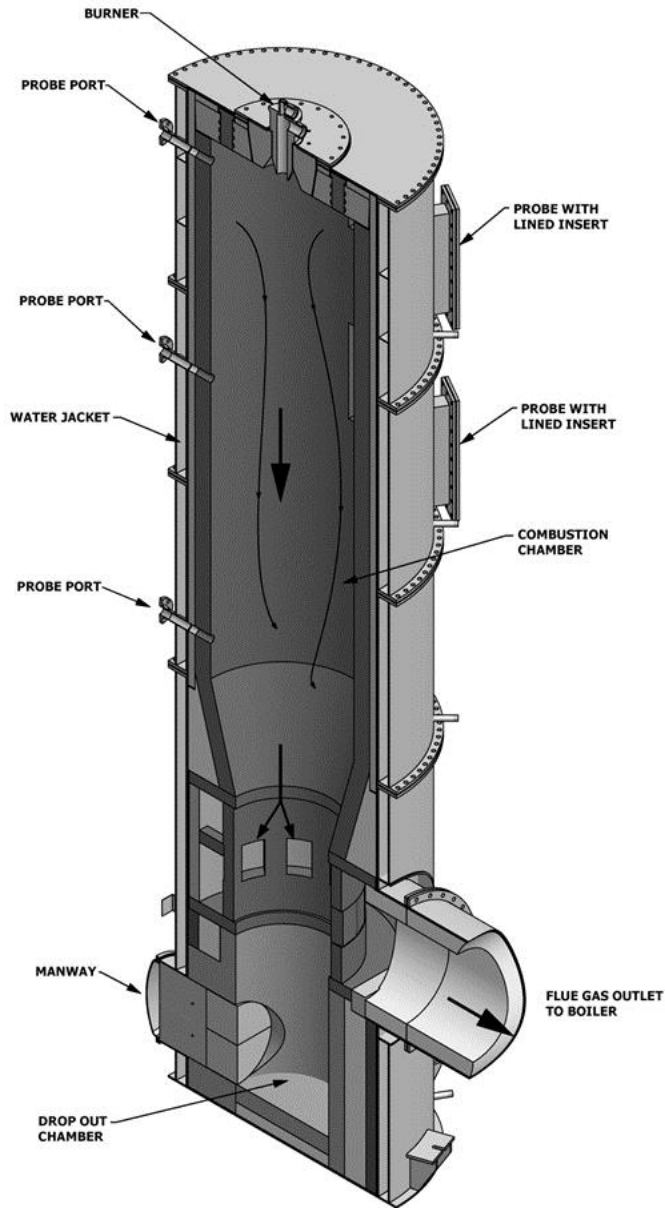


Figure A4.2: Cross section of the vertically down-fired combustor

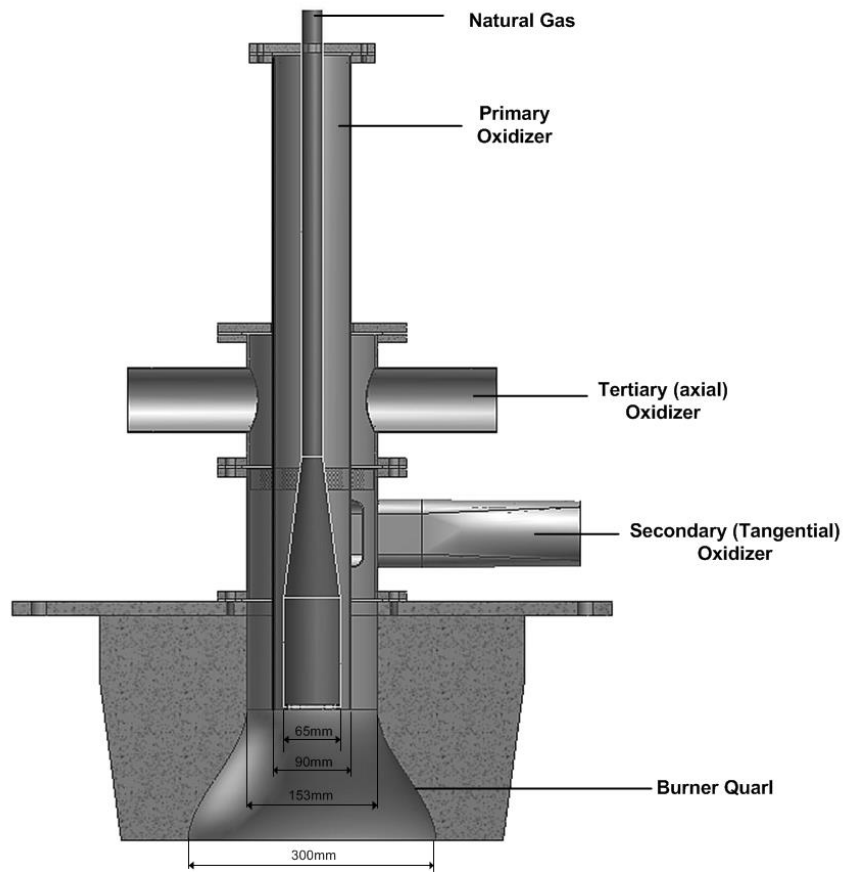


Figure A4.3: Burner of the test facility

## APPENDIX V: DESCRIPTION OF THE DROP-TUBE FURNACE

### A5.1. Introduction

A Lindberg/Blue M, Model HTF55342C Tube Furnace is a square-shaped electric heating device used as a laboratory-scale coal combustor. It is approximately 43.2cm long, 88.9cm wide, and 40.6cm tall. The Lindberg/Blue M, Model HTF55342C Tube Furnace, as seen in Figure A5.1, consists of 6 parts: a controller, a furnace, an inlet manifold system, a ceramic tube, an outlet dilution system, and a coal feeding system.

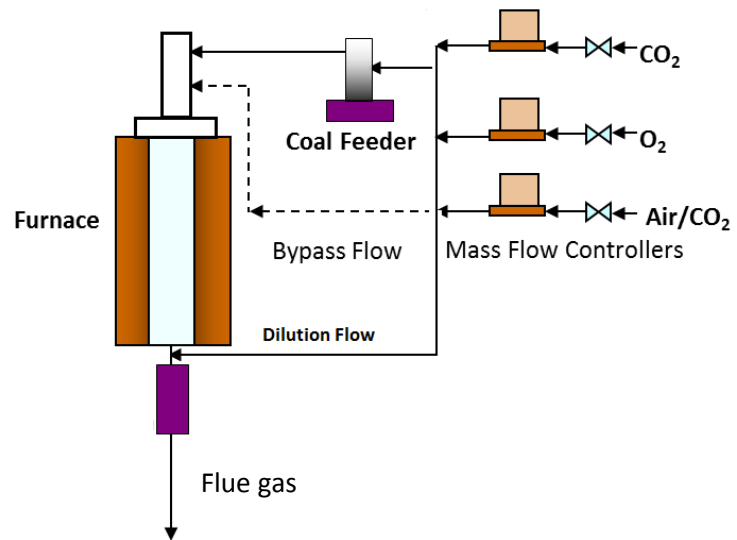


Figure A5.1. Picture and schematic drawing of the drop-tube furnace



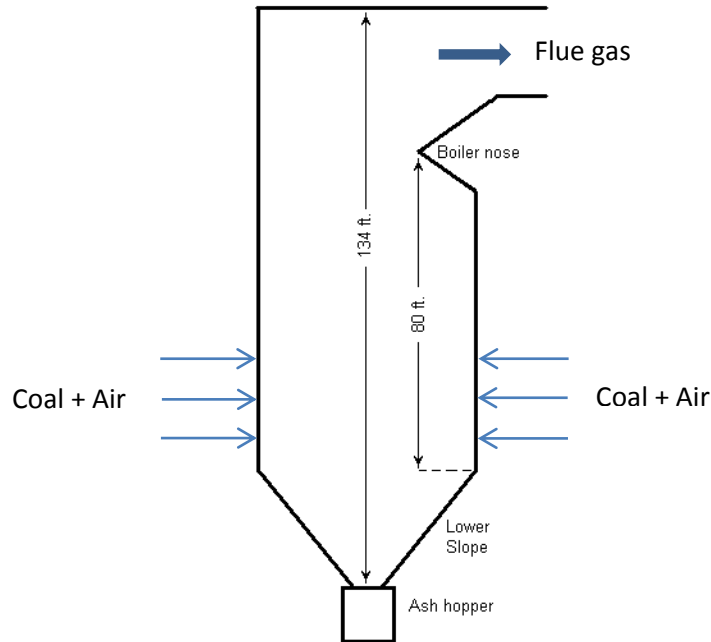


Figure A5.2 Schematic drawing of a 285 MW furnace (Provided by Ameren Energy)

The drop-tube furnace is a simple lab-scale combustion system. Thus there are large difference between real power plant and the drop-tube furnace. Figure A5.2 shows the schematic drawing of a 285 MW pulverized coal furnace (Edwards Unit 2, Ameren Energy). The furnace is 46 ft (14.0 m) across by 30 ft (9.1 m) deep and is 80 ft (24.4 m) tall from the top of the lower slope to the tip of the boiler nose. From the ash hopper opening to the roof the boiler height is 134 ft (40.8 m). Comparing figure A5.1 and figure A5.2, the differences are obvious:

- 1) The scale of our drop-tube is much smaller.
- 2) Furnace surface area/coal feeding rate is much larger in our drop-tube furnace
- 3) The equivalence ratio ( $<0.1$ ) in our drop-tube furnace is much smaller than that in real scale furnace ( $\sim 1.2$ )
- 4) The flow field in our drop-tube is much simpler (Plug flow)

## **A5.2. Detailed Description**

### *A5.2.1 The temperature controller*

The temperature controller includes advanced microprocessor-based digital control, a solid-state power module, on/off switch and thermocouple input jack. The digital control used here is microprocessor-based PID control (proportional, integral, derivative) with single segment, single set point and built-in adjustable high limit over temperature protection. The controller has simultaneous display of actual temperature vs. set point.

### *A5.2.2 The furnace*

The furnace is manufactured by Lindberg/Blue. It is a split hinged furnace with a set temperature range from 373 K to 1473 K (100°C to 1200°C). The furnace includes a central tube, a thermocouple, heating coils, and insulating materials. It is a split hinge case consists of cylindrical cavity surrounded by heating coils, which are embedded in a thermally insulating matrix. Temperature of the furnace is controlled via feedback from a thermocouple outside of the central tube wall by PID control.

### *A5.2.3 Inlet manifold piece*

The inlet manifold piece, shown in Figure A5.3, is made of a 45.7cm long and 4.76 cm outer diameter stainless steel pipe. There is a 6.4cm diameter and 0.8 cm thick round-shaped cap threaded on top center of the tube. As shown in the figure, there are four horizontal 0.9cm diameter and 4.4cm long tubes welded to the pipe on one side. The first smaller tube is located 3.8cm below the top cap and the four tubes are equal distanced (8.9cm) from each other. On the other side, there is a 1.3cm diameter and 7.0cm long coal inlet tube located 38.26 cm below the top cap. On the bottom of the tube, the other steel cap is welded to the pipe.

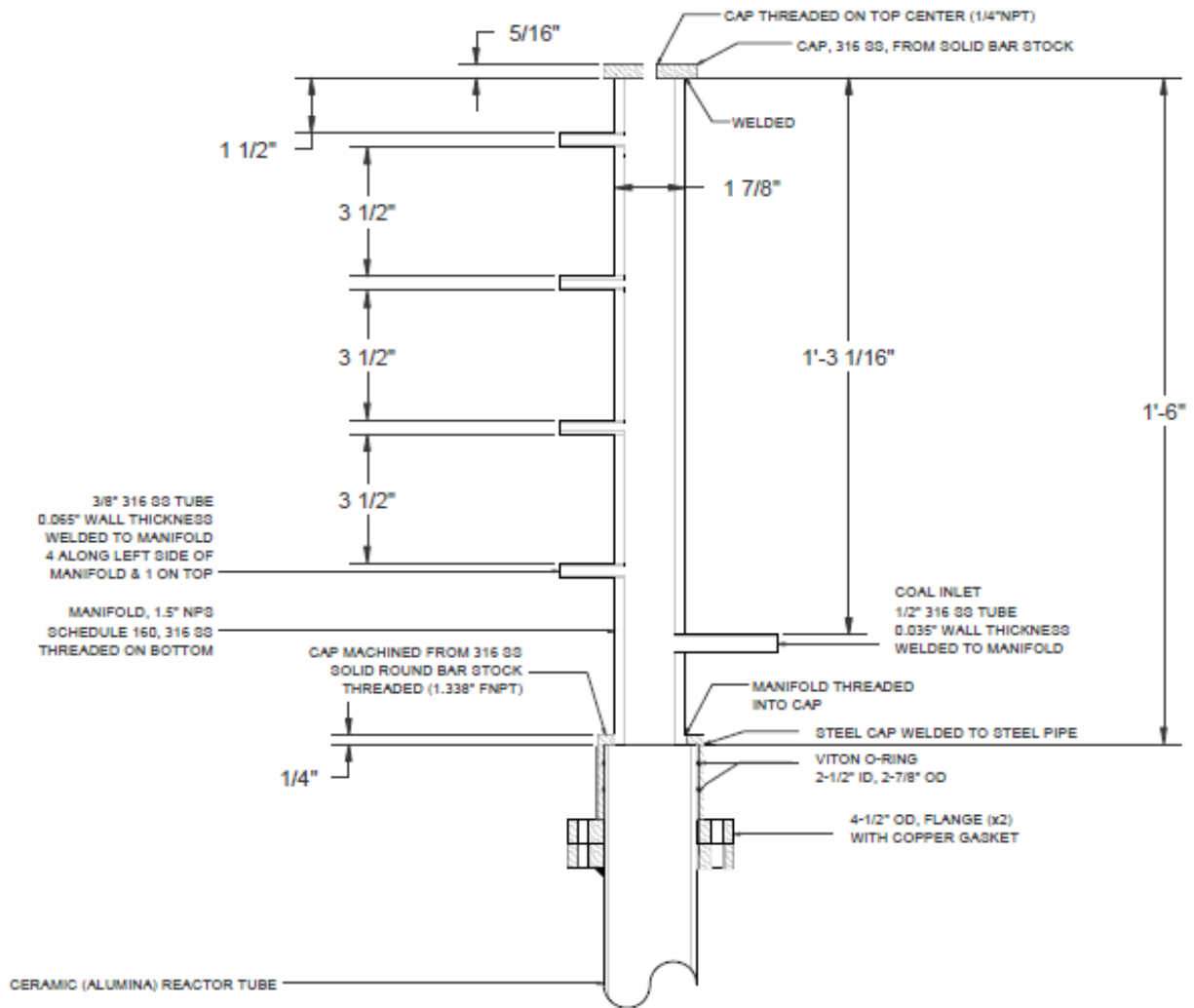


Figure A5.3. Overall inlet system into combustor (source: Smallwood's thesis(Smallwood 2005))

#### A5.2.4 Ceramic (alumina) reactor tube

The alumina reactor tube is 6.35 cm outside diameter, 5.72 cm inside diameter, and 121.92 cm long. It is connected to the pipe by a NPS schedule 40 tube in which two 6.35cm ID o-rings are put in before the ceramic tube. The o-rings would be pressed when the ceramic tube is placed in

the NPS tube hence the tension between the o-rings and the ceramic tube would seal the tube. And the position of the ceramic tube is fixed by a top and a bottom flange, both having 11.43 cm outer diameters.

#### A5.2.5 Outlet dilution pieces

The outlet dilution pieces, as shown in Figure A5.4, are consist of an outlet cap and conical reducers with holes for dilution air and they are connected to the ceramic reactor tube by a cap and two flanges similar to the ones used to connect the ceramic tube to the manifold piece. The conical reducers are two reducers which are welded together and many 0.16cm diameter holes (the horizontal distance between two holes is 1.3cm and vertical distance is 1.6cm) are drilled on the reducers to enable particle free clean air entering the dilution system.

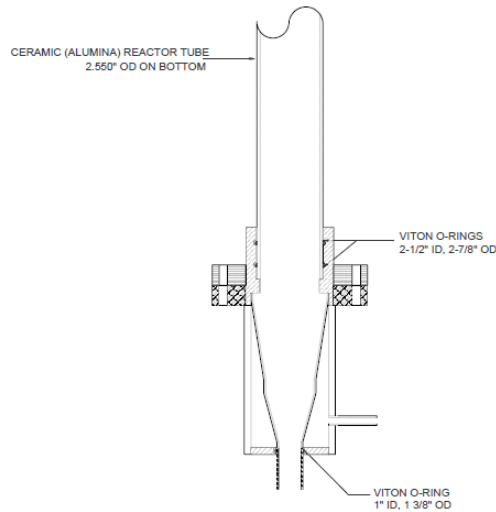


Figure A5.4. Outlet system at combustor exit (source: Smallwood's thesis(Smallwood 2005))

#### A5.2.6 Coal feeding system

A self-made coal feeder is used and its schematic drawing is shown in Figure A5.5. Coal particles are stored in a glass tube. Air is sent to the glass tube via a set of stainless steel tubes,

which can change their total length by sliding one tube into the other tube. Air flows out through a 1/8'' (0.3cm) stainless steel tube which is placed in the center of the coal feeder. Gas velocity around the entrance of the 1/8'' stainless steel tube is relatively high which enables air to carry coal particles at the entrance. If we fix the 1/8'' tube and push the glass tube up at a certain speed using a syringe pump, then coal particles would be carried away by air at a fixed rate. Therefore, the coal feeding rate can be controlled and calibrated. In order to keep the coal particle surface in the glass tube flat, a vibrator attached to the glass tube is used. Using a coal feeder, air can carry fixed amount of coal particles and enter the drop-tube furnace. The flow rate of the air (as a carrier) is set to be 1 LPM. The connection between the drop-tube furnace and coal feeder is shown in Figure 5.6A. The 1/8'' tube is inserted into the top part of the drop-tube furnace and then bended down.

Coal particles with carrier gas are delivered to the furnace through the 1/8'' tube. At the exit of the 1/8'' tube, gas flow will spread out, as well as Coal particles. The flow field was determined using FLUENT (fig. A5.6B). The velocity of gas in the center tube is much higher compared to gas velocity around the center tube. After gas is released from the center tube, some swirls are formed due to the high velocity in center tube. These swirls can help distribute coal particles on the cross section in the ceramic tube. Thus coal particle will not concentrate in the center line of the ceramic tube.

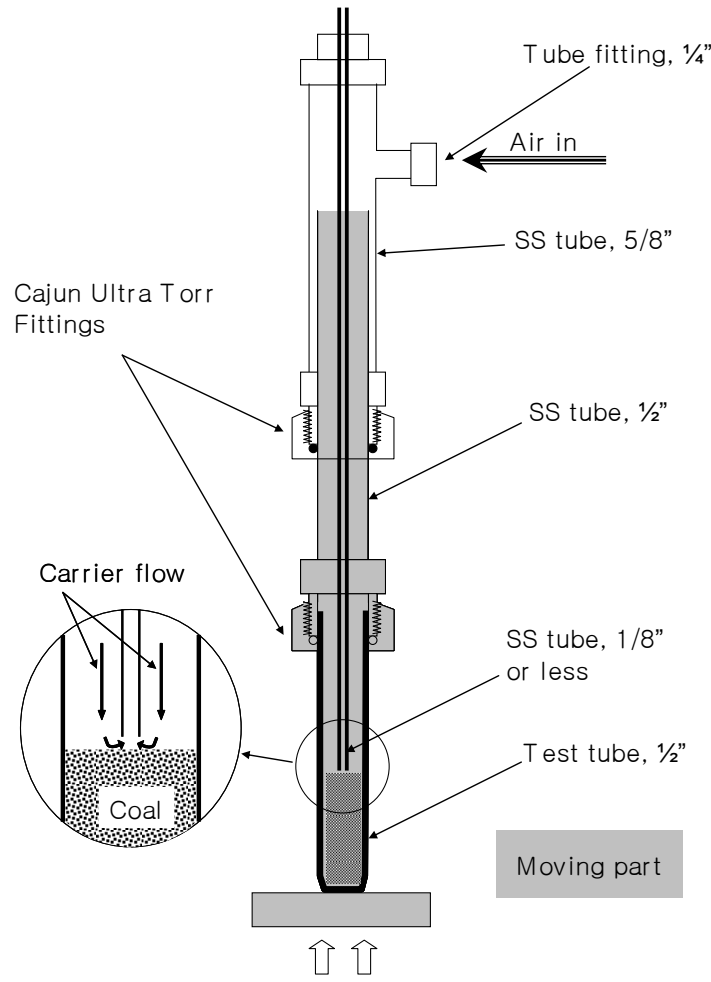
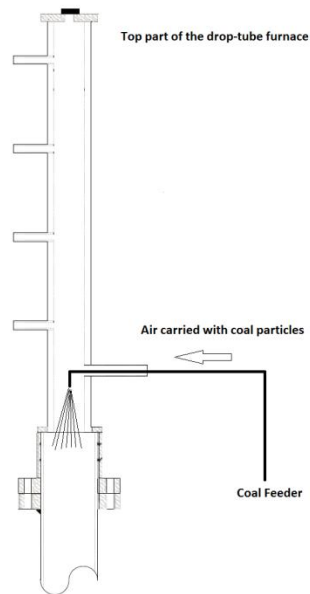


Figure A5.5. Schematic drawing of the coal feeder (source: William Linak)

A.



B.

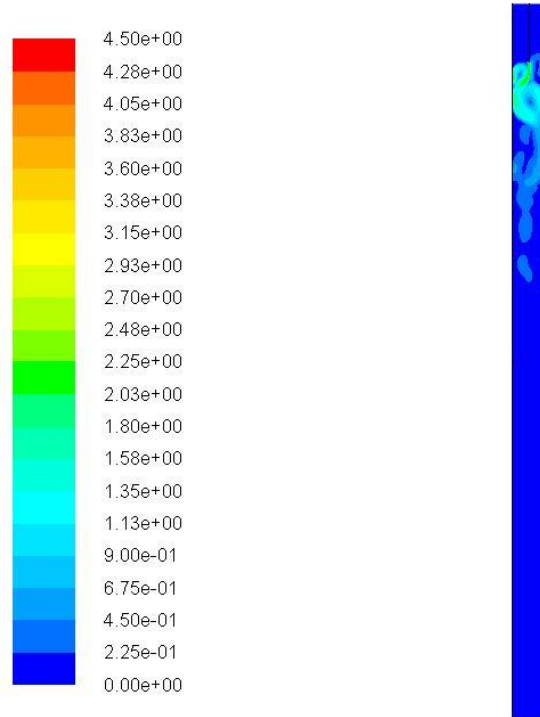


Figure A5.6. (A) Schematic drawing of the connection between the coal feeder and the drop-tube furnace; (B) Air velocity contour (unit: m/s) in the drop-tube furnace (calculated using *Fluent*)

### A5.3. Residence time calculations

Temperature profile inside reactor tube across its length at fixed temperature set point is measured by thermocouple. The temperature profile (shown in Figure A5.7) is used to calculate the residence time of air in the combustor by integrating across the length of the reactor tube. In our calculation, the combustion reactor tube is divided into 24 sections, two inches long each.

The average temperature in each of these sections is calculated (T1, T2, ... and T24, respectively) by averaging the temperatures at the beginning and the end of the sections. The second factor

used to calculate the residence time is the initial flow rate of air into the system and the assumption that the product of temperature and density is constant throughout the system. This principle can easily be derived from the Ideal Gas Law:  $PV = nRT$ ; where  $P$  is the pressure,  $V$  is the volume,  $n$  is the number of moles,  $R$  is the molar gas constant, and  $T$  is the temperature. Substituting  $n = m/M$  where  $m$  is the mass and  $M$  is the molar mass into equation, and rearranging, gives  $PM/R = (m/V) * T$ . Recognizing that  $m/V$  is density,  $\rho$ , the equation can be then be rewritten as  $PM/R = \rho T = \text{constant} = \rho_0 T_0 = 352.8 \text{ K kg/m}^3$ . Since the air flow rate at the inlet,  $Q_0$ , is constant, the mass flow rate ( $\rho * Q$ ) is also constant. These two principles allow for the calculation of residence times in the 24 sections of the combustor. For any given set point temperature, the residence time in the combustor can be calculated by calculating the density in each of the three sections, then calculating the flow rate in each of the three sections ( $Q_1, Q_2, \dots, Q_{24}$ , respectively), and substituting the flow rate values into the following equation:

$$t_R = \frac{\pi r^2 Q_1}{L_1} + \frac{\pi r^2 Q_2}{L_2} + \dots + \frac{\pi r^2 Q_{24}}{L_{24}}$$

According to our calculation, residence time for 3 LPM inlet air flow at 1100°C furnace set point temperature is approximately 23.3s.



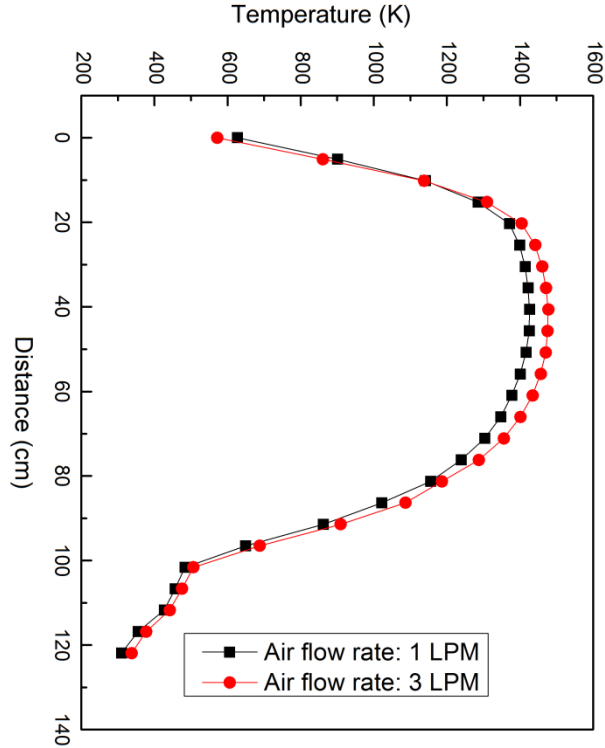


Figure A5.7. Temperature profile along the alumina tube when the furnace temperature is fixed at 1100°C

#### A5.4. Temperature history of a burning coal

Firstly, for simplicity, I will assume that a coal particle is heating up **without any chemical reaction**. Only heat convection and radiation are considered.

The energy balance equation for this particle is shown below. Heat transfer to the coal particle is through heat convection and radiation. Assuming that there is no temperature gradient inside the coal particle, then the heat flux is equal to the left hand side of Eq. 1.

$$mC_p \frac{\partial T_s}{\partial t} = q = 4\pi r_s^2 (T_g - T_s)h + \varepsilon_s \sigma (T_{wall}^4 - T_s^4) \text{ (Eq. 1)}$$

where  $m$  is the mass of coal particle,  $C_p$  is heat capacity,  $T_g$  is gas temperature,  $T_s$  is the temperature of coal particle (assuming no temperature gradient inside coal particle),  $q$  is the heat flow to coal particle,  $T_{\text{wall}}$  is tube wall temperature,  $\varepsilon_s$  is emissivity,  $\sigma$  is Stefan-Boltzmann constant,  $r_s$  is the radius of coal particle,  $h$  is heat transfer coefficient and  $k_g$  is thermal conductivity for air. The first term on the right hand side is representative of heat convection. The second term on the right hand side is representative of heat radiation.

Consider a coal particle (material: carbon, diameter: 50  $\mu\text{m}$ , initial temperature: 298 K). If we suddenly put this particle into a chamber with the temperature of 1373 K, the temperature of the coal particle vs. time can be easily obtained by solving Eq. 1 (for simplicity, we can neglect the heat conduction term, since it is much smaller than radiation term). Figure 1 shows the result. Since we do not know the emissivity, we calculated the result at 3 different emissivities: 0.01; 0.1 and 0.95. Emissivities of most materials range from 0.01 to 1. And the emissivity of carbon is about 0.95, which should be similar to coal.

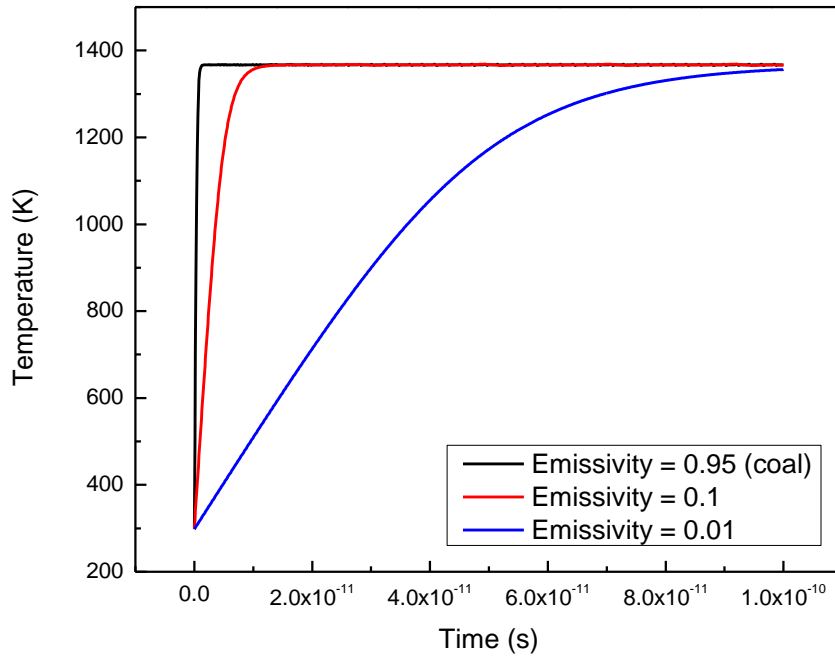


Figure A5.8. Temperature changing of a coal particle which is suddenly put into a hot chamber with the temperature at 1376 K

From Fig. A5.8, we can see that the heating up time for the coal particle is extremely short ( $\sim 1 \times 10^{-12}$  second) due to the rapid heat transfer through radiation, even when emissivity is low (0.01). Thus we can safely assume that the temperature of coal particle is always equal to gas temperature if all chemical reactions are frozen. Then we can plot temperature of coal particle vs. time in the furnace, since we know the gas temperature profile along the drop-tube. Fig. A5.9 shows the temperature changing of a coal particle in the DTF when the air flow rate is set to 3 LPM and the temperature of DTF is set to 1376 K. The residence time of a coal particle in the DTF is about 23 second. But the time during the temperature of coal particle larger than 1300 K

is only about 5 second. Figure 2 also shows different initial temperatures of a coal particle. Due to rapid heat transfer between coal particle and its surroundings, the temperature of the coal particle reaches its surrounding temperature in very short time. Then its temperature just follows the change of the surrounding gas temperature.

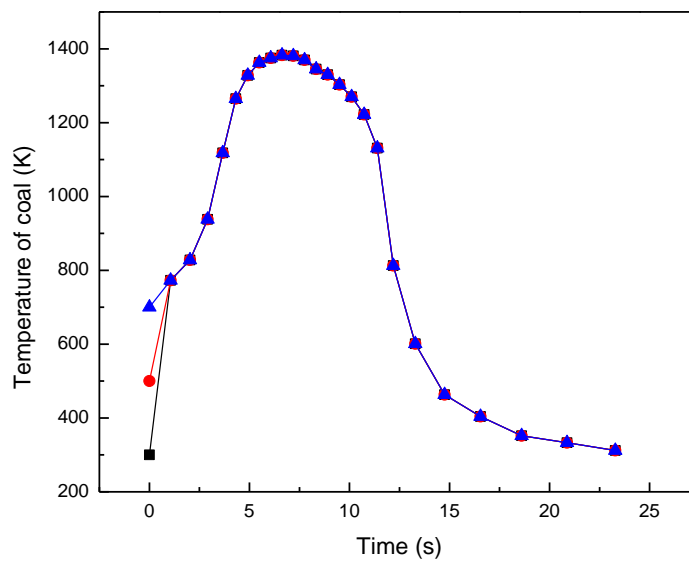


Figure A5.9. Temperature changing of a coal particle in the DTF used in AAQRL (the air flow rate is set to 3 LPM, the temperature of DTF is set to 1376 K, burning is not considered): Black Square: the initial temperature of the coal particle is 300 K; Red Circle: the initial temperature is 500 K and Blue Triangle: the initial temperature is 700 K.

Secondly, let's include the **burning of coal particle**.

Burning of a coal particle is very complicated, which includes pyrolysis, burning of volatiles and burning of char particle. Here, for simplicity, we assume coal particle is a pure carbon particle. And its size does not change during the combustion. We will use a One-film model to calculate the surface temperature of a burning carbon particle. This model is described in Turns' book in detail (Turns 2012). A brief introduction is shown below.

*Assumptions:*

- 1) It is a quasi-steady process
- 2) Carbon particle is burning in air. There is no interaction between particles
- 3) Only the reaction  $C+O_2=CO_2$  is considered. CO formation and oxidation are excluded.
- 4) The thermal conductivity, heat capacity and the product of the density and mass diffusivity are all constant. And lewis number ( $Le$ ) is equal to 1
- 5) There is no temperature gradient inside the carbon particle. The emissivity of carbon is 1

To calculate the surface temperature of carbon particle, we need write both mass conservation and energy conservation equations:

*Mass conservation:*

$$\dot{m}_c = (Y_{O_2,\infty} - 0)/(R_{kin} + R_{diff}) \quad (\text{Eq. 2})$$

Where  $\dot{m}_c$  is burning rate of carbon;  $Y_{O_2,\infty}$  is oxygen mass fraction in air;  $R_{kin}$  is kinetic “resistance” and  $R_{diff}$  is diffusion “resistance”, both of which are defined below:

$$R_{kin} = \frac{v_l R_u T_s}{4\pi r_s^2 MW_{mix} k_c P} \quad (\text{Eq. 3})$$

and

$$R_{diff} = \frac{v_I + Y_{O_2,s}}{\rho D 4\pi r_s^2} \quad (\text{Eq. 4})$$

Where  $v_I$  is mass stoichiometric coefficient ( $v_I = 2.664$  in this case),  $R_u$  is universal gas constant,  $MW_{mix}$  is mean molecular weight of air,  $k_c$  is kinetic rate constant of carbon oxidation,  $P$  is pressure,  $Y_{O_2,s}$  is oxygen mass fraction at carbon surface,  $D$  is mass diffusivity and  $\rho$  is air density.

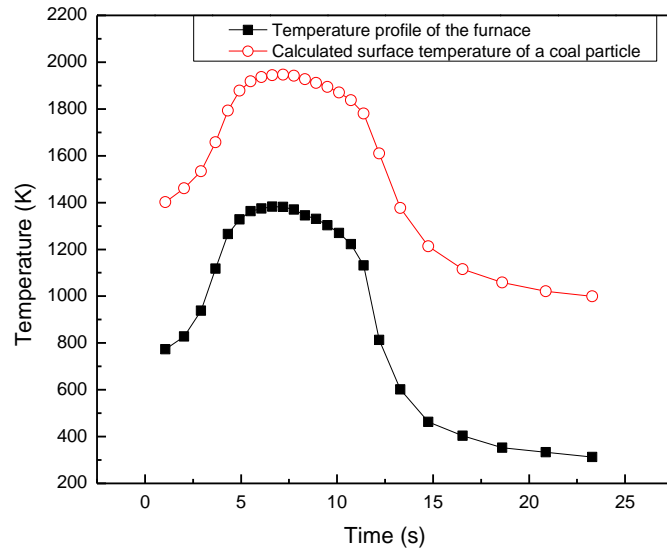
*Energy conservation*

$$\dot{m}_c \Delta h_c = -k_g 4\pi r_s^2 \frac{\partial T}{\partial r} \Big|_{r_s} + \varepsilon_s \sigma (T_s^4 - T_{sur}^4) \quad (\text{Eq. 5})$$

where  $\Delta h_c$  is enthalpy of carbon oxidation.

The equation 2 and 5 can be solved simultaneously, in order to calculate the surface temperature of carbon particle. According to the gas temperature profile along the drop-tube, the surface temperature of carbon particle can be obtained, since we assume that particle size does not change during the combustion. Figure 3 shows the changing of surface temperature of a 50  $\mu\text{m}$  carbon particle in the DTF.

A.



B.

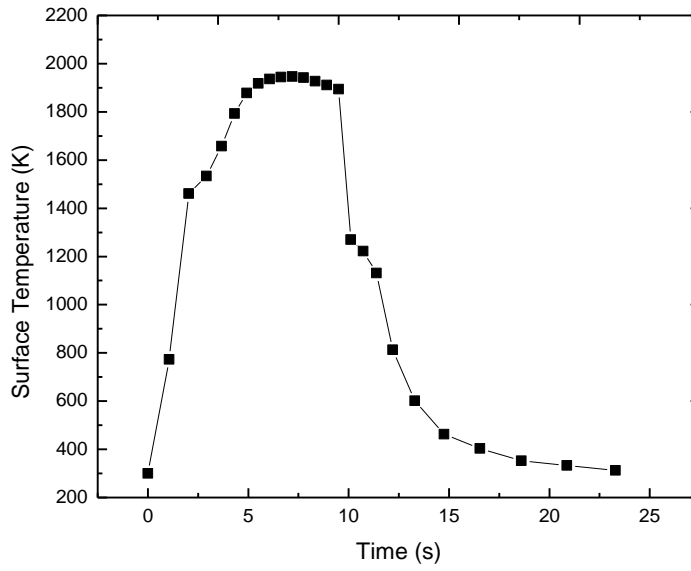


Figure A 5.10. (A) Calculated temperature changing of a coal particle in the DTF used in AAQRL (the air flow rate is set to 3 LPM, the temperature of DTF is set to 1376 K, constant burning is assumed); (B) Calculated temperature changing of a coal particle in the DTF (constant burning is NOT assumed)

According to Fig. A5.10A, carbon burning greatly increases the surface temperature of carbon. The maximum surface temperature is approaching to 2000 K. Figure A5.10A gives a better prediction on coal surface temperature than Fig. A5.9. However, it is still a rough estimation. The major drawback of Fig. 3 is that coal is not just carbon. For a 50  $\mu\text{m}$  carbon particle, it would burn out in about 0.2 second in our DTF. But, for coal particle, the burning process is much slower, since ash in coal will greatly slow down the diffusion of  $\text{O}_2$  and  $\text{CO}_2$ , thereby reducing the carbon oxidation rate. Therefore, Fig. A5.10A actually gives an upper limit of surface temperature of coal burning, while Fig. 2 gives a lower limit.

In reality, a coal particle will be heated in the drop-tube furnace from an initial temperature (room temperature). Then the coal particle starts to burn; and its surface temperature will increase drastically. But, devolatilization will also play an important role to retard increasing of temperature. Finally, the coal particle will burn out and leave the ash particles, whose surface temperature will quickly reach their surrounding gas temperature. If we assume that burnout time for coal particles is 10 seconds in our DTF (the exact number of burnout time needs to be calculated using a shrink core model which also integrated gas diffusion in ash layer), then Fig. A5.10B shows the temperature changing history for this coal particle, which is more realistic.



### **A5.5. Reference**

Smallwood, M. 2005. "Submicrometer Particle Formation and Mercury Capture During Powder River Basin Coal Combustion." Master thesis, Department of Environmental Engineering Science, Washington University in St. Louis.

## APPENDIX VI. ADVANCED INSTRUMENTATION FOR AEROSOL MEASUREMENT: AMS AND TAG

### A6.1. High-Resolution Time-of-Flight Aerosol Mass Spectrometer (HR-Tof-AMS)

The Aerodyne quadrupole Aerosol Mass Spectrometer (Q-AMS) was described in detail by (Canagaratna et al. 2007, Allan et al. 2003, Jimenez et al. 2003). HR-Tof-AMS is a newer version of AMS and has better mass-to-charge ratio ( $m/z$ ) resolution and faster response than the Q-AMS. The HR-Tof-AMS has been described in detail by DeCarlo et al. (2006). Briefly, aerosol particles are introduced into the AMS via the aerodynamic lens, which focuses the particles into a narrow beam. Particle size is resolved based on particle velocity across a time of flight chamber at the exit of the aerodynamic lens. Next, particles are impacted on a vaporizer where the non-refractory fraction is vaporized and immediately ionized using electron impact ionization. Finally, these ions are analyzed by a time-of-flight mass spectrometer. The vaporizer temperature was set to 600 °C. Coal combustion produces CO<sub>2</sub>, which will also contribute to some organic peaks like  $m/z$  28 and 44. A set of control experiments were conducted to determine and subtract the contribution of organic signal from background CO<sub>2</sub>. For each experimental condition, the AMS was running under the V-mode and the sampling time was about 15 min. And filtered, particle-free exhaust gas measured by AMS was used as the baseline. By using high-resolution mass spectra, the exact molecular formula of each organic peak (e.g. C<sub>x</sub>H<sub>y</sub>O<sub>z</sub>) was obtained, and overall elemental ratios for the entire mass spectrum was calculated. The method of elemental ratio calculation has been described by Aiken et al. (2007).

## A6.2 Thermal Desorption Aerosol Gas Chromatograph Mass Spectrometer (TAG)

The TAG system was designed to identify particulate organic compounds. Williams et al., (2006) provides an in depth description of the TAG system. Here is a brief introduction (Fig. A6.1): aerosol particles are firstly collected in an impactor; or a small square from the quartz filter containing particulates was inserted directly into this impactor. Then the temperature of this impactor increases to about 300 °C. Thus, the aerosol sample is thermally desorbed and converted into gas vapors, which were introduced into a gas chromatograph (GC) column to separate the compounds for detection. Compounds were detected using quadrupole mass spectrometry or a time-of-flight mass spectrometry.

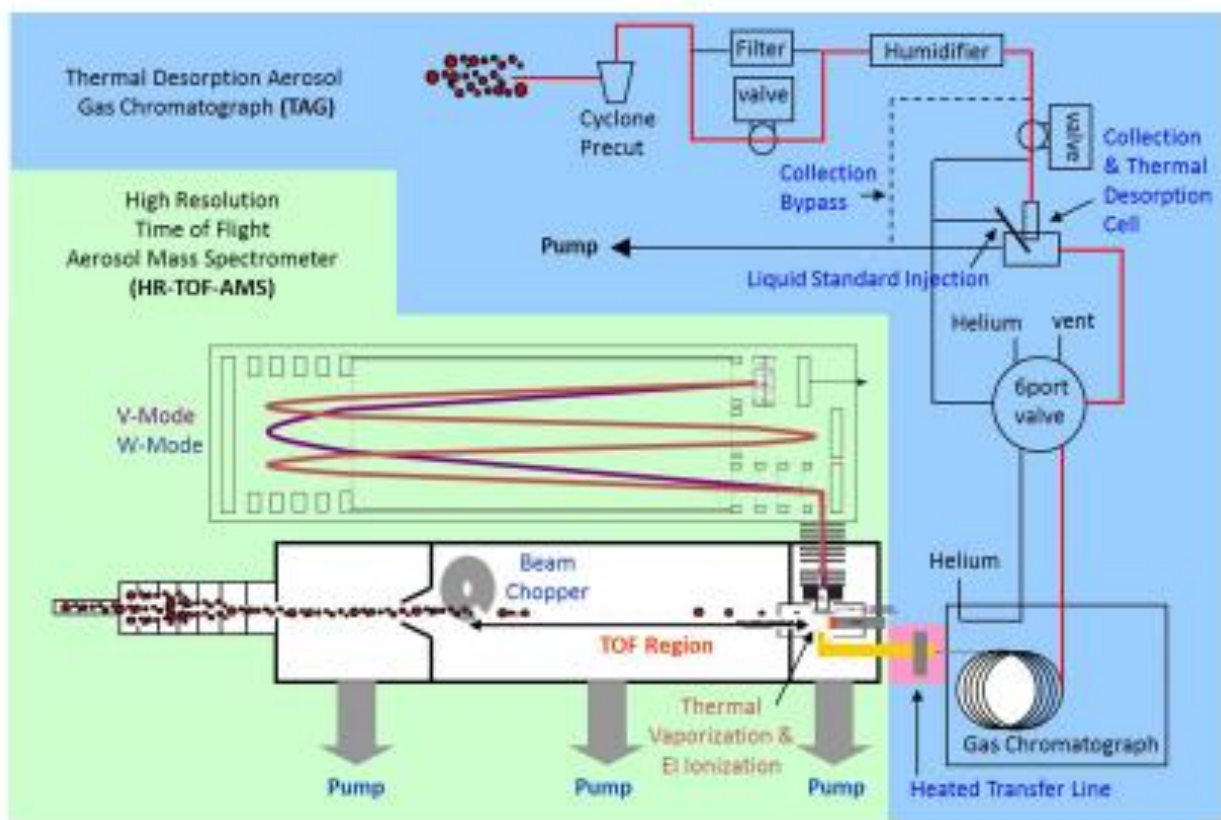


Figure A6.1 Schematic drawing of TAG (picture courtesy: Brent Williams)

### A6.3 References:

Allan, J. D., J. L. Jimenez, P. I. Williams, M. R. Alfarra, K. N. Bower, J. T. Jayne, H. Coe, and D. R. Worsnop. 2003. "Quantitative sampling using an Aerodyne aerosol mass spectrometer 1. Techniques of data interpretation and error analysis." *J. Geophys. Res.* no. 108 (D3):4090. doi: 10.1029/2002jd002358.

Canagaratna, M. R., J. T. Jayne, J. L. Jimenez, J. D. Allan, M. R. Alfarra, Q. Zhang, T. B. Onasch, F. Drewnick, H. Coe, A. Middlebrook, A. Delia, L. R. Williams, A. M. Trimborn, M. J. Northway, P. F. DeCarlo, C. E. Kolb, P. Davidovits, and D. R. Worsnop. 2007. "Chemical and microphysical characterization of ambient aerosols with the aerodyne aerosol mass spectrometer." *Mass Spectrometry Reviews* no. 26 (2):185-222. doi: 10.1002/mas.20115.

Jimenez, J. L., J. T. Jayne, Q. Shi, C. E. Kolb, D. R. Worsnop, I. Yourshaw, J. H. Seinfeld, R. C. Flagan, X. Zhang, K. A. Smith, J. W. Morris, and P. Davidovits. 2003. "Ambient aerosol sampling using the Aerodyne Aerosol Mass Spectrometer." *J. Geophys. Res.* no. 108 (D7):8425. doi: 10.1029/2001jd001213.

Williams, B. J., A. H. Goldstein, N. M. Kreisberg, and S. V. Hering. 2006. "An In-Situ Instrument for Speciated Organic Composition of Atmospheric Aerosols: Thermal Desorption Aerosol GC/MS-FID (TAG)." *Aerosol Science and Technology* no. 40 (8):627-638. doi: 10.1080/02786820600754631.

## APPENDIX VII. LIST OF PAPERS AND PRESENTATIONS

### PAPERS

1. **Wang, X.**; Williams, B. J.; Biswas, P., Emission Characteristics of Particulate Matter from Electrical Toy Cars: A New Indoor Aerosol Source. *To be submitted to Journal of the Air & Waste Management Association* **2014**.
2. **Wang, X.**; Cotter, E.; Williams, B. J.; Biswas, P., Relationship between Organic Aerosol Formation and Pyrolysis during Coal Combustion. *Submitted to Proceedings of the Combustion Institute* **2014**.
3. **Wang, X.**; Daukoru, S. M.; Torkamani, S.; Wang, W. N.; Biswas, P., Role of Flue Gas Recycle on Submicrometer Particle Formation during Oxy-Coal Combustion. *Proceedings of the Combustion Institute* **2013**, 34(2): 3479-3487.
4. **Wang, X.**; Williams, B. J.; Wang, X.; Tang, Y.; Yang, X.; Biswas, P., Characterization of Organic Aerosol Produced during Pulverized Coal Combustion in a Drop Tube Furnace. *Atmospheric Chemistry and Physics*, **2013**, 13, 10919-10932.
5. He, J.; **Wang, X.**; Wang, W. N.; Biswas, P., Elemental Mercury Oxidation in an Electrostatic Precipitator with In-Situ Soft X-rays. *In preparation*.

6. **Wang, X.;** Wang, H.; Huang, Y.; He, J.; Wang, W. N.; Cui, W.; Williams, B. J.; Yang, X.; Biswas, P., Evidence for A New Source of Nitrogen-Containing Organic Aerosol: Combustion of High Sulfur Content Coal. *To be submitted to Environmental Science & Technology Letters* **2014**.
7. **Wang, X.;** He, J.; Dhungel, B.; Wang, W. N.; Kumfer, B. M; Axelbaum, R. L.; Biswas, P., Characterization of Organic and Black Carbon Aerosols from Coal Combustion: An Experimental Study in a 1 Megawatt Pilot Scale Coal Combustor. *To be submitted to Energy & Fuels* **2014**.
8. **Wang, X.;** Li, S.; Wang, W. N.; Biswas, P., Mercury Removal from Coal Combustion by Injecting Vanadium Pentoxide ( $V_2O_5$ ) as High Temperature Sorbent. *In preparation*.
9. Wang, Y.; **Wang, X.;** Biswas, P., Measurement of Sub-3 nm particles in coal combustion flue gas. *In preparation*.
10. He, J.; **Wang, X.;** Wang, W. N.; Biswas, P., Secondary Aerosol Formation in Electrostatic Precipitator. *In preparation*.

## SELECTED PRESENTATIONS

1. American Association for Aerosol Research 32<sup>th</sup> Annual Conference, Portland, Platform presentation, 2013
  - Establishing the Role of Sulfur in Coal in Aerosol (Sulfuric Acid, Sulfate and Organic) Formation during Pulverized Combustion in a Drop-tube Furnace
  
2. Invited Talk at Fudan University, Shanghai, China, May 2013
  - Organic Aerosol Formation during Pulverized Coal Combustion
  
3. AIChE Annual Conference, Pittsburgh, Pennsylvania: Platform presentation, 2012
  - Characterization of Submicrometer Particles from Biomass-Coal Co-Firing in a Drop-Tube Furnace
  
4. AIChE Annual Conference, Pittsburgh, Pennsylvania: Platform presentation, 2012
  - Evaluation of Mercury Capture Technology Using Various Sorbents Injection
  
5. 35th International Symposium on Combustion, Warsaw, Poland: Platform presentation (Dr. Pratim Biswas presented for Xiaofei Wang) 2012
  - Role of Flue Gas Recycle on Submicrometer Particle Formation during Oxy-Coal Combustion
  
6. American Association for Aerosol Research 30<sup>th</sup> Annual Conference, Orlando, Platform presentation, 2011

- Characterization of Carbonaceous Aerosol Particles from Coal Combustion Using Aerosol Mass Spectrometry

7. American Association for Aerosol Research 30<sup>th</sup> Annual Conference, Orlando, Poster presentation, 2011

- Role of Flue Gas Recycle on Submicrometer Particle Formation during Oxy-Coal Combustion



## **APPENDIX VIII. LIST OF RAW DATA INCLUDED IN THE ATTACHED CD**

1. Raw data from particle size measurement (scanning mobility particle sizer data and aerodynamic particle sizer data)
2. Raw data from aerosol mass spectrometer
3. Raw data from XRF measurement

## **XIAOFEI WANG - CURRICULUM VITAE**

Aerosol & Air Quality Research Laboratory (AAQRL)  
Department of Energy, Environmental & Chemical Engineering  
Washington University in St. Louis  
St. Louis, MO, 63130  
Phone: 314-397-8632  
E-mail: [xiaofeiwang@go.wustl.edu](mailto:xiaofeiwang@go.wustl.edu)

### **EDUCATION**

**PhD Candidate, Energy, Environmental & Chemical Engineering**  
**Expected Graduation Date:** **May 2014**  
Washington University in St. Louis  
Thesis Topic: Fine particle and mercury formation and control during coal combustion  
Advisor: Pratim Biswas

**M.S., Environmental Science** **June 2009**  
Fudan University  
Thesis Title: Single particle analysis of ambient aerosols in Shanghai  
Advisor: Xin Yang

**B.S., Environmental Science** **June 2007**  
Fudan University

### **AWARDS AND HONORS**

- Dave Benferado Scholarship for Air Pollution Control and Waste Minimization Research, the Air & Waste Management Association, 2012
- Best Master Dissertation Award, Shanghai Municipal Education Commission, 2010
- McDonnell Scholar, Washington University in St. Louis, 2009 - Present
- Peabody Energy Corporate Fellow, 2009 - Present
- Graduate Scholarship for Outstanding Freshman, Fudan University: Second prize, 2007
- The People's Scholarship, Fudan University: Third prize, 2007
- Challenge Scholar Award for Outstanding Student Project of Scientific Innovation, Fudan University, 2006
- The People's Scholarship, Fudan University: Third prize, 2004
- Undergraduate Scholarship for Outstanding Freshman, Fudan University: Third prize, 2003

### **RESEARCH EXPERIENCE**

**Department of Energy, Environmental & Chemical Engineering**  
Washington University in St. Louis  
*PhD. Student, 2009 – present. Advisor: Pratim Biswas*  
Thesis Topic: Fine Particle and Mercury Formation and Control during Coal Combustion

- Characterized organic aerosols produced from pulverized coal combustion using various mass spectrometry, including high resolution aerosol mass spectrometer (HR-AMS), aerosol time-of-flight mass spectrometer (ATOFMS), thermal desorption aerosol gas chromatograph aerosol mass spectrometer (TAG-AMS). identified a major aerosol type from coal combustion in urban atmosphere using the new found characteristics of coal combustion aerosols
- Studied organic aerosol formation mechanism during pulverized coal combustion
- Studied mercury emission control from coal combustion using non-carbon based sorbents
- Investigated formation mechanism of submicrometer particles during conventional coal combustion, oxy-coal combustion and biomass/coal co-firing
- Led a project to evaluate the emissions of particulate matter and mercury from a 1 megawatt pilot-scale coal combustor and evaluate the performance of an electrostatic precipitator (ESP) with *in situ* soft X-ray
- Studied coal pyrolysis via both modeling and experimental approaches

### **Department of Environmental Science and Engineering**

Fudan University

*M.S. 2007 - 2009. Advisor: Xin Yang*

Thesis Title: Single particle analysis of ambient aerosols in Shanghai

- Found the evidence for high molecular weight nitrogen-containing organic salts in urban aerosols using ATOFMS; and proposed a formation mechanism of organic salts formation
- Studied particulate nitrate formation in an urban area using ATOFMS
- Developed some MATLAB codes for analysis of ATOFMS data

*B.S. 2007. Advisor: Xingnan Ye*

Thesis Topic: Construction and Characterization of an Aerosol Chamber at Fudan University

- Participated the construction of an aerosol chamber
- Tested its controls of humidity, pressure and temperature

### **JOURNAL PUBLICATIONS**

1. **Wang, X.**; Williams, B. J.; Biswas, P., Emission Characteristics of Particulate Matter from Electrical Toy Cars: A New Indoor Aerosol Source. *Submitted 2013*.
2. **Wang, X.**; Cotter, E.; Williams, B. J.; Biswas, P., Relationship between Organic Aerosol Formation and Pyrolysis during Coal Combustion. *Submitted to Proceedings of the Combustion Institute* (Accepted for oral presentation in 35<sup>th</sup> International Combustion Symposium) **2014**.
3. **Wang, X.**; Daukoru, S. M.; Torkamani, S.; Wang, W. N.; Biswas, P., Role of Flue Gas Recycle on Submicrometer Particle Formation during Oxy-Coal Combustion. *Proceedings of the Combustion Institute* **2013**, 34(2): 3479-3487.

4. **Wang, X.**; Williams, B. J.; Wang, X.; Tang, Y.; Yang, X.; Biswas, P., Characterization of Organic Aerosol Produced during Pulverized Coal Combustion in a Drop Tube Furnace. *Atmospheric Chemistry and Physics*, **2013**, 13, 10919-10932.
5. Yang, F.; Wang, X.; Zhang, Y.; **Wang, X.**; Chen, H.; Yang, X.; Chen, J., Real-time, single-particle measurements of ambient aerosols in Shanghai. *Frontiers of Chemistry in China* **2010**, 5, (3), 331-341.
6. **Wang, X.**; Gao, S.; Yang, X.; Chen, H.; Chen, J.; Zhuang, G.; Surratt, J. D.; Chan, M. N.; Seinfeld, J. H., Evidence for High Molecular Weight Nitrogen-Containing Organic Salts in Urban Aerosols. *Environmental Science & Technology* **2010**, 44, (12), 4441-4446.
7. Zhang, Y.; Yang, F.; Wang, M.; **Wang, X.**; Chen, H.; Yang, X., Single particle mass spectrometry of zinc and copper-containing aerosols in Shanghai. *Journal of Fudan University (Natural Science)* **2010**, (1), 51-59.
8. **Wang, X.**; Zhang, Y.; Chen, H.; Yang, X.; Chen, J.; Geng, F., Particulate Nitrate Formation in a Highly Polluted Urban Area: A Case Study by Single-Particle Mass Spectrometry in Shanghai. *Environmental Science & Technology* **2009**, 43, (9), 3061-3066.
9. Zhang, Y.; **Wang, X.**; Chen, H.; Yang, X.; Chen, J.; Allen, J. O., Source apportionment of lead-containing aerosol particles in Shanghai using single particle mass spectrometry. *Chemosphere* **2009**, 74, (4), 501-507.

#### PAPERS IN PREPARATION

1. He, J.; **Wang, X.**; Wang, W. N.; Biswas, P., Elemental Mercury Oxidation in an Electrostatic Precipitator with In-Situ Soft X-rays. *In preparation for Journal of the Air & Waste Management Association*.
2. **Wang, X.**; Cotter, E.; He, J.; Wang, W. N.; Williams, B. J.; Biswas, P., Establishing the Role of Sulfur in Coal in Aerosol (Sulfuric Acid, Sulfate and Organic) Formation during Pulverized Combustion in a Drop-tube Furnace. *In preparation for Environmental Science & Technology letters*.
3. **Wang, X.**; Li, S.; Wang, W. N.; Biswas, P., Mercury Removal from Coal Combustion by Injecting Vanadium Pentoxide ( $V_2O_5$ ) as High Temperature Sorbent. *In preparation for Environmental Engineering Science*.

#### ORAL PRESENTATIONS

1. American Association for Aerosol Research 32<sup>th</sup> Annual Conference, Portland, Platform presentation, 2013

- Establishing the Role of Sulfur in Coal in Aerosol (Sulfuric Acid, Sulfate and Organic) Formation during Pulverized Combustion in a Drop-tube Furnace
2. Invited Talk at Fudan University, Shanghai, China, May 2013
    - Organic Aerosol Formation during Pulverized Coal Combustion
  3. AIChE Annual Conference, Pittsburgh, Pennsylvania: Platform presentation, 2012
    - Characterization of Submicrometer Particles from Biomass-Coal Co-Firing in a Drop-Tube Furnace
  4. AIChE Annual Conference, Pittsburgh, Pennsylvania: Platform presentation, 2012
    - Evaluation of Mercury Capture Technology Using Various Sorbents Injection
  5. American Association for Aerosol Research 30<sup>th</sup> Annual Conference, Orlando, Platform presentation, 2011
    - Characterization of Carbonaceous Aerosol Particles from Coal Combustion Using Aerosol Mass Spectrometry
  6. Department Seminar, Environmental Science and Engineering, Fudan University, May 2008
    - The formation mechanism of nitrate in the individual particles over Shanghai in summer revealed by ATOFMS

## TEACHING EXPERIENCE

### Department of Energy, Environmental & Chemical Engineering

Washington University in St. Louis

*Teaching assistant:* Chemical Reaction Engineering, Fall 2010

- Help sections, office hours and grading

*Teaching assistant:* Heat Transfer, Fall 2011

- Grading

*Teaching assistant:* Introduction to Environmental Engineering, Spring 2012

- Lectures, office hours and grading

## SKILLS

**Laboratory skills:** High resolution aerosol mass spectrometer (AMS, Aerodyne Research Inc.), Aerosol time-of-flight mass spectrometer (ATOFMS, TSI Inc.), Thermal desorption aerosol gas chromatograph aerosol mass spectrometer (TAG-AMS, Aerodyne Research Inc.), Scanning mobility particle sizer, Aerodynamic particle sizer, Direct mercury analyzer, Gas phase mercury sampling, Transmission electron microscopy (TEM), Thermogravimetric Analysis (TGA, TA instruments), Drop-tube furnace, Flat-flame burner design, Modeling for aerosol dynamics, Distributed activated energy modeling for coal/biomass pyrolysis

**Computer skills:** Matlab, Igor, MS Excel, MS Word, MS Power Point

**Languages:** Mandarin: native speaker; English: fluent